State of Oregon
Oregon Department of Geology and Mineral Industries
Ian P. Madin, Interim State Geologist

OPEN-FILE REPORT O-15-05

COASTAL FLOOD HAZARD STUDY, CLATSOP COUNTY, OREGON

By Jonathan C. Allan[1], Peter Ruggiero[2], Gabriel Garcia[2],
Erica L. Harris[1], Jed T. Roberts[3], and Laura L. Stimely[1]

2015

[1]Oregon Department of Geology and Mineral Industries, Coastal Field Office, P.O. Box 1033, Newport, OR 97365
[2]College of Earth, Ocean and Atmospheric Sciences, Oregon State University, Corvallis, OR 97331
[3]Oregon Department of Geology and Mineral Industries, 800 NE Oregon St., Ste. 965, Portland, OR 97232

DISCLAIMER

This product is for informational purposes and may not have been prepared for or be suitable for legal, engineering, or surveying purposes. Users of this information should review or consult the primary data and information sources to ascertain the usability of the information. This publication cannot substitute for site-specific investigations by qualified practitioners. Site-specific data may give results that differ from the results shown in the publication.

Cover photograph: Coastal geomorphologist, J. Allan, maps the elevation of the beach at Arch Cape using a Real-Time Kinematic Differential Global Positioning System (RTK-DGPS). Photo taken by E. Harris, September 21, 2010.

Oregon Department of Geology and Mineral Industries Open-File Report O-15-05
Published in conformance with ORS 516.030

For additional information:
Administrative Offices
800 NE Oregon Street #28, Suite 965
Portland, OR 97232
Telephone (971) 673-1555
Fax (971) 673-1562
http://www.oregongeology.org
http://www.oregon.gov/DOGAMI/

TABLE OF CONTENTS

LIST OF FIGURES

LIST OF TABLES

1.0 INTRODUCTION

The objective of the Clatsop County coastal flood hazard project is to develop updated Digital Flood Insurance Rate Maps (DFIRM) and Flood Insurance Study (FIS) report for Clatsop County, Oregon (**Figure 1-1**). For this effort, the Oregon Department of Geology and Mineral Industries (DOGAMI) will be using newly acquired (2009) light detection and ranging data (lidar) to redelineate coastal and riverine flood hazards within Clatsop County, produce revised DFIRMs and a revised FIS report, and produce other mapping products useable at the local, state, and federal level for mitigation planning, risk analysis, and disaster response.

As part of the revision, DOGAMI has been contracted to perform detailed coastal flood hazard studies for several stretches of beach along the Clatsop County shoreline of the Pacific Ocean. These analyses are to include assessments of the 1% or 100-year extreme storm wave event and the associated calculated wave setup, runup and total water level (i.e., the wave runup superimposed on the tidal level) to help guide the determination of Special Flood Hazard Areas (SFHAs), the most significant being regions subject to high coastal flood risk (Zone VE), characterized with base flood elevations (BFEs) that are used to guide building practices. Additional modeling of the 0.2%, or 500-year, event will also be undertaken.

Detailed coastal flood analyses will be limited to the following key areas:

- the Clatsop Plains, which extends from the mouth of the Necanicum estuary to the south Columbia River jetty;
- Seaside, from the north side of Tillamook Head to the mouth of the Necanicum estuary;
- Cannon Beach, from Bird Rocks to Silver point;
- Arcadia Beach, from Silver Point to Hug Point;
- Arch Cape beach, from Hug Point to Arch Cape;
- Falcon Cove, from Arch Cape to the north side of Cape Falcon.

Aside from these areas, DOGAMI will develop revised Zone V for the remainder of the county shoreline. While the bulk of the shoreline has been mapped as Zone VE, portions of the coastline have been previously mapped "D" (e.g., immediately south of the Columbia River jetty) and "X" (e.g., area around Tillamook Head and small sections of shore south of Cannon Beach). These latter areas reflect areas that were previously not mapped using detailed hydraulic analyses. However, after consulting with FEMA and state government representatives, the decision has been made to revise these latter zones to better reflect the geomorphology of the coast, and in addition re-designate these areas as Zone V.

The development of coastal flood maps is complicated, due to its dependence on a myriad of data sources required to perform the wave transformations, runup, and overtopping calculations. These challenges are further compounded by an equally wide range of potential settings in which the data and methods can be applied, which range from dune to bluff-backed beaches, sites that may be backed by coastal engineering structures such as sea walls, riprap revetments, or wooden bulkheads, to gravel and hard rock shorelines. **Figure 1-2** broadly summarizes the various steps that are described in the ensuing sections in order to help understand conceptually the process that leads ultimately to the completed coastal flood hazard zones.

This report first examines the coastal geology and geomorphology of the Clatsop County shoreline, including a discussion of the erosion history of the coast. The results presented in this section will ultimately form the basis for defining the flood zones along the Clatsop coast. Section 3 presents the results of Real-Time Kinematic Differential Global Positioning Surveys (RTK-DGPS) of the detailed study sites established along the length of the Clatsop County shoreline, undertaken at the peak of the 2010/11 winter. These surveys are also compared with recent historical data derived from lidar data, which are used to help define the most eroded winter profile used in the runup calculations described in Section 6. Section 3 also documents various parameters associated with the measured beach profile data, including the beach-dune junction elevation, the beach slope and dune/bluff crest/top elevations.

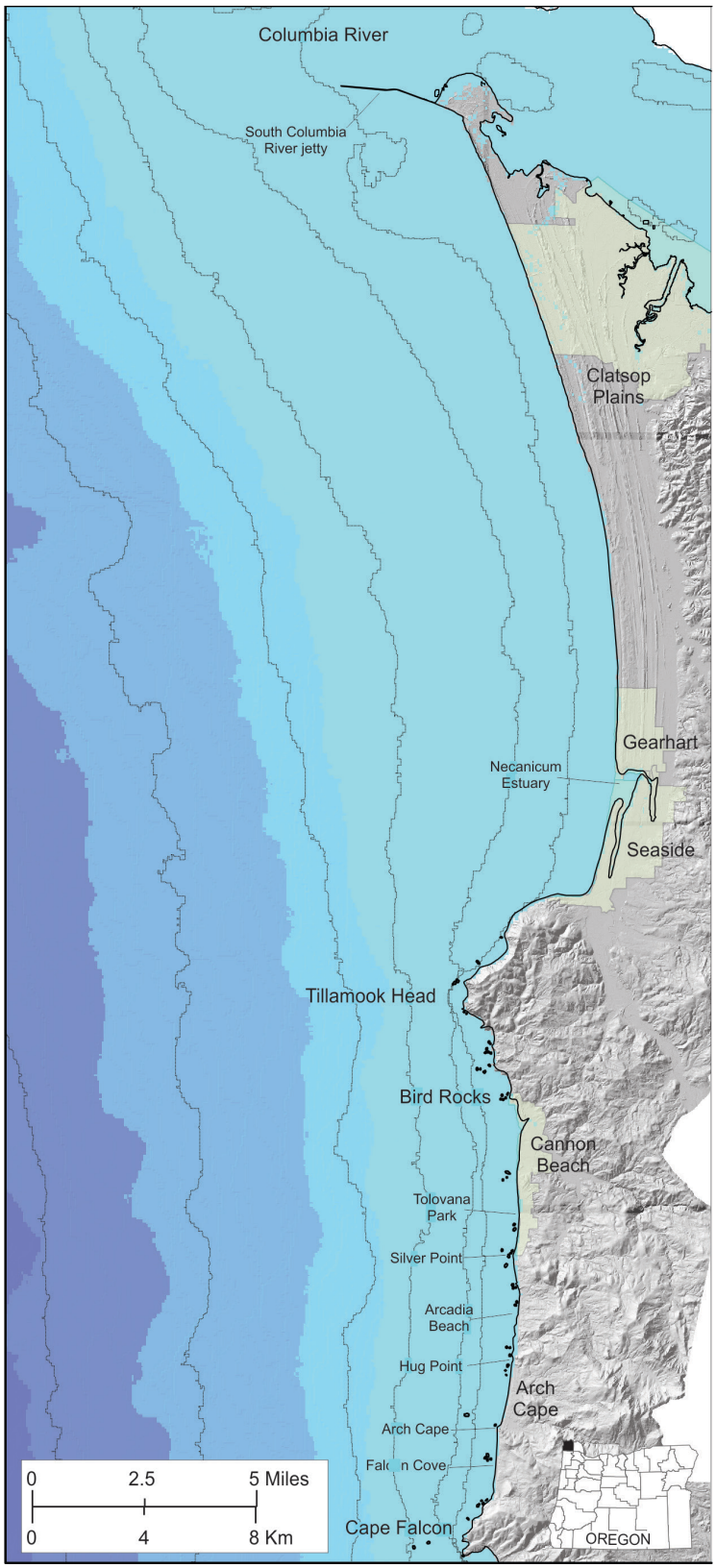

Figure 1-1. Location map of Clatsop County coastline.

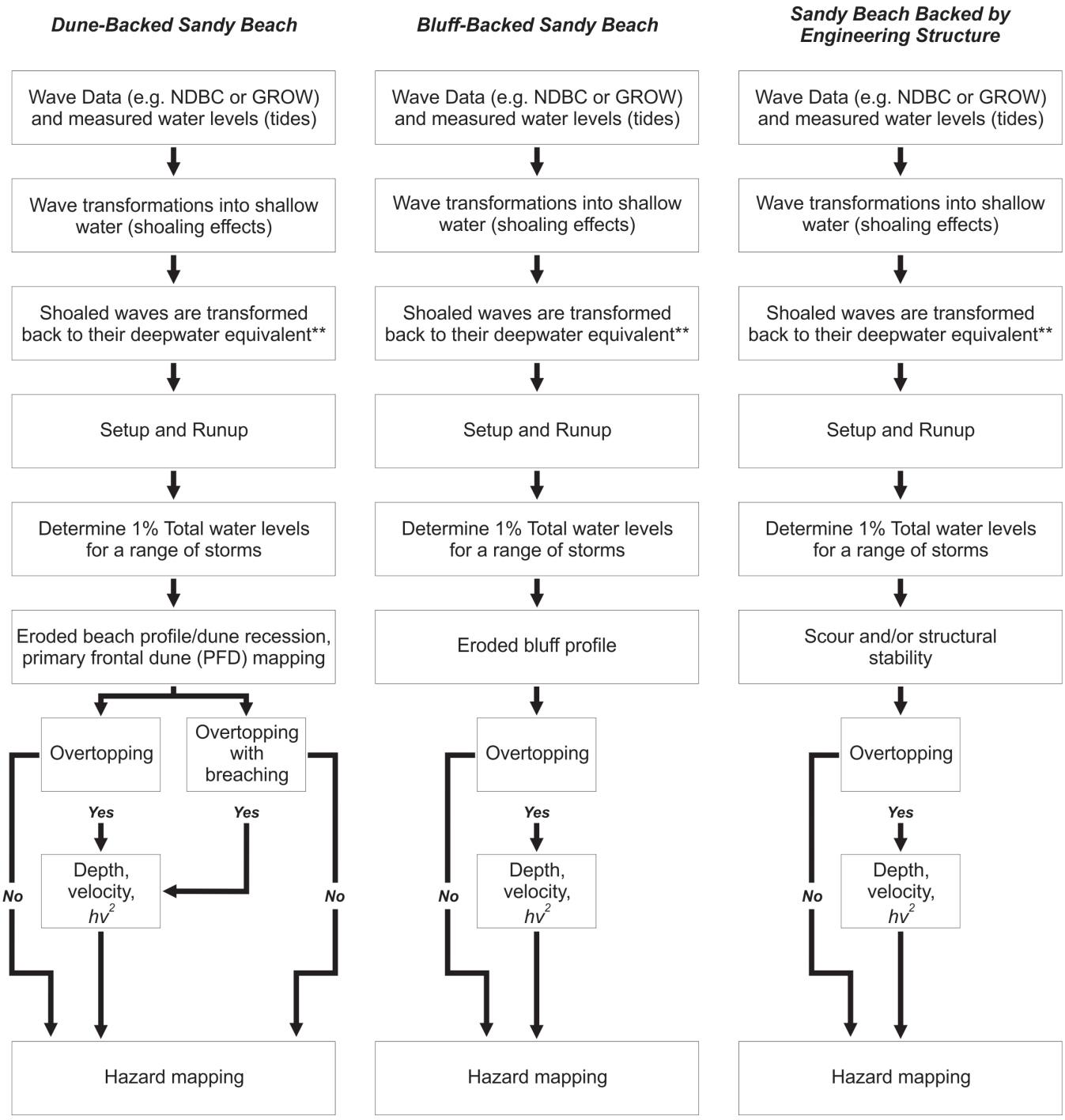

Figure 1-2. Three representative examples of the steps that may be taken to derive coastal flood hazard maps on the Pacific Northwest coast. **Note: The waves are first shoaled using numerical models in order to account for the effect of wave changes (refraction/diffraction) that take place across the shelf and in the nearshore. Because many coastal engineering equations (e.g., wave runup) require deepwater inputs, the "shoaled" waves are then converted back to their deepwater equivalence.

An examination of the tide data measured by the National Ocean Service (NOS) of the National Oceanographic Atmospheric Administration (NOAA) Astoria tide gauge located 23.5 km from the river's mouth (the greatest distant of any of the tide gauges from the open coast), and the South Beach, Yaquina Bay tide gauge, is presented in Section 4, including an analysis of the 1% and 0.2% *still water levels* (SWL). Section 5 describes the steps undertaken to develop a synthesized wave climate, critical for developing the input wave statistics used in calculating the wave runup. Section 5 also examines the procedures used to refract the waves from deep water into the nearshore using the SWAN (Simulating Waves Nearshore) wave model. Analyses of the wave runup, including the calculation of the 1% and 0.2% total water levels (T_{WL}) as well as any overtopping calculations is presented and discussed in Section 6.

Section 7 discusses the steps used to determine the degree of erosion that might occur on the dune-backed beaches, including the approach used to define the duration-reduced erosion factor, important for further establishing the initial conditions on which the runup and overtopping calculations are ultimately performed. Similar discussions are provided describing observations of bluff erosion, characteristic of a few discrete sections of the Clatsop County shoreline. Finally, Section 8 synthesizes all of the information and describes the steps taken to draft new flood maps along the Clatsop County shoreline.

2.0 COASTAL GEOLOGY AND GEOMORPHOLOGY OF CLATSOP COUNTY

Clatsop County is located on the northwest Oregon coast, between latitudes 46°15′33.16″N (Columbia River) and 45°46′59.24″N (just north of Cape Falcon), and longitudes 123°59′50.64″W and 123°21′47.55″W. The terrain varies from low elevation sandy beaches and dunes on the coast itself, to elevations over 900 m (e.g., Onion Peak reaches 933 m [3,064 ft]) farther inland). The coastal strip (**Figure 1-1**) is 57 km in length and varies in its geomorphology from wide sandy beaches backed by broad dunes, cobble and boulder beaches, and bluff backed shorelines. Bold headlands formed of resistant basalt (e.g., Cape Falcon and Tillamook Head) provide natural barriers to alongshore sediment transport, effectively dividing the county coastline into two littoral cells:

- Cape Falcon to Tillamook Head (Cannon Beach cell); and
- Tillamook Head to Pt Grenville on the Washington coast, the latter forming the 185 km long Columbia River littoral cell.

The county is bounded in the north by the Columbia River and the broad expanse of its lower estuary. Prior to jetty construction and discharge control, this river system historically transported large volumes of sediment to the coast that played a significant role in the evolution of the Clatsop Plains. To the south, smaller streams such as the Necanicum and Ecola Creeks flow out of the coast range. Due to their generally low flow discharge and the terrain they are down cutting into, these creeks carry little beach sediment to the coast today. Hence, there is no significant source of sediment to the coast today other than from erosion of the backshore. This is especially true of the coast south of Tillamook Head.

2.1 Local Geology

Along the Clatsop County coast the predominant geologic units consist of latest Holocene beach sand present along the full length of the coastline. These beaches are backed by a wide variety of geologic units that clearly influence the contemporary geomorphology of the coast today (Schlicker and others, 1972; Witter and others, 2009). Travelling north to south, the geology of the coast can be broadly divided into the following components:

- An extensive dune ridge sequence that forms the Clatsop Plains (**Figure 2-1**);
- Late Holocene gravels (pebbles to cobbles) and boulders that abut against Tillamook Head, where they form prominent, steep natural barriers to wave erosion. Furthermore, much of the City of Seaside is built on a 3.7-km-long spit composed of basalt cobbles that originated as rocky debris produced by landslides on Tillamook Head. Gravels are also prevalent along much of the Clatsop County shoreline forming a generally thin veneer at the back of the most beaches in southern Cannon beach, Hug Point and at Arcadia Beach. With progress south, the gravels increase in size and volume forming a more substantial gravel beach at Arch Cape, culminating with the impressive cobble berm at Falcon Cove;
- Late Pleistocene to Holocene colluvial deposits that overlay Middle Miocene, Intrusive Grande Ronde Basalt (e.g., much of Tillamook Head). These are fronted by late Holocene gravels and boulders (**Figure 2-2**);
- Relatively flat, late Pleistocene coastal terrace deposits on which most of the City of Cannon Beach and the community of Tolovana Park have been developed on (**Figure 2-3**). These sediments include well-cemented fluvial gravels, massive beach sand, and poorly bedded mud with fossil shell from estuarine environments. In many areas, low bluffs of the coastal terrace presently are protected from storm wave erosion by a ramp of dune sand and are well vegetated suggesting that they have been stable for some time;
- Between Silver Point and Hug Point, much of the shore can be characterize as consisting of unstable bluffs, with several major landslides. The geology in this region is characterized as mostly Astoria Formation (Middle to lower Miocene)

sandstone/mudstone units. Interspersed with Pleistocene terrace deposits (e.g., in the vicinity of Arcadia Beach), while in the south, exposures of Angora Peak sandstone form prominent bluffs.

- The community of Arch Cape occupies a broad coastal terrace with few active landslides impacting relatively low (<10 m high) bluffs. The entire shoreline is naturally armored by a gravel beach, which periodically is covered with sand during summer months (**Figure 2-4**).
- Finally, Cove Beach borders a crescent-shaped recess in the coast between Arch Cape and Cape Falcon. The small beach community of Falcon Cove that overlooks Cove Beach faces the most severe erosion and landslide hazards among coastal communities in southern Clatsop County. More than 65 percent of coastal bluffs backing Cove Beach show evidence of active or prehistoric mass movement (Witter and others, 2009). Deposits that comprise these bluffs are inferred to reflect mostly late Pleistocene rock avalanche deposits.

Figure 2-1. Looking south along the Clatsop Plains toward Tillamook Head in the distance (photo: E. Harris, DOGAMI, 2011).

Figure 2-2. Cobble and boulder beaches predominate around the Tillamook Head (photo: E. Harris, DOGAMI, 2011).

Figure 2-3. Haystack Rock at Cannon Beach. Homes present along the shore have been constructed on marine terrace deposits that form low, well vegetated bluffs (photo E. Harris, DOGAMI, 2011).

Figure 2-4. Gravel beach at Arch Cape (photo E. Harris, DOGAMI, 2011).

Much of the beach sand present on the Oregon coast consists of grains of quartz and feldspar. The beaches also contain small amounts of heavier minerals (e.g., garnet, hypersthene, augite, and hornblende [**Figure 2-5**]), which can be traced to various sediment sources along the Pacific Northwest coast (Clemens and Komar, 1988). For example, garnet and hypersthene is derived from the Klamath Mountains located in southern Oregon and in North California. Because the headlands today extend well out in deep water, they effectively limit sand transport around their ends under the current process regime. This suggests that these heavier minerals were probably transported northward along the coast at a time when sea level was much lower, with few barriers to interrupt their northward movement (Komar, 1997). With distance from their source, the sediments combined with other minerals derived locally from erosion processes in the coast range. As shown in **Figure 2-5**, the concentrations of garnet and hypersthene decrease to the north, while concentrations of of augite increase significantly; augite is a mineral that is prevalent in the volcanic rocks present throughout Tillamook County. At Tillamook Head the concentration of garnet is very small, suggesting that Tillamook Head reflects the most northerly transport of the garnet. North of Tillamook Head, it can be seen that concentrations of hypersthene and hornblende increase again. These latter sediments are derived from the Columbia River, which contributed to the formation of the Clatsop Plains, Long Beach Peninsula, and Grayland Plains. Thus, sediments derived from the Columbia River were transported mainly to the north, supplying the Washington coast and shelf.

With the end of the last glaciations, sea level rose rapidly and the beaches began to migrate landward. New sediments were derived from erosion of the coastal plain that makes up the continental shelf today. At around 5000-7000 years ago, the rate of sea level rise slowed as it approached its current level today (Komar, 1997). At this stage the prominent headlands would have begun to interrupt sediment transport. Modern barrier spits and beaches began to

form within the headland bounded littoral cells that make up the present coast today.

Along the Tillamook County coast, the beaches contain abundant concentrations of augite, indicative of their having been derived locally (**Figure 2-5**). This implies that at the time, rivers and streams were carrying these sediments out to the coast where they mixed with other sediments. These concentrations likely increased during the past 150 years as human settlement accelerated leading to increased deforestation (Peterson and others, 1984; Komar and others, 2004). This correspondingly contributed to increased sediment loads in the various rivers. However, analyses of the sediment characteristics in Tillamook Bay, the largest estuary in the county, indicated that while fine sediments pass through the estuary, the bulk of the coarser sediments remain behind where they accumulate as bars and shoals in Tillamook Bay (Komar and others, 2004). Furthermore, sediments within Tillamook Bay are predominantly of a marine origin (60%), while river sediments make up 40% of the sediment in the estuary. This finding is consistent with the work of Peterson and others (1984) and Clemens and Komar (1988), who observed that because of the combination of low river discharge and high tidal regime in Oregon estuaries, the majority of the estuaries are in fact natural "sinks" for the sediment. Thus, the beaches of Oregon receive very little sediment input from rivers and streams today. Accordingly, sediment supply is essentially confined to those areas backed by coastal bluffs, particularly those areas overlain by more erosive Pleistocene marine terrace sandstones (raised ancient beach and dune sands) and more recent Holocene dune sands that drape the landscape.

Prior to the 1940s, many of the barrier spits were devoid of significant vegetation. With the introduction European beach grass (*Ammophila arenaria*) in the early 1900s and its subsequent proliferation along the Oregon coast, the grass essentially contributed to the stabilization of the dunes and barrier spits. The product today is an extensive foredune system, which consist of large "stable" dunes containing significant volumes of sand. Accompanying the stabilization of the dunes, humans have settled on them, building in the most desirable locations, typically on the most seaward foredune. As will be shown throughout this report, construction of these homes and facilities in such areas poses a significant risk as periodically storms erode into the dunes. This has resulted in many cases where the foundations of homes may be undermined, eventually requiring riprap coastal engineering structures to mitigate the erosion problem.

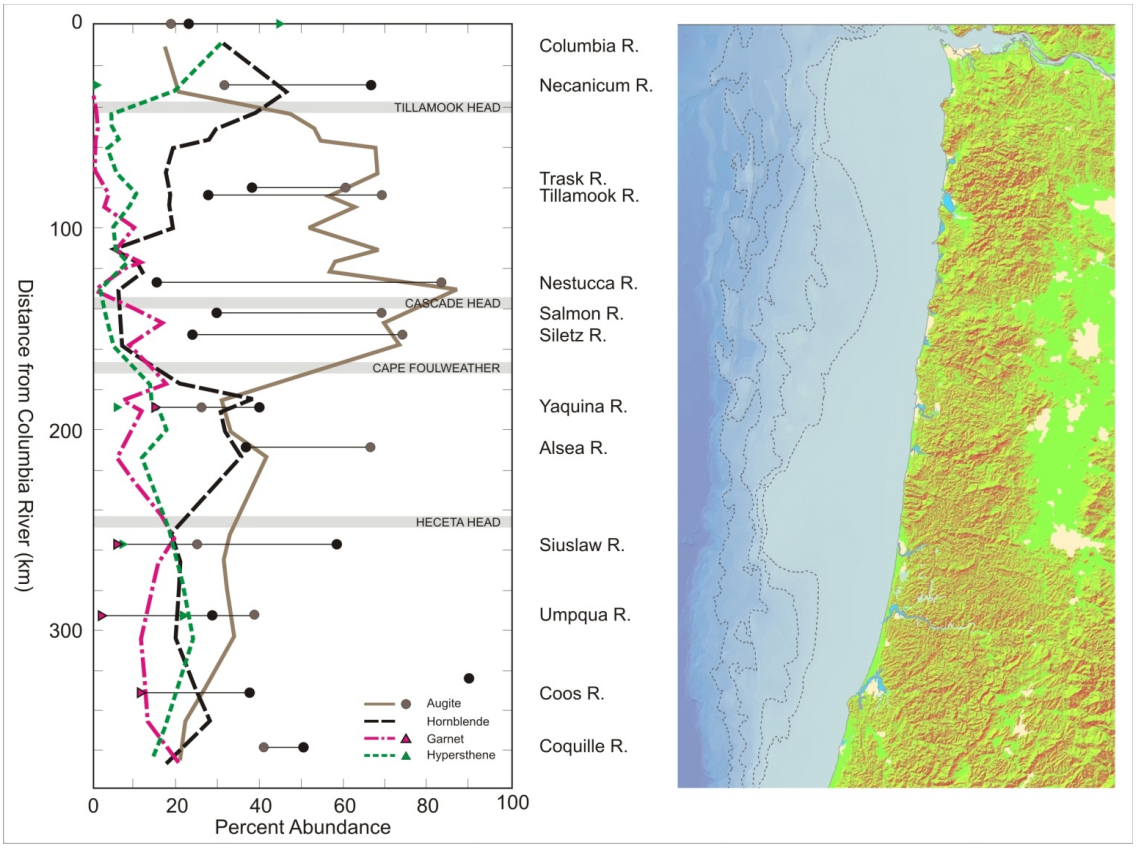

Figure 2-5. Variations in the percent abundances of various heavy minerals observed on the central to northern Oregon coast (after Clemens and Komar, 1988).

2.2 Tsunami Hazards Associated with the Cascadia Subduction Zone and from Distant Earthquake Sources

There is considerable geologic evidence from estuaries and coastal lakes along the Cascadia subduction zone that provides evidence for episodic occurrences of abrupt coastal subsidence immediately followed by significant ocean flooding associated with major tsunamis that swept across the ocean beaches and also traveled well inland through the bays and estuaries. Coastal paleoseismic records document the impacts of as many as 13 major subduction zone earthquakes and associated tsunamis over the past ~7,000 years (Witter and others, 2003; Kelsey and others, 2005; Witter and others, 2010), while recent studies of turbidite records within sediment cores collected in deep water at the heads of Cascadia submarine canyons provide evidence for at least 41 distinct tsunami events over the past ~10,000 years (Goldfinger and others, 2003; Goldfinger, 2009; Goldfinger and others, 2009). The length of time between these events varies from as short as a century to as long as 1,200 years, with the average recurrence interval for major Cascadia earthquakes (magnitude [M_W] > 9) estimated to be ~530 years (Witter and others, 2010).

The most recent Cascadia subduction zone earthquake occurred on January 26, 1700 (Satake and others, 1996; Atwater and others, 2005) and is estimated to have been a magnitude (M_W) 9 or greater based on the size of the tsunami documented along the coast of Japan. This event probably ruptured the full length (~1,200 km) of the subduction zone, based

on correlations between tsunami deposits identified at multiple sites along the length of the PNW coast.

There is now increasing recognition that great earthquakes do not necessarily result in a complete rupture of the Cascadia subduction zone (i.e., rupture along the full 1,200 km fault zone), such that partial ruptures of the plate boundary have occurred in the paleo-records due to smaller earthquakes with magnitudes (M_W) < 9 (Witter and others, 2003; Kelsey and others, 2005). These partial segment ruptures appear to occur more frequently on the southern Oregon coast, determined from paleotsunami studies (stratigraphic coring, radiocarbon dating and marine diatom analyses) undertaken at several locations on the southern Oregon coast, including Bradley Lake located just south of Bandon, the Sixes River and the Coquille estuary. According to Kelsey and others (2005), initial estimates of the recurrence intervals of Bradley Lake tsunami incursion is typically shorter (~380–400 years) than the average recurrence intervals inferred for great earthquakes (~530 years). Furthermore, they have documented from those records that local tsunamis from Cascadia earthquakes recur in clusters (~250–400 years) followed by gaps of 700–1,300 years, with the highest tsunamis associated with earthquakes occurring at the beginning and end of a cluster.

Recent analyses of the turbidite records (Goldfinger, 2009; Goldfinger and others, 2009) suggest that of the 41 events in the geologic past:

- 20 events were probably associated with a rupture of the full Cascadia subduction zone, characterized by a magnitude (M_W) ~9 or greater earthquake;
- 2-3 events reflected a partial rupture (~75%) of the length of the subduction zone, characterized by an estimated earthquake magnitude (M_W) of ~8.5–8.8 earthquake;
- 10-11 events were associated with a partial rupture (~50%), characterized by an estimated earthquake magnitude (M_W) of ~8.3–8.5 earthquake; and
- 8 events reflected a partial rupture (~25%), with an estimated earthquake magnitude (M_W) of ~7.6–8.4.

These last 19 shorter ruptures are concentrated in the southern part of the margin and have estimated recurrence intervals of ~240–320 years. Goldfinger (2009) estimated that time-independent probabilities for segmented ruptures range from 7-9% for full margin ruptures, to ~18% in 50 years for a southern segment rupture; time dependent rupture analyses indicate that the probability increases to ~25% in 50 years for the northern zone.

Aside from local tsunamis associated with the Cascadia Subduction Zone, the Oregon coast is also susceptible from tsunamis generated by distant events, particularly along the coast of Japan, along the Aleutian Island chain, and from the Gulf of Alaska. The most recent distant tsunami event occurred on March 11, 2011, when a magnitude (M_W) 9.0 earthquake occurred 129 km (80 mi) offshore from the coast of Sendai, northeast Honshu, Japan (Allan and others, 2012a). This earthquake triggered a catastrophic tsunami that within minutes inundated the northeast coast of Japan, sweeping far inland; most recent reports indicate 15,854 dead and another 3,155 missing. Measurements derived from a tide gauge on the impacted shore (Ayukawa, Ishinomaki, Miyagi Prefecture) recorded a tsunami amplitude of 7.6 m, before the gauge was destroyed by the initial tsunami wave (Yamamoto, 2011), while post-tsunami surveys indicate that the tsunami water levels within the inundation zone reached as high as 19.5 m (Mori and others, 2011). The tsunami also propagated eastward across the Pacific Ocean, impacting coastal communities in Hawaii and along the west coast of the continental United States — Washington, Oregon, and California.

Damage in Oregon, Washington, and northern California from the tsunami was almost entirely confined to harbors, including Depoe Bay, Coos Bay, Brookings in Oregon, and in Crescent City, California, having been moderated by the arrival of the tsunami's highest waves during a relatively low tide (Allan and others, 2012a). At Crescent City, an open-coast breakwater, the to-and-fro surge of the water associated with the tsunami waves overturned and sank 15 vessels and damaged 47, while several boats were swept offshore. Flood damage also occurred during the early hours of

March 12; for example, an RV park near the mouth of Elk Creek was flooded when a 1.05 m (3.4 ft) tsunami wave arrived, coinciding with high tide. The total damage to the Crescent City harbor and from the effects of the flooding has been placed at $12.5 million. At Brookings on the southern Oregon coast, 12 fishing vessels put to sea at about 6 am, prior to the arrival of the tsunami waves. However, the *Hilda*, a 220-ton fishing boat and the largest in the harbor, broke loose under the forces of the wave-induced currents, washing around the harbor and smashing into and sinking several other boats. Much of the commercial part of the harbor and about one third of the sports basin were destroyed; the total damage has been estimated at about $10 million.

Prior to the Tōhoku tsunami, the previous most significant distant tsunami occurred on March 27, 1964, when a magnitude (M_W) 9.2 earthquake occurred near Prince William Sound in Alaska, which generated a catastrophic local tsunami in Alaska, while the effects of the tsunami was also felt around the Pacific Basin. The tsunami caused significant damage to infrastructure in the coastal communities of Seaside and Cannon Beach and killed four people camping along Beverly Beach in Lincoln County.

In 2009, the Oregon Department of Geology and Mineral Industries (DOGAMI) initiated a multi-year study to accelerate remapping of the Oregon coast for tsunami inundation using state of the art computer modeling and laser based terrain mapping (lidar). The outcome of this effort was the creation of new and more accurate tsunami evacuation maps for the entire length of the coast. DOGAMI, in collaboration with researchers (Zhang and Baptista) at the Oregon Health and Science University (OHSU), Oregon State University (Goldfinger) and the Geological Survey of Canada (Wang), developed a new approach to produce a suite of next-generation tsunami hazard maps for Oregon (Priest and others, 2010; Witter and others, 2010). Modeling tsunami inundation on the southern Oregon coast was initiated late in 2009 and consisted of a range of scenarios, including 15 Cascadia events and two distant earthquake source events (e.g., 1964 Prince William Sound earthquake magnitude [M_W] 9.2 earthquake [Witter, 2008]). The last of the suite of new evacuation maps (TIM series) was released in 2013; the maps are also available in an online tsunami hazard portal (http://nvs.nanoos.org/TsunamiEvac).

Associated with great Cascadia earthquakes is a near instantaneous lowering (subsidence) of the coast by ~0.4 m (1.3 ft) to as much as 3 m (9.8 ft) (Witter and others, 2003). This process equates to raising sea level by the same amount along the entire Pacific Northwest coastline. Following the earthquake, coastal erosion is expected to accelerate everywhere as the beaches and shorelines adjusted to a new equilibrium condition that, over time, would likely decrease asymptotically (Komar and others, 1991). On the southern Oregon coast, Komar and others have suggested that the extensive development of sea stacks offshore from Bandon may be evidence for that erosion response following the last major subduction zone earthquake in 1700. Over the past century, the erosion appears to have stabilized, as there is little evidence for any progressive erosion trend. This suggests that the south coast is now being uplifted (estimated to be ~0.6 to 1.1 m) due to the Cascadia subduction zone having become locked again, such that strain is now building toward the next major earthquake. With the release of that energy and land subsidence, cliff erosion along the Bandon shore (and elsewhere on the Oregon coast) would be expected to begin again.

2.3 Coastal Geomorphology

On the basis of geology and geomorphology, the Clatsop County shoreline can be broadly divided into the following morphological beach types (**Figure 2-6** and **Figure 2-7**). These include:

1. ***Dune-backed beaches:*** Dune-backed beaches make up the bulk (54%) of the Clatsop County shoreline, much of which is associated with the Clatsop Plains. Dune-backed beaches also characterize a small section of the shore near Seaside and to the north of Ecola Creek in Cannon Beach (**Figure 2-1**). The geo-morphology of the beaches can be generalized as having wide, dissipative surf zones with low sloping foreshores that are backed by broad, high dunes containing significant sand volume (**Figure 2-6 and Figure 2-8**). Dune crest elevations are highest along the central portion of the Clatsop Plains where they reach 17.6 m (58 ft) and are generally lowest in southern Clatsop Plains. High dunes also characterize the shore on the north side of Ecola Creek in Cannon Beach (up to 18 m high). The average beach slope (tan β) for dune-backed beaches on the Clatsop Plains is 0.044 (σ = 0.010), with the lowest mean slopes occurring in the vicinity of Seaside (0.022 [σ = 0.006]).
2. ***Gravel/boulder beaches:*** At the south end of Seaside, a substantial cobble/boulder beach abuts against Tillamook Head, where they form prominent, steep natural barriers to wave erosion (**Figure 2-9**). Crest elevations of the cobble/boulder beach reach 7.6 m and exhibit a mean slope of 0.184 (σ = 0.022). Considerable flotsam exists along its crest, indicating that this stretch of shore is subject to periodic wave overtopping (**Figure 2-9**).

Cliffed shore: Cliffed shores make up the third largest (17.8%) geomorphic "type" in the county (**Figure 2-6** and **Figure 2-7**). Examples of this type of shore exist around Tillamook Head (**Figure 2-2**), and along discrete sections of the shore to the south of Cannon Beach. This particular shore type may be fronted by either prominent cobble/boulder beaches (e.g., Tillamook Head) or wide dissipative sand beaches, backed with a veneer of gravel (e.g., Arcadia Beach).

3. ***Bluff-backed beaches:*** Bluff-backed beaches are the second most prominent geomorphic type in Clatsop County comprising approximately 22.5% of the shore (**Figure 2-7**). This particular beach type dominates the shoreline south of Cannon Beach (**Figure 2-3**, **Figure 2-4**, **Figure 2-10**). The bluffs that back the beaches vary in height from ~7 m (23 ft) to greater than 40 m (131 ft). Beach slopes (tan β) seaward of the bluffs are similar to those observed on the Clatsop Plains, averaging about 0.046 (σ = 0.040). Geomorphically, these beaches may be characterized as "composite" using the terminology of Jennings and Shulmeister (2002), such that the beaches consist of a wide dissipative sandy beach, backed by a steeper upper foreshore composed of gravels. In addition, several of the bluff-backed sections are characterized by well-vegetated faces, indicating that they have not been subject to significant wave erosion processes along the toe of the bluffs during the late twentieth century.
5. ***Cobble berm backed by bluffs:*** Finally, an extensive cobble berm fronts moderately high bluffs in Falcon Cove at the south end of the county. Similar to the bluff-backed beaches to its north, this particular beach type is also characterized as of the "composite" type and is one of the most substantial of its type on the Oregon coast. Although it is fronted by a wide, dissipative sand beach, much of this is presently located below water and is mostly visible near low tide. However, prior to the storms of the late 1990s, the sand beach at Falcon Cove was more substantial and its loss is likely due to the removal of sand during the 1997-98 El Niño to the north around Arch Cape and into the Cannon Beach littoral cell.

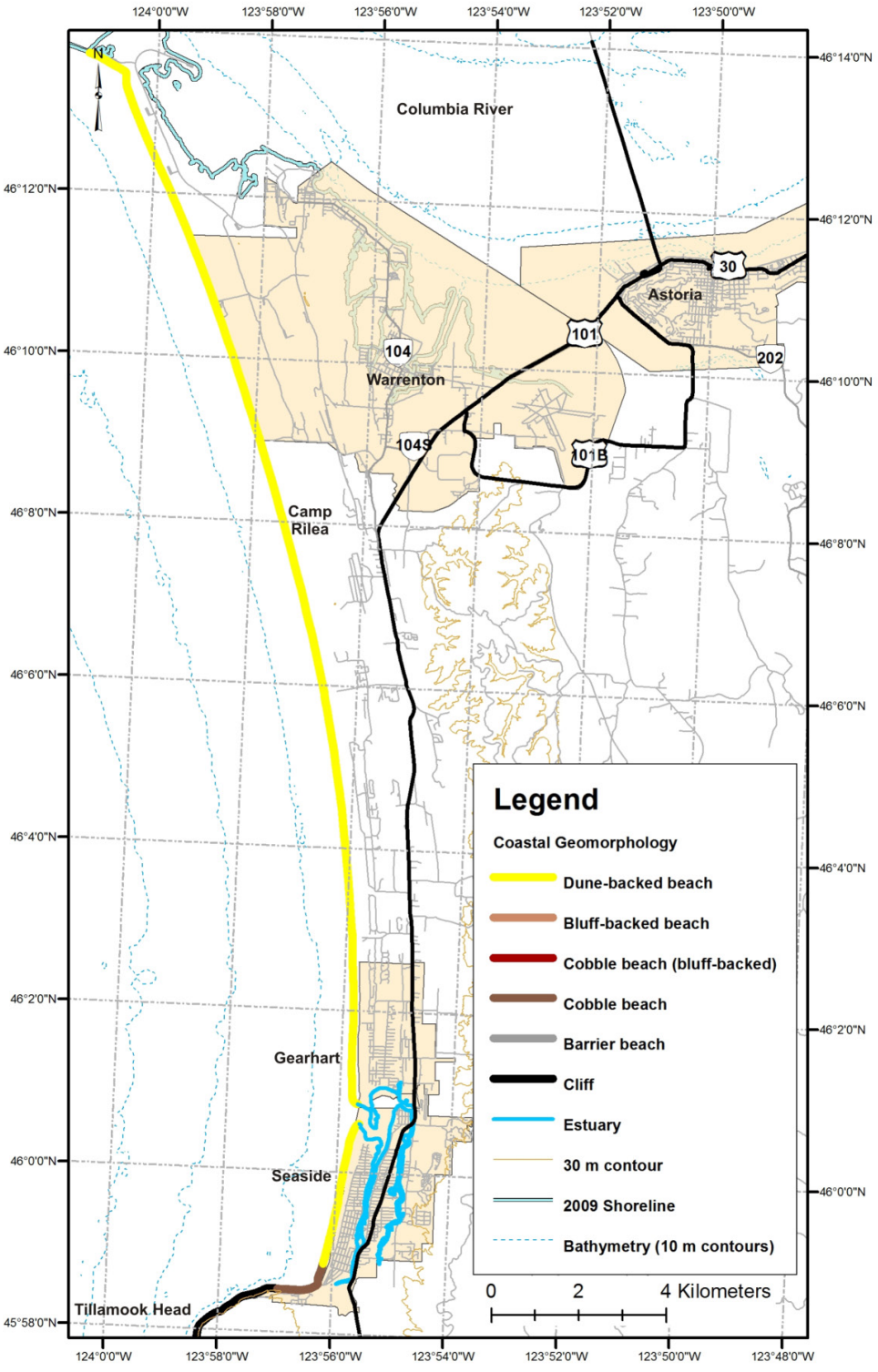

Figure 2-6. Geomorphic classification of the northern Clatsop County shoreline (Tillamook Head to the Columbia River).

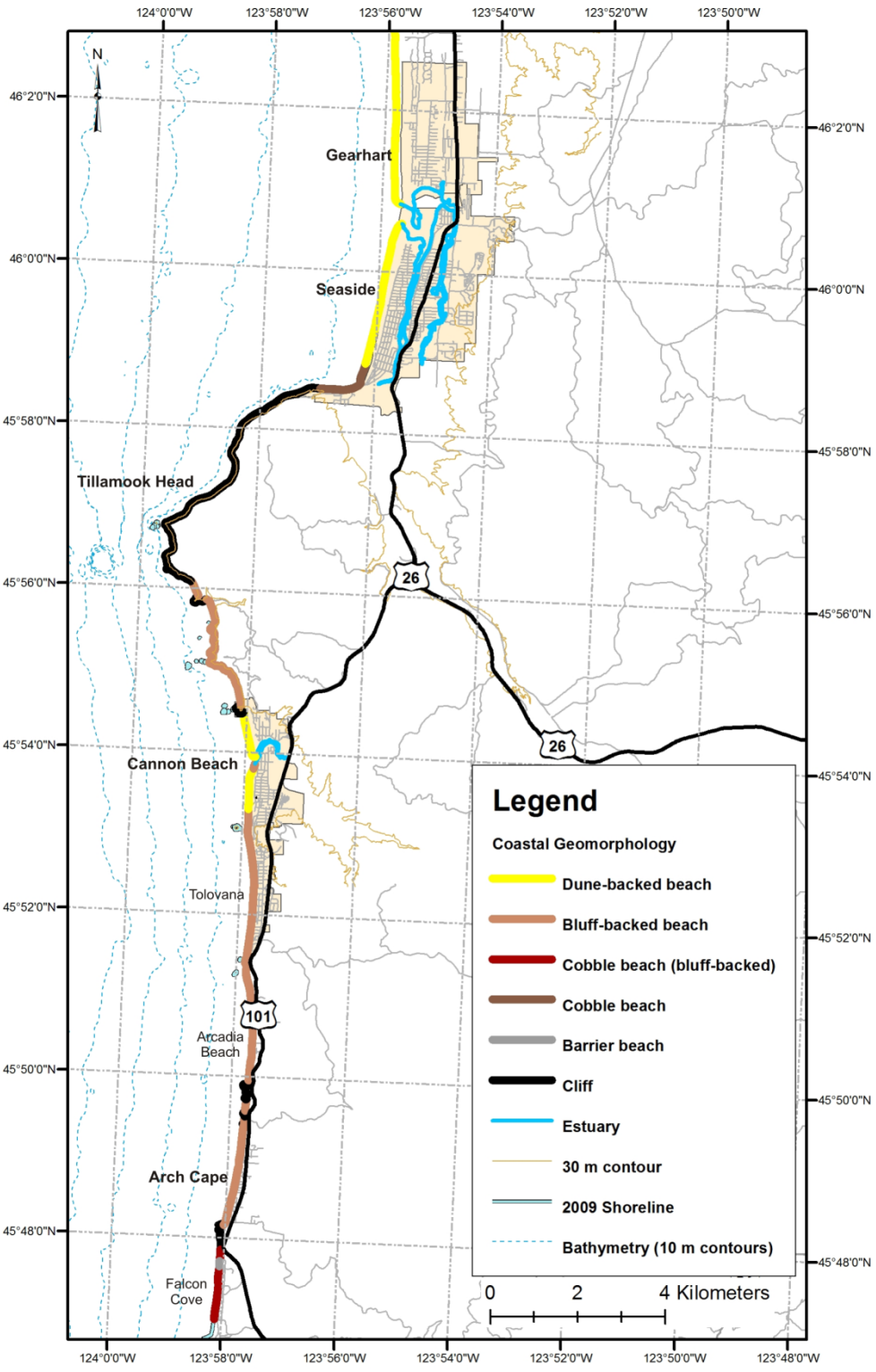

Figure 2-7. Geomorphic classification of the southern Clatsop County shoreline (Cape Falcon to Seaside).

Figure 2-8. The Clatsop Plains reflect a broad, progradational, dune sequence that rapidly advanced seaward following construction of the south Columbia River jetty. The beaches are wide, dissipative, and backed by a prominent primary frontal dune (photo: E. Harris, DOGAMI, 2011).

Figure 2-9. An extensive cobble/boulder berm at the south end of Seaside provides significant protection to properties built landward of it. Nevertheless, flotsam along the crest of the cobble berm indicates that this beach is periodically overtopped (photo: J. Allan, DOGAMI, 2010).

Figure 2-10. Bluff-backed beach in southern Cannon Beach formed in late Pleistocene coastal terrace deposits. Note the low-sloping beach in front of the bluffs that serve to dissipate the wave runup (photo: J. Allan, DOGAMI, 2010).

2.4 Coastal Erosion and Flood History

2.4.1 Clatsop Plains

The Clatsop Plains are an arcuate shaped coastline that extends from Tillamook Head in the south to the mouth of the Columbia River (MCR) (**Figure 2-6**). The plains form part of a smaller subcell (34 km in length) located within the much larger Columbia River littoral cell (CRLC), a 165-km coastal system that extends from Tillamook Head, Oregon, to Point Grenville, Washington. The Clatsop Plains coastline is characterized by wide, dissipative, surf zones and prominent longshore bars in the nearshore, while the beaches are backed by an extensive dune sequence (Cooper, 1958; Woxell, 1998). The frontal foredunes that immediately back the beaches range in height from ~8 m to over 16 m. These dunes increase in height from Seaside to Kyle Lake, and then decrease in height toward Clatsop Spit (Ruggiero and Voigt, 2000). The beaches are gently sloping (mean slope (tan β) of 0.032, ± 0.007), and have a somewhat lower beach slope when compared with slopes identified along the Tillamook County coastline (Allan and Priest, 2001).

For the past few thousand years, the shorelines of the CRLC, including the Clatsop Plains, have accreted, causing the coastline to prograde seaward by a few hundred to several thousand meters. This process is thought to have begun around 4,000 years ago, as the rate of sea-level rise slowed (Woxell, 1998). Woxell (1998) estimated that the Clatsop Plains historically accreted at an average rate of 0.7 m/yr (2.3 ft/yr) from about 4000 years BP to AD 1700. Between 1700 and 1885, accretion rates along the Clatsop Plains fell slightly to around 0.5 m/yr (1.6 ft/yr).

The year 1885 is significant because this was when construction of the south jetty was initiated, and the coastline began to prograde seaward by hundreds of meters. These changes were not constant, varying in

response to different phases of jetty construction, including the construction of the north jetty, and their subsequent maintenance and modification (Lockett, 1963). Following construction of the south jetty in 1902, Clatsop Spit grew northwards by about 4.6 km (2.9 mi) during a period of 50 years (**Figure 2-11**). A likely source of the sand that accumulated along Clatsop Spit was due to changes in the Columbia River inlet, which resulted in the development of shoals along the north side of the south jetty, and possibly from erosion of the mid-continental shelf region offshore from the Clatsop Plains (Lockett, 1963; Sherwood and others, 1990). Analyses by Gelfenbaum and others (2001) indicated that between the 1870s and 1926 the mid-continental shelf region and the inlet mouth lost about 364 million m^3 (476 million yd^3) of sand (**Figure 2-12**). Between the late 1800s and early 1920s, accretion rates along the Clatsop Plains have ranged from 2.0 to 5.8 m/yr (6.6 to 19 ft/yr), with an average rate of 3.3 m/yr (10.8 ft/yr), with the highest accretion rates identified near the MCR (Woxell, 1998).

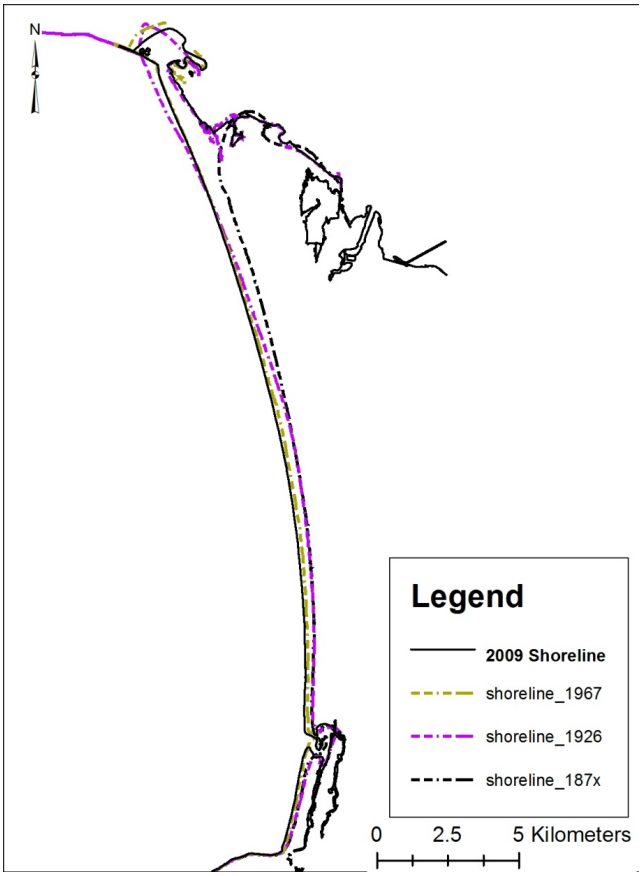

Figure 2-11. Clatsop Plains shoreline changes (1800s to 2009). Note the extent of shoreline progradation along the southern two-thirds of the coast, while the northern 4 km has been eroding since the late 1920s. Historical shorelines were derived from the Southwest Washington Coastal Erosion Study (Gelfenbaum and Kaminsky, 2002).

Since the mid 1920s the rate of coastal advance has slowed along the Clatsop Plains, while erosion has been the dominant shoreline response along the northern 4km of Clatsop Spit (**Figure 2-11**). For example, the northern end of Clatsop Spit eroded by some 200 to 250 m (650 to 820 ft) between 1926 and the 1950s. This response is probably related to ongoing erosion of the mid-continental shelf region

offshore from Clatsop Spit throughout this period (**Figure 2-13**); the product of reduced sand supplies from the Columbia River and possible dredging and disposal practices that commenced in the river. Furthermore, it is also likely that modifications made to the jetties during the 1930s may also account for some of the shoreline erosion. In contrast, the central part of the Clatsop Plains prograded significantly (total accumulation of 60 million m^3 (78 million cubic yards) of sand) throughout this period. The pattern of erosion and deposition identified adjacent to the mouth of the Columbia River (**Figure 2-13**), indicate that much of the eroded sand was displaced either seaward or to the north (Lockett, 1963; Sherwood and others, 1990; Gelfenbaum and others, 2001). In particular, the erosion of the outer tidal area has provided a large amount of sediment to the littoral system north of the Columbia River, which contributed to significant beach accretion along Long Beach and sedimentation in Willapa Bay. However, as noted by Sherwood and others (1990), the effects of this large sediment input may now be wearing off.

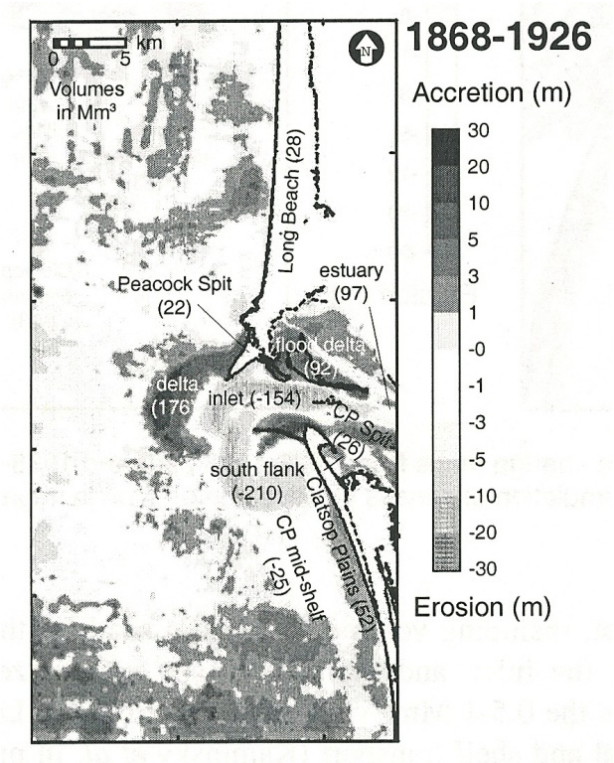

Figure 2-12. Estimated sand volume changes identified adjacent to the Columbia River for the period 1868 –1926 (Gelfenbaum and others, 2001). Note: Volume estimates are in millions of cubic meters (Mm^3).

Since the 1950s erosion of the spit appears to have stabilized somewhat. However, recent analyses using lidar, aerial photography, and beach surveys indicate that the central and northern Clatsop Plains continue to experience some erosion, while accretion dominates the southern end of the cell (Ruggiero and Voigt, 2000; Allan and Hart, 2008). Because of ongoing erosion offshore from Clatsop Spit and erosion adjacent to the spit tip, the U.S. Army Corps of Engineers (USACE) is now concerned that part of the south jetty may eventually be undermined through toe erosion. In addition, because the northern tip of Clatsop Spit is only 380–700 m (1,200–2,300 ft) wide, there are also concerns that this section of the spit could be breached, which would result in the formation of a second river mouth.

To better understand the changes taking place within the CRLC, the Washington Department of Ecology (WDoE) and the U.S. Geological Survey (USGS) initiated a joint study, the Southwest Washington Coastal Erosion Study (SWCES), to examine the causes of erosion hotspots that had begun to appear along the CRLC. As part of this effort, the WDoE and the USGS developed and implemented a beach-monitoring program along the full length of the CRLC. Within the Clatsop Plains subcell, six beach monitoring sites were established in 1997 and have been surveyed on a seasonal basis since their inception. In 2005, a "technology transfer" was implemented between the WDoE and DOGAMI staff that resulted in DOGAMI staff taking over the monitoring of the Clatsop beach profile sites (http://nvs.nanoos.org/BeachMapping). Analyses of these data indicate continued aggradation in the dunes, along the bulk of the shoreline, while the northern tip continues to experience erosion, particularly adjacent to the south jetty.

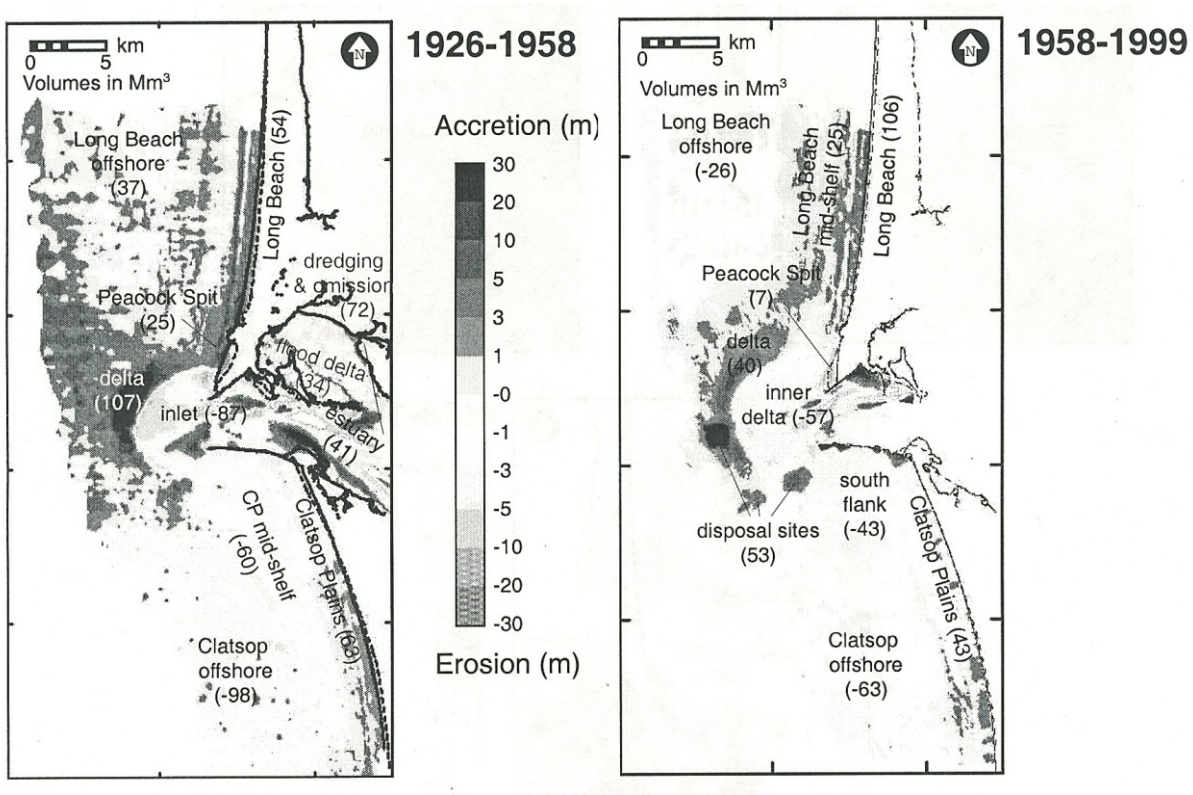

Figure 2-13. Estimated sand volume changes identified adjacent to the Columbia River for the periods 1926–1958 and 1958–1997 (Gelfenbaum and others, 2001). Note: Volume estimates are in millions of cubic meters (Mm^3).

2.4.2 Seaside

Prior to the 1920s, much of the Seaside shoreline consisted of a composite beach comprising a steep, gravel barrier berm fronted by a sandy beach, which extended as far north as about 18th Avenue near the mouth of the Necanicum estuary (Leach, 1989). Today, however, the beach reflects a wide, dissipative beach system. Importantly, the active beach foreshore today is now located some 110 to 190 m farther seaward from its position in the late 1930s, but now backed by low dunes (particularly in the south and north) or the Seaside promenade (a seawall), which runs along much of the shore.

Shoreline changes in the town of Seaside are provided in **Figure 2-14**. For the purposes of this study, we have extrapolated a variety of shorelines, including NOS topographic "T" sheets (primarily 1920s era), aerial photographs (1939, 1967, and 1995–2009), and tidal (MHHW) datum-based shorelines from lidar data. Detailed reviews of shoreline mapping techniques, including the use of NOS T-sheets and aerial photographs, are given by Anders and Byrnes (1991), Gorman and others (1998), Moore (2000) and Allan and others (2003). The 1939 photos have been rubbersheeted in Esri® ArcGIS® so that they can be compared with more recent orthorectified images of the area. (The process by which an historical aerial photograph can be distorted to allow it to be seamlessly joined to an adjacent geographic layer of matching imagery, such as an orthorectified aerial photograph. The rubbersheeting process uses common ground control points (GCPs) evident in both photographs to perform the distortion.) In addition, we have typically derived two shorelines: a wet/dry sand line used when comparing shorelines derived from NOS "T" sheets, orthorectified aerial photos and tidal datum-based shorelines, and a vegetation line that can be compared with 1967 and 2009 orthorectified aerial photos of the coast.

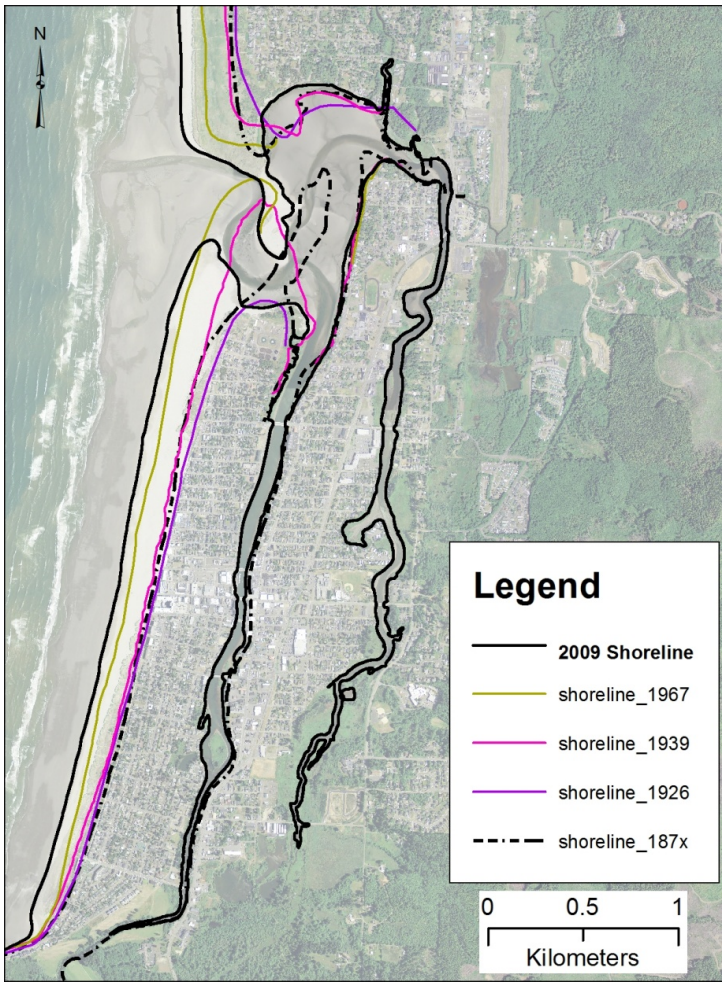

Figure 2-14. Historical shoreline changes at Seaside (1800s to 2009).

Evident from the figure is that the beach has been steadily accreting since the early 1920s, much of which is now dominated by a wide, dissipative, sand beach. As noted above, this response is related to large-scale sediment adjustments that have taken place around the mouth of the Columbia River and offshore from the Clatsop Plains following jetty construction. Included in **Figure 2-14** is a shoreline derived from 1939 aerial photographs flown by the USACE following a major storm in January 1939; this event has been previously described as a 75-year event (FEMA, 2010). Analyses of these data indicate that the beach at the time was significantly narrower, such that the high water line was within about 30–40 m (98–130 ft) from the Seaside promenade, which tracks along the western edge of the town. The promenade was built in 1921 and has proved highly effective, with no reports of damage to the adjacent infrastructure, seawall, or as a result of overtopping (Leach, 1989). Today, the promenade in the south and north is located as much as 140 m from the active beach. However, midway along the promenade beach sand is actively transported landward by Aeolian processes where it piles up on the backshore and against the promenade (**Figure 2-15**). In response, the city of Seaside now implements a dune management program such that the developing dunes are periodically lowered in order to maintain views to the ocean. Finally, there is no evidence of the promenade having been impacted by waves in recent decades, which is largely a function of the width of the beach today and the growth of dunes along much of the shore.

Figure 2-15. The Seaside promenade that runs parallel to the ocean and the "turnaround" near mid photo. Periodic beach and dune grading occurs just north of Turnaround in order to mitigate sand aggradation adjacent to the promenade and in order to retain vistas of the ocean (photo: E. Harris, DOGAMI, 2011).

An extensive cobble and boulder beach dominates the shore around Tillamook Head, and along the southern portion of the beach at Seaside. The Seaside gravel beach forms an "L" shape, trending north-south at Seaside and east-west on the south flank of Tillamook Head. In this region there is evidence for several older beach deposits, demonstrating the occurrence of previous aggradational phases that is related to influxes of sediment in response to landslides along the northern flank of Tillamook Head (Allan and others, 2005). This section of the coast is stable, although it is periodically overtopped during major storms, evident by the presence of drift logs along the crest of the cobble berm.

Finally, **Figure 2-14** also highlights the variability at the mouth of the Necanicum estuary, which has fluctuated to the north and south by about 900 m. These changes are largely a function of variations in the prevailing wave climate, alongshore sediment transport processes and as a result of riverine discharge. Of interest, although the barrier spit tip on both sides of the estuary have eroded and shifted considerably over the years, the eastern shoreline within the lower estuary has experience relatively little erosion.

2.4.3 Cannon Beach

Major coastal storms battered the Cannon Beach area on January 3, 1939, December 2 and 3, 1967, February 18, 1976, and most recently in January 1983 and February 1986 (FEMA, 2010). These storms have resulted in significant ocean flooding at times, the product of flooding associated with Ecola Creek, coupled with high tides, locally induced surges and large waves. The latter processes serve to cause Ecola Creek to back up, which leads to flooding in low-lying areas adjacent to the town, including the sanitary facilities located within the flood plain (**Figure 2-16**). For example, a particularly significant flood on December 2-3, 1967, resulted in water ponding to an elevation of 3.5 m (11.5 ft), a depth of 0.76 m (2.5 ft) above the street surface, at the intersection of 2nd and Hemlock Streets, the center of the city's business district (FEMA 2010). Approximately 35 stores and business establishments, several public buildings, the conference complex, and three residential properties were flooded. Water and sanitary facilities were damaged, creating a health hazard. Similar, but less severe, flooding has occurred three other times in the last 20 years.

Figure 2-16. Oblique view looking east over downtown Cannon Beach toward the sanitary ponds (photo: E. Harris, DOGAMI, 2011).

Analyses of the shoreline variability along the Cannon Beach shore indicates no predominant trends of erosion immediately south of Ecola Creek, while the beach north of the creek has prograded seaward by 40–60 m since 1967, enabling large dunes to form at the back of the beach (**Figure 2-16** and **Figure 2-17**). This is most evident when comparing the location of the main vegetation line in 1939, 1967 and most recently in 2009. Farther south near Tolovana Park, similar efforts to identify the vegetation line in 1939 and 1967 indicate that much of this shore has remained relatively stable, having experience minimal change (erosion or accretion) over the years, and particularly since the late 1960s.

Nevertheless, despite any obvious trends and patterns in shoreline response south of Ecola Creek, it is clearly evident that this beach has periodically been affected by major storms. Evidence for this include the presence of numerous coastal engineering structures, including riprap (the most common structure), followed by a few concrete seawalls, and wooden bulkheads. For example, a substantial wooden bulk-

head has been constructed along 270 m of the shore fronting downtown Cannon Beach (between 2nd and 3rd Street), while a major seawall built after the January 1939 storm is located in front of the Ecola Inn (**Figure 2-18**). Analysis of the permit record held by the Oregon State Parks and Recreation Department, who manages the public beach, indicates that many of the smaller riprap structure were constructed in the early 1970s (~73-74) and following the 1982-83 El Niño. Of interest, however, very few structures were constructed after the major 1997-98 El Niño (second strongest on record) and in particular following the extreme 1998-99 winter, which generated the equivalent of four 100-year storms in the space of two months (Allan and Komar, 2002).

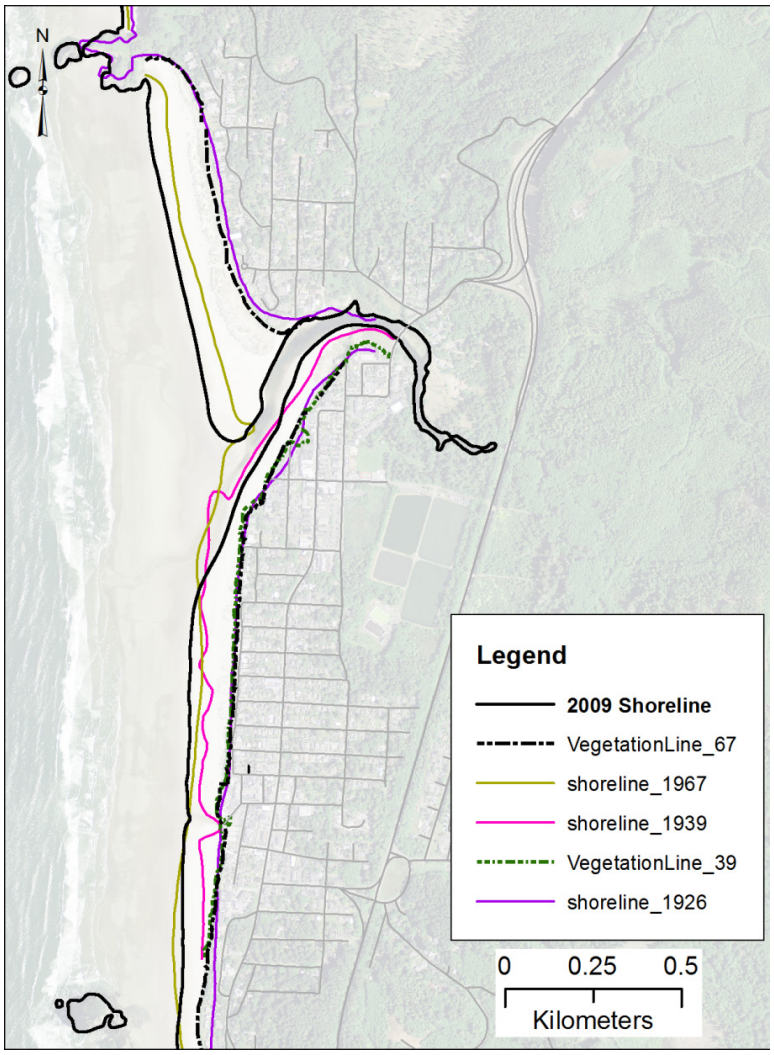

Figure 2-17. Historical shoreline changes at Cannon Beach (1926–2009).

Figure 2-18. A seawall constructed in front of the Ecola Inn in Cannon Beach. The wall was built following the January 3, 1939, storm (photo: J. Allan, DOGAMI, 2010).

2.4.4 Arch Cape

Shoreline changes in the Arch Cape subcell are broadly similar to those observed along the Cannon Beach shore. **Figure 2-19** documents various responses from 1928 to the presence. As can be seen from **Figure 2-19** the shoreline in 1939 and 1967 track farther seaward of its position in 2009. This would imply that the shore is actively eroding. However, in reality this simply highlights the strong seasonal excursions that PNW beaches are subject to, which can be as much as 20–30 m (65–100 ft), and even greater during an El Niño climate event. Hence, a better measure of long-term changes is to assess changes taking place on the backshore. **Figure 2-18** includes vegetation lines determined from 1939 and 1967 photos, overlaid on a 2009 aerial photograph. In general, the southern half of the Arch Cape subcell indicates little long-term evidence for erosion or accretion, with vegetation lines in 1939, 1967 and 2009 tracking very close to each other (**Figure 2-19** and **Figure 2-20**). However, in the northern half of Arch Cape there is some suggestion that this section has been slowly eroding landward, with most of the change having taken place between 1939 and 1967. Estimated rates of erosion are low ~0.03 – 0.1 m, with the calculated photo errors (uncertainty) producing numbers as large as the rates themselves, reinforcing the fact that the long-term change is slow. Regardless, it is interesting to note that the bulk of the existing coastal engineering present in the Arch Cape subcell is located in the northern third of the shore (**Figure 2-21**). Furthermore, the majority of these were constructed in the early 1980s, with a few having been built in the late 1970s.

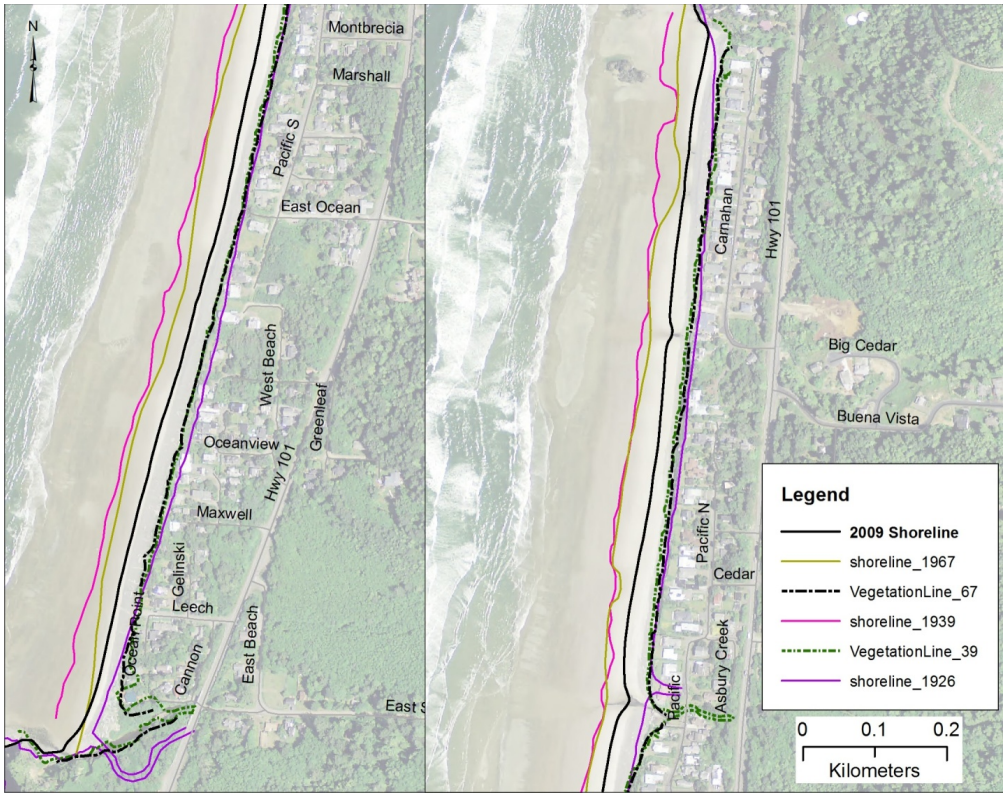

Figure 2-19. Historical shoreline changes at Arch Cape (1926–2009).

Figure 2-20. Viewing look north at Arch Cape. The entire beach is backed by a prominent gravel berm containing shingle to cobble size particles and is further backed by low bluffs. The bluff faces exhibit few signs of recent erosion, evident by the well-vegetated bluff face. Note the prominent seawall (mid-photo) constructed to protect one particular home (photo: E. Harris, DOGAMI, 2010).

Figure 2-21. Coastal engineering in the Arch Cape subcell. Top) view looking north in Arch Cape highlighting a low wooden bulkhead and seawall constructed along the toe of a bluff formed in marine terrace deposits. Bottom) View south showing a riprap structure fronted by a prominent gravel berm in the north end of Arch Cape (photo: J. Allan, DOGAMI, 2010).

2.4.5 Falcon Cove

By far the highest erosion rates observed along the Clatsop County shore occur in Falcon Cove, located between Cape Falcon and Arch Cape at the very south end of the county. More than 65 percent of coastal bluffs backing Cove Beach show evidence of active or prehistoric mass movement (Witter and others, 2009). Deposits that comprise these bluffs are inferred to reflect mostly late Pleistocene to Holocene colluviums that are easily eroded. As noted previously, the coastal geomorphology reflects a wide dissipative sandy beach backed by a prominent cobble berm and bluffs.

Figure 2-22 documents the shoreline history in Falcon Cove. An attempt was made to rubbersheet a single 1939 photo at the south end of the pocket beach, the results of which are included in the figure. While suitable ground-control points could be identified in the southern half of the photo, the northern half lacked sufficient points. Hence, vegetation results derived from the 1939 photo likely contain higher errors compared with other Clatsop County sites to the north. In general, erosion rates in the southern half of Falcon Cove have ranged from about 0.1 m to 0.4 m since 1967. If we include results from the 1939, these numbers effectively double for a number of sites.

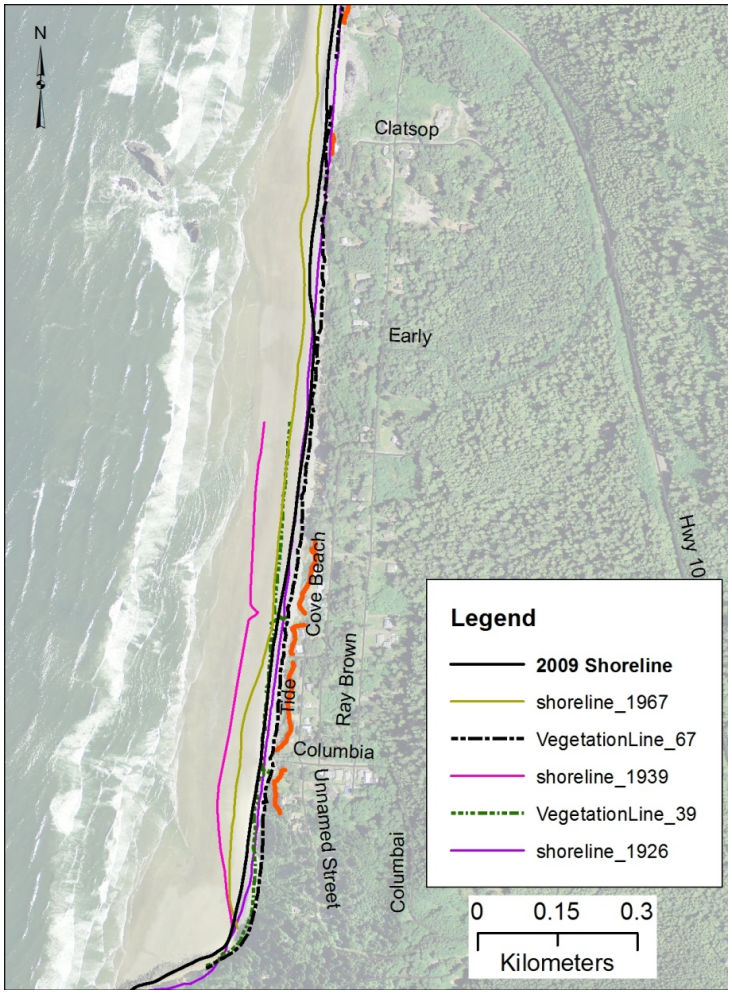

Figure 2-22. Historical shoreline changes at Falcon Cove (1926–2009). Bold red line denotes problem sites where bluffs are actively eroding and homes are either already affected or could be affected soon.

3.0 BEACH AND BLUFF MORPHOLOGY ASSESSMENTS

Field surveys were undertaken during the 2010/11 winter along several sections of the Clatsop County coastline, including the Clatsop Plains, Seaside, Cannon Beach, Tolovana Park, Arcadia beach, Arch Cape, and Falcon Cove beaches. These surveys serve two important objectives:

1. To establish beach profile transects along discrete but representative sections of the shoreline's geomorphology/geology, including sections of coast where coastal engineering structures have been constructed, for the purposes of coastal hydraulic analyses.
2. To provide representative measurements of the beach in its most eroded state (i.e., most eroded winter profile) whether it be derived from lidar or Global Positioning System (GPS) data, in order to define the morphology, elevations, and slope of the beach face for use in subsequent wave runup and over-toping computations.

Surveying along the Clatsop Plains was initially carried out in September 2010, and most recently in February 2011. In both cases, the surveys were completed late in the winter season when Oregon beaches are typically in their most eroded state (Aguilar-Tunon and Komar, 1978; Komar, 1997; Allan and Komar, 2002; Allan and Hart, 2008). A total of 85 beach profile transects were established along the length of Clatsop County (**Figure 3-1** and **Figure 3-2**) and can be subdivided according to the following sites:

- the Clatsop Plains: 14 sites;
- Seaside: 17 sites;
- Cannon Beach: 17 sites;
- Arcadia Beach: 3 sites;
- Arch Cape: 10 sites; and
- Falcon Cove: 6 sites.

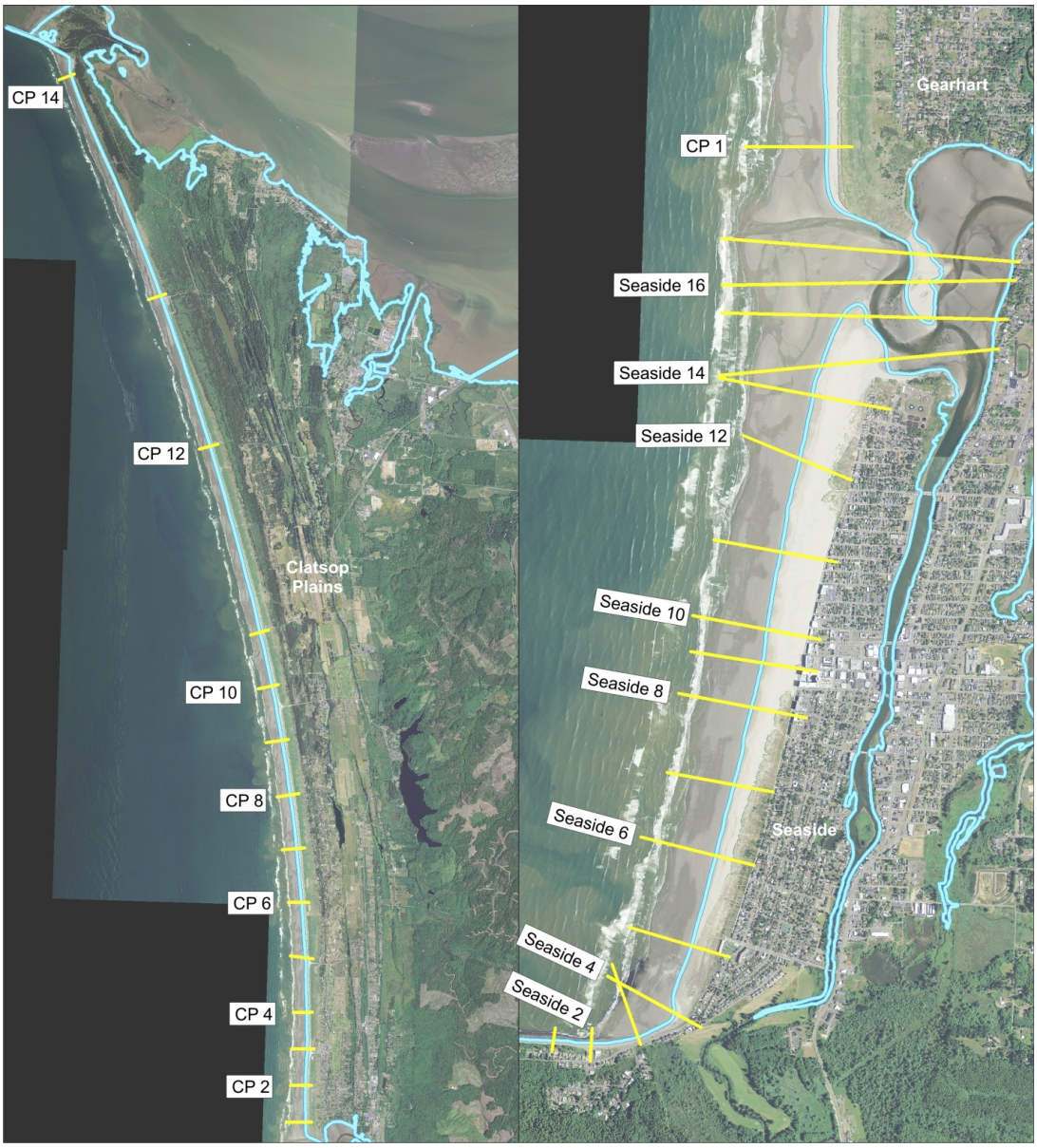

Figure 3-1. Location map of beach profiles measured along the Clatsop Plains and adjacent to Gearhart (left) and at Seaside (right) in Clatsop County.

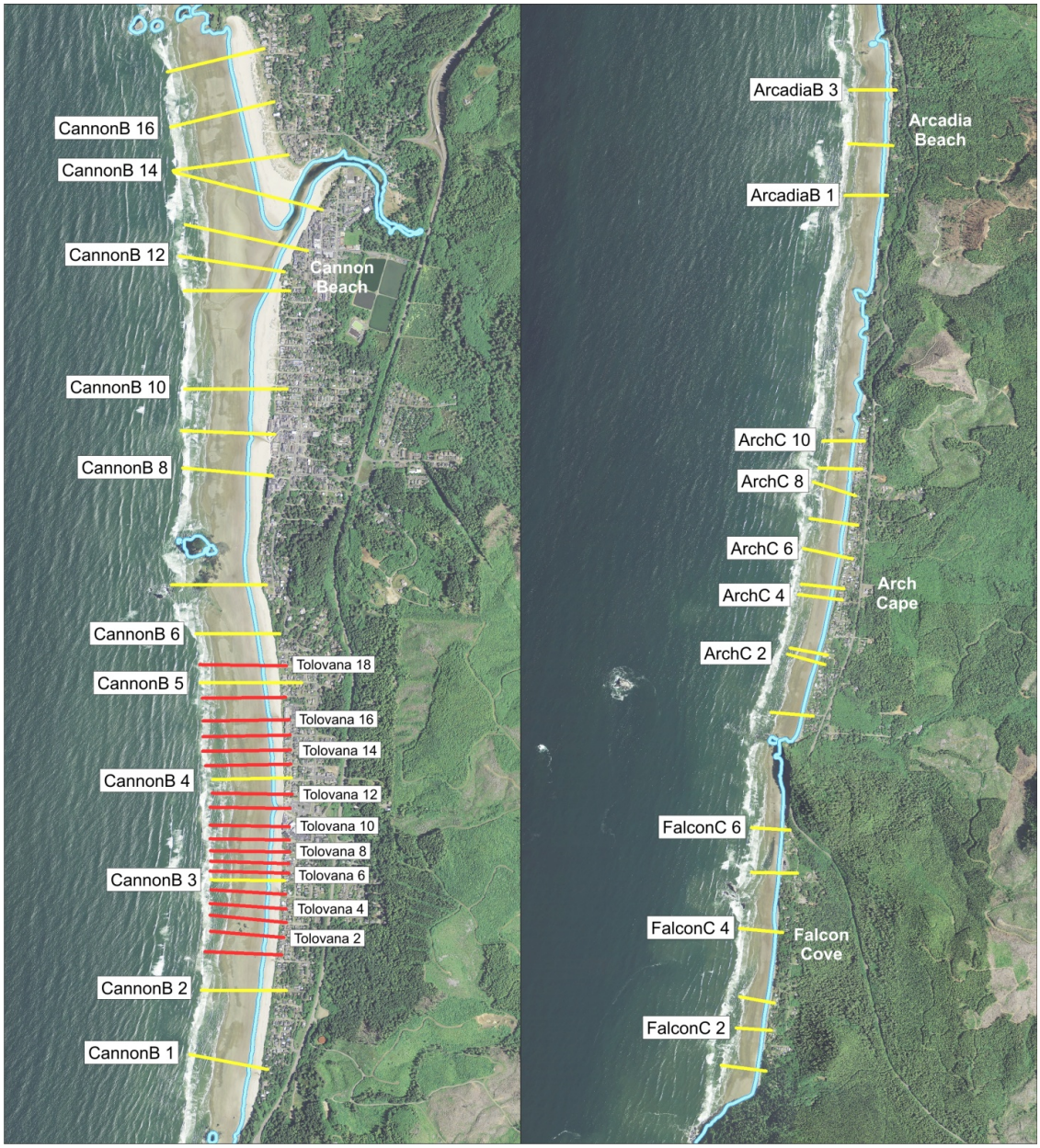

Figure 3-2. Location map of beach profiles measured at Cannon Beach (yellow) and near Tolovana Park (red) (left) and at Arcadia Beach, Arch Cape, and Falcon Cove (right) in Clatsop County.

3.1 Survey Methodology

Beach profiles that are orientated perpendicular to the shoreline can be surveyed using a variety of approaches, including a simple graduated rod and chain, surveying level and staff, Total Station theodolite and reflective prism, Light Detection and Ranging (lidar) airborne altimetry, and Real-Time Kinematic Differential Global Positioning System (RTK-DGPS) technology. Traditional techniques such as leveling instruments and Total Stations are capable of providing accurate representations of the morphology of a beach but are demanding in terms of time and effort. At the other end of the spectrum, high-resolution topographic surveys of the beach derived from lidar are ideal for capturing the three-dimensional state of the beach over an extended length of coast within a matter of hours; other forms of lidar technology are now being used to measure nearshore bathymetry out to moderate depths, but are dependent on water clarity. However, lidar technology remains expensive and is impractical along small segments of shore and, more importantly, the high cost effectively limits the temporal resolution of the surveys and hence the ability of the end-user to understand short-term changes in beach morphology (Bernstein and others, 2003).

Within this range of technologies, the application of RTK-DGPS for surveying the morphology of both the subaerial and subaqueous portions of the beach has effectively become the accepted standard (Morton and others, 1993; Ruggiero and Voigt, 2000; Bernstein and others, 2003; Ruggiero and others, 2005), and has been the surveying technique used in this study. The GPS is a worldwide radio-navigation system formed from a constellation of 24 satellites and their ground stations, originally developed by the U.S. Department of Defense; in 2007 the Russian Government made their GLONASS satellite network available increasing the number of satellites to ~46 (as of February 2011). In its simplest form, GPS can be thought of as triangulation with the GPS satellites acting as reference points, enabling users to calculate their position to within several meters (e.g., using inexpensive off the shelf hand-held units), while survey grade GPS units are capable of providing positional and elevation measurements that are accurate to a centimeter. At least four satellites are needed mathematically to determine an exact position, although more satellites are generally available. The process is complicated because all GPS receivers are subject to error, which can significantly degrade the accuracy of the derived position. These errors include the GPS satellite orbit and clock drift plus signal delays caused by the atmosphere and ionosphere and multipath effects (where the signals bounce off features and create a poor signal). For example, hand-held autonomous receivers have positional accuracies that are typically less than about 10 m (<~30 ft), but can be improved to less than 5 m (<~15 ft) using the Wide Area Augmentation System (WAAS). This latter system is essentially a form of differential correction that accounts for the above errors, which is then broadcast through one of two geostationary satellites to WAAS enabled GPS receivers.

Greater survey accuracies are achieved with differential GPS (DGPS) using two or more GPS receivers to simultaneously track the same satellites enabling comparisons to be made between two sets of observations. One receiver is typically located over a known reference point and the position of an unknown point is determined relative to that reference point. With the more sophisticated 24-channel dual-frequency RTK-DGPS receivers, positional accuracies can be improved to the sub-centimeter level when operating in static mode and to within a few centimeters when in RTK mode (i.e., as the rover GPS is moved about). In this study we used Trimble® 24-channel dual-frequency R7/R8 and 5700/5800 GPS receivers. This system consists of a GPS base station (R7 and/or 5700 unit), Zephyr Geodetic antenna (model 2), HPB450 radio modem, and R8 (and/or 5800) "rover" GPS (**Figure 3-3**). Trimble reports that both the R7/R8 and 5700/5800 GPS systems have horizontal errors of approximately ±1 cm + 1 ppm (parts per million × the baseline length) and ±2 cm in the vertical (Trimble, 2005).

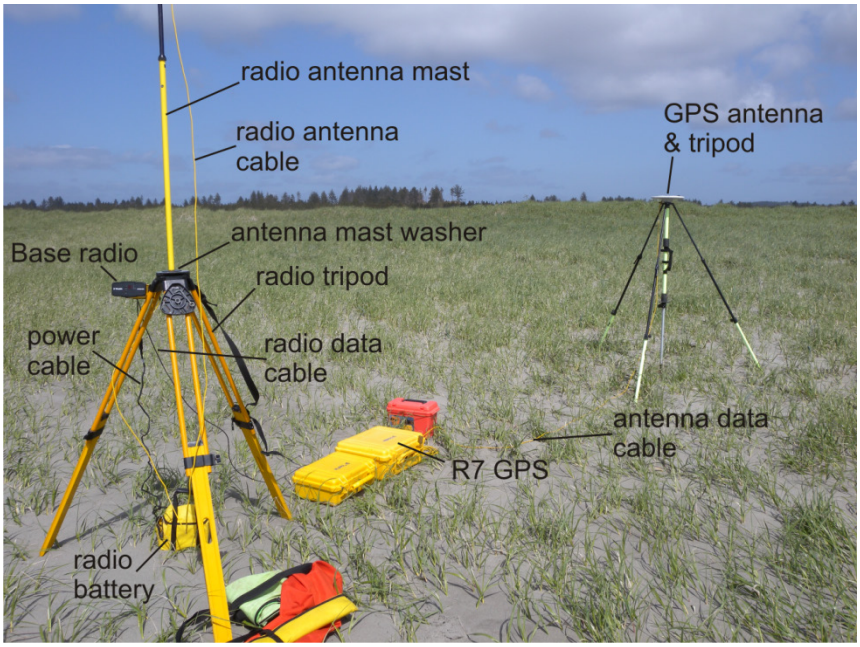

Figure 3-3. The Trimble R7 base station antenna in operation on the Clatsop Plains. Corrected GPS position and elevation information is then transmitted by an HPB450 Pacific Crest radio to the R8 GPS rover unit.

To convert a space-based positioning system to a ground-based local grid coordinate system, a precise mathematical transformation is necessary. While some of these adjustments are accomplished by specifying the map projection, datum and geoid model prior to commencing a field survey, an additional transformation is necessary whereby the GPS measurements are tied to known ground control points (**Figure 3-4**). This latter step is called a GPS site calibration, such that the GPS measurements are calibrated to ground control points with known vertical and horizontal coordinates using a rigorous least-squares adjustments procedure. Performing the calibration is initially undertaken in the field using the Trimble TSC2 GPS controller and then re-evaluated in the office using Trimble Business Office software (v2.5).

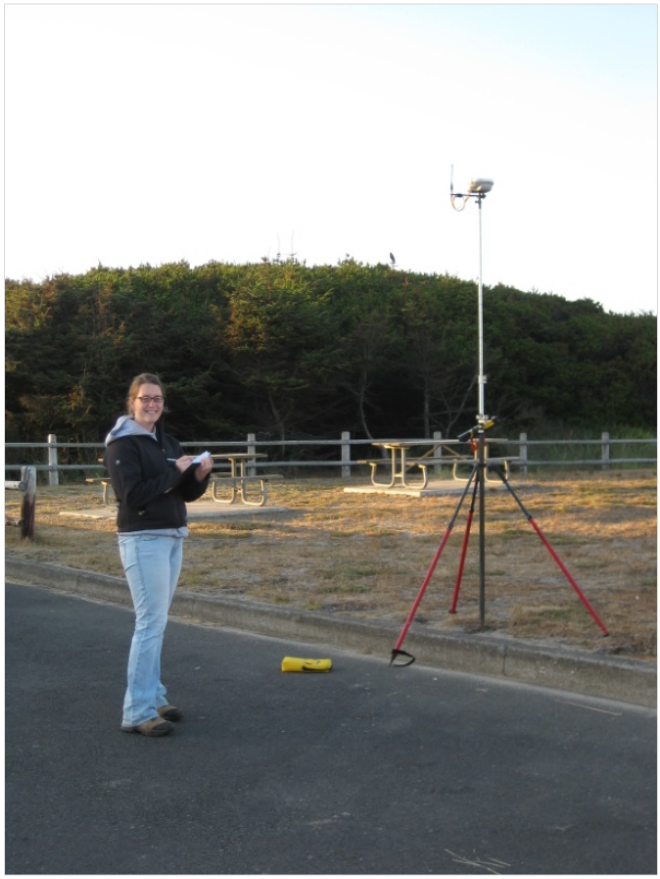

Figure 3-4. A 180-epoch calibration check is performed on a survey monument established by DOGAMI in Bob Straub State Park (Pacific City) in Tillamook County. This procedure is important for bringing the survey into a local coordinate system and for reducing errors associated with the GPS survey.

3.1.1 Clatsop County survey control procedures

Survey control (**Table 3-1**) along the Clatsop County shore was provided by occupying several benchmarks established by National Geodetic Survey (NGS), Watershed Sciences, Inc. (WSI), and by the Coastal Field Office of DOGAMI. In 2009, WSI established numerous temporary benchmarks (as well as reoccupied many NGS benchmarks) along the northern Oregon coast in order to calibrate lidar surveys of the northern Oregon coast. Coordinates assigned to these monuments were derived using the Online Positioning User Service (OPUS) maintained by the NGS (http://www.ngs.noaa.gov/OPUS/). In many cases, the same benchmarks were observed multiple times and the horizontal and vertical coordinates were continually updated, while the root-mean square (rms) errors associated with the multiple reoccupations were found to be low (typically sub-centimeter). Given the high level of accuracy assigned to the WSI monuments, we used their coordinates and elevations in place of NGS reported values to perform GPS site calibrations along the Clatsop County shoreline. (More detailed information about the survey procedures used by WSI can be found in their report on the 2008/09 lidar collected on the central to northern Oregon coast.) Besides the WS and NGS benchmarks, coastal staff at DOGAMI have established additional benchmarks along sections of the coast in order to further densify survey control in those areas. The approaches used to established the benchmarks are fully described in the reports by Allan and Hart (2007, 2008). For this study we used one DOGAMI benchmark (NEH 8) located in the town of Manzanita to help calibrate our GPS surveys of the beaches between Cape Falcon and Cannon Beach.

For beach surveys undertaken at Seaside and along the Clatsop Plains, survey control was provided by three NGS benchmarks: DELRAY, SEASIDE RM 2, and KIM (**Table 3-1**), while survey control south of Seaside was provided by one NGS benchmark (CANN), a WS benchmark (FEMA2 PW3), and a DOGAMI benchmark (NEH8). Additional survey control and field checking was provided using OPUS) (Soler and others, 2011). OPUS provides a simplified way to access high-accuracy National Spatial Reference System (NSRS) coordinates using a network of continuously operating GPS reference stations (CORS, http://www.ngs.noaa.gov/CORS/). In order to use OPUS, static GPS measurements are typically made using a fixed height tripod for periods of 2 hours or greater. OPUS returns a solution report with positional accuracy confidence intervals for adjusted coordinates and elevations for the observed point. In all cases we used the Oregon State Plane coordinate system, northern zone (meters), while the vertical datum is relative to the North American Vertical Datum of 1988 (NAVD88).

At the NEH8 DOGAMI monument, we performed two separate occupations of the site late in 2011, which were calibrated against the Oregon Real Time GPS Network (ORGN, http://www.theorgn.net/), established and maintained by ODOT and partners. The ORGN is a network of permanently installed, continuously operating GPS reference stations (essentially a CORS network similar to those operated and maintained by the NGS) that provide real-time kinematic (RTK) correctors to field GPS users over the internet via cellular phone networks. As a result, GPS users that are properly equipped to take advantage of these correctors such as the Trimble system used in this study, can survey in the field to the 1-cm horizontal accuracy level in real time. The derived coordinates are entirely consistent with the coordinate system and elevations determined through multi-hour occupations and submitted to OPUS for post-processing, but with the significant advantage of taking considerable less time.

For surveys undertaken along the Clatsop Plains and adjacent to Seaside, the R7 GPS base station was located on NGS monument AH7031 (DELRAY, **Table 3-1**), using a 2.0-m fixed-height tripod. Survey control was provided by undertaking 180 GPS epoch measurements (~3 minutes of measurement per calibration site) using two calibration sites (**Table 3-1**), enabling us to perform a GPS site calibration which brought the survey into a local coordinate system. This step is critical in order to eliminate various survey errors that may be compounded by factors such as poor satellite geometry, multipath, and poor atmospheric conditions, combining to increase the

total error to several centimeters. **Table 3-2** shows the relative errors identified when compared against the original reported values determined by the NGS. To further validate the accuracy of the GPS base station, OPUS solutions were derived from multiple >5 hours of static GPS measurements on benchmark AH7031 (DELRAY). **Table 3-2** indicates that horizontal and vertical errors at the GPS base station (AH7031) were less than 1 cm (i.e., within one standard deviation [σ]). Comparisons with the reported NGS horizontal coordinates similarly indicate nominal differences (~4 cm in the *x* coordinate and <1 cm in the *y* coordinate). However, as can be seen from **Table 3-2** there is a notable difference in the reported height, with the NGS derived value being about 0.13 m below the mean OPUS solution. NGS notes that several of their benchmarks along the Clatsop Plains coast do in fact differ by > 0.1 m when compared with GPS derived height solutions; it is presently not clear why there are reported differences between NGS derived values and observed OPUS solutions on the Clatsop Plains. Given the small differences between multiple OPUS derivations (**Table 3-2**), we used the mean value defined for the AH7031 site, and similarly used OPUS derivations from multi-hour GPS occupations of the other benchmarks. Furthermore, using this approach we are entirely consistent with the survey control procedures developed by WSI in their collection of lidar for DOGAMI around the state of Oregon.

For surveys undertaken along the southern Clatsop County coastline, the R7 GPS base station was located on NGS monument RD4216 (CANN, **Table 3-1**) located adjacent to Highway 101 near Cannon Beach. The GPS receiver was again mounted on a 2.0-m fixed-height tripod. Survey control was provided by undertaking 180 GPS epoch measurements using two calibration sites (**Table 3-1**). Similar to our approach along the Clatsop Plains, comparisons with multi-hour occupations of the primary base station site determined using OPUS solutions indicate very small differences between the surveys, with horizontal errors being less than 1 cm, while the vertical error is less than 2 cm. Comparisons with the reported NGS horizontal coordinates for the CANN site again indicate nominal differences (~7 cm in the *x* coordinate, < 1 cm in the *y* coordinate, and ~2 cm in the vertical). Differences between the two NEH8 occupations were found to be negligible (**Table 3-2**). Overall, these results indicate good across-the-board coherence in the derived coordinates and elevations, which in turn provides confidence in the reduced beach profile transect values.

Table 3-1. Survey benchmarks used to calibrate GPS surveys of the beach at Seaside and along the Clatsop Plains, and in southern Clatsop County. Asterisk signifies the location of the GPS base station during each respective survey. NGS denotes National Geodetic Survey monument, WSI denotes Watershed Sciences, Inc. monument, NGS/OPUS signifies OPUS derivation solution, and ORGN signifies Oregon Real Time GPS Network.

Study Area	Primary Identification (PID) Name	Designation	Northing (m)	Easting (m)	Elevation (m)
Seaside/	AH7031* - WSI/OPUS1	DELRAY	270262.871	2234745.433	11.672
Clatsop Plains	RD1141 – NGS/OPUS1	SEASIDE RM 2	264386.402	2234392.295	7.278
	AH7029 – NGS/OPUS1	KIM	281697.729	2233078.885	28.439
Cannon Beach/	RD4216* - NGS/OPUS1	CANN	249672.887	2231374.944	30.577
Arch Cape/	FEMA2_PW3 – WSI/OPUS1	FEMA2_PW3	254233.448	2231555.564	3.999
Falcon Cove	NEH8 – DOGAMI/ORGN2	NEH8	234997.630	2232106.115	9.101

Notes: Coordinates are expressed in the Oregon State Plane Coordinate System, northern zone (meters) and the vertical datum is NAVD'88.

[1]Control provided using both horizontal and vertical values (average of several multi-hour static GPS occupations);

[2]Control provided using both horizontal and vertical values derived by averaging two separate GPS occupations with survey control provided by ORGN.

Table 3-2. Comparison of horizontal and vertical coordinates derived by the NGS, WSI, DOGAMI, and OPUS solutions.

Study Area	Primary Identification (PID) Name	Solution	Northing (m)	Easting (m)	Elevation (m)
Clatsop Plains	AH7031	WS	270262.8714	2234745.433	11.672
		OPUS	270262.871	2234745.436	11.684
		OPUS	270262.88	2234745.426	11.676
		OPUS	270262.869	2234745.431	11.671
		OPUS	270262.864	2234745.435	11.663
		Mean	**270262.8714**	**2234745.433**	**11.672**
		σ	0.006	0.004	0.009
		NGS	-0.043	-0.009	0.132
	RD1141	OPUS	264386.395	2234392.291	7.275
		OPUS	264386.401	2234392.299	7.247
		OPUS	264386.41	2234392.295	7.312
		Mean	**264386.402**	**2234392.295**	**7.278**
		σ	0.008	0.004	0.033
		NGS	-0.054	-0.003	-0.019
	AH7029	OPUS	281697.718	2233078.896	28.416
		OPUS	281697.741	2233078.868	28.463
		OPUS	281697.727	2233078.892	28.439
		Mean	**281697.729**	**2233078.885**	**28.439**
		σ	0.012	0.015	0.024
		NGS	0.042	0.026	-0.139
Cannon Beach	RD4216	OPUS	249672.800	2231374.939	30.600
		OPUS	249672.892	2231374.936	30.561
		OPUS	249672.892	2231374.948	30.582
		OPUS	249672.886	2231374.949	30.568
		OPUS	249672.881	2231374.949	30.572
		Mean	**249672.887**	**2231374.944**	**30.577**
		σ	0.005	0.006	0.015
		NGS	-0.072	-0.008	-0.023
	FEMA2_PW3	WS	254233.448	2231555.564	3.999
	NEH8	ORGN	234997.641	2232106.115	9.121
		ORGN	234997.618	2232106.114	9.080
		Mean	**234997.630**	**2232106.115**	**9.101**
		σ	0.016	0.001	0.029

After completion of a local site calibration, cross-shore beach profiles were surveyed with the R8 GPS rover unit mounted on a backpack, worn by a surveyor (**Figure 3-5**). This was undertaken during periods of low tide, enabling more of the beach to be surveyed. The approach was to generally walk from the landward edge of the primary dune or bluff edge, down the beach face and out into the ocean to approximately wading depth. A straight line, perpendicular to the shore was achieved by navigating along a predetermined line displayed on a hand-held Trimble TSC2 computer controller, connected to the R8 receiver. The computer shows the position of the operator relative to the survey line and indicates the deviation of the GPS operator from the line. The horizontal variability during the survey is generally minor, being typically less than about ±0.25 m either side of the line (**Figure 3-6**), which results in negligible vertical uncertainties due to the relatively uniform nature of beaches characteristic of much of the Oregon coast (Ruggiero and others, 2005). Based on our previous research at numerous sites along the Oregon coast, this method of surveying can reliably detect elevation changes on the order of 4-5 cm, that is well below normal seasonal changes in beach elevation, which typically varies by 1–2 m (3–6 ft) (Ruggiero and others, 2005; Allan and Hart, 2007, 2008).

Figure 3-5. Surveying the morphology of the beach at Bandon using a Trimble 5800 "rover" GPS.

Analysis of the beach survey data involved a number of stages. The data was first imported into MathWorks® MATLAB® (a suite of computer programming languages) using a customized script. A least-squares linear regression was then fit to the profile data. The purpose of this script is to examine the reduced data and eliminate those data point residuals (e.g., **Figure 3-6**) that exceed a ±0.75-m threshold (i.e., the outliers) either side of the predetermined profile line. The data are then exported into a Microsoft® Excel® database for archiving purposes. A second MATLAB script takes the Excel profile database and plots the survey data (relative to the earlier surveys) and outputs the generated figure as a Portable Network Graphics (png) file. Appendix B shows the reduced beach profile plots for the Clatsop County transects.

To supplement the GPS beach and bluff data, high resolution lidar data measured by WSI in 2009 for DOGAMI were also analyzed and integrated into the beach profile data set. This was especially important for backshore areas where it was not possible to easily survey with the GPS gear. In addition, lidar data flown by the USGS/NASA/NOAA in 1997, 1998, and 2002 were also used to extend the time series of the beach and bluff profile data. In particular, the 1998 lidar data measured at the end of the major 1997-98 El Niño was analyzed, providing additional measurements of the beach in an eroded state that can be compared with more recent winter surveys of the beach. The 1997, 1998, and 2002 lidar data were downloaded from NOAA's Coastal Service Center (http://coast.noaa.gov/dataregistry/search/collection/info/coastallidar) and gridded in ArcGIS using a nearest neighbor algorithm to produce a digital elevation model (DEM). Distance and elevation data were then extracted from the lidar DEM.

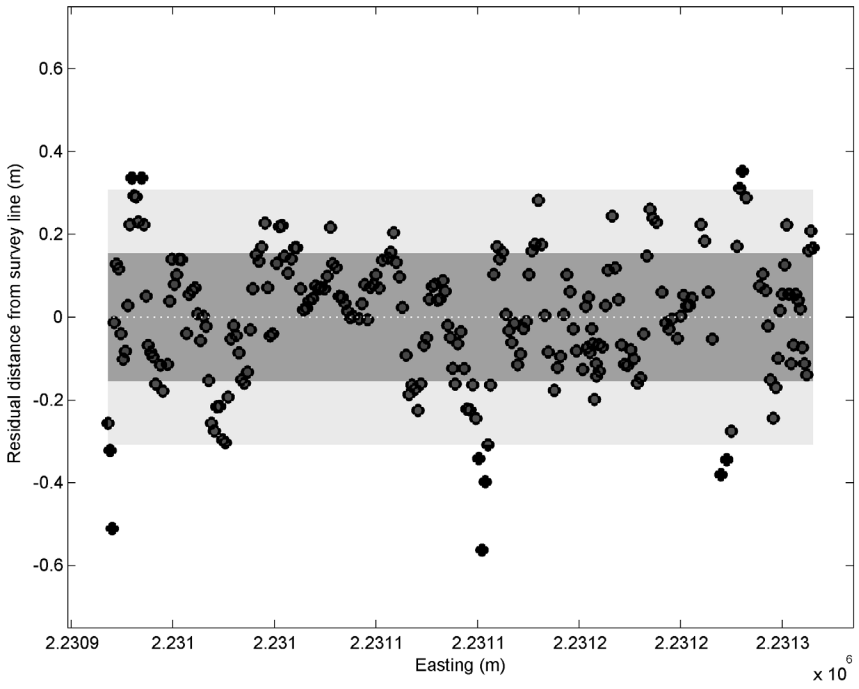

Figure 3-6. Residuals of GPS survey points relative to zero (transect) line. Example reflects the Cannon Beach 10 profile line. Dark grey shading indicates 68.3% of measurements located ±0.15 m (1σ) from the transect line, while 95.5% (2σ) of the measurements are located within ±0.30 m of the profile line (grey shading).

3.2 Beach Characterization

Analyses of the beach profile data were undertaken using additional scripts developed in MATLAB. The profile analysis script requires the user to interactively locate the positions of the seaward edge and crest of the Primary Frontal Dune (PFD) backing the beach, and then evaluate the beach-dune juncture (E_j) elevations and beach slopes (tan β) for the 1997, 1998, 2002, 2008/2009, 2010, and 2011 surveys along each of the profile sites. Beach slope was determined by fitting a linear regression through the measured GPS data. In all cases, the slope of the beach face was determined to be the region of the beach located between Mean Sea Level (~1.4 m, MLLW) and the highest observed tide (~3.8 m, MLLW), an approach that is consistent with methodologies adopted by Ruggiero and others (2005) and Stockdon and others (2006). Determination of the location of the beach-dune junctures (E_j) was accomplished interactively using the MATLAB script and from local knowledge of the area. In general, the beach-dune juncture (E_j) reflects a major break in slope between the active part of the beach face and the toe location of the primary dune or bluff. For most sites along the Oregon coast, the beach-dune junctures (E_j) typically occurs at elevations between about 4-6 m (NAVD88). **Figure 3-7** provides an example of identified beach-dune junctures (E_j) determined for one site (Cannon bch15) immediately north of Ecola Creek in Cannon Beach. In this example, it is apparent that the dune has experienced considerable accretion during the past decade, with the dune face having prograded seaward by 36.5 m (120 ft) since 1997 as measured at the 10 m (33 ft) contour elevation. Analysis of the profile data indicates that the beach-dune juncture (E_j) has varied in elevation, a function of repeated phases of both erosion and accretion events. As of winter 2011, an erosion scarp had formed and the beach-dune juncture reflected the toe of the scarp, located at an elevation of 4 m (13.1 ft). However, in this example the MLWP beach-dune juncture is associated with the 1998 beach-dune juncture, which is located at an elevation of 4.87 m, while the slope of the beach is best captured by the March 2011 winter survey. **Figure 3-7** also identifies the crest of the primary dune as well as the landward boundary of the *primary frontal dune* (PFD). These latter data are used later to develop or refine VE and V-zones (where no detailed coastal study is undertaken).

To estimate beach erosion and profile changes for a specific coastal setting that occurs during a particular storm, it is essential to first estimate the initial conditions of the morphology of the beach prior to the actual event of interest (Northwest Hydraulic Consultants, 2005). This initial beach profile is referred to as the Most Likely Winter Profile (MLWP) condition for that particular coastal setting. The MLWP was assessed based on an examination of the combined surveyed profiles and lidar data. **Figure 3-8** provides an example for one particular site on the Clatsop Plains (14). In contrast to **Figure 3-7**, the GPS survey undertaken in March 2011 was found to best characterizes the MLWP. Landward of the dune crest, information on the backshore topography was derived by incorporating the actual measured GPS data because those data provided the best representation of the actual ground surface. Where GPS survey data were not available, we used topographic data derived from the 2009 lidar flown for DOGAMI.

.

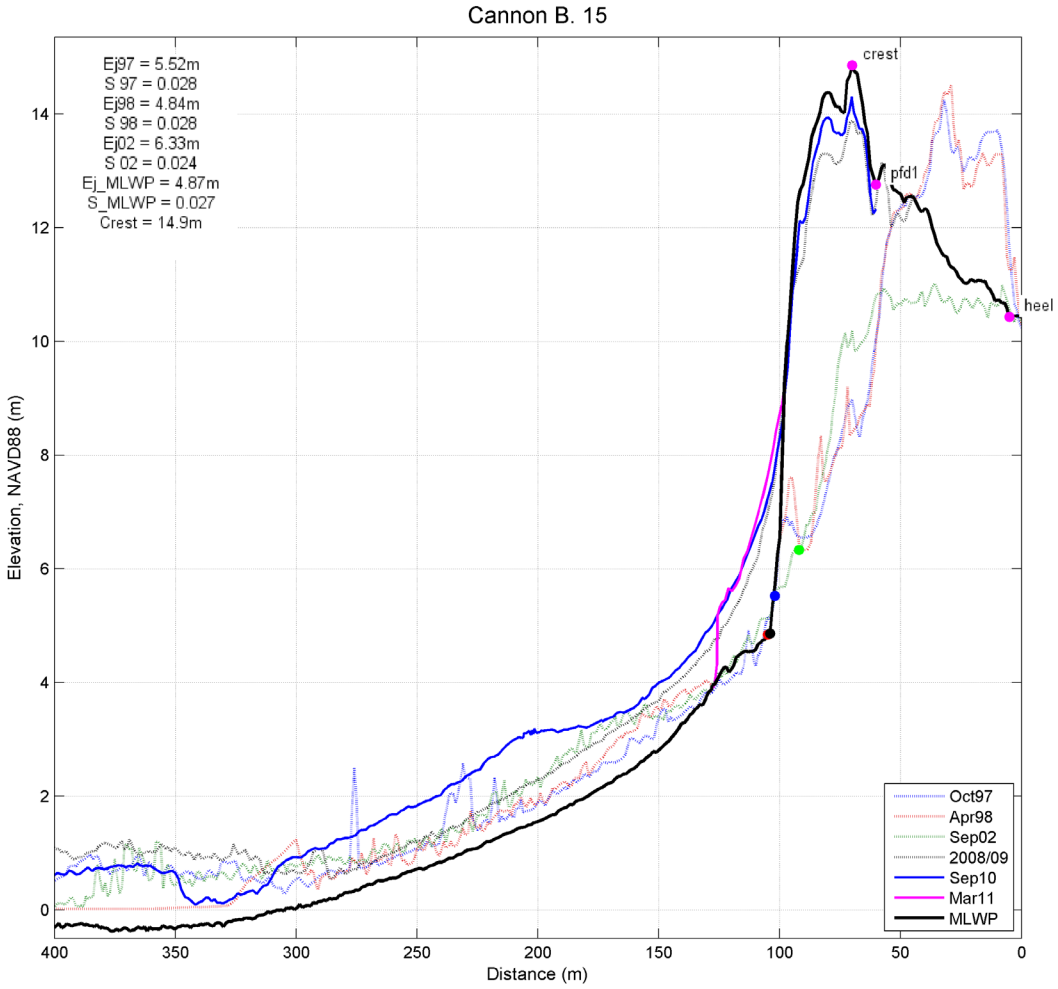

Figure 3-7. Plot showing beach-dune junctures (black, blue, red, and green dots) and slopes identified from various surveys at the Cannon Beach 15 profile site. In this example, the MLWP beach-dune juncture elevation corresponds to the 1998 lidar survey. The dune crest and primary frontal dune location (PFD) are characterized by the magenta circles. The plot also provides a dramatic example of recent accretion along this section of Cannon Beach.

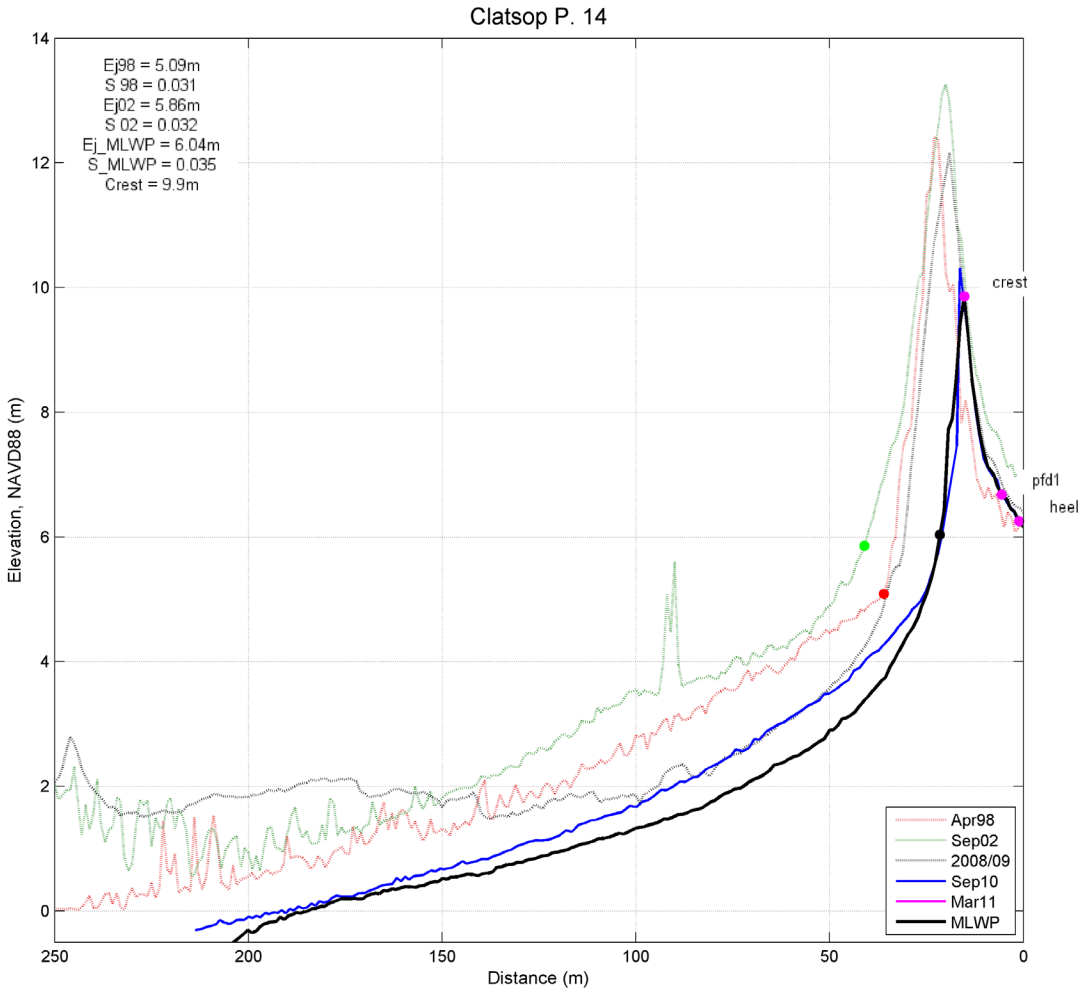

Figure 3-8. Example plot of the combined beach profile data for the Clatsop Plains 14 site. Note the amount of erosion affecting this site, with the beach having retreated landward by ~10.5 m (34.5 ft). The beach-dune juncture is characterized by black, red, and green dots; the dune crest and PFD locations are in magenta.

Table 3-3 summarizes the various morphological parameters identified for each transect site along the Clatsop County coastline, including their geomorphic classification. **Figure 3-9** provides a plot of the alongshore changes in beach slopes (tan β), mean sediment grain sizes (M_z), beach-dune and beach-bluff juncture (E_j) elevations, and the dune crest and/or bluff top heights. In general, the steepest slopes is confined to those beaches with coarse sediments on the foreshore, while sites exhibiting generally lower beach slopes typically occur near the mouths of estuaries and creeks (e.g., the Necanicum estuary at Seaside). At many of the beach study sites, sediment grain sizes vary both in the along-shore and cross-shore directions. For example, beaches in southern Clatsop may be characterized as "composite" using the nomenclature of Jennings and Shulmeister (2002), consisting of a wide dissipative sandy beach composed of fine to medium sand (M_z ranges from 2.8Ø to 2.1Ø (0.14 mm to 0.23 mm [Peterson and others, 1994]), **Figure 3-9**), backed by a thin veneer of gravel on the upper foreshore (e.g., Arcadia and Tolovana Beach). In contrast, the beach at Arch Cape exhibits a substantial gravel berm on the upper foreshore that backs a wide dissipative beach, providing significant protection to the backshore (Allan and others, 2005). Southern Clatsop beaches are further distinct from those in northern Clatsop (e.g., Clatsop Plains), which consist of pure sand beaches composed of fine to medium sand, wide dissipative surf zones, broad gently sloping foreshores, and are backed by massive dunes.

The coarsest beaches typically occur near headlands and along those beaches backed by coastal bluffs. For example, as described in Section 2 an extensive cobble and boulder beach dominates the shore around Tillamook Head, and along a portion of the beach at Seaside. The predominant source of the cobbles and boulders is from landslides along the northern flank of Tillamook Head (Allan and others, 2005). One such event occurred early in 1987 and released an estimated 230,000 m^3 (300,000 yd^3) of material onto the beach (Tom Horning, personal communication, 2005). The landslide debris was rapidly redistributed along the shore, moving at an estimated 3.2 km (2 mi) per month. By July 1987 it had formed a barrier spit across the beach near where the berm curves again to the north (**Figure 3-10**). By September 1987, the sediment had migrated onto the existing gravel beach but continued to travel to the north, eventually causing the beach at U Avenue (located near the Seaside 5 profile site) to prograde seaward by 45 m (150 ft). Grain size measurements by Allan and others (2005) indicated that the cobbles range in size from -5.7 to 6.1Ø (52–69 mm) and tend to predominate on the upper portion of the beach foreshore, while abundant boulders located in the inter-tidal region lower on the profile provide considerable protection to the beach foreshore (**Figure 3-11**). As can be seen from **Figure 3-9**, beach slopes in southern Seaside peak at ~8 to 11° (tan β = 0.15 to 0.2), and is entirely consistent with measurements undertaken by Allan and others (2005)

Table 3-3. Identified beach morphological parameters from the most eroded winter profile along the Clatsop Plains. Parameters include the beach-dune junction elevation (Ej_MLWP), beach slope (tan *β*) and a site description.

Reach	Profile Number	Dune Crest/Bluff Top (m)	*Ej_MLWP* (m)	Beach Slope (tan *β*)	Description
Clatsop Plains	1	10.972	5.024	0.036	dune-backed
	2	12.504	5.561	0.028	dune-backed
	3	11.543	5.483	0.024	dune-backed
	4	13.003	6.222	0.028	dune-backed
	5	14.539	5.344	0.025	dune-backed
	6	14.099	6.342	0.031	dune-backed
	7	13.892	6.377	0.032	dune-backed
	8	13.819	6.455	0.029	dune-backed
	9	13.405	6.554	0.029	dune-backed
	10	14.180	6.508	0.027	dune-backed
	11	15.313	6.533	0.033	dune-backed
	12	16.059	5.628	0.029	dune-backed
	13	15.960	5.997	0.031	dune-backed
	14	6.215	6.21	0.038	dune-backed
Seaside	1	15.152	6.484	0.149	cobble berm backed by high bluff
	2	8.918	5.639	0.165	cobble berm backed by high bluff
	3	6.570	6.570	0.186	sand backed by cobble berm
	4	6.810	6.810	0.028	sand backed by cobble berm
	5	5.916	5.890	0.039	sand backed by cobble berm
	6	7.634	5.778	0.045	dune-backed
	7	7.472	5.576	0.026	dune-backed
	8	9.501	5.845	0.018	dune-backed
	9	8.258	5.326	0.015	sand backed by seawall
	10	7.894	6.379	0.021	sand backed by seawall
	11	7.255	5.114	0.022	sand backed by seawall
	12	9.679	4.362	0.014	dune-backed
	13	8.019	4.680	0.009	dune-backed
	14	7.410	4.28	0.007	sand backed by low bluff
	15	6.864	3.149	0.005	sand backed by low bluff
	16	5.800	2.400	0.005	sand backed by riprap/low bluff
	17	5.418	2.330	0.005	dune-backed
Cannon Beach	1	16.651	4.869	0.026	sand backed by high bluff
	2	9.438	4.348	0.030	sand backed by riprap/mod high bluff
	3	10.043	5.173	0.031	sand backed by seawall
	4	7.903	5.200	0.030	sand backed by low bluff
	5	7.035	4.713	0.028	sand backed by riprap/low bluff
	6	12.826	4.285	0.027	sand backed by high bluff
	7	16.011	4.607	0.032	sand backed by riprap/high bluff
	8	15.746	6.869	0.031	sand backed by high bluff
	9	6.805	4.129	0.023	sand backed by seawall
	10	9.752	6.966	0.028	sand backed by mod high bluff
	11	11.490	5.186	0.049	dune-backed
	12	10.964	4.231	0.051	sand backed by riprap/mod high bluff
	13	6.709	4.127	0.009	sand backed by seawall
	14	6.841	4.184	0.020	sand backed by riprap
	15	14.857	4.867	0.038	dune-backed
	16	16.764	4.723	0.043	dune-backed
	17	15.060	4.056	0.033	dune-backed

Reach	Profile Number	Dune Crest/Bluff Top (m)	*Ej_MLWP* (m)	Beach Slope (tan *β*)	Description
Tolovana	1	8.290	4.696	0.031	sand backed by cobble, riprap/low bluff
	2	7.006	4.663	0.029	sand backed by cobble/low bluff
	3	7.832	4.938	0.030	sand backed by cobble, riprap/low bluff
	4	8.222	4.942	0.028	sand backed by riprap/low bluff
	5	7.708	4.509	0.026	sand backed by cobble, riprap/low bluff
	6	8.193	4.323	0.025	sand backed by riprap/low bluff
	7	7.697	4.812	0.025	sand backed by riprap/low bluff
	8	7.300	5.011	0.026	sand backed by riprap/low bluff
	9	8.229	5.218	0.027	sand backed by riprap
	10	7.644	4.130	0.029	sand backed by riprap/concrete foundation
	11	6.662	4.122	0.024	sand backed by riprap
	12	7.609	4.344	0.029	sand backed by riprap/low bluff
	13	7.955	4.565	0.028	wooden bulkhead/low bluff
	14	7.629	4.218	0.027	sand backed by riprap/low bluff
	15	7.537	4.070	0.025	sand backed by riprap/low bluff
	16	7.458	4.040	0.026	sand backed by riprap/low bluff
	17	7.980	4.528	0.026	sand backed by riprap/low bluff
	18	8.974	4.941	0.029	sand backed by cobble, riprap/low bluff
Arcadia	1	15.322	6.201	0.060	sand, gravel backed by high bluff
	2	17.825	5.713	0.034	sand, gravel backed by high bluff
	3	12.366	4.925	0.038	sand backed by mod high bluff
Arch Cape	1	6.876	6.876	0.026	sand backed by gravel berm
	2	11.576	7.005	0.103	sand backed by gravel, riprap/low bluff
	3	8.001	5.221	0.087	sand backed by gravel, riprap/low bluff
	4	16.761	7.131	0.143	sand backed by gravel/mod high bluff
	5	12.149	5.291	0.168	sand backed by gravel /seawall
	6	7.001	5.485	0.048	sand backed by gravel /riprap
	7	15.219	6.849	0.079	sand backed by gravel /high bluff
	8	18.065	4.031	0.071	sand backed by gravel/bulkhead/high bluff
	9	8.462	6.663	0.101	sand backed by gravel/low bluff
	10	7.897	5.366	0.085	sand backed by gravel, riprap/low bluff
Falcon Cove	1	15.935	7.027	0.167	sand, cobble berm backed by high bluff
	2	20.150	6.414	0.198	sand, cobble berm backed by high bluff
	3	15.612	6.091	0.165	sand, cobble berm backed by high bluff
	4	11.844	6.927	0.177	sand, cobble berm backed by high bluff
	5	6.453	1.250	0.224	sand backed by cobble barrier
	6	11.585	5.388	0.176	sand, cobble berm backed by high bluff

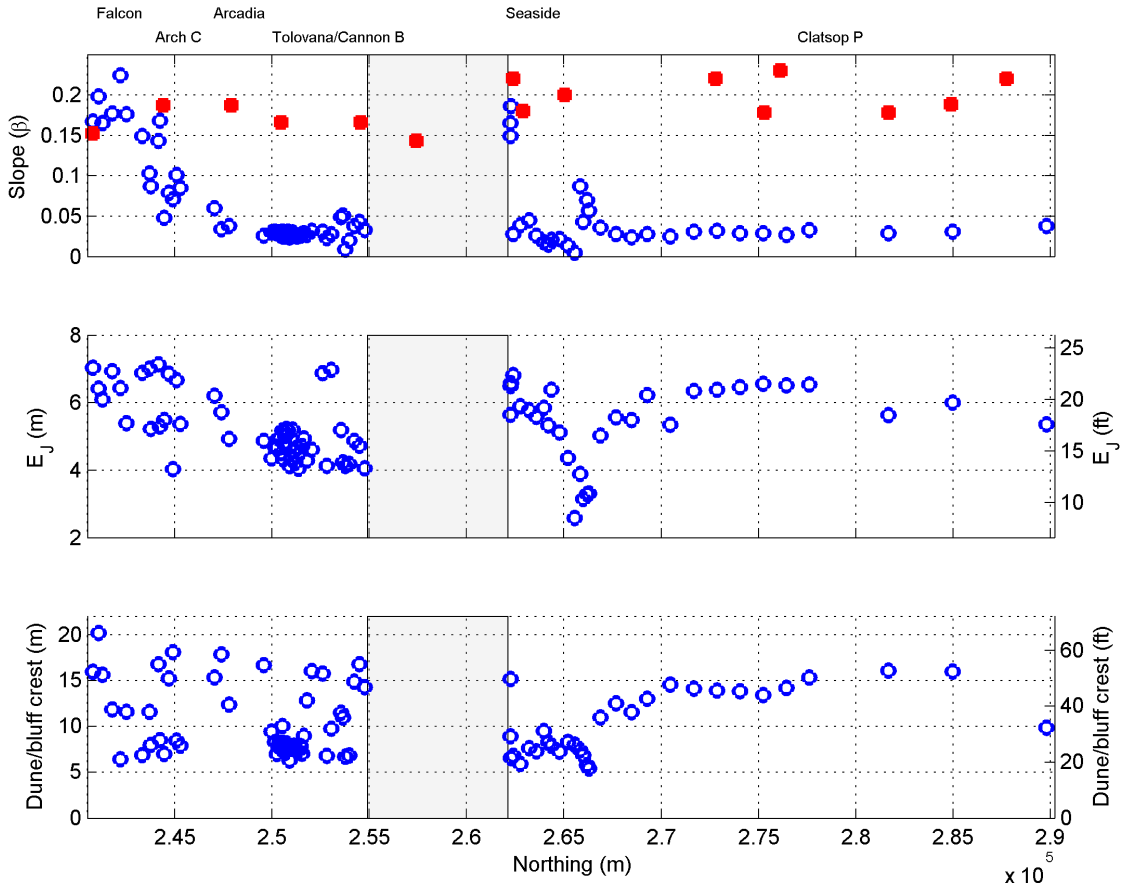

Figure 3-9. Alongshore changes in beach slopes (tan β), beach-dune juncture (Ej) elevations, and dune/bluff crest/tops along Clatsop County. Red squares indicate mean sediment grain sizes measured by Peterson and others (1994).

Figure 3-10. Oblique aerial photo (view to southeast) of a migrating cobble-boulder berm that developed at the cove at Seaside's southern shoreline from the 1987 landslide on Tillamook Head. Within one month the berm connected to the north-south beach at the upper left corner of the photo. Larger winter surf pushed the rubble onto the original east-west shoreline (foreground in lower right of photo), killing all intertidal sea life. Waves then moved the cobbles and boulders westward with negligible progradation of the east-west shoreline and onto the north-south beach where the material formed a series of coalescing berms that shifted the shoreline 300 ft westward. The rocky material continues to advance slowly northward along the beach, driven by winter surf (photo: courtesy of Paul D. See).

Figure 3-11. Gravel beach at Seaside and along Tillamook Head. A) Adjacent to the Seaside 3 profile site. The presence of logs at the beach crest indicates the maximum wave runup height (about 6 m [19.6 ft]) achieved during the most recent storm event. B) At Seaside 1, the lower portion of the gravel beach is protected by a boulder toe, with the finer gravels having been pushed up the cobble face to form the crest of the beach. Note the well-vegetated backshore and marine cliff landward of the cobble beach. The survey staff near the bottom of the photo shows 0.3-m (1-ft) graduations and indicates the size of the boulder toe (photo: J. Allan, DOGAMI, 2010).

In southern Clatsop County, gravels and cobbles back broad sandy beaches at several locations, including the shore near Tolovana Park in Cannon Beach, Arcadia Beach, Hug Point and at Arch Cape (**Figure 3-1** and **Figure 3-2**). Gravels in these areas tend to be slightly smaller (-5.44 to -5.96ø [43–62 mm]) when compared with the gravels at Seaside. Furthermore, with the exception of Arch Cape, the gravels tend to form a thin veneer at the back of the beach and as a result may be periodically covered by sand in the summer. **Figure 3-9** indicates that the beach slopes in the Arch Cape area are relatively steep varying from ~2.9 to 10° (tan β = 0.05–0.18).

The gravel beach at Falcon Cove is without doubt one of the more dramatic example of erosion identified on the Oregon coast. Along much of its length the gravel beach fronts an actively eroding bluff. At least two homes have had to be moved landward, and several other homes remain threatened. At the north end of the beach, the gravel forms a barrier beach that has impounded a lake behind it. However, the site is subject to frequent overtopping, as evidenced by the many logs and debris along the crest of the berm and on its landward side leading into the lake. The beach is actively being fed by gravel and boulders from the south end of the cell in the form of landslides off Cape Falcon, while the south-central portion of Cove Beach is primarily supplying sand and colluvial material to the system. As material is released from Cape Falcon, the sediment is rapidly transported northward along the beach where it is assimilated into the gravel beach. The gravel beach is characterized by a wide range of grain sizes, from coarse sand and granules to large cobbles. The sediment is classified as "well sorted," which indicates a uniform mixing of the predominant grain sizes present on the beach. Mean grain sizes (MzØ) ranged from −5.74Ø (53 mm) in the south to −6.19Ø (73 mm) in the north. **Figure 3-9** indicates that the beaches in Falcon Cove are steep varying from ~9 to 14° (tan β = 0.16–0.26).

Sandy beaches throughout Clatsop County are classified as having fine to medium sand (M_z range from 2.8Ø to 2.1Ø [0.14 to 0.23 mm]) (Peterson and others, 1994), with little to no evidence of alongshore variation (**Figure 3-9**). As a result, these beaches tend to be broad, are backed by bluffs or dunes, have low slopes (mean tan β = 0.029 (σ = 0.008), and hence are characterized with wide, dissipative surf zones.

Figure 3-9 also plots the beach/dune and beach/bluff juncture elevations (Ej) for the various study sites. In general, values for Ej tend to be highest along the shores of Falcon Cove, portions of Arch Cape, southern Seaside and along the length of the Clatsop Plains (mean = 5.6 – 6.4 m). In contrast, the lowest Ej values are confined to much of the Cannon Beach shore (mean = 4.75 m) and within the Necanicum estuary. In addition, **Figure 3-9** indicates the bluff top, structure crest, and or dune crest heights. Because these heights are indicative of the potential for flooding, with higher crests generally limiting flood overtopping, it can be seen that the risk from coastal flooding and inundation is likely to be highest along much of the shores in Seaside, Tolovana/Cannon Beach, and at Arch Cape. Along the remainder of the shore, the beaches are protected by prominent bluffs (e.g., Falcon Cove) and/or dunes (e.g., Clatsop Plains) with crest elevations that range from 14 to 21 m (46 – 69 ft) that effectively preclude wave overtopping and hence inundation in those areas. Nevertheless, some of these sites are subject to erosion hazards that likely will influence the extent of the flood zones in those areas, after factoring the potential for erosion from storms.

3.3 Recent Coastal Changes in Clatsop County

This section briefly reviews beach profile changes that have occurred during the past decade, having been documented by lidar and recent GPS surveys of the shore.

The overall approach used to define the morphology of the beach and dune system, including the location of the PFD along the length of county shoreline, and shoreline changes over the past decade, was based on detailed analyses of lidar data measured by the USGS/NASA/NOAA in 1997, 1998, and 2002 and by DOGAMI in 2009. However, because lidar data flown by the USGS/NASA/NOAA is of relatively poor resolution (~1 point/m^2) and reflects a single return (i.e., includes vegetation where present), while the lidar data flown by DOGAMI has a higher resolution (8 points/m^2), and was characterized by multiple returns enabling the development of a bare-earth DEM, determination of the most critical beach/dune morphological features was based entirely on analysis of the 2009 lidar data.

Lidar data flown in 1998 and 2002 were downloaded from NOAA's Coastal Service Center, and gridded in ArcGIS using a TIN algorithm; a similar approach was undertaken with the 2009 lidar data. Transects spaced 25 m apart were cast for the full length of the county coastline using the Digital Shoreline Analysis System (DSAS) developed by the USGS (Thieler and others, 2009). For each transect, xyz values for the 1997, 1998, 2002 and 2009 lidar data were extracted at 1-m intervals along each transect line and saved as a text file using a customized ArcGIS script.

Processing of the lidar data was undertaken in MATLAB using a custom beach profile analysis script developed by DOGAMI. This script requires the user to interactively define various morphological features including the dune/bluff crest/top, bluff slope (where applicable), landward edge of the PFD, beach-dune juncture elevations for each year, and the slope of the beach foreshore.

3.3.1 Clatsop Plains beach changes

Figure 3-12 shows the profile changes measured at four of the transect sites: SEA12 (Seaside), Rilea (CP11), Iredale (CP13), and Eastjetty (CP14). Beginning in the north at the CP14 site, **Figure 3-12** indicates that the Eastjetty site exhibited little change between 1998 and 2002. However, since ~2006 the Eastjetty site has been steadily eroding back landward, causing the foredune width to narrow over time. In total, the dune has eroded landward by 21.6 m (70.8 ft). Today, the remnant dune is narrow and could easily breach in a single storm.

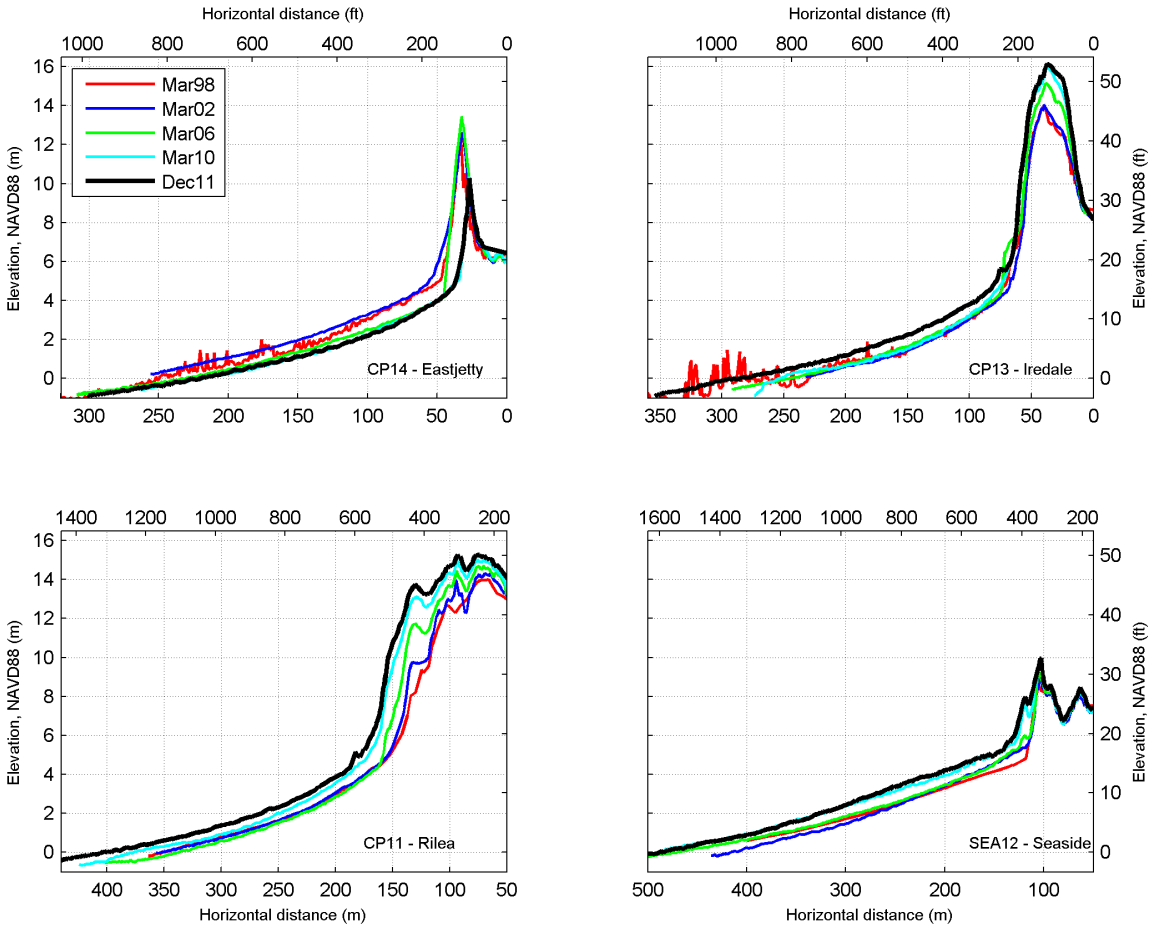

Figure 3-12. Measured beach morphological changes carried out between 1998 and 2011 for selected sites on the Clatsop Plains from winter surveys undertaken by WDOE and DOGAMI in each year.

Farther south at the CP13 (Iredale) site, morphological changes of the beach there again indicate the impact of the storms of the late 1990s, which caused the beach to initially erode landward. However, since then the beach has been gradually rebuilding and by 2005 had essentially rebuilt itself. Probably the most significant change occurring at the Iredale site is the degree of aggradation occurring on the crest of the foredune (**Figure 3-12**). As can be seen in the figure, between 1998 and 2011 the foredune grew vertically by ~2 m (6.5 ft), resulting in a net gain of 180 m^3 of sand per meter of beach ($m^3.m^{-1}$) or 235 yd^3 per yard of beach. With progress south along the plains, aggradation on the foredune become even more significant, while changes on the beach face tend to be relatively minor. For example, net volume gains were measured at CP13 (Rilea) (517 $m^3.m^{-1}$ [676 $yd^3.yd^{-1}$]) and at CP5 (Delray) (298 $m^3.m^{-1}$ [389 $yd^3.yd^{-1}$]). Given that the mean shoreline position at each of the beach profile sites has not changed substantially (i.e., prograded seaward), the bulk of the sediment volume gains reflect aggradation on the primary foredune. The pattern of beach aggradation continues to the south to the SEA12 (Seaside) profile site (**Figure 3-12**), which indicates that the beach there has also been gaining sand over the past decade, although at a much slower pace when compared with the beach to the north.

Figure 3-13 shows the net shoreline change (1997–2009) as measured at the 6 m (19.6 ft) contour elevation derived for the Clatsop Plains to Seaside coastline. The 6 m contour was used because this particular elevation provides a better measure of the long-term response of the beach, while lower elevations tend to be dominated by large seasonal excursions (Allan and others, 2003; Allan and Hart, 2008). These results generally confirm the observed responses described above for specific transects along the Clatsop Plains. In general, **Figure 3-13** indicates that erosion dominates the northern tip of the Clatsop Plains (profiles 0–18), a region of little significant change (profiles 19–240), a region of active accretion which increases to the south (profiles 241–700), and then decreases toward the Necanicum Estuary (profiles 701–971), and an area characterized by large shoreline excursions around the mouth of the estuary. Along the Seaside coastline, the lidar data indicate that this section is also accreting, though it is characterized by large fluctuations along the shore as ephemeral dunes form, aggrade, and are subsequently reworked by aeolian processes.

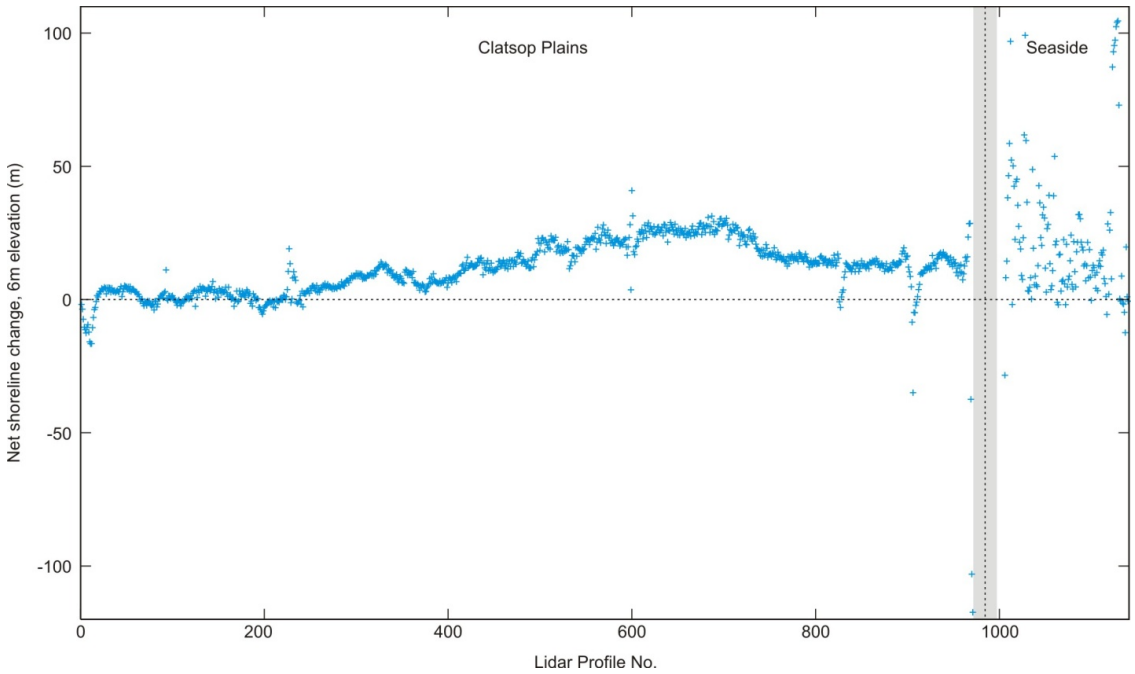

Figure 3-13. Net shoreline excursions along the Clatsop Plains and Seaside as measured at the 6m (19.6 ft) contour for the period 1997–2009. Grey band denotes the location of the Necanicum Estuary.

3.3.2 Seaside to Falcon Cove beach changes

Similar analyses of coastal change have been derived for the reminder of the Clatsop County shoreline. **Figure 3-14** presents those results for the coast from Cannon Beach south to Falcon Cove. Overall, shoreline changes are much lower when compared with beaches in the north and probably reflects the fact that this shore has limited sediment inputs that are largely derived from erosion into the coastal bluffs. As can be seen in **Figure 3-14**, the results confirm that significant accretion has occurred on the north side of Ecola Creek in Cannon Beach. Accretion also characterizes the section of shore to the north of Haystack Rock (north of the CannonB 8 profile site, **Figure 3-2**). In contrast, much of the shore between Haystack Rock and the CannonB1 profile site has experienced a small amount of erosion, ranging from negligible to several meters over the past 12 years. This pattern characterizes much of the shore between Arcadia Beach and Arch Cape. Again, the degree of erosion over the past decade is relatively small. In contrast, beaches with the Arch Cape littoral cell are mostly stable, having accreted several meters as the gravel berm gained more sediment and built higher. Finally, Shoreline changes in Falcon Cove indicate significant erosion (up to 15 m of retreat) in the central to northern half of the cell, while the south end is relatively stable having gained additional cobble. However, these latter responses probably reflect mostly fluctuations in the position and volume of the cobble berm that fronts the bluffs. For example, analyses of the actual transects in this area indicate that the bluffs themselves have eroded by no more than several meters during the past 15 years.

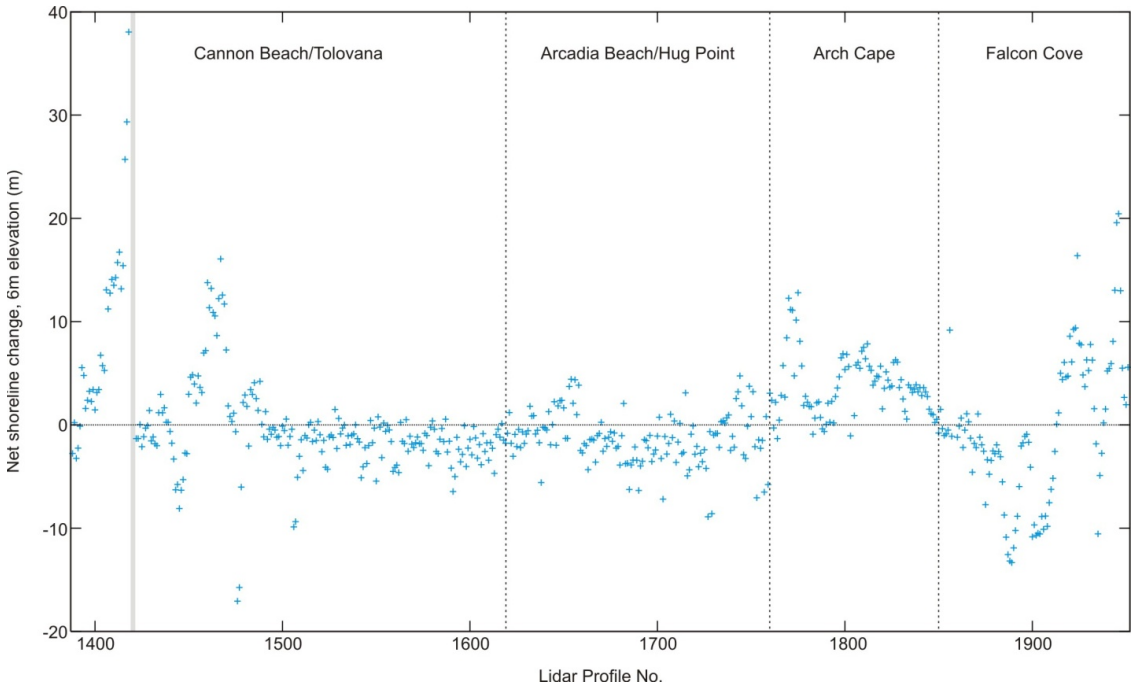

Figure 3-14. Net shoreline excursions along the southern Clatsop County coastline as measured at the 6m (19.6 ft) contour for the period 1997–2009. Grey band denotes the location of Ecola Creek.

3.4 Bathymetry

Important for calculating wave transformations and determining nearshore beach slopes is information on the local bathymetry offshore from the Clatsop County coast. For the purposes of this study we have adopted two approaches:

1. For the purposes of SWAN numerical wave modeling, we used bathymetric data compiled by the National Geophysical Data Center (NGDC), an office of NOAA for the purposes of developing an integrated bathymetric-topographic DEM for tsunami inundation modeling.
2. For erosion assessments and wave runup calculations, we used bathymetric data collected in late summer 2010 with the aid of personal watercrafts (Ozkan-Haller and others, 2009).

For the purposes of developing an integrated bathymetric-topographic DEM that can be used for tsunami inundation modeling, NGDC has compiled detailed bathymetric data across the continental shelf from multiple agencies. The synthesized bathymetric-topographic DEM (Astoria [http://www.ngdc.noaa.gov/dem/squareCellGrid/download/454] and Garibaldi [http://www.ngdc.noaa.gov/dem/squareCellGrid/download/249]) is a 1/3 arc-second (approximately 10 m [~33 ft]) DEM of the northern Oregon coast that spans all of Clatsop County, and includes the offshore rocks, small islands, and reefs that would affect wave shoaling. The DEM was generated from a diverse suite of digital data sets that span the region (Carignan and others, 2009a, b). A summary of the data sources and methods used to synthesize the data to develop the Astoria and Garibaldi DEMs is described in the reports by Carignan and others (2009a, 2009b). In general, the best available data were obtained by the NGDC and shifted to common horizontal and vertical datums: North America Datum 1983 (NAD 83) and Mean High Water (MHW).

NGDC used shoreline, bathymetric, and topographic digital data sets (**Figure 3-15**) from several U.S. federal, state and local agencies (e.g., NOS, Office of Coast Survey (OCS) and Coastal Services Center (CSC), USGS, USACE, and the Oregon Department of Fish and Wildlife/Marine Resource Program (ODFW). Having converted all the data to a common coordinate system and vertical datum, the grid data were checked for anomalous data and corrected accordingly. Because the data sets, particularly in deep water and near to the coast, were relatively sparse, further manipulation and smoothing was required to create a uniform grid. These products were then compared with the original surveys to ensure grid accuracy. According to Carignan and others (2009a) the final DEM is estimated to have an accuracy of up to 10 m (~33 ft), while some portions of the grid are more accurate (e.g., the coastal strip where high-resolution lidar data was available). The bathymetric portion of the data set is estimated to have an accuracy of between 0.1 m (0.33 ft) and 5% of the water depth, again depending on the type of survey data that was used to calibrate the final grid development.

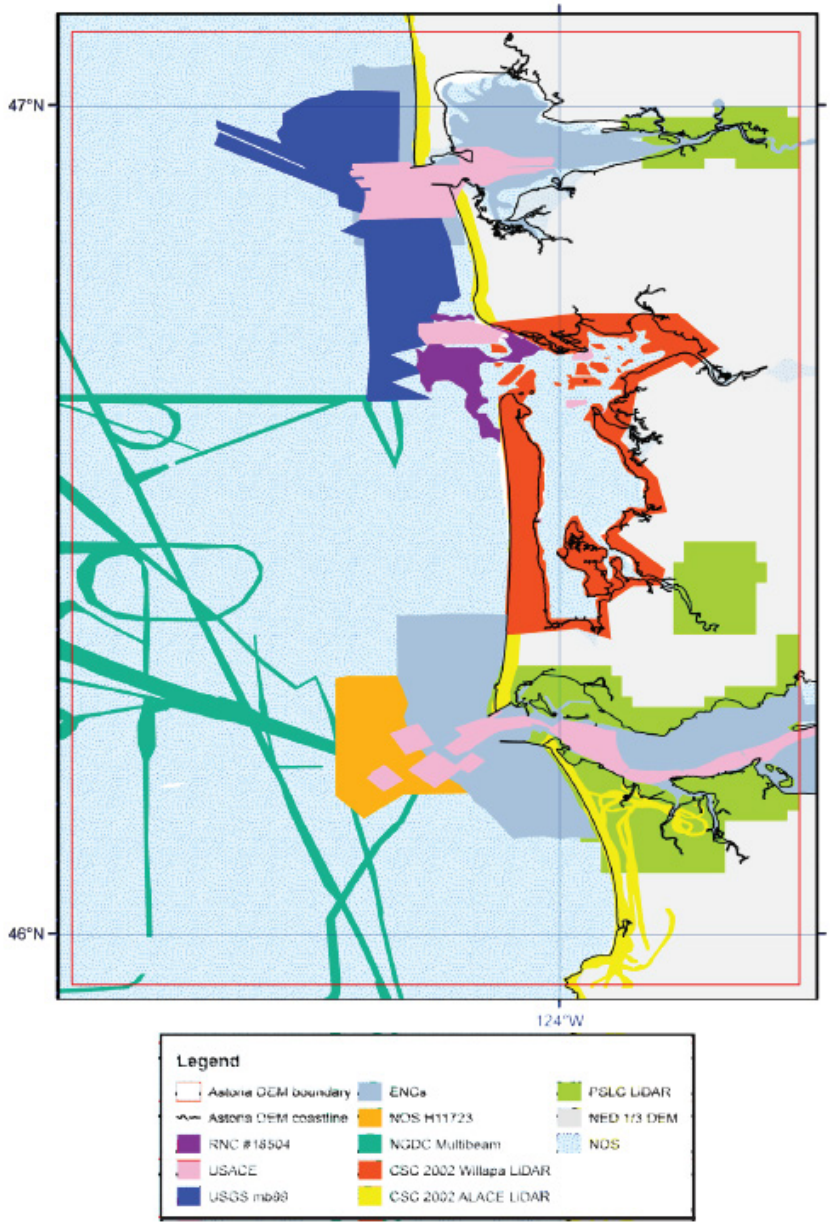

Figure 3-15. U.S. federal, state, and local agency bathymetric data sets used to compile the Astoria DEM (Carignan and others, 2009a).

Finally, despite all these efforts it is important to note that a limitation of the DEMs being developed by NGDC is the virtual absence of suitable bathymetric data in the nearshore (effectively landward of the 10 m [33 ft] bathymetry contour), because few survey boats are able to venture into this highly turbulent and dangerous portion of the surf zone. The exception to this is where surveys have been undertaken by the USACE in the entrance channels to estuaries where navigable water depths need to be maintained. Thus, there is some uncertainty about estimating nearshore slopes for the surf zone due to the absence of sufficient data for this region, with the user having to make some assumptions based on the best available data

that is present outside the surf zone and information at the shoreface. This is a recognized problem with all coastal flood analyses. To resolve this problem, we used a Coastal Profiling System (CPS) that has been developed for nearshore bathymetric surveys by Dr. Peter Ruggiero, Department of Geosciences, OSU (Ruggiero and others, 2005). The CPS consists of a highly maneuverable personal watercraft that is equipped with a survey grade GPS receiver and antenna, an echo sounder and an on board computer. Repeatability tests undertaken by Ruggiero and colleagues indicate sub-decimeter accuracy on the order of 0.15 m (0.5 ft) (Ozkan-Haller and others, 2009). **Figure 3-16** provides an example of the CPS system, while **Figure 3-17** presents the mapped coverage of our bathymetric surveys undertaken in the 2009 summer. An example of two of the bathymetric transects undertaken in Clatsop County is presented in **Figure 3-18**.

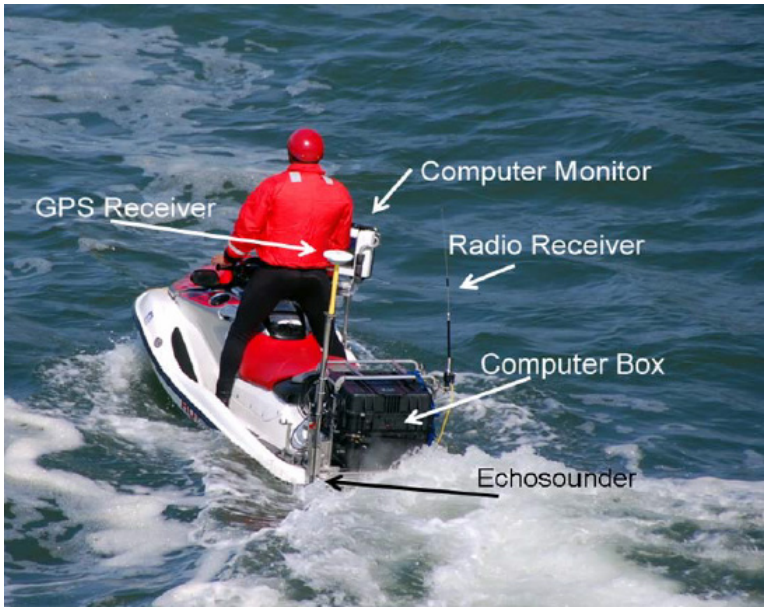

Figure 3-16. Data acquisition boat and onboard equipment (photo: courtesy of P. Ruggiero, OSU).

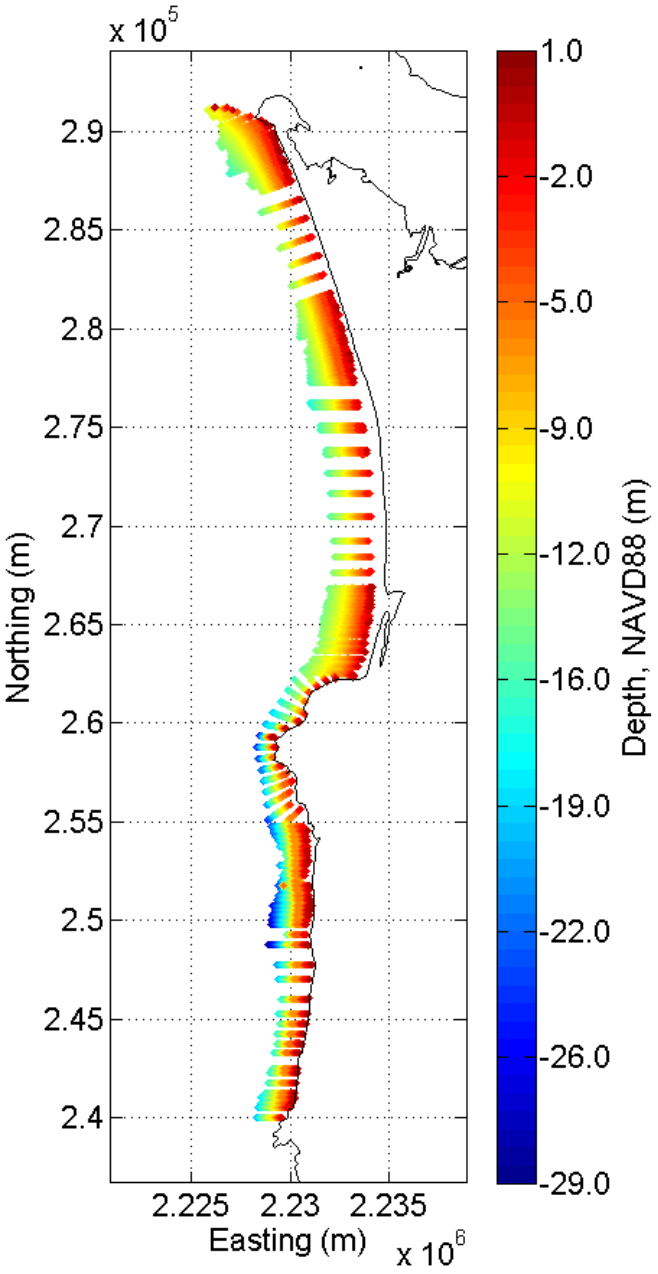

Figure 3-17. Collected bathymetry transects measured offshore the coast of the north Umpqua Spit near Winchester Bay, Oregon.

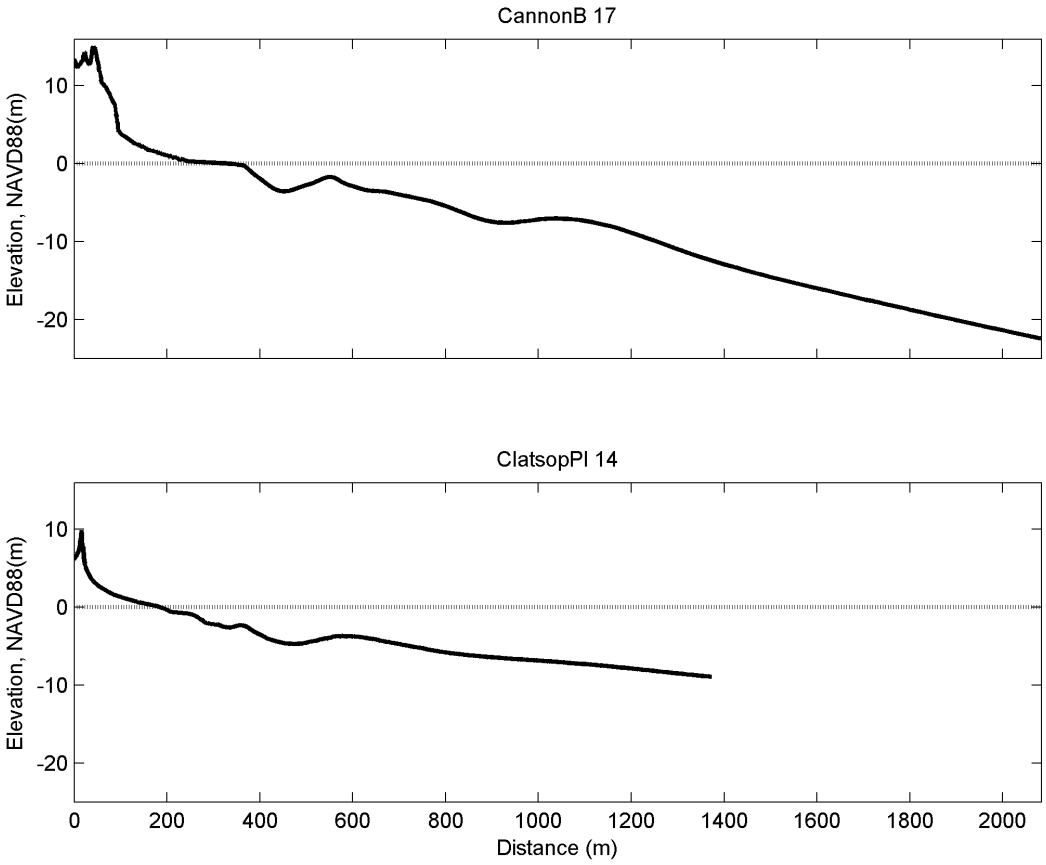

Figure 3-18. Combined topographic and bathymetric cross-shore transects measured offshore from Cannon Beach and near the tip of the Clatsop Plains showing the presence of multiple sand bars. Note the contrasting nearshore slopes between the two sites, with steeper topography observed at Cannon beach and wider shallower topography offshore the tip of Clatsop Spit.

4.0 TIDES

Measurements of tides on the Oregon coast are available from various tide gauges operated by NOS (http://www.tidesandcurrents.noaa.gov/map/index.shtml?type=PreliminaryData&region=Oregon). Hourly tidal records are available from the following coastal sites (**Table 4-1**): Willapa Bay, Washington (Toke Point, #9440910), the Columbia River (Astoria, #9439040), Tillamook Bay (Garibaldi, #9437540), Newport (South Beach, #9435380), Coos Bay (Charleston, #9432780) and at Port Orford (#9431647) on the southern Oregon coast. Long-term tidal records are also available from the Crescent City tide gauge (#9419750), located in northern California. In addition to the above, hourly tide data are also available at a site near Hammond, located close to the mouth of the Columbia River. This latter site is operated by the Center for Coastal Margin Observation & Prediction and has been in operation now for several years. (Recently [April 2011], NOS installed a new tide gauge at Hammond. The NOS gauge was not examined here.) The objective of this section is to establish which tide gauge would be most appropriate in applications directed toward FEMA wave and total water level analyses for the Clatsop Coast. Results presented here will also help guide future TWL analyses scheduled for Tillamook and Lincoln Counties.

The eight tide gauges, including their available records, in this region are listed in **Table 4-1**. **Figure 4-1** maps the locations of the most pertinent tide gauges present on the central to northern Oregon coast, along with the locations of various wave buoys operated by the National Data Buoy Center (NDBC) and the Coastal Data Information Program (CDIP), and Global Reanalysis of Ocean Waves (GROW) Fine Northeast Pacific wave hindcast data. These latter stations are pertinent to discussions of the wave climate and modeling described in Section 5, and ultimately in calculations of wave runup and overtopping.

As can be seen in **Table 4-1**, a number of the gauges have long records (30+ years) suitable for coastal flood analyses. The longest tide-gauge records (87 and 80 years, respectively) are from Astoria (AST), located 23.5 km up-channel from the mouth of the Columbia River, and at Crescent City (CC) in northern California. The South Beach (SB) and Toke Point (TP) gauges have moderately long records on the order of 45 and 43 years, respectively (**Table** 4-1); the SB gauge is located within Yaquina Bay, about 2 km from the open coast, and the TP gauge is close to the mouth of Willapa Bay. The shortest records (about 6 years), are those for Garibaldi (GB), located near the mouth of Tillamook Bay, and Hammond (HM), located approximately 7 km from the mouth of the Columbia River. All hourly tide data were purchased from NOS and were processed using various scripts developed in MATLAB. In addition to the measured tides, hourly tide predictions were calculated for all years using NOS tide prediction program, NTP4.

Table 4-1. Pacific Northwest NOAA tide gauges. Note the Hammond tide gauge is operated and maintained by CMOP (OHSU).

Gauge Site	Gauge Location	Record Interval	Years
Washington			
Toke Point (TP)	Willapa Bay, near the inlet mouth	Oct. 1968 – present	43.6
Oregon			
Astoria (AST)	Astoria	Feb.1925 – present	*87.2*
Hammond (HM)	Hammond, near the inlet mouth	Feb. 2006 – present	6.2
Garibaldi (GB)	Tillamook Bay, near the inlet mouth	July 2005 – present	6.8
South Beach (SB)	Yaquina Bay, near the inlet mouth	Feb. 1967 – present	*45.2*
Charleston (CH)	Coos Bay, near the inlet mouth	Apr. 1970 – present	*42*
Port Orford (PO)	Port Orford, open coast harbor	Oct. 1977 – present	*34.6*
California			
Crescent City (CC)	Crescent City, open coast harbor	Sep. 1933 – present	*79.4*

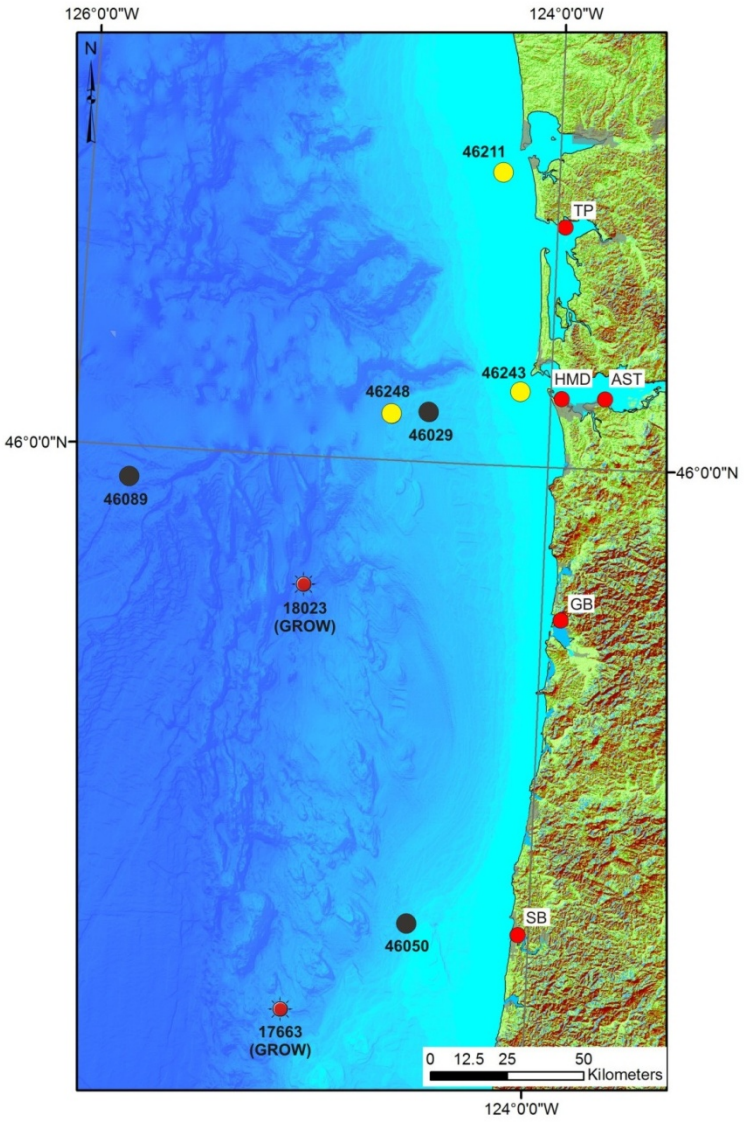

Figure 4-1. Location map of NDBC (black) and CDIP (yellow) wave buoys, tide gauges (red) and GROW wave hindcast stations (red suns). NDBC is National Data Buoy Center of NOAA and CDIP the Coastal Data Information Program (CDIP) of Scripps Institution of Oceanography. Note: NDBC Buoy #46005 referenced in this report is located 540 km (335 mi) west of the Columbia River mouth.

4.1 Tide Characteristics on the Central to Northern Oregon Coast

Tides along the Oregon coast are classified as moderate, with a maximum range of up to 4.3 m (14 ft) and an average range of about 1.8 m (6 ft) (Komar, 1997). There are two highs and two lows each day, with successive highs (or lows) usually having markedly different levels. Tidal elevations are given in reference to the mean of the lower low water levels (MLLW), and can be easily adjusted to the NAVD88 vertical datum (MLLW to NAVD88 conversions may be performed using values provided for a specific tide gauge by the NOS or by using the VDATUM [http://vdatum.noaa.gov/] tool developed by NOAA..) As a result, most tidal elevations are positive numbers with only the most extreme lower lows having negative values.

Initial analyses of the measured tides focused on developing empirical probability density function (PDF) plots of the measured tidal elevations for each of the tide gauges located between Newport, Oregon and Willapa Bay, Washington. The objective here is to assess the measured tides along the Oregon/Southwest Washington coast in order to identify any significant characteristics (including differences) between the gauges. **Figure 4-2** presents a series of PDF plots from each of the gauges. Because the gauges are characterized by varying record lengths, we have initially truncated the analyzed data to the period 2006 to 2011, when measurements were available from all five gauges.

As seen in the top plot of **Figure 4-2**, the gauges can be broadly characterized into two distinct regions. Those along the central and northern Oregon coast (SB and GB) indicate a slightly higher incidence of water levels between ~1.25 m and 2.25 m (4.1-7.4 ft, i.e., MSL to MHW). In contrast, the AST, HM, and TP gauges located in the Columbia River and in southern Washington indicate a lower incidence of water levels in that same range. These differences are probably related to a combination of effects associated with the regional oceanography (upwelling, shelf currents, and Coriolis effects that deflect the currents toward the coast), and effects from the Columbia River plume (Legaard and Thomas, 2006). The lower plot in **Figure 4-2** shows the same PDF, but now clipped to span tidal elevations between 2 and 4 m (6.5 to 13 ft). On the basis of this latter plot, the higher water levels characteristic of TP clearly stand out. In terms of determining ultimately which tide gauge on which to base the still water level time series, these initial results strongly suggest that we can effectively rule out Toke Point as a candidate site, as it consistently yields much higher water levels and surges (described later), which are probably a function of its location at the mouth of a broad inlet and the potential for additional wind setup along the length of the bay. At the high water level end of the plot, differences between the four remaining gauges are relatively minor.

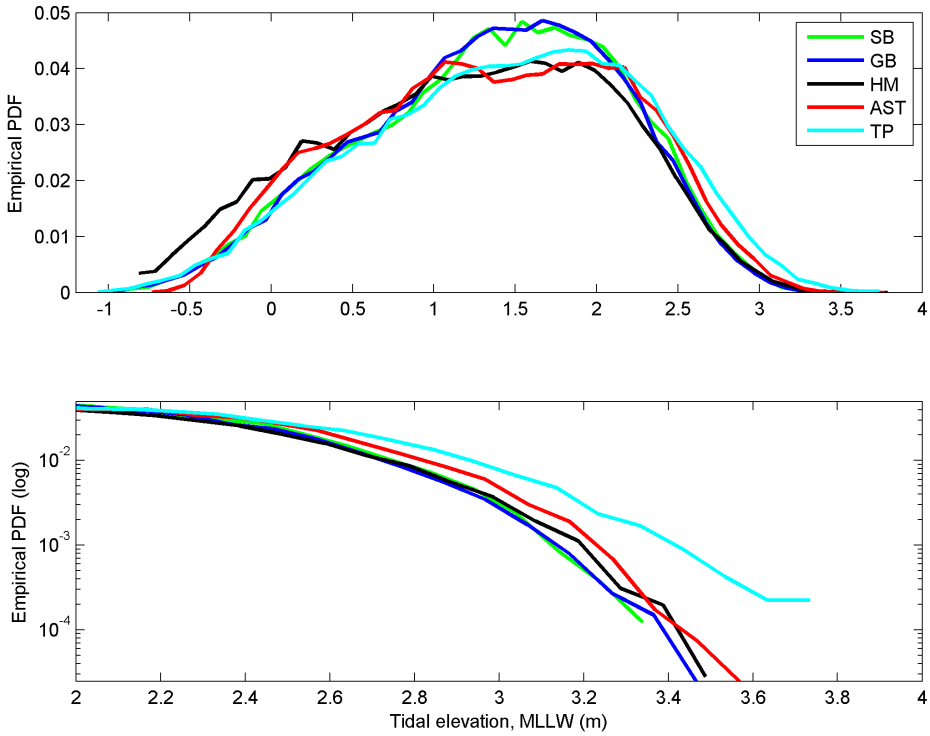

Figure 4-2. Empirical probability density function plots for various tide gauges for overlapping years of data (2006–2011). Top) probability density function plots showing the complete range of tidal elevations, Bottom) truncated to higher water levels.

Figure 4-3 is broadly similar to **Figure 4-2**, with the exception that the PDFs now include the complete time series of data measured by the respective tide gauges. In this latter plot we have excluded the HM tide gauge due to its short record, and Toke Point due to its unique site within the mouth of Willapa Bay. In general, the AST gauge is characterized by a higher incidence of water levels between about −0.18 and 1.0 m (−0.6 to 3.3 ft), and again between 2.1 and 3.5 m (6.9 to 11.5 ft). This contrasts with the SB and GB gauges, which show a higher incidence of water levels between ~1.0 and 2.0 m (3.3 to 6.6 ft). As noted previously, these differences are probably caused by regional oceanographic factors. Detailed examination of the hourly tides indicate that the higher incidence of AST water levels in the wings of the PDF reflect the fact that both the Higher Highs and Lower Highs are greatest at AST when compared with SB and GB, while the Lower Lows and Higher Lows are generally lower at AST compared with SB and GB.

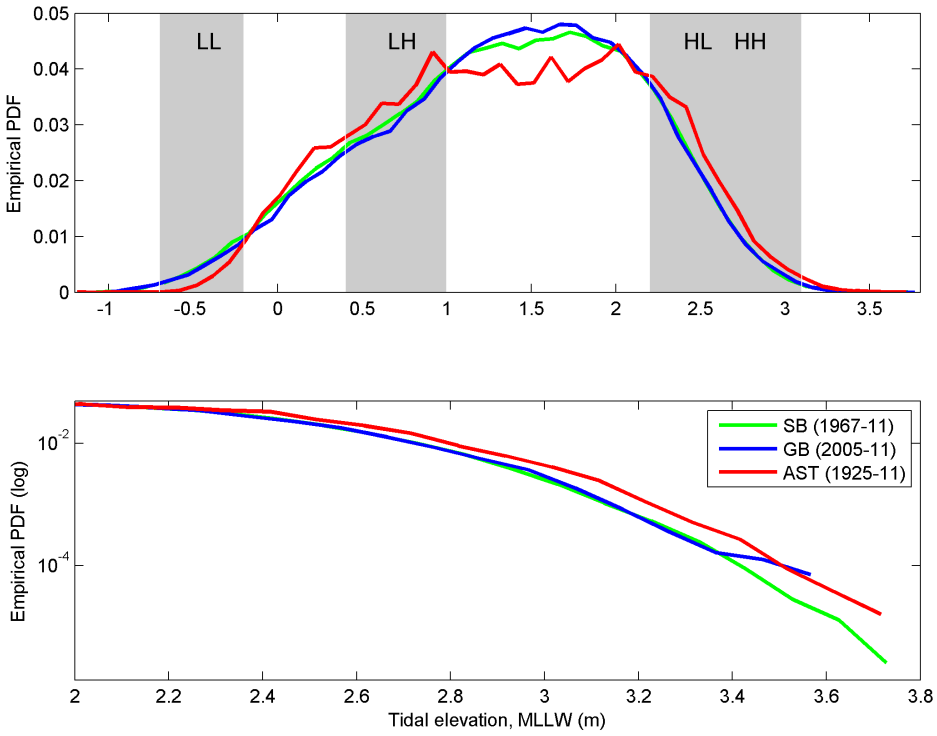

Figure 4-3. Empirical PDFs for SB, GB, and AST based on all available data. Top) probability density function (PDF) plot showing the complete range of tidal elevations. LL, LH, HL, and HH denote the Lower Lows, Lower Highs, Higher Lows and Higher Highs in the tide data. Bottom) PDF truncated to higher water levels.

At the extreme high end of the complete PDF plots (**Figure 4-3**), the highest water levels measured at AST, GB and SB are, respectively, 3.76, 3.62, 3.71 m (12.3, 11.9, 12.2 ft). These results equate to a difference of 0.05 m (0.16 ft) between AST and SB and 0.14 m (0.46 ft) between AST and GB, while indicating the absence of any real latitudinal trend with the extreme water levels. Furthermore, differences between these values and those reported by NOS for the respective stations differ by no more than 2 cm. The larger difference between the GB and AST gauges when compared with the SB gauge is entirely due to the shortness of the Garibaldi measurement record (~6 years). Overall, the relative consistency in the PDF plots generated for each gauge, particularly at the more extreme end of the measured water levels, is indicative of the areal impact of major North Pacific extratropical storms, which can affect stretches of coast up to 1,500 km in length (932 mi, i.e., 3 times the length of the Oregon coast) (Davis and Dolan, 1993; Allan and Komar, 2002).

4.2 Seasonal Changes

Figure 4-4 presents a plot of the characteristic seasonal cycles determined for the three gauges, AST, GB, and SB, to further examine their consistencies. All three gauges depict the typical seasonal cycle that reflects the combination of ocean upwelling effects along the coast, and seasonal reversals in the California current system. The Astoria gauge has been divided into two time periods that reflect conditions prior to Columbia River dam control (~ mid 1960s, dotted line), and post dam conditions (solid black line). The reason for the latter is that the AST gauge exhibits seasonal characteristics that are not apparent

in the other coastal tide gauges (including TP), that is entirely a function of Columbia River discharge flows (Sherwood and others, 1990; Burgette and others, 2009).

Prior to dam and irrigation control on the Columbia River, the seasonal cycle at the AST tide gauge was characterized by generally higher monthly mean sea levels in May through June (**Figure 4-4**), decreasing to a minimum between August and September. Between September and February, the ocean water levels increase reaching peaks in December and February. The high mean monthly sea levels observed between May and July are entirely due to the occurrence of spring freshets (i.e., high discharge flows due to spring snow melt (Sherwood and others, 1990)).

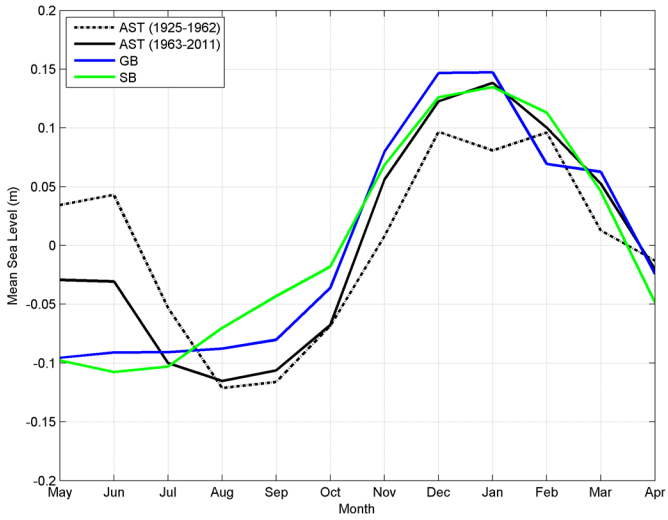

Figure 4-4. Seasonal plot of tides along the central to northern Oregon coast.

Following dam control, the incidence of high mean sea levels during spring at the AST tide gauge is clearly reduced (**Figure 4-4**), while the timing of these events remains essentially unchanged although the period of higher spring mean sea levels has in fact been shortened slightly by about 1 month. In contrast, the seasonal pattern between October and March is essentially the same for AST as it is for SB and GB, with all three sites experiencing peak water levels in January, while the broad shape of the curve is effectively the same. As noted by Sherwood and others (1999), with the introduction of river control on the Columbia River in the mid-1960s for the purposes of flood control and for irrigation use, the incidence of spring freshets were reduced by up to 40% compared with the natural regime. This change is captured in **Figure 4-4** by the marked drop in monthly mean sea levels observed from May to July. Interestingly, under conditions today there is essentially little difference in the seasonal water levels between the three gauges during the critical winter period (October to March) when storms are affecting this northern part of the Oregon coast.

Finally, although not shown in **Figure 4-4**, all the tide gauges are strongly influenced by the El Niño Southern Oscillation phenomena, which periodically causes mean sea levels along the U.S. West Coast to increase (Komar and others, 2011). This response is due to an intensification of the processes, especially enhanced ocean sea surface temperatures offshore from the Oregon coast. This occurred particularly during the unusually strong 1982-83 and 1997-98 El Niños, whereby mean sea levels increased by approximately 20–25 cm (~0.8 ft) above the normal seasonal

cycle in mean sea level depicted in **Figure 4-4** (i.e., for a total mean sea level rise of up to 50 cm [1.6 ft] relative to the preceding summer). As a result, under these latter conditions wave swash processes are able to reach to much higher elevations on the beach, potentially eroding dunes and bluffs.

4.3 Oregon Storm Surges

The actual level of the measured tide can be considerably higher than the predicted tides provided in standard Tide Tables, and is a function of a variety of atmospheric and oceanographic forces, which ultimately combine to raise the mean elevation of the sea. These latter processes also vary over a wide range of timescales, and may have quite different effects on the coastal environment. For example, strong onshore winds coupled with the extreme low atmospheric pressures associated with a major storm can cause the water surface to be locally raised along the shore as a storm surge, and have been found in tide-gauge measurements to be as much as 1.5 m (4.9 ft) along the Pacific Northwest coast (Allan and Komar, 2002). However, during the summer months these processes can be essentially ignored due to the absence of major storms systems.

Analyses have been undertaken to examine the non-tidal residuals and ultimately the storm surges identified at the various tide gauges on the northern Oregon coast. The objective of this analysis is to provide a better understanding of the spatial and temporal variability of storms as they track across the North Pacific, the magnitudes (and frequency) of the surges, and the potential differences in the non-tidal residuals between the gauges due to variations in the storms tracks, barometric pressures and winds. This last point is particularly important in terms of finalizing the tide gauge time series to be used in the Clatsop total water level analyses.

For the PNW, the measured water level (h_t) at a particular tide gauge is given by the following relationship:

$$h_t(t) = z_o + X_{at}(t) + X_{oc}(t) + S(t) \qquad \text{(Eq. 4-1)}$$

where z_o is the mean water level, X_{at} is the predicted astronomical tide, X_{oc} is the altered mean water level due to ocean processes (water temperatures, currents and El Niño "sea level" waves), and S is the contribution by the storm surge at time t. The predicted astronomical tide for the specific tide gauge is calculated by using its harmonic constituents:

$$x_t = \sum_{i=1}^{M} H_i \cos(\sigma_i t + \varphi_i) \qquad \text{(Eq. 4-2)}$$

where H_i is the amplitude of the constituent i, σ_i is its frequency, and φ_i the phase of the constituent, M being the number of tidal constituents included in the analysis.

4.4 Non-Tidal Residual Analyses

The procedures used to analyze the non-tidal residuals and storm surge incidence follow those developed by Allan and others (2011), which used a harmonic analysis method of least squares (HAMELS) approach developed in MATLAB to estimate the amplitude and phase for any set of tidal constituents at each of the tide gauge sites (Boon, 2004). The purpose here is to develop a predicted time series of the water levels produced entirely by astronomic forces that excludes the seasonal component produced by oceanographic processes on the West Coast; the seasonal component can be integrated into tide predictions through the solar annual (Sa) and solar semiannual (Ssa) tide and is integrated as an *average term* in the predicted tides provide by NOS.

HAMELS analyses of tide gauge data have previously been completed for the SB and TP tide gauges (Allan and others, 2011). Thus, similar analyses were undertaken using the AST and GB tide gauges. The specific steps included the following:

- HAMELS was used to derive an estimate of the amplitude and phase for the tidal constituents. This was initially done using just a spring/summer data set for testing purposes and then expanded to the full year of data;

- Having determined the tidal constituents, HAMELS was used to derive the astronomic tide predictions for the entire record on a year-by-year basis (eliminates any long-term trend). The non-tidal residuals (NTRs) were calculated by subtracting the astronomic tide from the measured tides;
- The NTR time series were then filtered using a moving average filter (averaged over ±30 days) with zero phase shift, and the seasonal cycle was removed from the NTRs;
- The winter standard deviation was calculated and those events exceeding 2*σ were used to define individual surge events (Zhang and others, 2001).

Figure 4-5 presents a plot of the derived NTRs for the South Beach (SB), Garibaldi (GB), and Astoria (AST) tide gauges. These data reflect the corresponding NTRs associated with the Higher Highs and Higher Lows of the diurnal tidal cycle, which were determined using a peak detection algorithm in MATLAB. Analyses here span the period of record for the respective tide gauges. Correlation (R^2) values calculated for the three plots are 0.91, 0.69, and 0.79, respectively, with the strongest correlation found between the SB and GB tide gauges on the open coast, while the weakest correlation was between the SB and the AST tide gauges.

Figure 4-6 presents the actual time series of deseasoned NTRs derived for the SB, GB, and AST tide gauges for the 2005-06 winter. In this example, the NTRs have been time adjusted to a single station. As can be seen in this example, the SB and GB tide gauges tends to track very closely to each other, consistently capturing the same peaks and troughs. In contrast, the AST gauge shows larger fluctuations, when compared to the other tide gauges. These differences are further highlighted in the anomaly plot (**Figure 4-6** bottom), which indicates more subtle differences between SB and GB tide gauges, with both gauges characterized by anomalies that reach as much as 0.2 m (0.65 ft). In contrast, anomalies between the GB and AST tide gauges reveal much larger differences. While differences here to a large degree reflect differences in the position of the storms relative to the tide gauges, the storm's barometric pressures, winds, and the associated wave forcing along the coast, the fluctuations shown for the AST gauge suggest that other factors (e.g., Columbia River discharge) may be exerting as strong influence on the observed patterns between GB and AST. Overall, differences between the SB and GB tide gauges probably reflect mostly subtle shifts in the timing of the events as they impact the coast, reinforcing our confidence that the effects of North Pacific extratropical storms are indeed widespread, affecting large tracts of the coast at similar times.

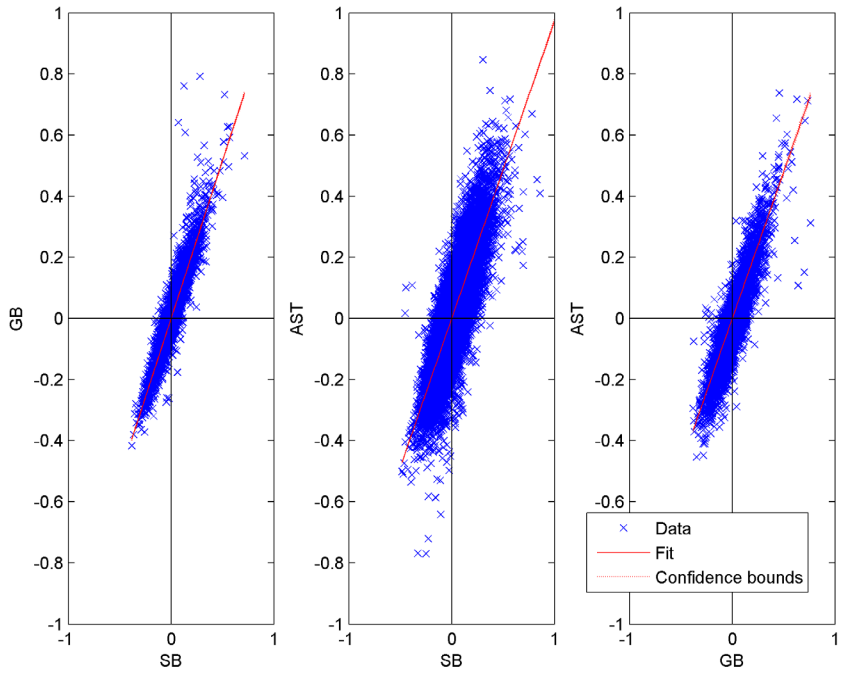

Figure 4-5. Comparison of non-tidal residuals determined for SB versus GB, SB versus AST, and GB versus AST tide gauges. Values plotted here reflect the daily peak values.

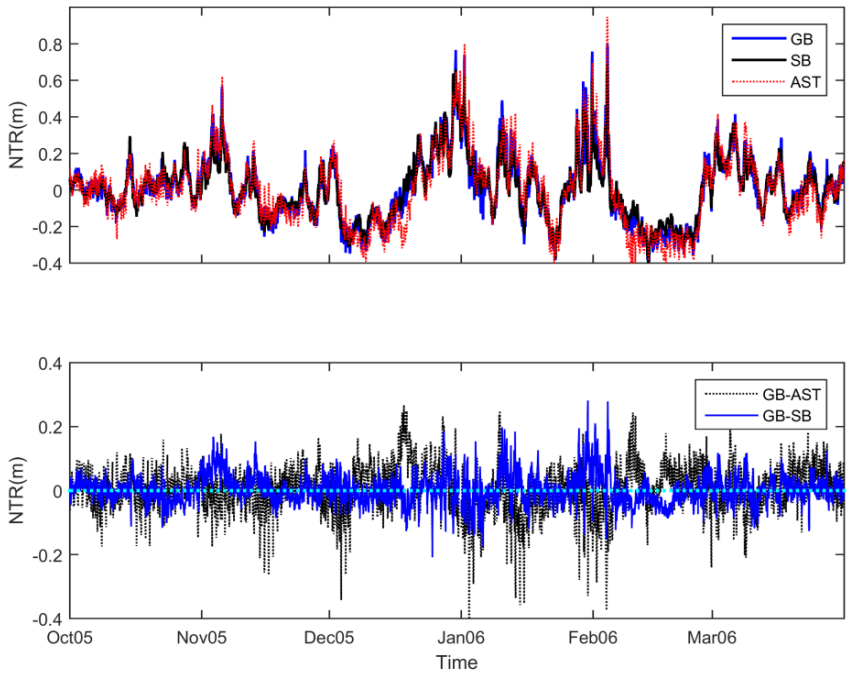

Figure 4-6. Top) Comparison of non-tidal residuals (NTR) and bottom) Differences between the SB, GB, and AST tide gauges for the 2005-06 winter.

Having identified the NTRs for each of the tide gauges, individual storm surge events have been identified following the procedures of Zhang and others (2001) and Allan and others (2011). **Figure 4-7** (left) presents a log number plot of all surge events for SB, GB, and AST gauges; here we include similar analyses performed on the TP tide gauge. The plot indicates that for the most part the four gauges are showing relatively similar patterns in terms of the storm surge magnitudes. In general, the mean storm surges increase northward (0.45 m [1.5 ft] at SB to 0.66 m [2.2 ft] at TP), while the highest surges have occurred at TP (1.62 m [5.3 ft]) and SB [1.42 m [4.7 ft]); despite its significantly longer record, the highest surge observed at AST reached 1.1 m (3.6 ft). **Figure 4-7** (right) presents the empirical CDF calculated for the four gauges, further highlighting the progressive shift in the surge magnitudes to the north. Again, the TP gauge stands out as an exception, further confirming why this site should be excluded as the time series of water levels for the Clatsop coast.

Taken together, these analyses confirm that the two open coast tide gauges located in Newport on the central Oregon coast and at Garibaldi in Tillamook Bay, overall provide the best measure of the open-coast still water levels, important in FEMA total water level and overtopping analyses. The main distinction between these two stations is the length of available measurements, with the Newport site having the longest record (~45 years), and Garibaldi having the shortest. Furthermore, based on our analyses, we believe that the measured tides at Astoria (located 23 km upriver from the coast), is significantly influenced by Columbia River flows that it should not be used in FEMA flood analyses for the Clatsop County open coast.

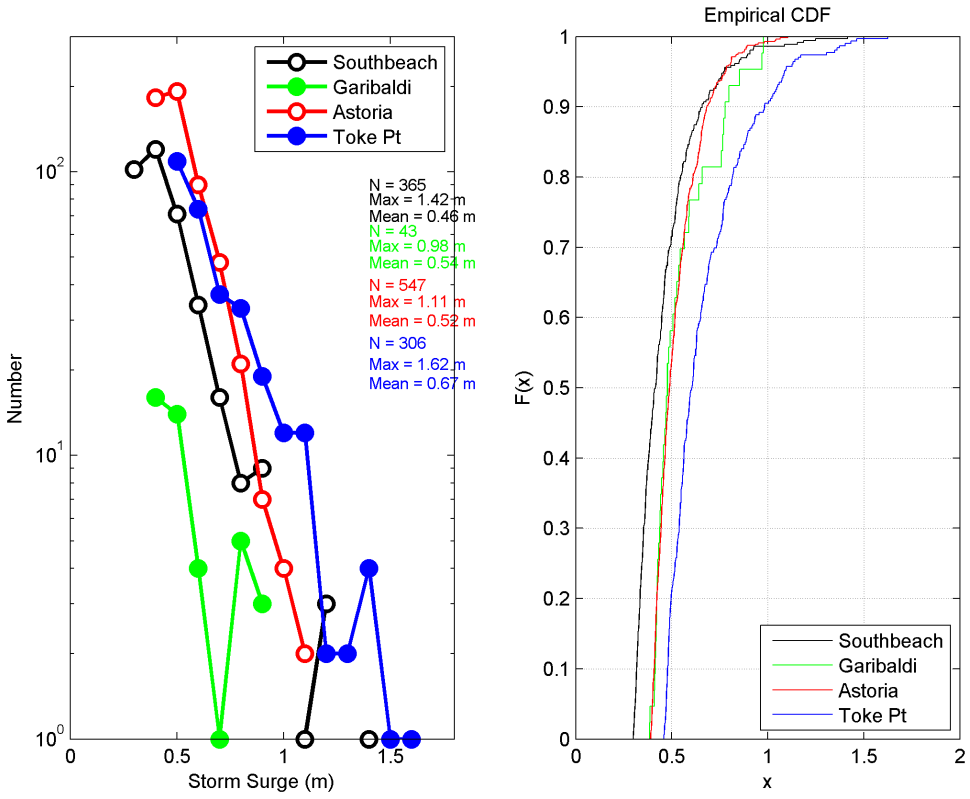

Figure 4-7. Plot of non-tidal residuals (NTR) anomalies calculated from the difference between AST and SB NTRs.

4.5 Clatsop County Tides

For the purposes of this study, we have based our *still water level* (SWL) and *wave runup* calculations on a combined time series that encompasses tides measured at the South Beach gauge (#9435380) in Yaquina Bay (1967-2005), and from the Garibaldi tide gauge (#9437540) in Tillamook Bay (2005-present), for a combined time series of 1967–2011. **Figure 4-8** shows the tidal elevation statistics derived from the South Beach tide gauge (the longest temporal record), with a mean range of 1.91 m (6.3 ft) and a diurnal range of 2.54 m (8.3 ft). The highest tide measured from this record reached 3.73 m (12.2 ft), recorded in December 1969 during a major storm. These values are comparable to those measured at the Garibaldi site (mean = 1.9 m, diurnal = 2.53 m), with the only real difference being the fact that this latter gauge recorded a peak water level of 3.64 m (11.9 ft) in December 2005 due to its shorter record.

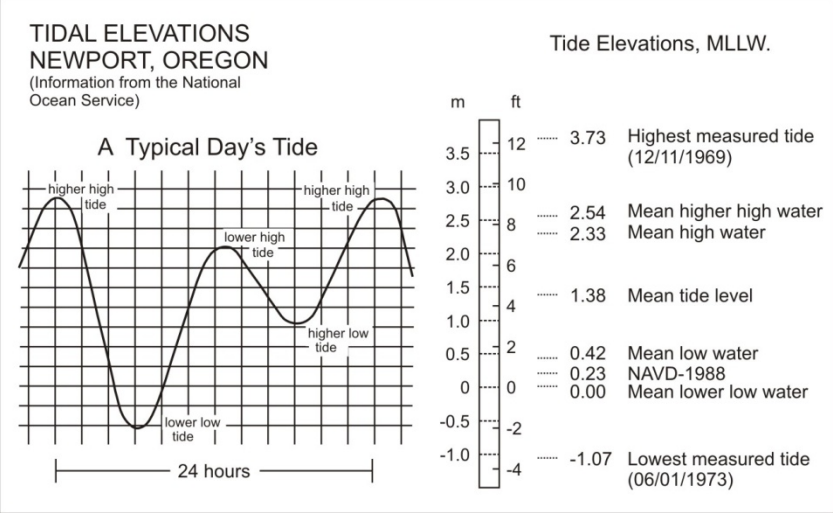

Figure 4-8. Daily tidal elevations measured at South Beach, Newport on the central Oregon coast. Data from NOS (http://www.co-ops.nos.noaa.gov/waterlevels.html?id=9435380).

As noted previously, tides on the Oregon coast tend to be enhanced during the winter months due to warmer water temperatures and the presence of northward flowing ocean currents that raise water levels along the shore, persisting throughout the winter rather than lasting for only a couple of days as is the case for a storm surge. This effect can be seen in the monthly averaged water levels derived from the combined time series (**Figure 4-9**), but where the averaging process has removed the water-level variations of the tides, yielding a mean water level for the entire month. Based on 45 years of data, the results in **Figure 4-9** show that on average monthly-mean water levels during the winter are nearly 25 cm (0.8 ft) higher than in the summer. Water levels are most extreme during El Niño events, due to an intensification of the processes, largely enhanced ocean sea surface temperatures offshore from the Oregon coast. This occurred particularly during the unusually strong 1982-83 and 1997-98 El Niños. As seen in **Figure 4-9**, water levels during those climate events were approximately 25–30 cm (0.8–1 ft) higher than the seasonal peak, and as much as 56 cm (1.8 ft) higher than during the preceding summer, enabling wave swash processes to reach much higher elevations on the beach during the winter months, with storm surges potentially raising the water levels still further.

Aside from seasonal to interannual effects of climate events on ocean water levels, also of interest are the long-term trends associated with relative sea level changes due to climate change along the Clatsop County coastline. **Figure 4-10** presents results from an analysis of the combined SB/GB time series based on a separate analysis of the summer and winter tide levels. For our purposes, "winter" is defined as the combined average tide level measured over a three-month period around the peak of the seasonal maximum in winter water levels, typically the months of December through February. Similarly, "summer" water levels reflect the combined average tide level measured over a three-month period around the seasonal minimum, typically the months between May through July when water levels also tend to be less variable (Komar and others, 2011). As observed previously in **Figure 4-9**, the winter tidal elevations are systematically displaced upward by about 25 cm (0.8 ft) above the summer, with the difference between the regression lines reflecting the seasonal change in ocean water levels from summer to winter. **Figure 4-10** also emphasizes the extremes associated with major El Niños, with the peaks between the 1983 and 1997 major events having been systematically shifted upward over the years due to relative sea level changes along this particular section of the coast. In contrast, the summer regression line is characterized by significantly less scatter in the residuals because it effectively excludes the influence of storms and El Niños that are dominant during the winter. With this approach, it can be seen that the central Oregon coast is slowly being transgressed at a rate of ~1.29 ± 0.89 $mm.yr^{-1}$, and is slightly lower than that reported by NOS (~2.18 ±0.85 $mm.yr^{-1}$). This difference is due to the SB tide gauge having been affected by localized subsidence, particularly in the late 1960s/early 1970s that has continued to decrease over time up until the mid 1990s (Burgette and others, 2009). Since then, repeat surveys of NGS benchmark indicate that the land appears to be now stable.

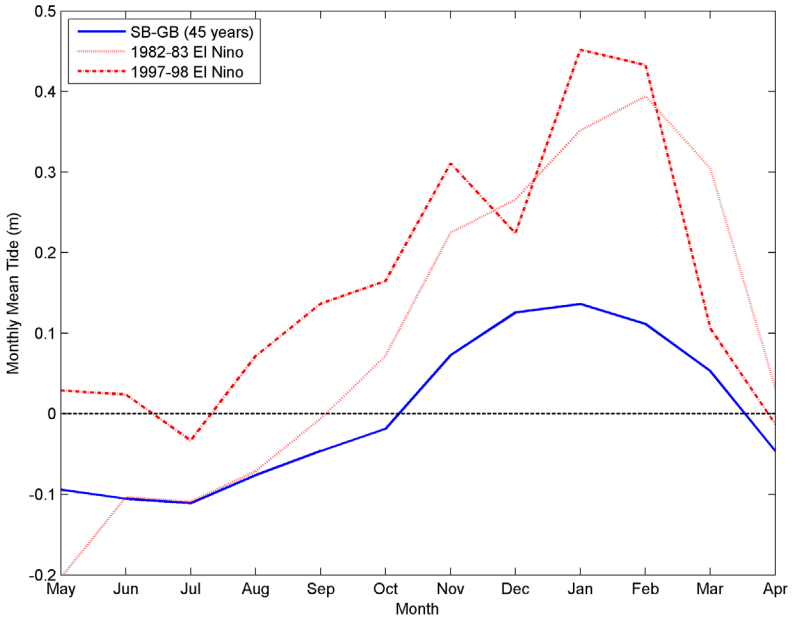

Figure 4-9. Seasonal cycles in monthly-mean water levels based on data from the combined South Beach/Garibaldi measured tides.

Finally, it is important to appreciate that the trends shown in **Figure 4-10** reflect relative sea level changes due to the fact that the PNW coast of Oregon and Washington is locally influenced by changes in the elevation of the land due to regional tectonics as well as by the global rise in sea level, with the net change being important to both coastal erosion and flood hazards. **Figure 4-11** presents a synthesis of both tectonic land elevation changes and sea level trends derived for multiple stations along the PNW coast (Komar and others, 2011), correlated against differential surveys of first-order NGS benchmarks (e.g., Burgette and others, 2009), and GPS CORS stations. Results here indicate that in general the southern Oregon coast is an emergent coast with tectonic uplift of the land outpacing sea level rise. In contrast the central to northern Oregon coast is slowly being transgressed by sea level. In the far north in Clatsop County, the overall pattern suggests that this portion of the coast varies from slight submergence in the southern County to emergent in the north along the Clatsop Plains.

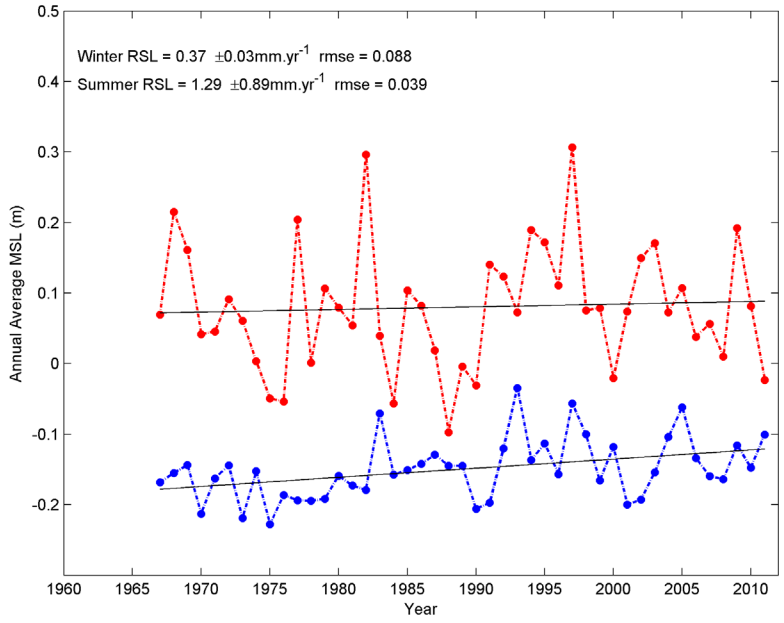

Figure 4-10. The trends of "winter" (red) and "summer" (blue) mean sea levels measured by the SB/GB tide gauges. Results for the summer regression are statistically significant, while the estimated winter rate is not significant at the 95% confidence level.

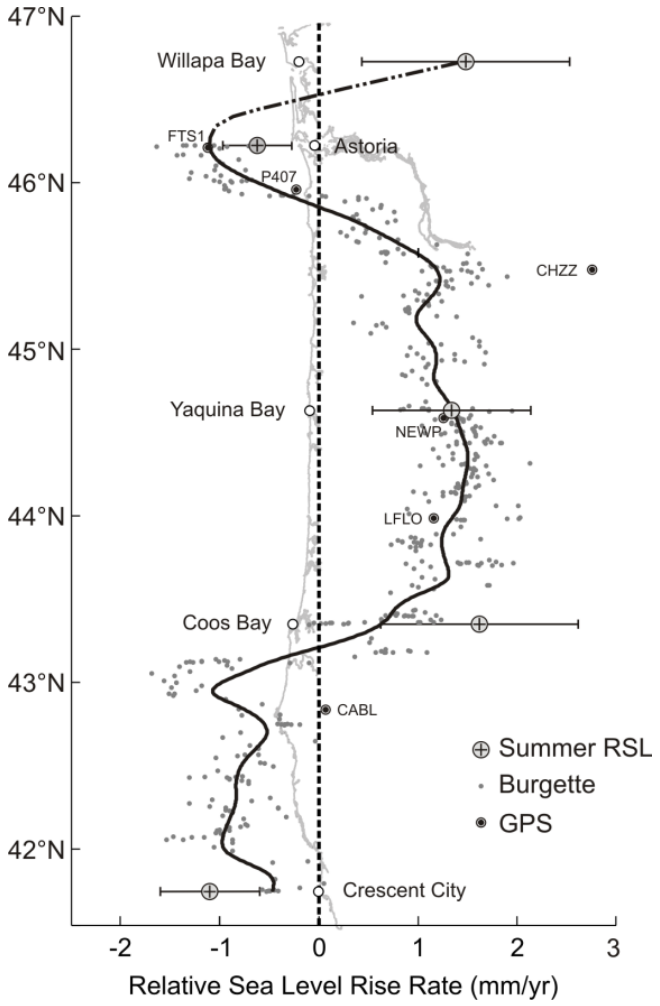

Figure 4-11. Assessments of changes in RSLs based on tide gauge records compared with benchmark and GPS measurements of land-elevation changes, with their corresponding RSL rates obtained by adding the 2.28 mm/yr PNW eustatic rise in sea level (Komar and others, 2011).

4.6 Still Water Level (SWL)

The still water level (SWL) is the sum of the predicted astronomical tide listed in Tide Tables, plus the effects of processes such as an El Niño or storm surge that can elevate the measured tide above the predicted tide (Northwest Hydraulic Consultants, 2005). Of importance to erosion and flooding hazards are the extremes of the measured tides. In conventional analyses of extreme values, the general assumption is that the data being analyzed (e.g., the annual maxima) represent independent and identically distributed (stationary) sequences of random variables. The generalized extreme value (GEV) family of distributions is the cornerstone of extreme value theory, in which the cumulative distribution function is given as:

$$G(z, \mu, \sigma, \xi) = \exp\left\{-\left[1 + \xi\left(\frac{z-\mu}{\sigma}\right)\right]^{-1/\xi}\right\} \qquad (4.3)$$

defined on

$$\left\{z: 1 + \frac{\xi(z-\mu)}{\sigma} > 0\right\},$$

where the parameters satisfy $-\infty < \mu < \infty$, $\sigma > 0$, $-\infty < \xi < \infty$ (Coles, 2001). The model has three parameters; μ is a location parameter, σ is a scale parameter, and ξ is a shape parameter. The EV-II (Frechet) and EV-III (Weibull) classes of extreme value distributions correspond respectively to the cases of $\xi > 0$ and $\xi < 0$. When $\xi = 0$, equation 4.3, collapses to the Gumbel or EV-I type extreme value distribution. By inferring the shape parameter ξ (estimated here, along with the other parameters, by maximizing the log-likelihood function), the data themselves determine the most appropriate type of tail behavior and it is not necessary to make an a priori assumption about which individual extreme family to adopt as in a classical Weibull-type extreme wave height analysis (Coles, 2001).

The GEV is often applied to annual maxima data in an approach referred to as the annual maximum method (AMM). However, one of the primary shortcomings of fitting an extreme-value distribution with annual maximum data is that useful information about the extremes is inherently discarded, particularly when data are sampled on either a daily or hourly basis (as in the case of the measured tides and deep-water significant wave heights measured by the Oregon tide gauges and NDBC wave buoys). Two well known approaches exist for characterizing extremes by utilizing data other than simply annual (block) maxima. The first is based on the behavior of the r-largest-order statistics within a block, for low r, and the second is based on exceedances above a high threshold value. For the purposes of this study, we use the peak-over-threshold (POT) approach for determining the extreme SWL and wave heights.

In the peak-over-threshold (POT) method, a high threshold, u, is chosen in which the statistical properties of all exceedances over u and the amounts by which the threshold is exceeded are analyzed. It is assumed that the number of exceedances in a given year follows a Poisson distribution with annual mean νT, where ν is the event rate and T = 1 year, and that the threshold excesses $y > 0$ are modeled using the Generalized Pareto Distribution (GPD) given by:

$$H(y, \sigma, \xi) = 1\text{-}\left(1 + \frac{\xi y}{\sigma}\right)^{-1/\xi} \qquad \text{(Eq. 4-4)}$$

where ξ is the shape parameter of the GEV distribution and σ is a scale parameter related to GEV parameters by $\sigma = \sigma + \xi(u - \mu)$. The event rate can also be expressed in a form compatible with the GEV distribution provided that

$$\nu = (1 + \frac{\xi(u-\mu)}{\sigma})^{-1/\xi}.$$

Estimates of extreme quantiles of the distributions are obtained by inverting the distributions in equation 4.4. For GPD-Poisson analyses the N-year return level, y_N, is given as:

$$y_N = \mu + \frac{\sigma}{\xi}\left[(N n_y \zeta_u)^{\xi} - 1\right] \qquad \text{(Eq. 4-5)}$$

where n_y is the number of observations per year and ζ_u is the probability of an individual observation exceeding the threshold u.

Figure 4-12 presents results of the GEV analyses for the combined SB/GB measured tides. In constructing this plot, we used a threshold of 3.06 m (10 ft). Included in the figure are the calculated 1- through 500-year SWLs. As can be seen in **Figure 4-12**, the 1% SWL calculated for the combined time series is 3.71 m (12.2 ft, relative to MLLW). When adjusted to the NAVD88 vertical datum, this value becomes 3.60 m (11.8 ft, NAVD88); note the adjustment from NAVD88 to MLLW is calculated to be 0.108 m (0.35 ft) at the GB site. (The NAVD88 to MLLW adjustment at the GB site was calculated using the VDATUM tool developed by NOAA [http://vdatum.noaa.gov/]) The 500-year SWL is estimated to be 3.68 m (12.1 ft) relative to the NAVD88 vertical datum. As observed previously, the highest tide measured in the combined time series reached 3.62 m (11.9 ft, relative to NAVD88).

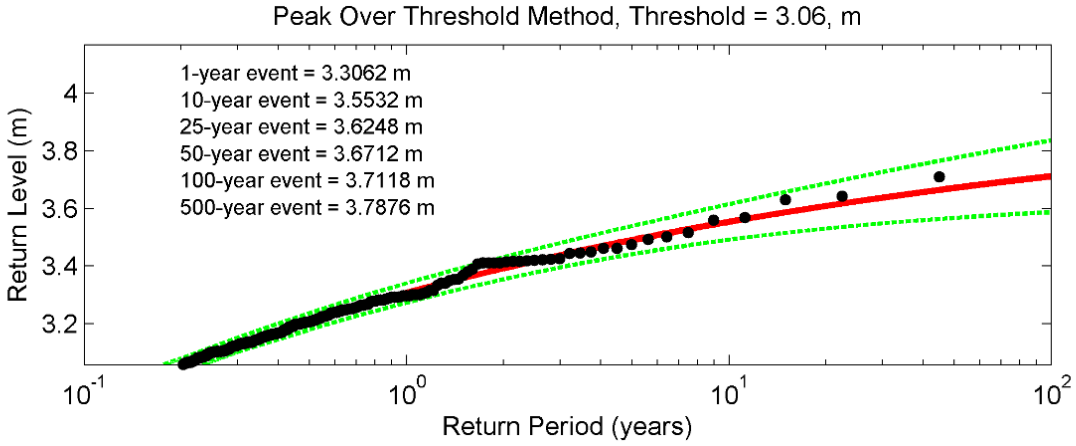

Figure 4-12. Extreme-value analyses of the still water level (SWL) determined for the combined South Beach/Garibaldi tide gauge time series. These data are relative to the MLLW vertical datum. Black dots reflect the discrete peak tidal events and the red line is the extreme value distribution fit to those data. Green dashed line reflects the 95% confidence boundary.

5.0 PACIFIC NORTHWEST WAVE CLIMATE

The wave climate offshore from the Oregon coast is one of the most extreme in the world, with winter storm waves regularly reaching heights in excess of several meters. This is because the storm systems emanating from the North Pacific travel over fetches that are typically a few thousand miles in length and are also characterized by strong winds, the two main factors that account for the development of large wave heights and long wave periods (Tillotson and Komar, 1997). These storm systems originate near Japan or off the Kamchatka Peninsula in Russia, and typically travel in a southeasterly direction across the North Pacific toward the Gulf of Alaska, eventually crossing the coasts of Oregon and Washington or along the shores of British Columbia in Canada (Allan and Komar, 2002).

Wave statistics (heights, periods, and more recently, wave direction) have been measured in the Eastern North Pacific using wave buoys and sensor arrays since the mid 1970s. These data have been collected by the National Data Buoy Center (NDBC) of NOAA and by the Coastal Data Information Program (CDIP) of Scripps Institution of Oceanography (**Figure 4-1**). The buoys cover the region between the Gulf of Alaska and Southern California and are located in both deep and intermediate to shallow water over the continental shelf. The NDBC operates some 30 stations along the West Coast of North America, while CDIP has at various times carried out wave measurements at 80 stations. Presently, there are two CDIP buoys operating offshore from the mouth of the Columbia River (#46243 and #46248) and three NDBC buoys (Washington [#46005], Tillamook [#46089], and Columbia River Bar [#46029]); note that buoy #46005 is located ~540 km (335 mi) directly west of the Columbia River mouth. Wave measurements by NDBC are obtained hourly (CDIP provides measurements every 30 minutes) and are transmitted via satellite to the laboratory for analysis of the wave energy spectra, significant wave heights, and peak spectral wave periods. These data can be obtained directly from the NDBC through their website (http://www.ndbc.noaa.gov/maps/Northwest.shtml).

An alternate source of wave data appropriate for FEMA flood modeling is hindcast wave data such as the Global Reanalysis of Ocean Waves Fine Northeast Pacific Hindcast (GROW-FINE NEPAC), purchased through Oceanweather, Inc., and Wave Information Studies (WIS; http://wis.usace.army.mil/) hindcasts developed by the USACE (Baird, 2005). GROW is a global wave model, while GROW Fine Northeast Pacific extends the original model by incorporating a higher-resolution analysis (4 times as many data nodes), basin-specific wind adjustments based on QUIKSCAT scatterometry, enhancements due to Southern Ocean swells, and inclusion of shallow water physics (Oceanweather Inc., 2010). These data can ultimately be applied to offshore structure design, tow-analysis, operability, and other applications where wind and wave data are required. Standard products from GROW include time series of wind and wave parameters (including sea/swell partitions), extreme criteria, operability statistics, and wave spectra (Oceanweather Inc., 2010). The advantage of GROW as opposed to measured data is that it provides a continuous time series of wave and wind data suitable for FEMA flood modeling. In contrast, measured data obtained from wave buoys may be characterized by significant data gaps due to the instruments having come off their mooring or from instrument failure. The main disadvantage of GROW Fine Northeast Pacific data is that the data are modeled based on basin-scale wind models and data, and the data time series is 3 hourly as opposed to hourly as provided by the buoys. For the purposes of this study, we have explored both data sets in order to define the most appropriate time series of wave data. To that end, GROW Fine Northeast Pacific data were purchased for three nodes offshore the Oregon coast. **Figure 4-1** identifies the location of two of the GROW sites, station #18023 located offshore from southern Clatsop /northern Tillamook County and #17663 offshore from Lincoln County. Besides the hourly measured wave buoy data, we obtained wave hindcast information on the deepwater wave climate deter-

mined through comparisons with the WIS station located adjacent to NDBC buoy 46005.

Analyses of the wave climate offshore from Clatsop County were undertaken by DOGAMI staff, and as a subcontract to Dr. Peter Ruggiero, College of Earth, Ocean, and Atmospheric Sciences (CEOAS), OSU, and included numerical analyses of the 1% or 100-year extreme total water levels, which reflect the calculated wave runup superimposed on the tidal level (i.e., the still water level [SWL]) to help determine the degree of coastal flood risk along the coast of Clatsop County.

OSU performed a series of tests and analyses including wave transformations, empirical wave runup modeling, and total water level modeling. For the purposes of this study, OSU used the SWAN (Simulating Waves Nearshore) wave model to transform deepwater waves to the nearshore (typically the 20 m (65.6 ft) contour). The transformed waves were then linearly shoaled back into deep water to derive a *refracted deepwater equivalent wave parameterization* (wave height and peak period) that can be used to calculate runup levels, which combined with tides, are used to estimate the flood risk along the county's shoreline.

In our Coos County FEMA study (Allan and others, 2012b), the approach we developed involved several stages:

1. A time series of deepwater wave heights and periods was first defined for a particular location offshore of the shelf break, which we used to calculate an initial wave runup and total water level time series based on two representative beach slopes characteristic of beaches in the Coos County detailed study areas.
2. Using the above approach, we defined ~135 discrete storm events for the two different slope types. Based on these events, we transformed the deepwater wave statistics associated with these events into the nearshore (20 m water depth) to account for wave refraction and shoaling effects. Depth limited breaking, wind growth, quadruplets, and triad interactions were all turned off in the SWAN runs. The derived nearshore wave statistics were then converted back to their adjusted deepwater equivalent wave height in order to perform the wave runup analyses and ultimately compute the 1% total water levels.

The main limitations associated with this approach were:

1. Only a very limited number of model runs were performed, ~135 per representative beach slope.
2. Because we used only two representative beach slopes, we may have missed a particular wave condition (wave height [H_s], period [T_P], direction [D_d]) and beach slope (tan β) combination that resulted in a higher TWL at the shoreline.
3. The structural function approach used to generate the initial extreme TWLs and therefore to pick the offshore wave conditions input in SWAN is fundamentally limited. Nature gave us only 1 combination of waves and water levels during the 30 years we used to generate input conditions, which is not necessarily a statistically robust sample.

For the purposes of the Clatsop County study, including other detailed FEMA coastal studies already completed for Oregon, we have developed a more refined approach that reflects the following enhancements.

1. Rather than steps 1 and 2 as described for our Coos County study, modeling will be carried out based on analyses of the full range of wave and tide combinations observed over the historical period. This approach will ultimately provide a more robust measure of the 1% (and other desired return periods) total water levels.
2. We have developed a lookup table approach for analyzing thousands of possible storm combinations rather than only a few hundred as performed in Coos County. The general idea is that a "lookup table" can be developed by transforming all combinations of wave quadruplets (H_S, T_P, D_d, and water levels). We used SWAN to compute the transformed wave characteristics of these waves up to wave breaking.
3. Our approach still suffers from the third limitation listed above for the Coos County study.

The area over which the SWAN grid was set up is shown in **Figure 5-1**. In general, our analyses proceeded in the following order:

1. Develop a long time series of both measured (NDBC) and modeled (WIS) wave conditions (~30 years long) at approximately the shelf edge offshore of the study area;
2. Run the SWAN model with a full range of input conditions, using constant offshore boundary conditions, to compute bathymetric induced wave transformations up to wave breaking.
3. Develop "lookup tables" from the suite of SWAN simulations.
4. Transform the long time series through the "lookup tables" such that we generate alongshore varying long time series at approximately the 20-m depth contour throughout the study area.
5. Use the deep water equivalent alongshore varying wave conditions and the appropriate measured tides from the combined Yaquina Bay/Garibaldi time series to compute time series of T_{WL}s for 85 beach profiles along the Clatsop coast. These include transects established on the Clatsop Plains (14 sites), Seaside (17 sites), Cannon Beach (17 sites), Arcadia Beach (3 sites), Arch Cape (10 sites), and Falcon Cove (6 sites).
6. Using a Poisson-generalized Pareto distribution, compute the 1-, 10-, 25-, 50-, 100-, and 500-year T_{WL} elevations using a peak-over-threshold (POT) approach.
7. Compare extreme T_{WL}s with topographic elevations of various beach-backing features to determine the potential extent of coastal flooding during extreme events.

The following sections describe in more detail the various procedures used in each of the aforementioned steps in this analysis.

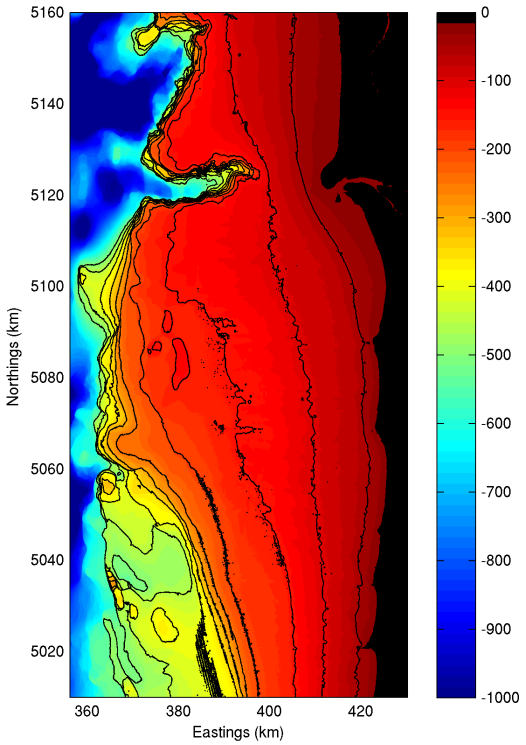

Figure 5-1. The SWAN model domain developed for the Clatsop County coast. The model bathymetry was developed using 1/3 arc-second (~10 m) DEMs downloaded from the NOAA's NGDC. Color scale reflects depth in meters.

5.1 Development of a Synthesized Wave Climate for Input into SWAN

Our primary goal was to use existing measured and hindcast wave time series to generate as long a record of the deep-water wave climate as possible for the offshore boundary of the SWAN model, approximately the edge of the continental shelf break. To this end, we downloaded all available National Data Buoy Center (NDBC; http://www.ndbc.noaa.gov/) and Coastal Data Information Program (CDIP; http://cdip.ucsd.edu/) hourly wave buoy data in the region for several wave buoys. **Figure 5-2** shows the various buoys used to derived a synthesized northern Oregon coast wave data set (data availability shown in **Figure 5-3**). Besides the hourly measured wave buoy data, we also obtained wave hindcast information on the deepwater wave climate determined through the Wave Information Studies (WIS; http://wis.usace.army.mil/) (Baird & Associates, 2005). For the purposes of this study, we used wave hindcast data determined for station 81067 (**Figure 5-2**), which is located adjacent to NDBC buoy #46005. While NDBC #46005 has a high quality, long record of data (1975–2012), it is located in 2,981 m (9,780 ft) of water and is over 400–500 km (250–310 mi) from the shelf edge. Therefore, NDBC #46089, a shelf-edge, deepwater buoy, was selected as the priority buoy to be used in the SWAN analyses. A buoy (Columbia River #46029) located on the shelf was also included in this analysis, reverse shoaled to deep water to account for wave height changes in intermediate depths. Because of the variation in locations and water depths of the buoys, we needed to develop a methodology to transform these "off-shelf" and "on-shelf" waves to the "shelf-edge" offshore boundary condition of the SWAN model. This was necessary as the wave climates observed at 46005 and 46029 are significantly different than the climate observed at the Tillamook offshore buoy (**Figure 5-4**).

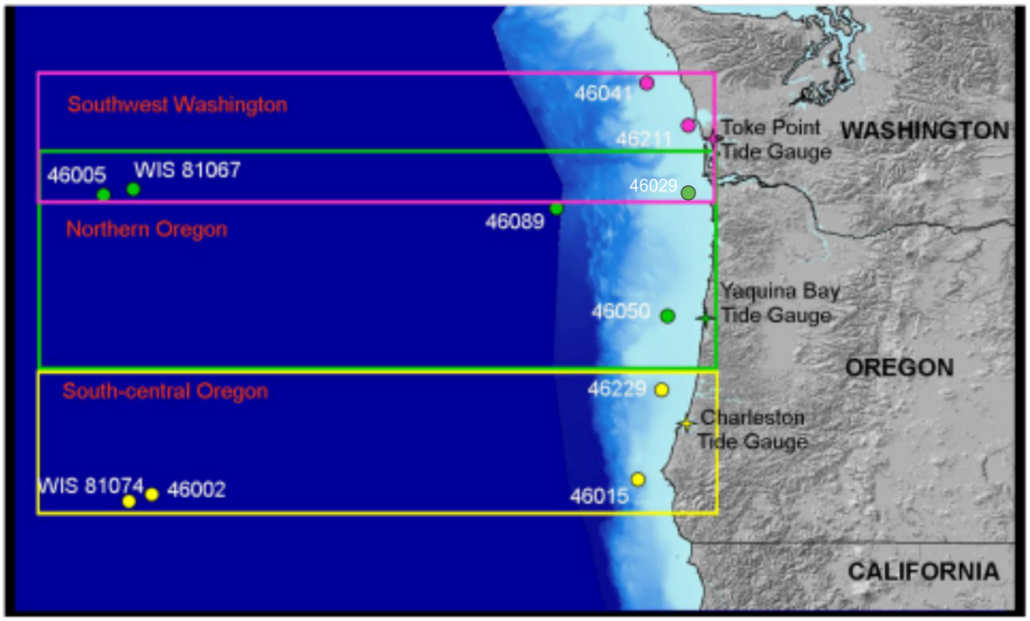

Figure 5-2. Map showing the regional divisions from which synthesized wave climates have been developed.

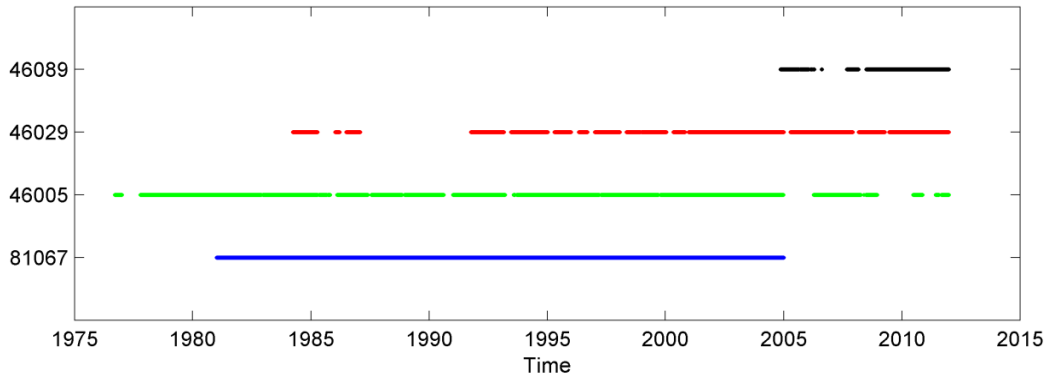

Figure 5-3. Available wave data sets timeline (after Harris, 2011).

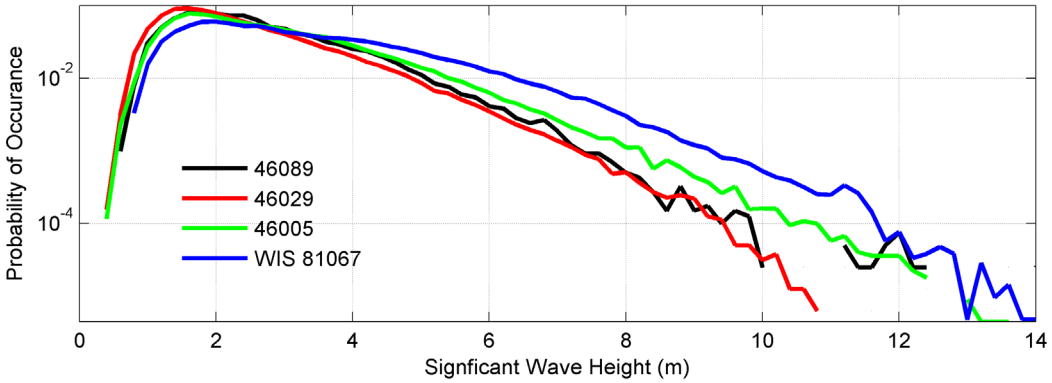

Figure 5-4. Differences in the empirical probability distribution functions of the on shore and off shore buoys.

To transform the 46005 and 46029 waves to the shelf edge, we created wave period bins (0–6, 6–8, 8–10, 10–12, 12–14, 14–16, 16–21, and 21–30 s[1]) to evaluate if there has been a wave period dependent difference in wave heights observed at Washington 46005 and Columbia River 46029 compared with the Tillamook buoy. For our comparisons, the time stamps associated with waves measured at either 46005 or 46029 were adjusted based upon the group celerity (for the appropriate wave period bin) and travel time it takes the wave energy to propagate to the wave gauge locations. For example, for waves in the period range 10–12 s the group celerity is about 8.3 m/s, and therefore it takes 13 hours for the energy to propagate from 46005 to the Tillamook buoy (**Figure 5-5**).

[1] The NDBC wave buoys only relatively coarsely resolve long-period waves. Between 21 and 30 s, only a wave period of 25 s is populated in the data set. There are no 30-s waves in the time series. Of the waves with periods between 16 s and 20 s, over 80 percent of them are at approximately 16 s. Only a relatively few waves in the record have recorded periods of 17, 18, and 19 s. This coarse resolution in the raw data determined our choice of period bin widths.

After correcting for the time of wave energy propagation, the differences in wave heights between the two buoys, for each wave period bin, were examined in two ways as illustrated in **Figure 5-5**:

1. A best fit linear regression through the wave height differences was computed for each wave period bin; and
2. A constant offset was computed for the wave height differences for each period bin.

Upon examination of the empirical probability density functions (PDF) of the buoys' raw time series (using only the years where overlap between the buoys being compared occurred) and after applying both transformation methods (**Figure 5-6**), it was determined that the constant offset method did a superior job of matching the PDFs, particularly for the high wave heights. Therefore, a constant offset adjustment dependent on the wave period was applied to the wave heights from the Washington 46005 and Columbia River 46029 buoys. Because the WIS hindcast data used in this study was also located well beyond the boundary of the SWAN model (basically at the location of 46005), the same series of steps comparing WIS wave heights to the Tillamook buoy was carried out, with a new set of constant offsets having been calculated and applied.

After applying the wave height offsets to the necessary buoys, gaps in the time series of Tillamook 46089 were filled in respectively with the Columbia River and Washington buoys. Where there were still gaps following this procedure we then filled in the time series with the corrected WIS data. Because wave transformations (particularly refraction) computed by SWAN are significantly dependent on wave direction, when this information was missing in the buoy records it was replaced with WIS data for the same date in the time series (but the wave height and period remained buoy observations where applicable).

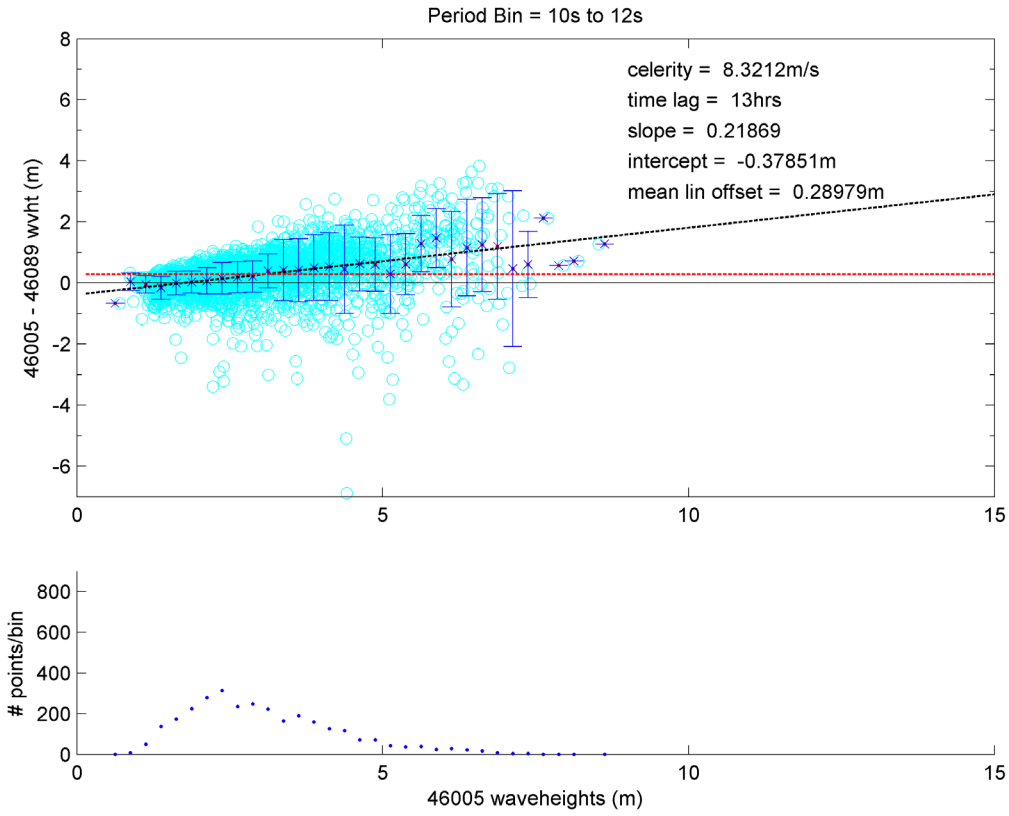

Figure 5-5. Example development of transformation parameters between the Washington buoy (#46005) and the Tillamook (#46089) buoy for period range 10 s to 12 s. In the top panel the dashed black line is the linear regression and the dashed red line is the constant offset. Blue error bars represent the standard deviation of the wave height differences in each period bin (Harris, 2011).

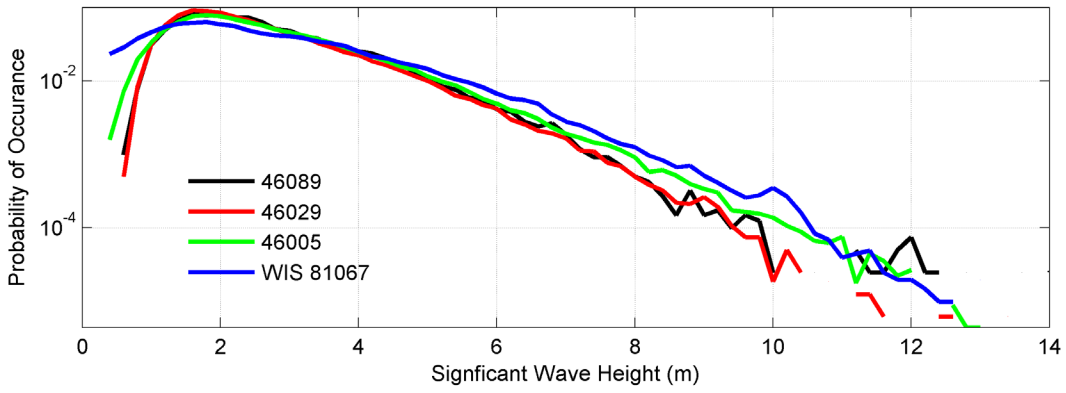

Figure 5-6. Adjusted probability density functions (corrected using the constant offset approach) for buoy 46005 (green line), buoy 46029 (red line) and WIS station 81067 (blue line) as compared to the raw probability density function for buoy 46089 (black line).

The final synthesized wave time series developed for Clatsop County extends from late 1980 through to 31st December, 2011 and consists of approximately ~31 years of data (measurements including at least wave height and periods) (**Figure 5-7**). Forty-six percent of the synthesized wave climate is from NDBC 46029, 32% from NDBC 46005, 15% from NDBC 46089, and 7% from WIS station 81067. As can be seen from **Figure 5-7A**, the wave climate offshore from the northern Oregon coast is episodically characterized by large wave events (> 8 m [26 ft]), with some storms having generated deepwater extreme waves on the order of 14.5 m (48 ft). The average wave height offshore from Clatsop County is 2.5 m (8.2 ft), while the average peak spectral wave period is 10.8 s, although periods of 20–25 s are not uncommon (**Figure 5-7B**).

The PNW wave climate is characterized by a distinct seasonal cycle that can be seen in **Figure 5-8** by the variability in the wave heights and peak periods between summer and winter. (The groupings evident in the peak periods (**Figure 5-7B**) are directly from the data and are a product of the data processing methods used by the NDBC to establish the wave frequencies and hence periods. It is for this reason that we chose coarse wave period bins for long period waves [i.e., > 16 s].) Monthly mean significant wave heights are typically highest in December and January (**Figure 5-8**), although large wave events (>12 m [39.4 ft]) have occurred in all of the winter months except October. The highest significant wave height observed in the wave climate record is 14.5 m (48 ft). In general, the smallest waves occur during late spring and in the summer, with wave heights typically averaging ~1.5 m during the peak of the summer (July/August). These findings are consistent with other studies that have examined the PNW wave climate (Tillotson and Komar, 1997; Allan and Komar, 2006; Ruggiero and others, 2010b). **Figure 5-7C** shows a probability density function determined for the complete time series, while **Figure 5-7D** is a cumulative frequency curve. The latter indicates that for 50% of the time waves are typically less than 2.2 m (7.2 ft), and less than 4.3 m (14.1 ft) for 90% of the time. Wave heights exceed 6.7 m (22 ft) for 1% of the time. However, although rare in occurrence, these large wave events typically produce the most significant erosion and flooding along the Oregon coast.

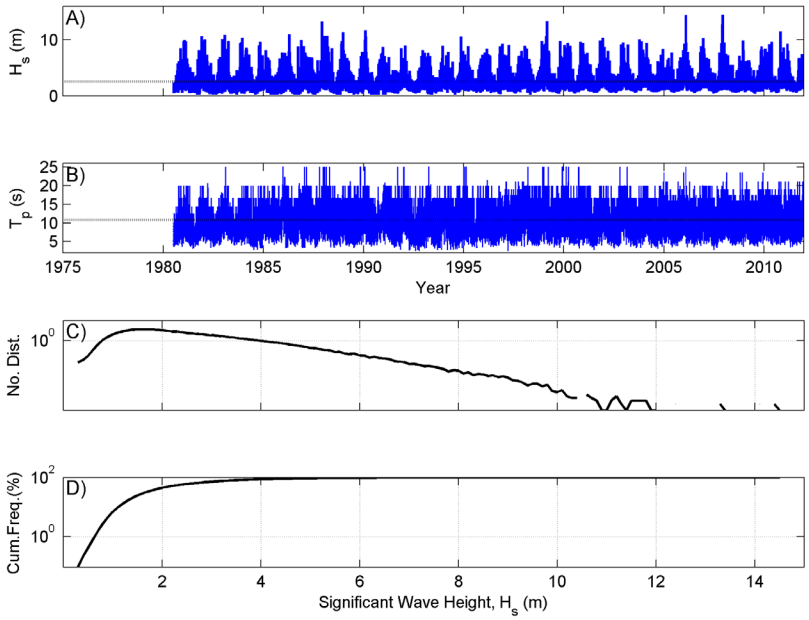

Figure 5-7. Synthesized wave climate developed for Clatsop County. A) Significant wave height with mean wave height denoted (dashed line), B) Peak spectral wave period with mean period denoted (dashed line), C) Probability distribution of wave heights plotted on a semi-log scale, and D) Significant wave height cumulative frequency curve plotted on a semi-log scale.

Finally, **Figure 5-9** provides a wave rose of the significant wave height versus direction developed for the northern Oregon coast. In general, the summer is characterized by waves arriving from the northwest, while winter waves typically arrive from the west or southwest (Komar, 1997). This pattern is shown in **Figure 5-9**, which is based on separate analyses of the summer and winter directional data developed from the synthesized time series. As can be seen in **Figure 5-9**, summer months are characterized by waves arriving from mainly the west-northwest (~48%) to northwesterly quadrant (~42%), with few waves out of the southwest. The bulk of these reflect waves with amplitudes that are predominantly less than 3 m (9.8 ft). In contrast, the winter months are dominated by much larger wave heights out of the west (~23%), and to a lesser extent the northwest (~5.8%), while waves from the southwest account for ~21% of the waves.

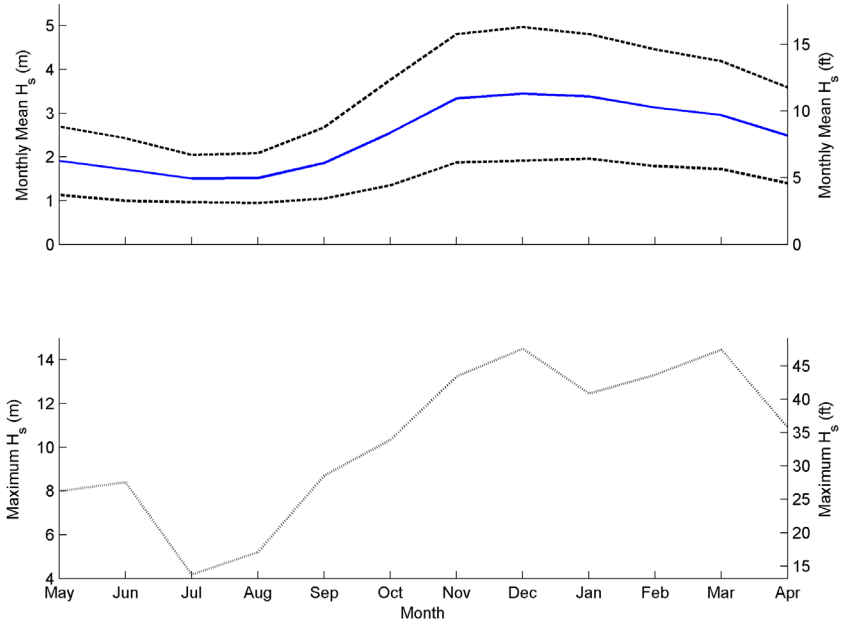

Figure 5-8. Seasonal variability in the deepwater wave climate offshore from the northern Oregon coast. Top) The monthly average wave height (blue line) and standard deviation (dashed line); Bottom) The maximum monthly significant wave height.

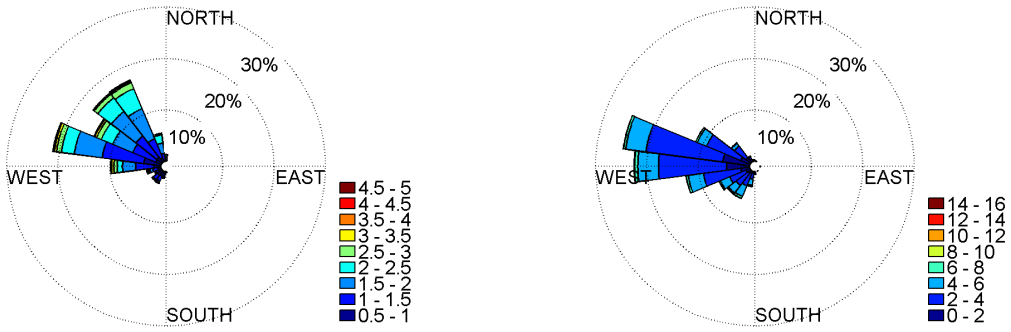

Figure 5-9. Left) Predominant wave directions for the summer months (June–August), and Right) winter (December–February). Colored scale indicates the significant wave height in meters.

5.2 Comparison of GROW versus Measured Waves

This section presents a more detailed analysis of GROW Fine Northeast Pacific wave hindcast data compared with measured waves obtained from selected wave buoys offshore from the Oregon coast. The objective is to better define the degree of congruence between these two contrasting data sets in order to assess their relative strengths and weaknesses. The approach used here is similar to the tide analyses presented in Section 4, using empirical probability density functions (PDFs) to assess the shapes of the distributions. For the purposes of this analysis, PDF plots were derived for the GROW station (#18023) and for NDBC wave buoys 46089, located 66 km (41 mi) northwest of 18023 (**Figure 4-1**), and 46005 (not shown on map), located 540 km (335 mi) west of the Columbia River mouth.

The first plot (**Figure 5-10**) presents a series of significant wave height empirical PDFs for all measured data from NDBC buoys 46005 and 46089 as well as the GROW hindcast data from site 18023. Data from the stations span the following time frames: NDBC 46005 from 1976 through 2010; NDBC 46089 from 2004 through 2010; GROW 18023 from 1980 through 2009. Based on these PDFs, it is immediately apparent that the GROW data contains a larger number of smaller wave heights (in the 2- to 3-m range) than those measured by the buoys. Additionally, examination of the log-scale plot (bottom of **Figure 5-10**) indicates that the GROW hindcast at 18023 tends to underestimate the more extreme wave heights (waves >7m), which are the most important for inundation and erosion vulnerability studies. **Table 5-1** lists general statistics of the various data sets where the maximum wave height modeled by GROW is shown to be nearly 3 meters lower than that measured by the 46089 buoy. In contrast, GROW indicates on average slightly higher peak periods when compared with the NDBC stations. While differences between NDBC 46005 and NDBC 46089 may simply reflect buoy locations relative to the tracks of the storms, differences between 46089 and GROW 18023 are almost certainly entirely due to the ability of the numerical model to hindcast the waves. Because NDBC station 46089 spans a much shorter measurement period compared with 46005 and the GROW site, the results from the full PDFs may be construed to be misleading. To better assess this potential bias, we again performed analyses of the truncated time series, which revealed near identical results to those presented in **Figure 5-10**. Summary statistics for the truncated time series are included in **Table 5-1**. **Figure 5-11** shows a PDF of the peak periods for 46005, 46089 and GROW for the time period of 2004-2009. This last plot clearly indicates that GROW is tending to overestimate the higher peak periods when compared with the measured data.

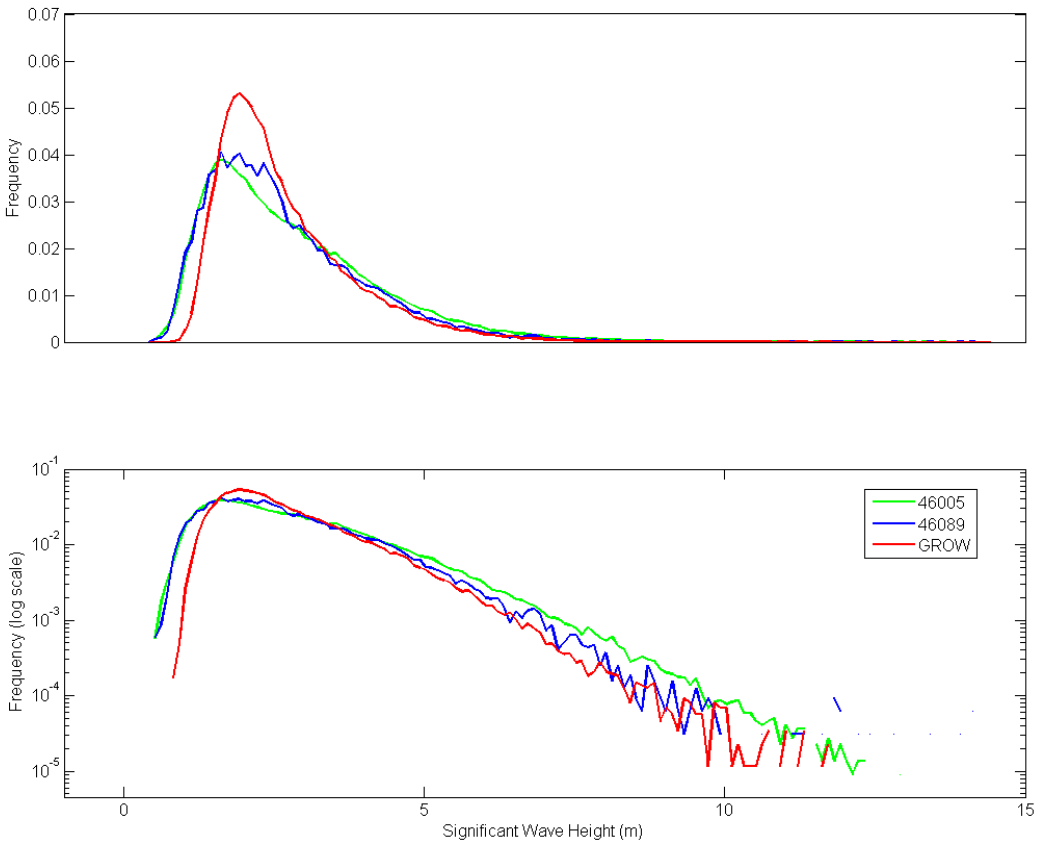

Figure 5-10. PDFs of significant wave heights plotted on Top) normal and Bottom) log scales. Plots include all existing data from these stations.

Table 5-1. General statistics of the NDBC buoy and GROW data sets based on the complete time series of data, and truncated time series. Note: *H* denotes the significant wave height and *T* is the wave period.

	46005	**46089**	**GROW**
Data Availability	1976–present	2004–present	1980–2009
Mean *H*	2.8 m	2.7 m	2.6 m
Max *H*	13.6 m	14.5 m	11.7 m
Min *H*	0.2 m	0.4 m	0.72 m
H Standard Dev.	1.4 m	1.3 m	1.1 m
Mean *T*	10.8 s	11.1 s	12.6 s
Data Availability	2004–2009	2004–2009	2004–2009
Mean *H*	2.8 m	2.6 m	2.6 m
Max *H*	12.7 m	14.5 m	11.7 m
Min *H*	0.5 m	0.4 m	0.9 m
H Standard Dev.	1.4 m	1.3 m	1.1 m
Mean *T*	10.6 s	11.1 s	12.7 s

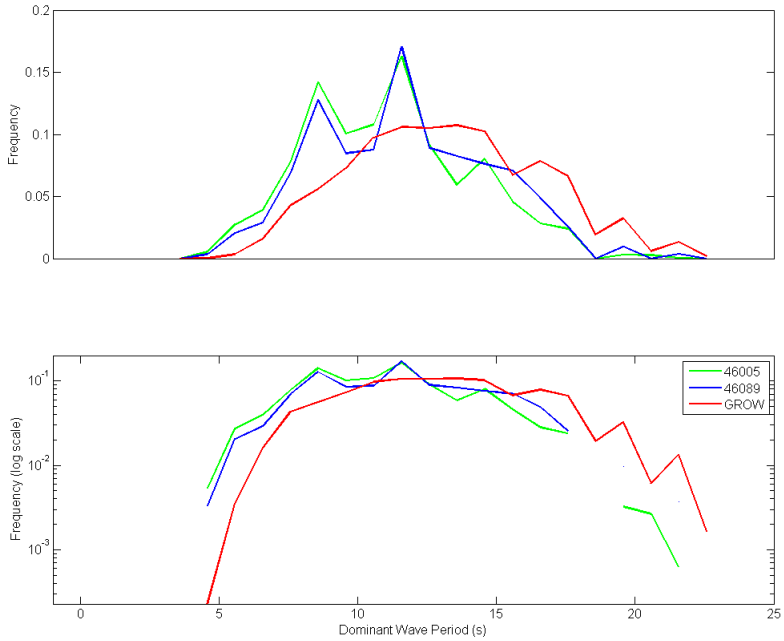

Figure 5-11. PDFs of peak wave periods from 2004 through 2009 on a Top) normal and Bottom) log plot.

Having examined PDFs of the various data sets, additional analyses were carried out for selected individual storms in order to better assess how well GROW is performing. The approach adopted was to select the five largest storms measured by the NDBC 46089. The storm events were selected by using a 3-day filter to ensure the selection of independent storm events. Once the peak of the storm was identified, the data (±2 days) were plotted with the GROW data. **Figure 5-12** presents results from two of the five selected storms. In general, our results indicate that while the timing of the events seems to be accurately determined by the GROW model, the magnitude is often lower than that measured by the wave gauges. This result may be due to the GROW approach of only estimating model results every 3 hours as opposed to NDBC's hourly buoy measurements. As a result, sampling at 3 hourly intervals has the potential to miss the peak of the storms. In fairness to GROW, the 3-hourly sampling probably reflects the fact that modeling waves on an hourly basis is dependent on having temporally and spatially suitable meteorological information, which remains a challenge for large-scale regional models.

Finally, we also compared 2% exceedance extreme runup values estimated using the Stockdon and others, (2006) approach and waves from the buoys and the GROW station. These results are presented in **Figure 5-13** and were calculated using a representative beach slope (tan β) of 0.04, which is typical for Oregon beaches. Only data from 2004 through 2009 were included in these calculations to provide a standard time frame for the comparison. Results indicate that, just as with the significant wave height PDFs, the extreme runup levels (>2.5 meters) are underestimated by the GROW model, while the highest calculated runup differs by about 0.4 m (1.3 ft). Although the difference in the calculated runup between GROW and our measured time series is not as large as expected, the shape of the PDF plot would potentially reduce the number of storms available for defining the 100-year wave runup and total water level, as well as in overtopping, inundation and erosion analyses as required for FEMA detailed coastal studies. Based on these findings, we have concluded that all subsequent modeling of waves for Clatsop County should be based as much as possible on the measured wave time series, as opposed to using GROW hindcast data.

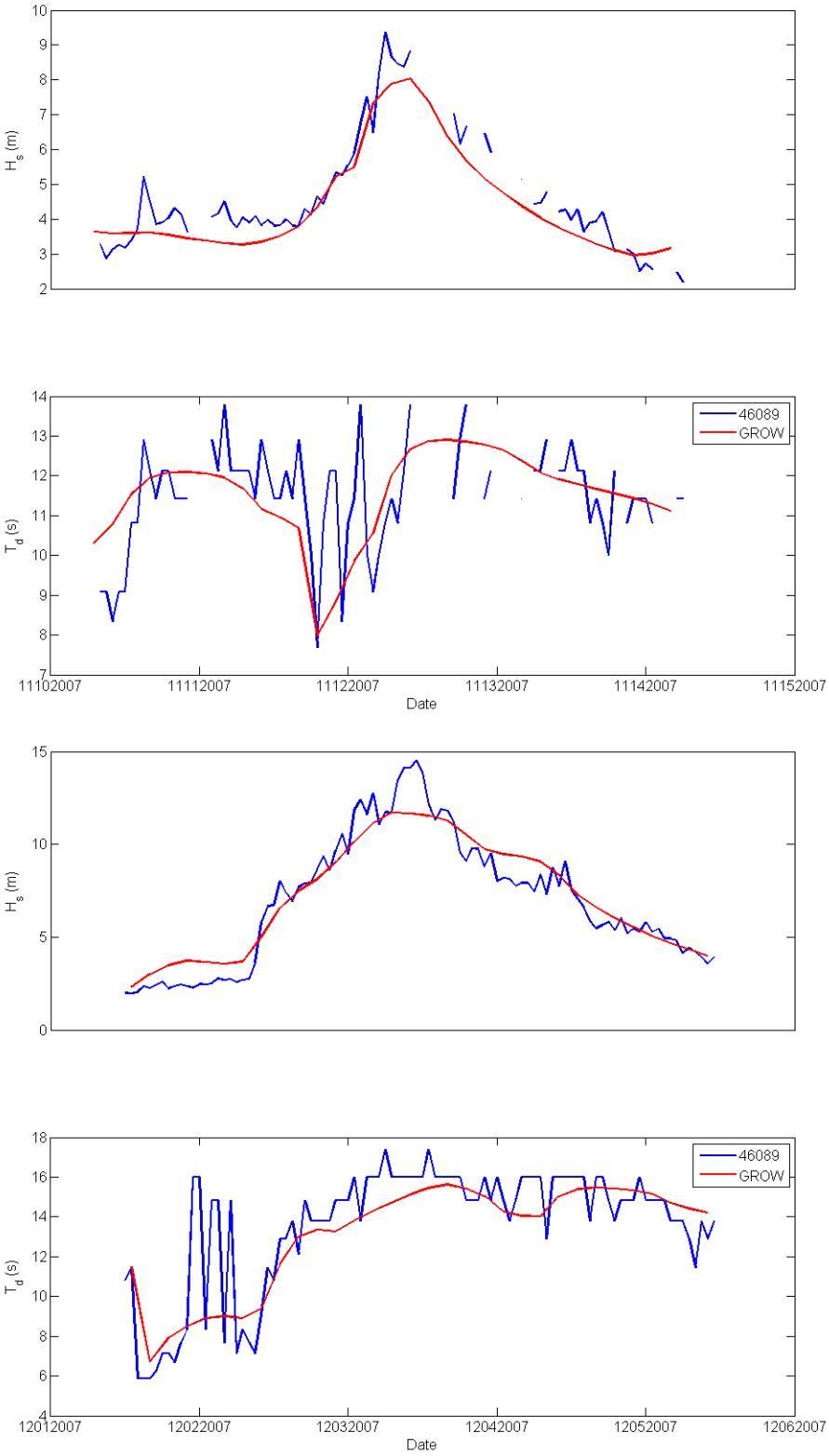

Figure 5-12. Two examples of storms where measured and modeled waves are compared. Top) Storm on November 12, 2007, and Bottom) Major storm event on December 3rd, 2007.

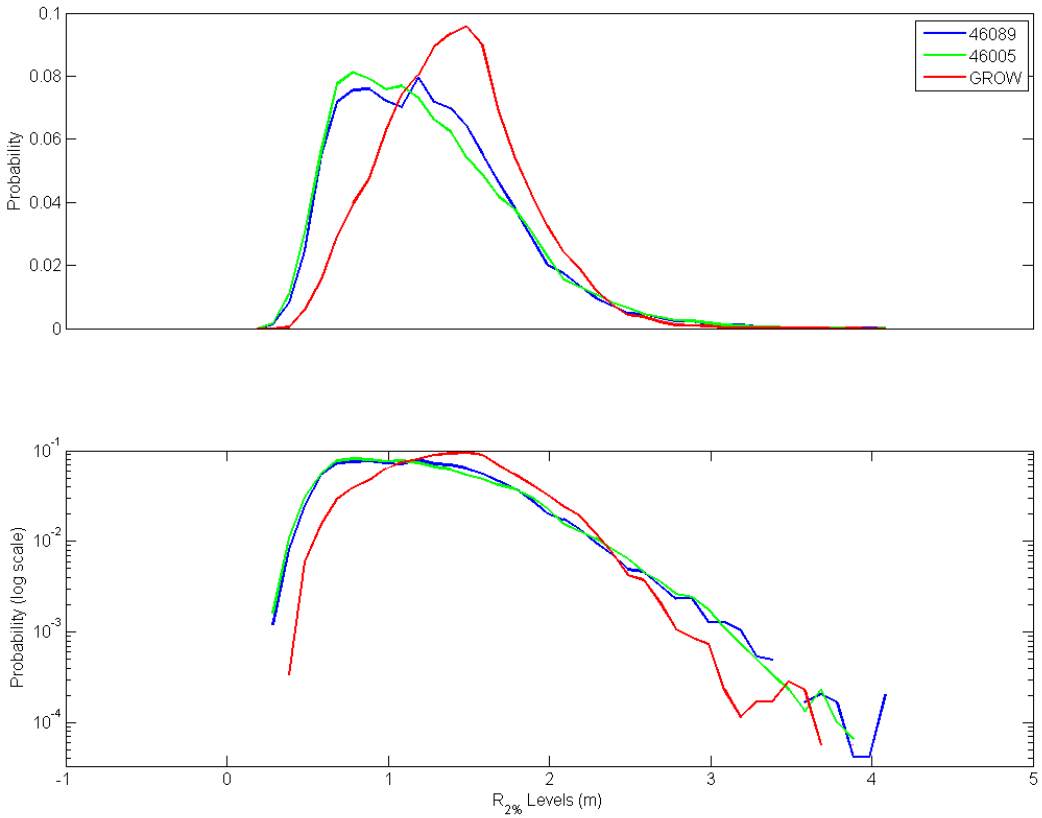

Figure 5-13. PDFs of calculated 2% extreme runup elevations for NDBC 46005, 46089 and GROW hindcast results. An average beach slope of 0.04 was used for runup calculations. The bottom plot is the same as the top, but with the y-axis having been plotted using with a logarithmic scale in order to emphasize the higher wave runup characteristics.

5.3 SWAN Model Development and Parameter Settings

We used the historical bathymetry assembled by the National Geological Data Center (NGDC) (described in Section 3.4) and created a model grid that covers a large portion of the northern Oregon coast (**Figure 5-1**).

SWAN (Simulating WAves Nearshore) version number 40.81, a third generation wave model developed at the Technical University of Delft in the Netherlands (Booij and others, 1999; Ris and others, 1999), was used in this study. The model solves the spectral action balance equation using finite differences for a spectral or parametric input (as in our case) specified along the boundaries. For the Clatsop County study, the cross-shore and alongshore resolution of the model grid used is 75 × 100 m. The total grid area is 74 km × 150 km in length, which yields 987 × 1,500 computational nodes. The SWAN runs were executed in stationary mode and included physics that account for shoaling, refraction, and breaking, while model settings varying from the default values are discussed in more detail below.

The north, south and west boundaries of the model were specified using grid coordinates and forced using a parameterized JONSWAP spectrum. The functions for spectral peakedness parameters γ and nn in the JONSWAP directional spectra are given as:

$$\gamma = \begin{cases} 3.3 & if\ Tp < 11s \\ 0.5Tp - 1.5 & if\ Tp \geq 11s \end{cases}$$
$$nn = \begin{cases} 4 & if\ Tp < 11s \\ 2.5Tp - 20 & if\ Tp \geq 11s \end{cases} \qquad (5.1)$$

Thus, the directional distribution is generated by multiplying the standard JONSWAP frequency spectrum by $\cos^{nn}(\theta - \theta_{peak})$ (Smith and others, 2001). Wind wave spectra are broad (low γ and nn values) while swell typically have narrow distributions (high γ and nn values). The values used in the SWAN wave modeling were based on the input peak periods which ranged $4.055 \leq \gamma \leq 11.03$ and $7.775 \leq nn \leq 42.65$. To ensure that the wave directional spread is sufficiently resolved by the model, we specified directional bins giving a 4-degree directional resolution. The spectrum was discretized in frequency space with 29 bins from 0.032 to 1 Hz. Wind was not included in the SWAN simulations and therefore no energy growth due to wind, or quadruplet wave-wave interactions occur in the simulations. Triad interactions, diffraction, and wave setup also were not activated in the model. We used the Janssen frictional dissipation option, which has a default friction coefficient of 0.067 m^2/s^3. No model calibration was performed in this study, although several numerical experiments were implemented to test various assumptions in the wave modeling (e.g., not to use winds).

5.3.1 Wind effects

The decision not to model the effect of winds on wave growth over the continental shelf in our Coos County study was based on two observations:

- To develop our combined wave time series described previously, we performed a "statistical" wave transformation between buoy 46002 and the buoys at the edge of the continental shelf and found that in general the wave heights during storm events decreased even with hundreds of kilometers of additional fetch. Without understanding the details of this phenomenon (e.g., white capping versus wind wave growth) and with no data for calibration we felt that attempting to model wind growth would add to the uncertainty of our input wave conditions.
- We also have previous experience with SWAN wave modeling in the region (U.S. Pacific Northwest) in which sensitivity runs including winds were performed with only minor impact on results (Ruggiero and others, 2010a).

To test the validity of the assumptions made in our Coos County study, several wave modeling experiments were performed to specifically examine the role of additional wind wave development over the shelf. The basic question addressed is: How much do wind fields result in wave growth between the location of the GROW stations that were purchased (an off-shelf location roughly equivalent to the offshore extent of the Tillamook (46089) buoy shown in **Figure 4-1**) and

the inner shelf. The latter was defined as the 100 m (300 ft) isobath. To address this question, hindcast waves were modeled for the months of January and February (i.e., peak of the winter season) and for two representative years (2006 and 2010). The wave modeling was accomplished by running a regional Eastern North Pacific (ENP) model and a 3 arc-min grid for the Oregon coast, with the outer boundary coinciding with the Tillamook buoy station (**Figure 5-14**). The model runs were forced by analyzed Global Forecast System winds with a temporal resolution of 6 hours and a spatial resolution of 1 arc-degree. A similar run was undertaken without winds over the same 3 arc-min grid, just propagating the boundary conditions. Hindcast wave data were obtained from selected points across the shelf at contour depths of 500, 400, 300, 200, and 100 m along a cross-shore transects from the offshore GROW station (A and B in **Figure 5-14**).

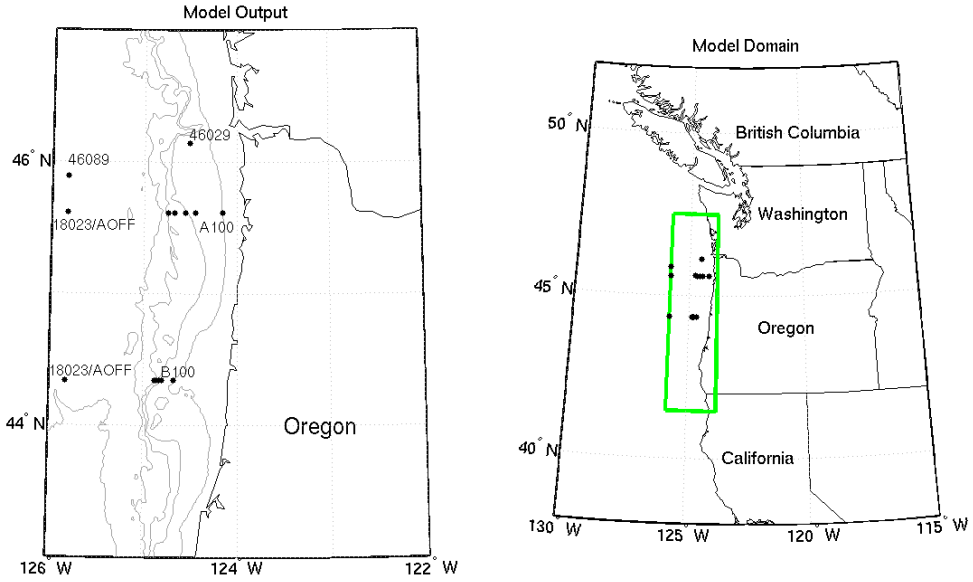

Figure 5-14. Left) Map showing the locations of the northern Oregon coast buoys, and transect lines (A and B), and Right) model domain.

Results from the model runs (with and without winds) are presented in **Figure 5-15** and **Figure 5-16**. Modeled and measured waves for two NDBC buoys (46089 and 46029) are included for comparative purposes (**Figure 5-17** and **Figure 5-18**). In general, our experiments indicated that although the addition of wind sometimes changed the timing of the large wave events, producing at times a relatively large % error for part of the "wave hydrograph," the peaks of the wave events showed very little difference between cases where wind was included or excluded (**Figure 5-15** and **Figure 5-16**). Furthermore, in the majority of cases, the differences in the derived wave heights between model runs including (excluding) wind (no wind) were on the whole minor. This finding was also observed in the derived peak wave periods, which appear to be virtually identical in all the plots. Of greater concern in these model tests, are the occasional large differences between the modeled runs (irrespective of whether wind/no wind is applied) and the actual measurements derived from NDBC wave buoys (**Figure 5-17** and **Figure 5-18**), as well as the GROW data derived for station 18023. These latter findings will be explored in more detail later in this section.

These experiments support our decision to not include wind growth in our model runs; therefore, quadruplet wave-wave interactions were also not incorporated in the simulations. Further, wave setup is not included in the simulations because we extract the transformed wave parameters at the 20-m depth contour and use the Stockdon and others (2006) empirical model to compute wave runup (which incorporates setup) along the coast.

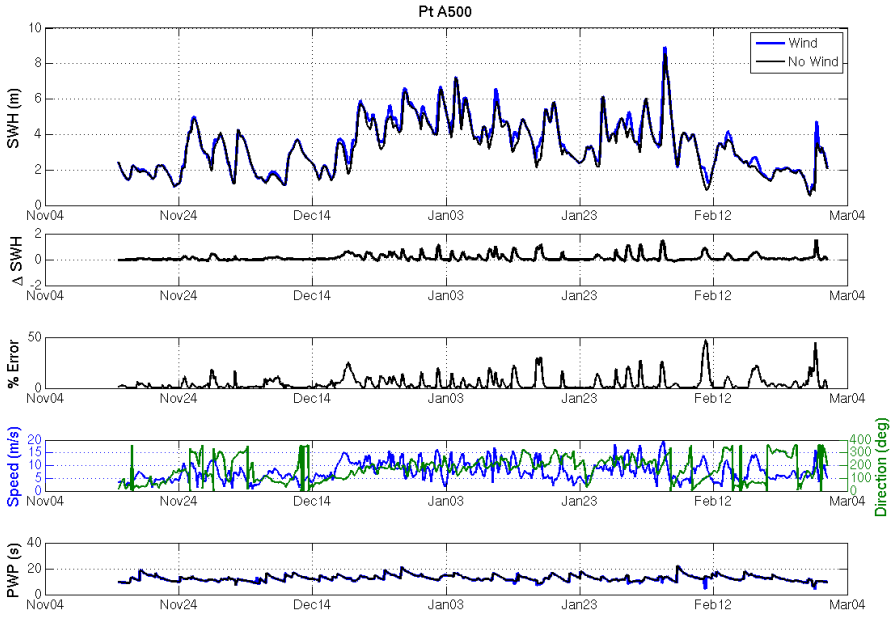

Figure 5-15. Model-model comparison at 500-m depth on transect A for the 2006 simulation.

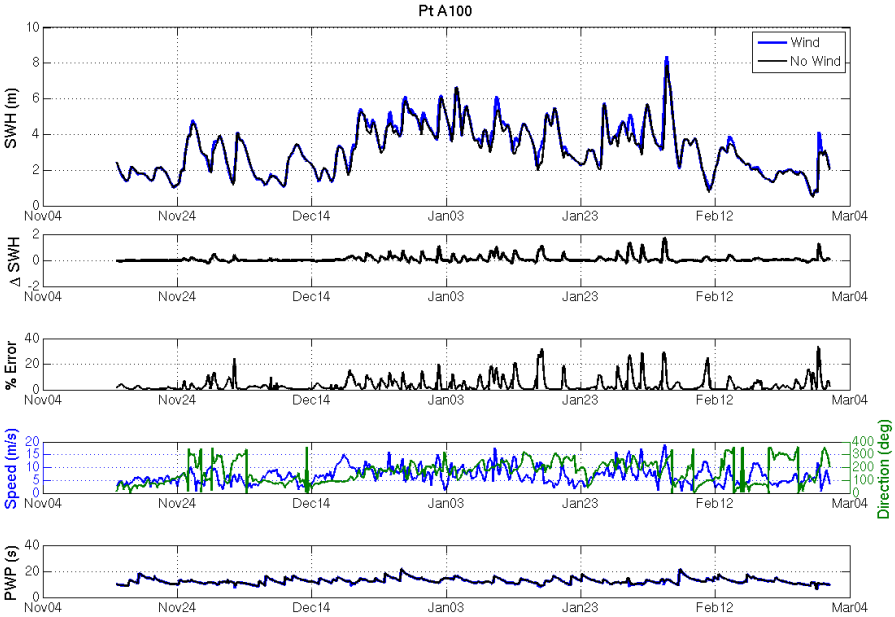

Figure 5-16. Model-model comparison at 100-m depth on transect A for the 2006 simulation.

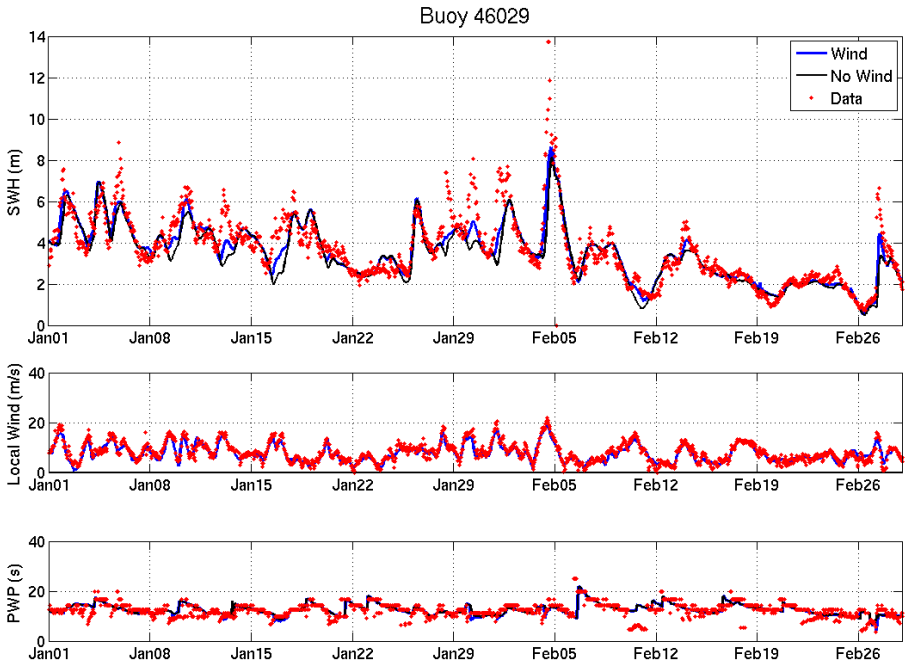

Figure 5-17. Model data comparison at NDBC buoy #46029 for the 2006 simulations.

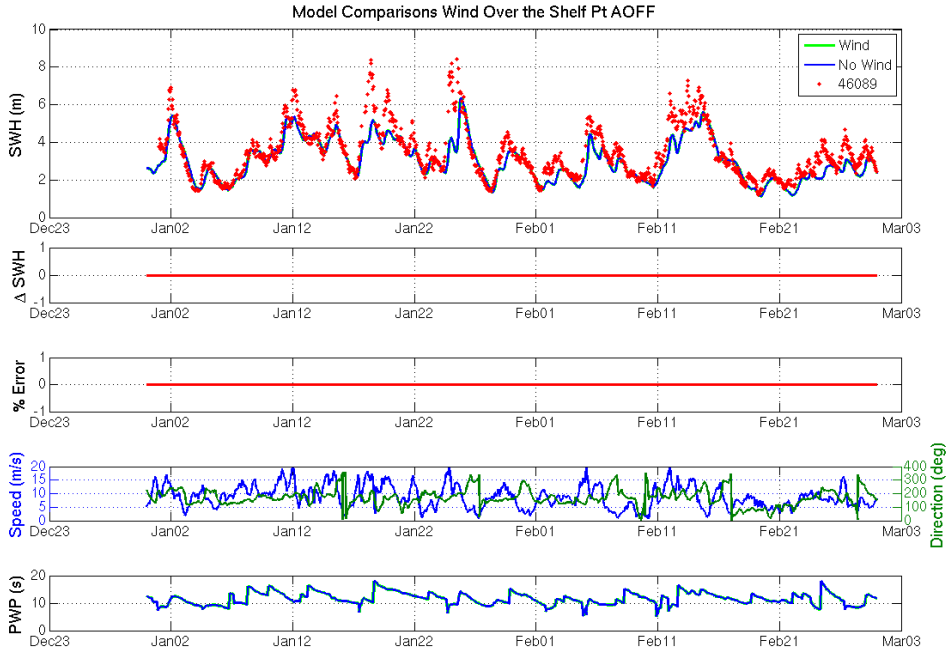

Figure 5-18. Model data comparison at Station Aoff (GROW station location) versus 46089 for the 2010 simulations.

5.3.2 Frictional and Whitecapping Dissipation of the Wave Energies

Additional testing was undertaken to explore the effect of not including friction and whitecapping. **Figure 5-19** and **Figure 5-20** provide two test-case conditions, associated with a significant wave height of 10 m and peak period of 20 s, with the waves approaching from a direction of 285 degrees (NW), while the second case is for a significant wave height of 14 m, peak period of 14 s, with the waves approaching from a direction of 270 degrees (W). **Figure 5-19** indicates that for this particular condition, the modeled results are relatively similar until immediately prior to wave breaking, where significant differences arise. However, as the significant wave height increases (**Figure 5-20**) the effect of excluding bottom friction and whitecapping becomes considerably larger. The exclusion of these processes results in an overestimation of wave heights prior to breaking. Therefore, we have chosen to include frictional dissipation and dissipation due to whitecapping in our modeling.

5.3.3 Look up table development

Having demonstrated that winds have little impact in terms of additional wave development across the continental shelf of Oregon, our next goal was to develop an efficient methodology that could be used to minimize the total number of SWAN runs needed to perform the actual wave modeling and transformations, while ensuring that we resolve the influence of varying parameters on the wave transformations. To do this we discretized the significant wave height (H_s), peak period (T_p), wave direction (D_p), and water level (WL) time series.

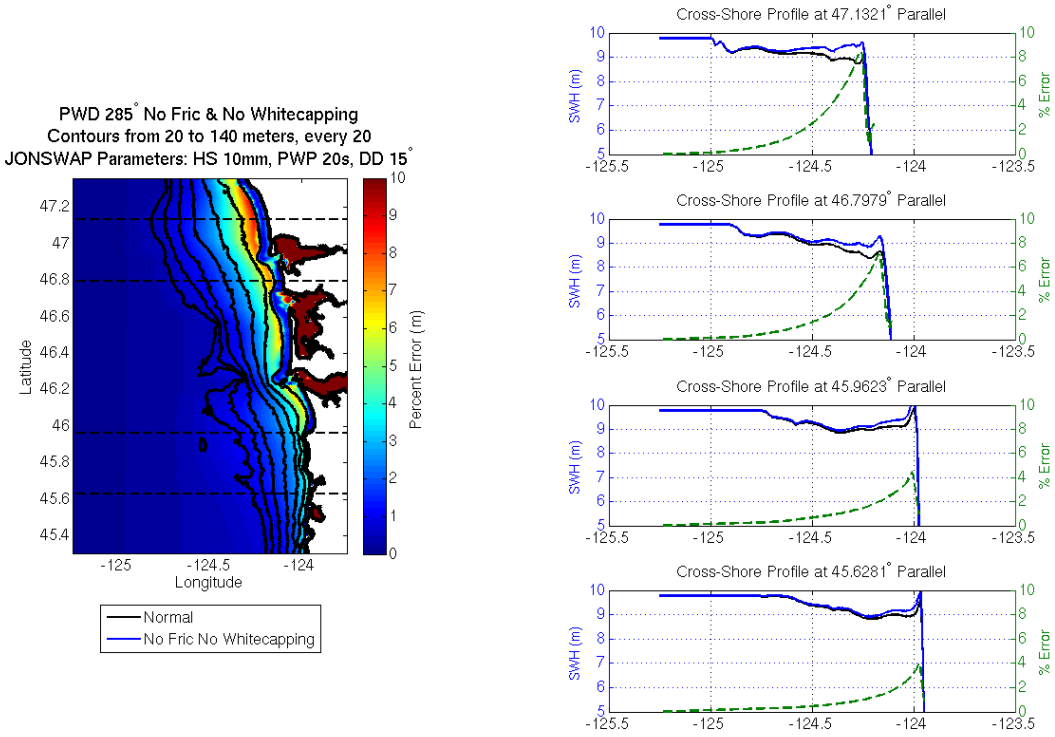

Figure 5-19. The impact of ignoring bottom frictional dissipation and dissipation due to whitecapping for a 10-m significant wave height with a peak period of 20 s approaching from a direction of 285 degrees.

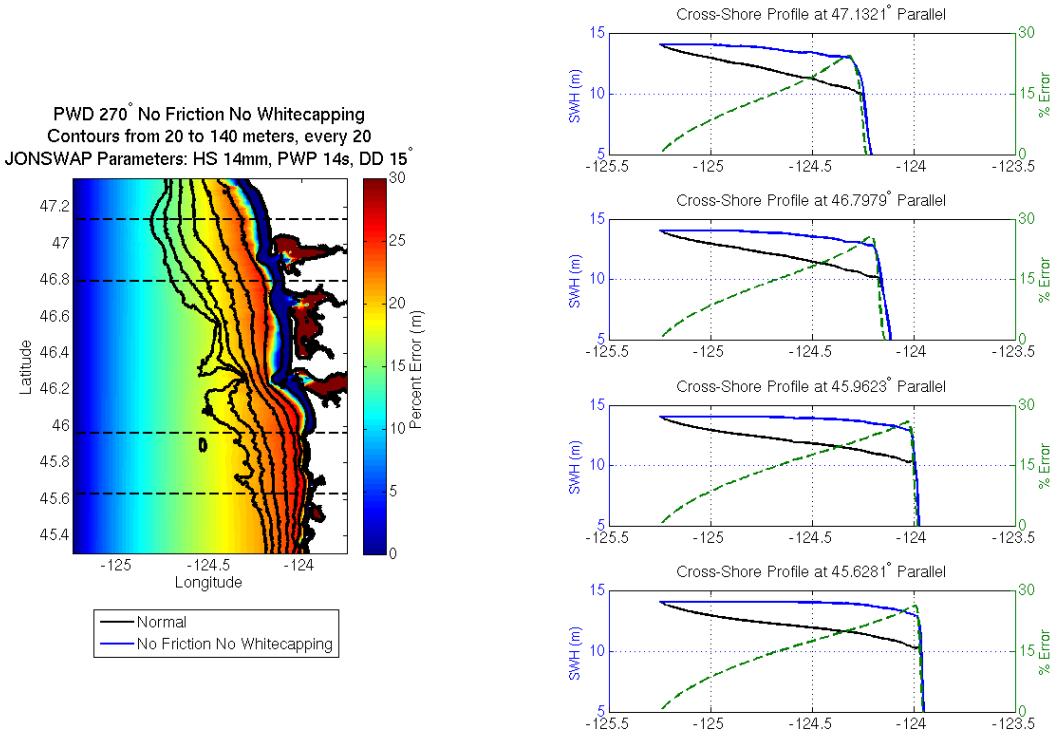

Figure 5-20. The impact of ignoring bottom frictional dissipation and dissipation due to whitecapping for a 14-m significant wave height with a peak period of 14 s approaching from a direction of 270 degrees.

For the direction bins (D_p), the bin widths were made approximately proportional to the probability distribution function of the GROW time series (and the synthesized wave climate time series). In application of this approach, 10 directional bins have been created that have approximately an equal probability of occurrence (**Figure 5-21**). As defined, the bin edges are: D_p = [170, 225, 240, 251, 260, 268, 277, 288, 304, 331, 370] and are subsequently refined in SWAN to D_p = [170, 225, 240, 250, 260, 270, 280, 290, 305, 330, 370], resulting in 11 directional cases for our SWAN runs. At the bin edges, linear interpolation is used to derive the wave parameters. From initial sensitivity runs, we have determined that these bin widths are more than adequate. **Figure 5-22** shows the result of interpolating over a 20-degree bin spacing.

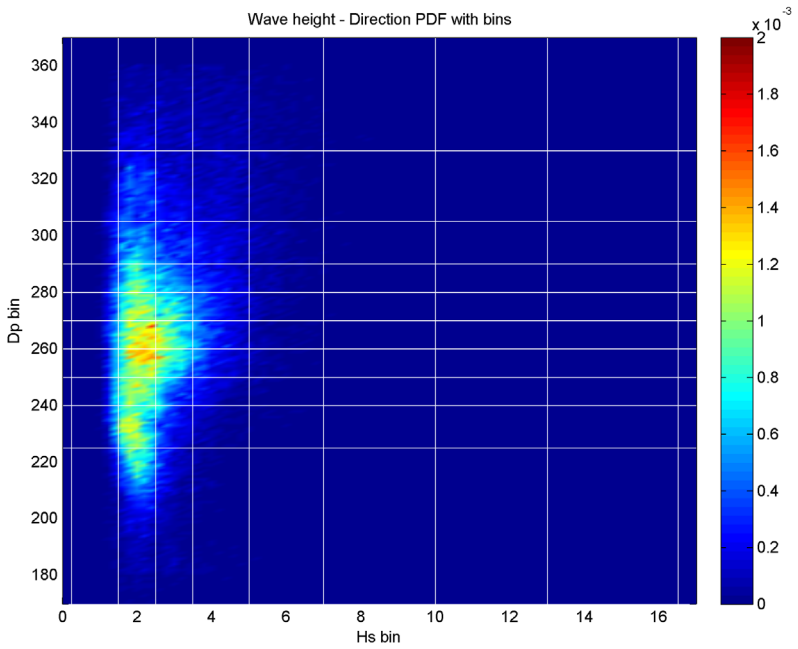

Figure 5-21. Joint probability of wave height and dominant direction derived from the GROW time series. Overlaid in white are the wave height and direction bins for use in the wave modeling on the Clatsop coast.

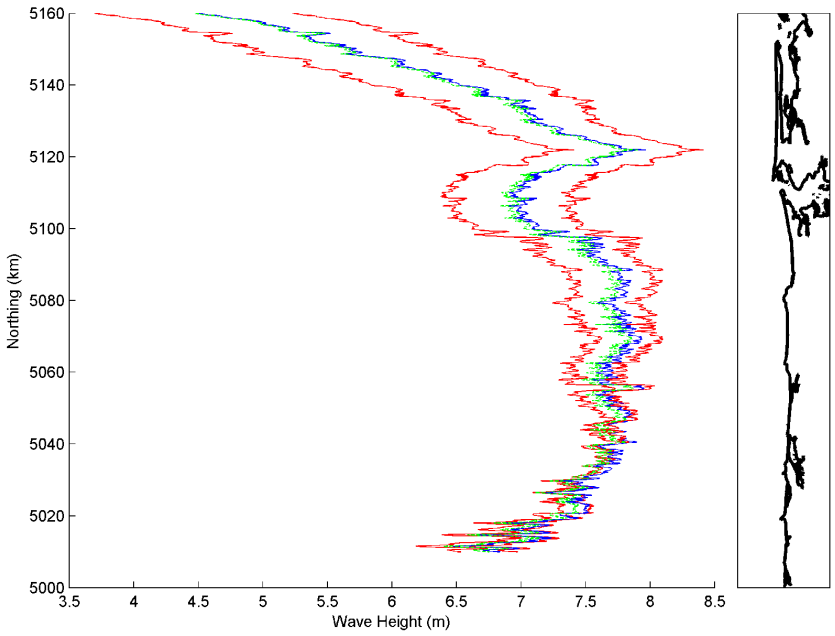

Figure 5-22. SWAN wave modeling and calculated alongshore wave variability using the look-up table approach. The left red line represents the alongshore variable wave height at the 20-m depth contour for an incident angle of 240 degrees (H_s = 10, T_p = 15 s) and the right red line is for an angle of 260 degrees. The blue line is the wave height for an angle of 250 degrees as modeled in SWAN while the green line is the linearly interpolated wave heights using the look-up table. Note that this is a preliminary SWAN model run, meant for testing the interpolation scheme, and the lateral boundary conditions are not dealt with in the same manner as in our production SWAN runs.

For the significant wave heights bins, we identified the following deepwater significant wave heights for inclusion in SWAN: H_s = [0.25, 1.5, 2.5, 3.5, 5, 7, 10, 13, 16.5], which gives us nine cases. From our sensitivity tests, we found that a bin width of 3 m for large waves is sufficient for resolving the linearly interpolated wave conditions (**Figure 5-23**). In the case of the deepwater peak periods, our analyses identified the following period bins for inclusion in SWAN: T_p = [2, 6, 9, 11, 13, 15, 17, 20, 23, 26], which provides a total of 10 additional cases. From our sensitivity tests, we found that the linear interpolation approach for wave period is not quite as good as for direction and wave height. Because wave period affects breaking, shoaling, and whitecapping, there is significant variability in the wave transformations as a function of wave period. For our sensitivity run of H_s = 10 m, and D_p = 260 degrees, **Figure 5-24** illustrates the impact of linear interpolation. However, for the most part in our parameter space we will have interpolation errors only around 10%. In this particular example the maximum error is only approximately 4 %.

Figure 5-25 presents the joint probability of wave height and peak period from the GROW time series. The white dots represent bin centers, from a much smaller mesh, in which this combination of H_s and T_p does not exist in the GROW time series. The red line represents the theoretical wave steepness limit below which waves are non-physical. We can use this information to reduce the overall matrix of model runs.

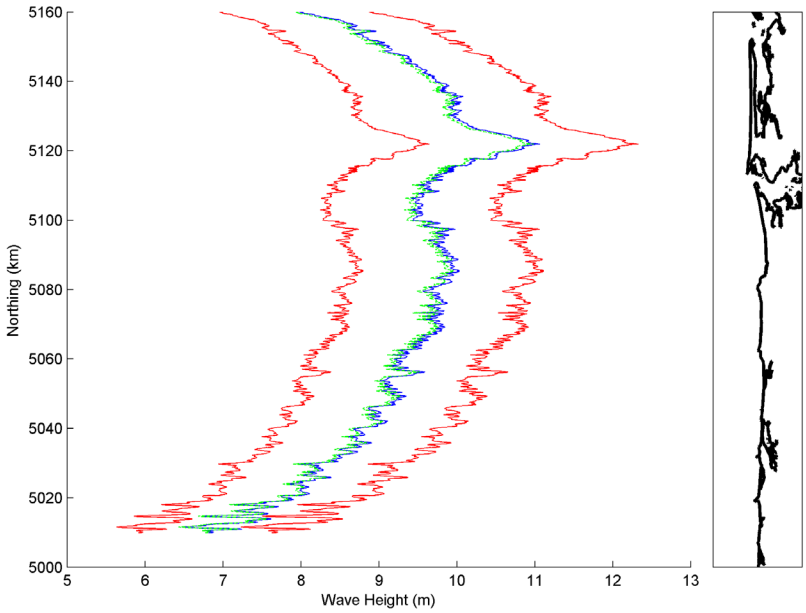

Figure 5-23. SWAN wave modeling and calculated alongshore wave variability using the look-up table approach for an 11-m and 15-m wave. In this example the red lines are the alongshore varying wave height for an 11-m and 15-m incident wave height in 20 m. The blue line is the modeled transformed 13-m wave height, while the green represents a linear interpolation between the 11- and 15-m results.

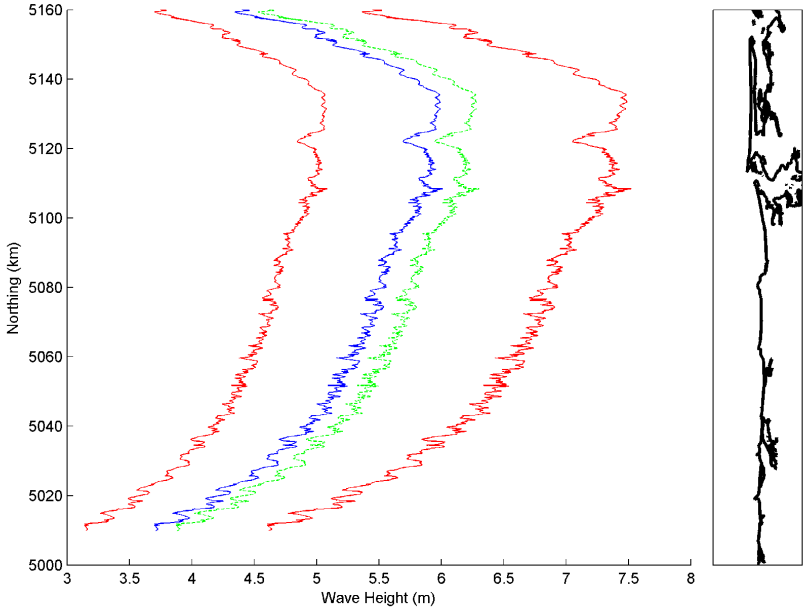

Figure 5-24. SWAN wave modeling and calculated alongshore wave variability using the look-up table approach for a 10-m wave. In this example the red lines are the alongshore varying wave height for a 10-m wave arriving from 260 degrees for 20 s and 24 s. The blue line is the modeled wave height for 22 s, and the green line represents a linear interpolation.

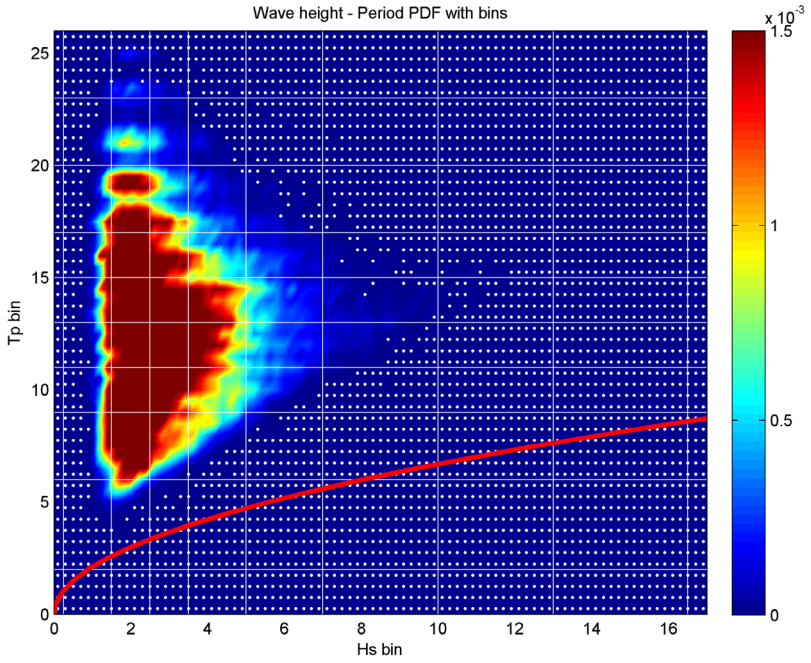

Figure 5-25. Joint probability of wave height and peak period from the GROW time series. The white dots represent bin centers, from a much smaller mesh, in which this combination of H_s and T_p does not exist in the GROW time series. The red line represents the theoretical wave steepness limit below which waves are non-physical.

Figure 5-26 is the joint probability of peak period and dominant wave height shown here for completeness. Finally, we illustrate our bin choice on the individual parameter PDFs in **Figure 5-27** (buoy data).

In summary, the lookup tables were generated using all wave parameter cases and two contrasting water levels. Our sensitivity tests indicated that varying water levels have a negligible impact on the model and linearly transformed waves. The following matrix of SWAN runs is considered for lookup table development for transforming waves offshore from Clatsop County.

D_p = [170, 225, 240, 250, 260, 270, 280, 290, 305, 330, 370] - 11 cases
H_s = [0.25, 1.5, 2.5, 3.5, 5, 7, 10, 13, 16.5] - 9 cases
T_p = [2, 6, 9, 11, 13, 15, 17, 20, 23, 26] - 10 cases
WL = [-1.5, 4.5] – 2 cases

In total, this equates to 1980 model cases that can be used for linearly interpolating the waves from a time series of data. However, **Figure 5-25** indicates that several H_s–T_p combinations are physically not realistic. Multiplying these bins by the D_p and WL bins means that we can eliminate 242 bins for a new total of only 1,738 model runs.

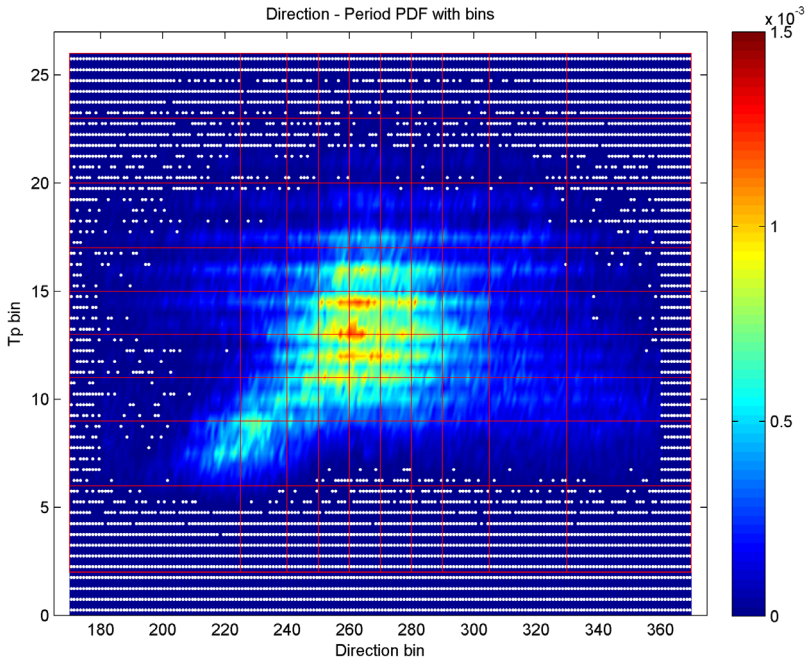

Figure 5-26. Joint probability of dominant direction and peak period from the GROW time series. The white dots represent bin centers, from a much smaller mesh, in which this combination of D_p and T_p does not exist in the GROW time series. The red lines depict the boundaries of the bin edges.

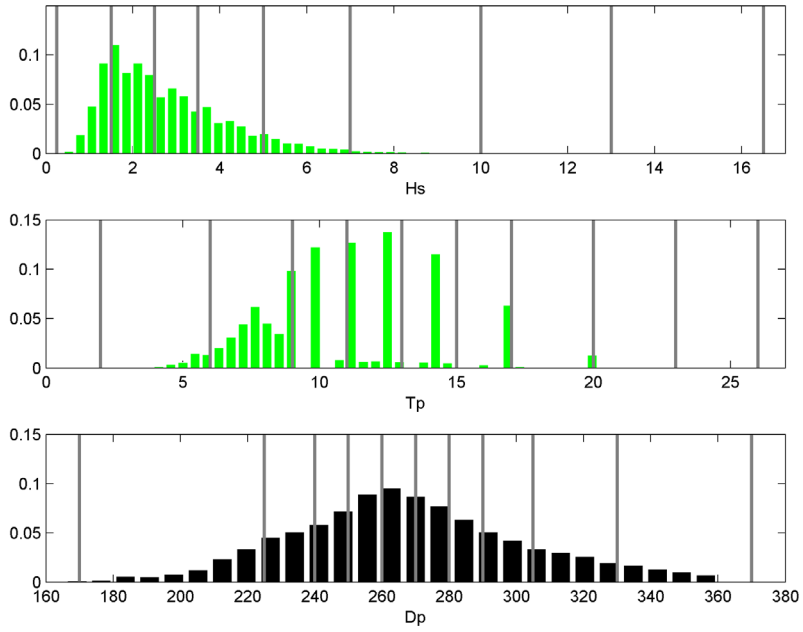

Figure 5-27. Individual parameter PDFs and bin edges using the combined buoy wave time series.

5.4 Summary of SWAN Results

Significant alongshore variability is apparent in many of the conditions examined with SWAN (**Figure 5-28**). Differences on the order of 3 m in significant wave height along the 20-m isobaths are not uncommon in Clatsop County. To calculate the wave runup along the County's shoreline we subsequently extracted the wave characteristics along the 20-m contour, or the seaward most location where the wave breaking parameter equaled 0.4, throughout the model domain (right panel **Figure 5-28**). Because all of the parametric runup models used in this study rely on information on the deep-water equivalent wave height and peak periods as inputs, we then computed the linear wave theory shoaling coefficient and back shoaled our transformed waves to deep-water. These transformed deep-water equivalent waves were then used to calculate the wave runup and generate the T_{WL} conditions used in the subsequent extreme value analysis.

To confirm that our approach of interpolating wave transformations using lookup tables yields acceptable results, we ran several additional SWAN runs that were not part of our original matrix. These additional runs extended across a range of conditions, including extreme events capable of forcing high water levels at the coast. We then compare the results from using the lookup tables to these additional direct SWAN computations at the 20 m contour location. **Figure 5-29** to **Figure 5-31** show a sample of these results for wave heights, peak periods, and directions respectively, for a SWAN run driven with an offshore boundary condition of H_s = 11.5, T_p = 18.5, D_p = 320, and a water level of 4.5 m NAVD88. In all cases, the % error between the lookup table and direct computation is low, averaging well less than 5%. In only a few locations, near model boundaries or inlets, are the errors significant. None of the transects analyzed in detail for extreme flooding later in this report are near those problem locations.

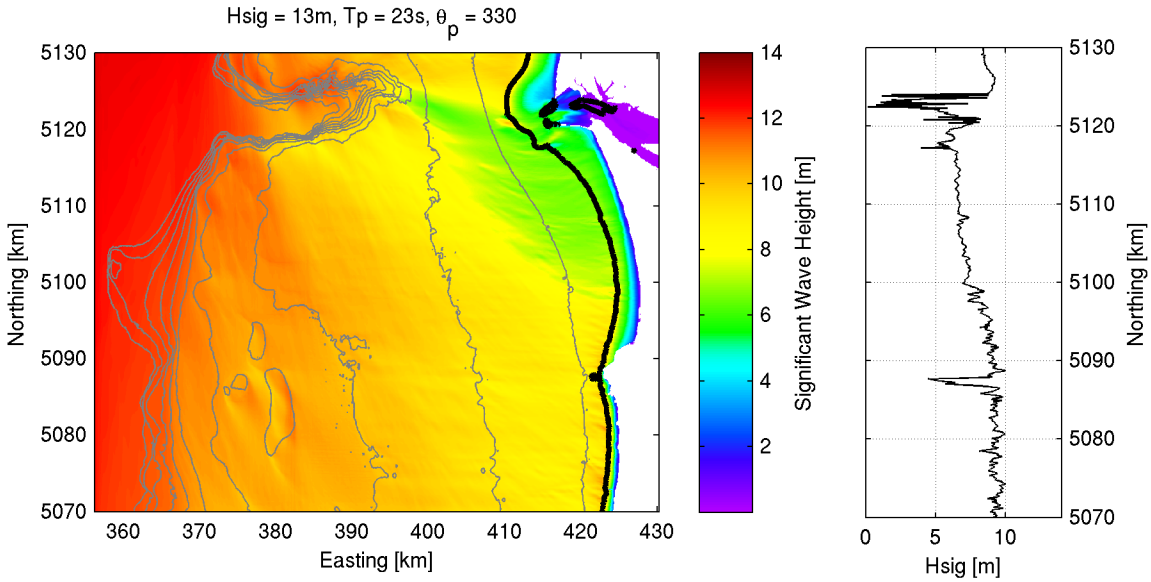

Figure 5-28. Example SWAN simulation, for an offshore significant wave height 13 m, peak wave period 23 s, and peak wave direction of 330 degrees. Left) Significant wave height in the modeling domain is shown in colors. Dissipation processes result in reduced inner shelf wave height. Contour lines are drawn from 50 to 500 m every 50 m in grey and 20 m in black. Right) Modeled significant wave height extracted at 20-m water depth.

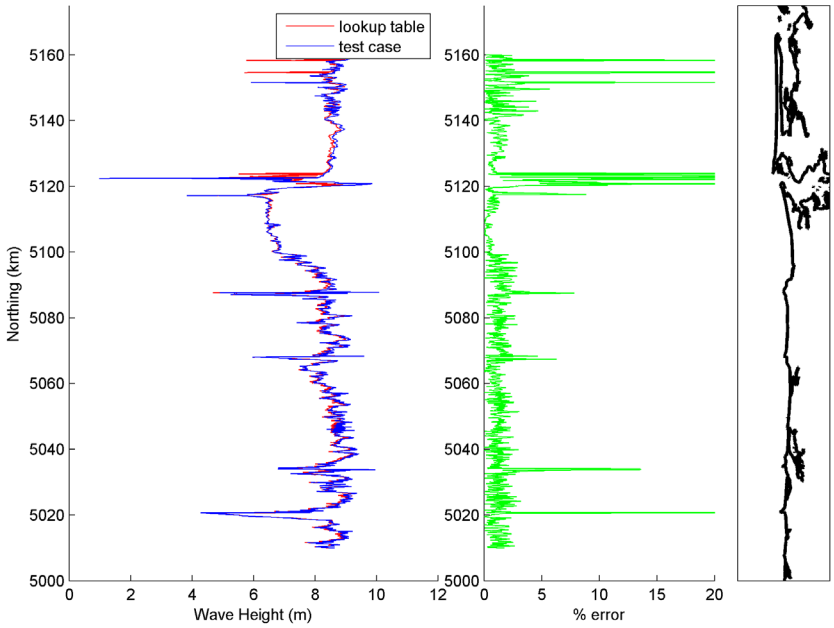

Figure 5-29. Comparison of alongshore varying wave height at the 20-m contour extracted from the lookup tables (red line) and from a direct SWAN computation (blue line) with an offshore boundary condition characterized as H_s = 11.5, T_p = 18.5, D_p = 320, and a water level of 4.5 m NAVD88.

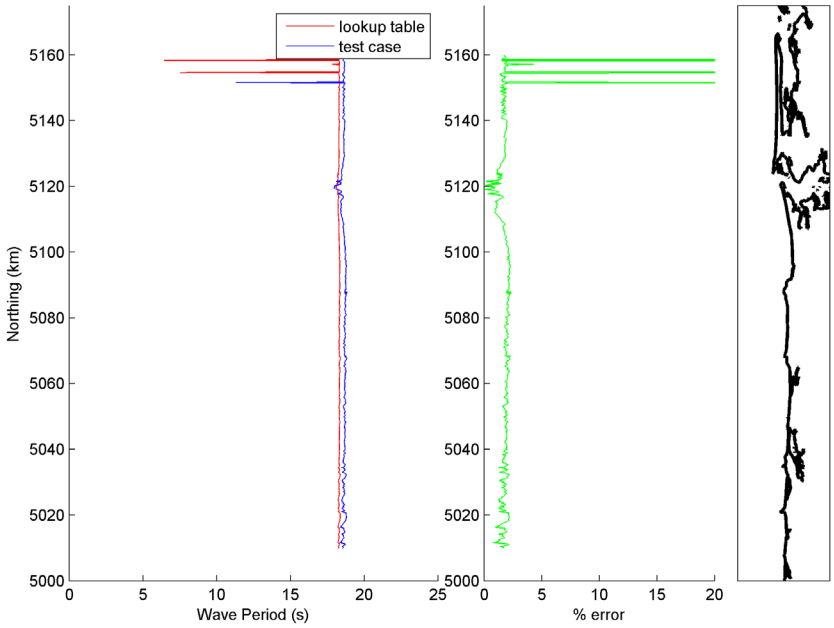

Figure 5-30. Comparison of alongshore varying wave period at the 20-m contour extracted from the lookup tables (red line) and from a direct SWAN computation (blue line) with an offshore boundary condition characterized as H_s = 11.5, T_p = 18.5, D_p = 320, and a water level of 4.5 m NAVD88.

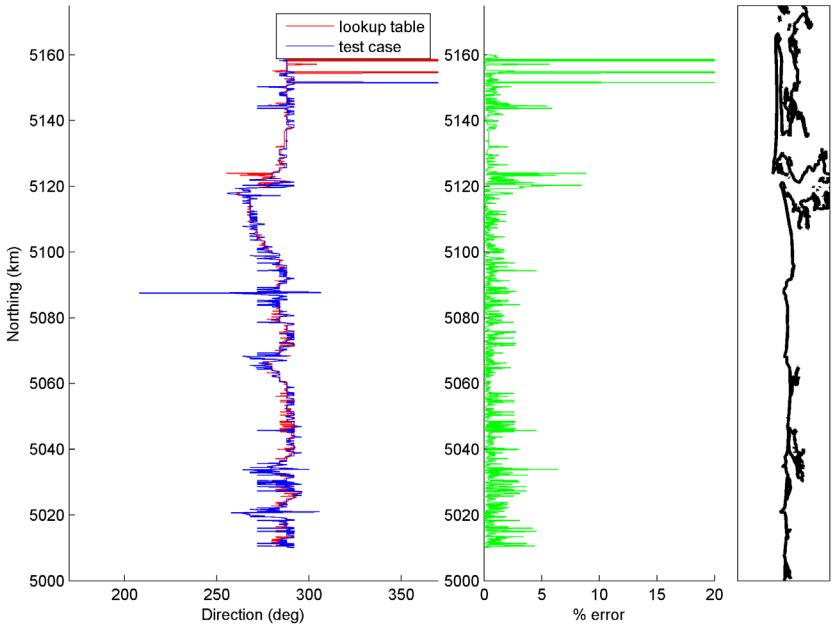

Figure 5-31. Comparison of alongshore varying wave direction at the 20-m contour extracted from the lookup tables (red line) and from a direct SWAN computation (blue line) with an offshore boundary condition characterized as H_s = 11.5, T_p = 18.5, D_p = 320, and a water level of 4.5 m NAVD88.

6.0 WAVE RUNUP AND OVERTOPPING

Wave runup is the culmination of the wave breaking process whereby the swash of the wave above the still water level is able to run up the beach face, where it may encounter a dune, structure, or bluff, potentially resulting in the erosion, or overtopping and flooding of adjacent land (**Figure 6-1**). Runup, *R*, or wave setup plus swash, is generally defined as the time-varying location of the intersection between the ocean and the beach, and as summarized is a function of several key parameters. These include the deepwater wave height (H_o or H_s), peak spectral wave period (T_p), the wave length (L_o) (specifically the wave steepness, H_o/L_o), and through a surf similarity parameter called the Iribarren number,

$$\xi_o = \frac{\beta}{\sqrt{H_o/L_o}},$$

which accounts for the slope (β) of a beach or an engineering structure, as well as the steepness of the wave.

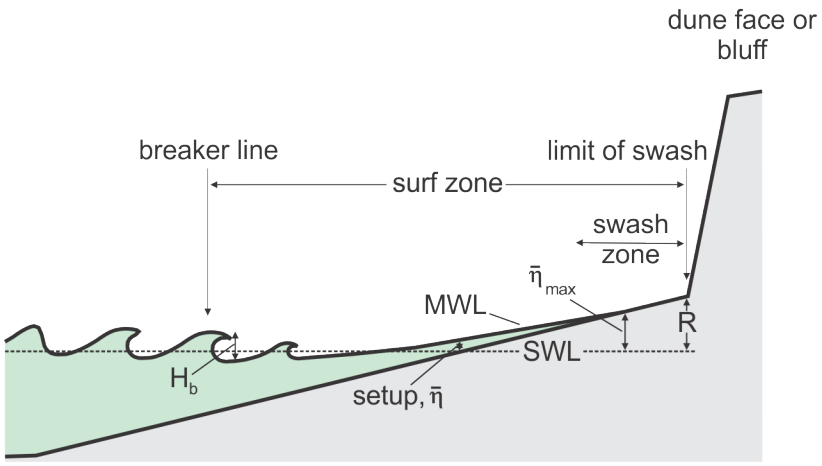

Figure 6-1. Conceptual model showing the components of wave runup associated with incident waves (modified from Hedges and Mase, 2004).

The total runup, *R*, produced by waves includes three main components:

- wave setup, $\overline{\eta}$;
- a dynamic component to the still water level, $\hat{\eta}$; and
- incident wave swash, S_{inc}

$$R = \overline{\eta} + \hat{\eta} + S_{inc} \qquad (6.1)$$

Along the Pacific Northwest Coast (PNW) of Oregon and Washington, the dynamic component of still water level, $\hat{\eta}$, has been demonstrated to be a major component of the total wave runup due to relatively high contributions from infragravity energy (Ruggiero and others, 2004). This process occurs due to a transfer of energy from the incident wind-generated waves to the longer-period infragravity wave energy, the division being placed at ~20-s periods. On the dissipative beaches of the Oregon coast, it is the infragravity energy that increases swash runup levels during major storms, and is ultimately responsible for erosion and overwash events. The combination of these processes produces "sneaker waves," yielding the most extreme swash runup levels.

A variety of models have been proposed for calculating wave runup on beaches (Ruggiero and others, 2001; Hedges and Mase, 2004; Northwest Hydraulic Consultants, 2005; Stockdon and others, 2006). Here we explore two approaches available for runup calculations along Clatsop County, Oregon. These included the runup model developed by Stockdon and others (2006) and the direct integration method (DIM) described in NHC (2005).

6.1 Runup Models for Beaches

6.1.1 Stockdon runup model

For sandy beaches, Stockdon and others (2006) developed an empirical model based on analyses of 10 experimental runup data sets obtained from a wide variety of beach and wave conditions, including data from Oregon (Ruggiero and others, 2004), and by separately parameterizing the individual runup processes: setup and swash. Stockdon and others (2006) proposed the following general relationship for the elevation of the 2% exceedance elevation of swash maxima, R_2, for any data run:

$$R_2 = 1.1[\bar{\eta} + \frac{S}{2}] \tag{6.2}$$

where:

$$S = \sqrt{(S_{inc})^2 + (\hat{\eta})^2} \tag{6.3}$$

and:

$$\bar{\eta}, S_{inc}, \hat{\eta} = f(H_o, T_o, \beta_f)$$

where β_f is the slope of the beach face, and S reflects both the dynamic, $\hat{\eta}$, and incident swash, S_{inc}, components. The 1.1 coefficient value was determined because the swash level assumes a slightly non-Gaussian distribution. The final parameterized runup equation is:

$$R_{2\%} = 1.1\left(0.35\tan\beta\,(H_oL_o)^{\frac{1}{2}} + \frac{[H_oL_o(0.563\tan\beta^2 + 0.004)]^{\frac{1}{2}}}{2}\right) \tag{6.4}$$

which may be applied to natural sandy beaches over a wide range of morphodynamic conditions. In developing equation 6.4, Stockdon and others (2006) defined the slope of the beach as the average over a region ±2σ around the wave setup, $\bar{\eta}$, where σ is the standard deviation of the continuous water level record, η(t). Simply put, the setup reflects the height of the mean-water level (MWL) excursion above the SWL, such that the slope is determined to span the region around this MWL. For Clatsop County, the slope of the beach was determined by fitting a linear regression through those data points spanning the region located between 2 to 4 m.

Combining equation 6.4 with the measured water level at tide gages produces the total water level, T_{WL} at the shore, important for determining the erosion or flood risk potential. Given that equation 6.4 has been derived from quantitative runup measurements spanning a range of beach slopes (beach slopes ranged from 0.01 to 0.11 and Iribarren numbers [**ξ**], ranged from 0.1 [fully dissipative conditions] to ~2.2 [reflective conditions], Table 1 of Stockdon and others [2006]), the model is valid for the range of slopes and conditions observed along the Clatsop County coastline and elsewhere on the Oregon coast.

6.1.2 Direct integration method—beaches

The FEMA coastal flood mapping guidelines (NHC, 2005) for the U.S West Coast presents an alternative method for calculating runup. According to NHC (2005), the direct integration method (DIM) approach allows for the wave and bathymetric characteristics to be taken into consideration, specifically the spectral shape of the waves and the actual bathymetry can be represented. Here we review the parameterized set of

runup equations that may be used to calculate runup on beaches. The equations are based on a parameterized JONSWAP spectra and uniform beach slopes.

Similar to equation 6.1, the runup of waves using DIM can be defined according to its three components that include the wave setup, $\overline{\eta}$, a dynamic nent, $\widehat{\eta}$, and the incident band swash, S_{inc}. Wave setup can be calculated using:

$$\overline{\eta} = 4.0\, F_H F_T F_{Gamma} F_{slope} \qquad (6.5)$$

while the root mean square (rms) of the dynamic component, $\widehat{\eta}_{rms}$, may be estimated using:

$$\widehat{\eta}_{rms} = 2.7\, G_H G_T G_{Gamma} G_{slope} \qquad (6.6)$$

where the units of $\overline{\eta}$ and $\widehat{\eta}_{rms}$ are in *feet* and the factors (F) are for the wave height (F_H and G_H), wave period (F_T and G_T), JONSWAP spectrum narrowness (F_{Gamma} and G_{Gamma}), and the nearshore slope (F_{slope} and G_{slope}). These factors are summarized as a series of simple equations in Table D.4.5-1 (NHC, 2005). For the purposes of defining an average slope, NHC recommended that the nearshore slope be based on the region between the runup limit and twice the wave breaking depth, h_b, where:

$$h_b = H_b / k \qquad (6.7)$$

and

$$H_b = 0.39 g^{0.2} \left(T_p H_o^2\right)^{0.4} \qquad (6.8)$$

where H_b is the breaker height calculated using equation 6.8 (Komar, 1998), g is acceleration due to gravity (9.81 m/s), and for the purposes here k (breaker depth index) can be taken to be 0.78. Thus, one important distinction between the DIM and Stockdon methods for calculating runup, is the method used to define the beach slope; the former accounts for a larger portion of the nearshore slope, while the latter is based on the slope calculated around the mid beachface.

To derive the statistics of the oscillating wave setup and the incident swash components, the recommended approach is to base the calculations on the standard deviations (σ) of each component. The standard deviation of the incident wave oscillation (σ_2) on natural beaches may be calculated from:

$$\sigma_2 = 0.3 \xi_o H_o \qquad (6.9)$$

Because the standard deviation of the wave setup fluctuations (σ_1) is proportional to equation 6.6, the total oscillating component of the dynamic portion of the wave runup can be derived from:

$$\widehat{\eta_T} = 2.0 \sqrt{\sigma_1^2 + \sigma_2^2} \qquad (6.10)$$

Combining the results of equations 6.10 and 6.5 yields the 2% wave runup, and when combined with the tidal component results in the total water level, T_{WL}.

6.1.3 Comparison between the Stockdon and DIM runup calculations

Fundamentally, the wave runup model proposed by Stockdon and others (2006) and the DIM method described in NHC (2005) are similar, because both models account for the three components of runup described in equation 6.1. Here we examine the runup results derived from both models based on a range of conditions characteristic of the Clatsop County shoreline (**Figure 6-2** and **Figure 6-3**). We focus on our results from Clatsop, because this is where we first tested both approaches, before settling on one approach for calculating all subsequent runup for the Oregon coast.

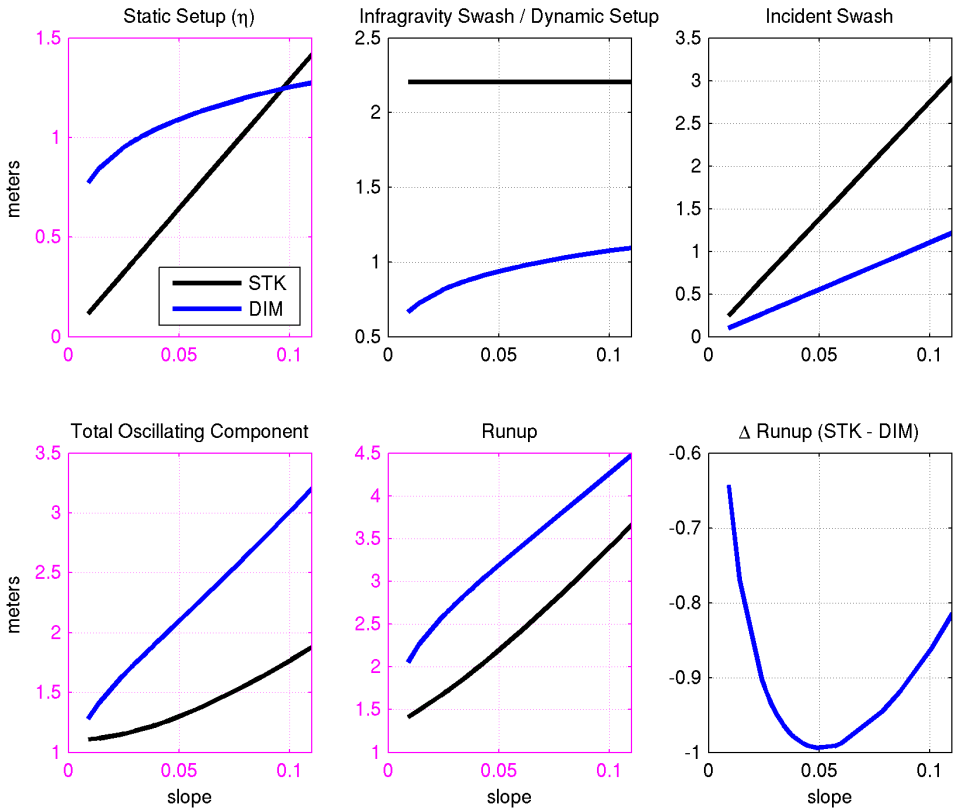

Figure 6-2. Calculated setup, swash and runup using the Stockdon and DIM runup equations. In this example, slope values are defined similarly for both methods, at a mid-beach elevation range of 2–4 m (6.6–13 ft). A 6 m (19.7 ft) significant wave height, 12-s peak wave period, and 270° wave direction were used to drive the models. Due to the semi-empirical nature of the equations, only the magnitudes of the subplots outlined in magenta are directly comparable (the two panels showing swash results are not directly comparable). The total oscillating component compares the results from equation 6.3 (S/2) with equation 6.10.

Figure 6-2 provides a comparison of the various calculated parameters (setup, infragravity swash, incident swash, total oscillating component, and runup) determined using the Stockdon and DIM approaches. In this example, we use the same slope defined for the mid-beach region in order to provide a direct comparison between DIM and Stockdon. Upper estimates have been truncated to tan β = 0.11, which reflects the slope limit on which Stockdon has been tested. In contrast, it is unclear the range of slope conditions on which DIM may be applied as there is no quantitative field testing of this particular formulation. As can be seen in **Figure 6-2**, although there are notable differences in the various parameterizations, the derived runup (bottom, middle plot) is similar. Nevertheless, as can be seen from the ΔR plot (bottom right), the DIM approach tends to estimate a slightly higher runup when compared to Stockdon, which in this example reaches a maximum of ~1 m (3.3 ft) for a beach slope of 0.04 to 0.05. Thus, overall, we can conclude that the two approaches are performing in a similar fashion when tested using the same slope.

Figure 6-3 presents a similar suite of comparisons under the same hydrodynamic conditions. Therefore the Stockdon and others (2006) results are identical to **Figure 6-2** in all panels. However, in this example we now account for the appropriate nearshore slope in the DIM runup calculations as defined above in

Section 6.1.2. We do this by computing the DIM runup components for this hydrodynamic condition at all of the 85 Clatsop County transects that we analyze in detail in this report using the full nearshore slope. The DIM values are, however, plotted against the foreshore beach slopes defined for all 85 transects in order to make the comparisons with Stockdon meaningful. As can be seen in **Figure 6-3**, application of the near-shore slope significantly changes the magnitudes of all the runup components, and in particular reduces the calculated runup when compared to Stockdon for most foreshore slopes. In general, at lower slopes (tan β < 0.05) runup calculated by DIM is slightly higher than Stockdon, which reverses at steeper slopes (tan β > 0.05). This pattern is consistent with analyses performed by Allan and others (2012) in Coos County.

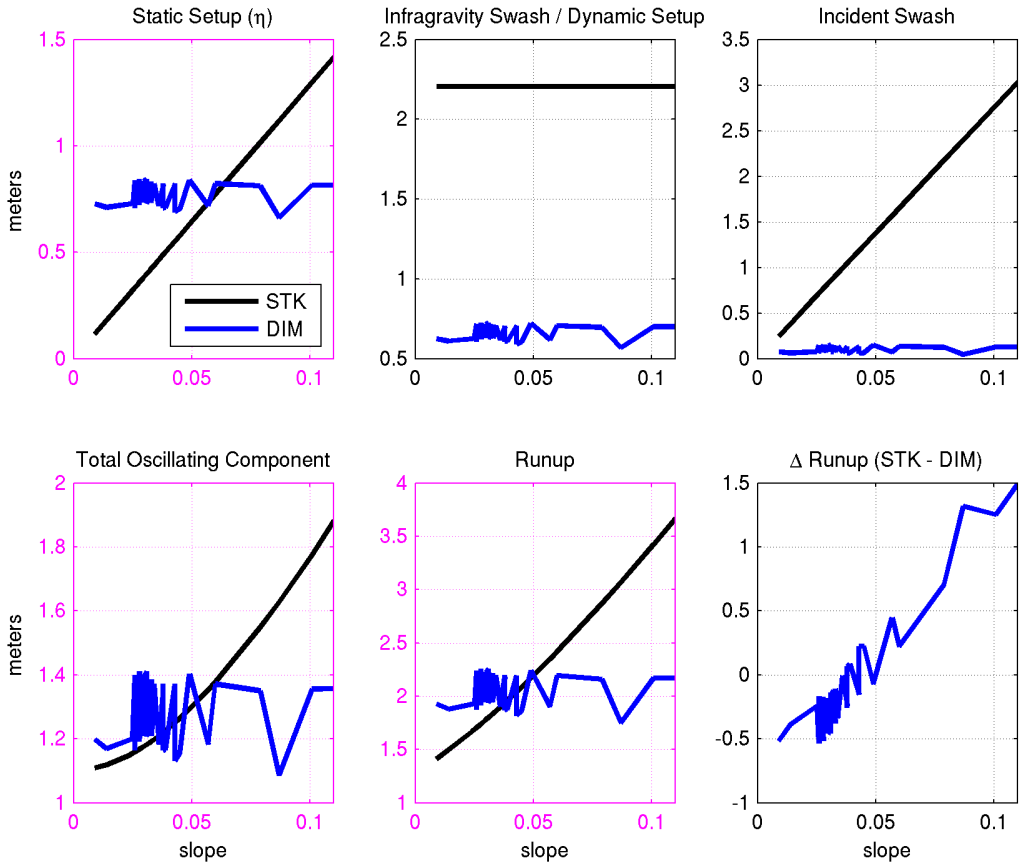

Figure 6-3. Total water level calculations using the Stockdon (foreshore slope) and DIM runup equations (nearshore slope). A 6m (19.7ft) significant wave height, 12s peak wave period, and 270° wave direction was used to drive the models. Due to the semi-empirical nature of these equations only the magnitudes of the subplots outlined in magenta are directly comparable. The results for DIM are sorted in ascending order as a function of foreshore beach slope.

Most interesting in the comparisons shown in **Figure 6-3** is that the DIM runup components actually do not vary as a function of the foreshore slope. The total runup (**Figure 6-3** bottom-center) produced by DIM is relatively constant, oscillating between 1.7 and 2.3 m (5.6 and 7.5 ft). The oscillations are due primarily to the variability in the nearshore slopes, which are a function of wave height (equations 6.7 and 6.8). Because waves in the PNW are relatively large and upper shoreface slopes relatively shallow, the DIM

runup values are controlled by the nearshore slope with little influence from the upper beach. This lack of dependence on the foreshore is in contrast to field measurements made in Oregon (Ruggiero and others, 2004) in which runup is clearly a function of the foreshore slope. Because the Stockdon model has been extensively validated against measured runup data, including measurements on the Oregon coast (e.g., Ruggiero and others, 2001, 2004) together with qualitative observations of runup during storms by DOGAMI staff at multiple sites along the coast, 1% extreme values of T_{WLS} calculated for sandy beaches along the Clatsop County coast will be based primarily on the Stockdon and others (2006) model.

6.2 "Barrier" Runup Calculations

6.2.1 Introduction

According to NHC (2005), an alternate approach is recommended for use in calculating runup on steep barriers. By definition, *barriers include "steep dune features and coastal armoring structures such as revetments"* (NHC, 2005, p. D.45-10), although little guidance is offered in terms of the range of slopes to which this alternate approach would apply. Throughout this document we use the generic term *barrier* to define the range of morphological and engineering conditions where barrier runup calculations may apply. In general, runup on barriers depends not only on the height and steepness of the incident waves defined through the Iribarren number or breaker parameter ($\xi_{m-1,0}$), but also on the geometry (e.g., the slope of the barrier and/or if a berm is present), design characteristics of the structure and its permeability.

The recommended approach for calculating runup on barriers is to use the TAW (Technical Advisory Committee for Water Retaining Structures) method, which provides a mechanism for calculating the runup, adjusted for various reduction factors that include the surface roughness, the influence of a berm (if present), and effects associated with the angle of wave approach (van der Meer, 2002; Northwest Hydraulic Consultants, 2005; Pullen and others, 2007). According to NHC (2005) the TAW method is useful as it includes a wide range of conditions for calculating the wave runup (e.g., both smooth and rough slopes), and because it agrees well with both small- and large-scale experiments.

Figure 6-4 is a conceptual model of the various components required to determine the extent of runup on barriers. Of importance is first determining the 2% Dynamic Water Level ($DWL_{2\%}$) at the barrier, which includes the combined effects of the measured still water level (SWL), the wave setup ($\bar{\eta}$) and the dynamic portion ($\hat{\eta}$) of the runup (**Figure 6-4**), which is then used to establish the spectral significant wave height (H_{mo}) at the toe of the "barrier" (NHC, 2005).

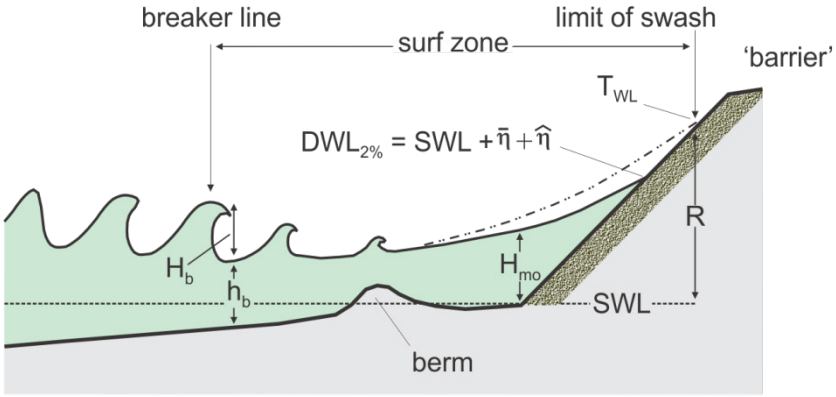

Figure 6-4. Wave runup on a beach backed by a structure or bluff (modified from NHC, 2005).

The general formula for calculating the 2% wave runup height on barriers is given in a non-dimensional form by equation 6.11:

$$\frac{R_{2\%}}{H_{mo}} = c_1 . \gamma_b . \gamma_f . \gamma_\beta . \xi_{m-1,0} \qquad (6.11)$$

with a maximum of:

$$\frac{R_{2\%}}{H_{mo}} = \gamma_f . \gamma_\beta \left(c_2 - \frac{c_3}{\sqrt{\xi_{m-1,0}}} \right)$$

where:

$R_{2\%}$ = wave runup height exceeded by 2% of the incoming waves,

H_{mo} = spectral significant wave height at the structure toe,

c_1, c_2, and c_3 = empirical coefficients with:

γ_b = influence factor for a berm (if present)

γ_f = influence factor for roughness element of slope

γ_β = influence factor for oblique wave attack

$\xi_{m-1,0}$ = breaker parameter:

$$\left(\tan \beta / \left(H_{mo} / L_{m-1,0} \right)^{0.5} \right),$$

$\tan \beta$ = slope of the "barrier,"

$L_{m-1,0}$ = the deepwater wave length $\left(g T_{m-1,0}^2 / 2\pi \right)$,

$T_{m-1,0}$ can be calculated from $T_p/1.1$, where T_p is the peak spectral wave period.

Substituting the empirical coefficients derived from wave tank experiments and incorporating a 5% upper exceedance limit into the general equations of 6.11 (van der Meer, 2002; Pullen and others, 2007), runup on barriers may be calculating using:

$$R_{2\%} = H_{mo}\left(1.75 . \gamma_b . \gamma_f . \gamma_\beta . \xi_{m-1,0}\right), where\ 0 < \gamma_b . \xi_{m-1,0} < 1.8 \qquad (6.12)$$

with a maximum of:

$$R_{2\%} = H_{mo}\left(1.0 . \gamma_f . \gamma_\beta \left(4.3 - \frac{1.6}{\sqrt{\xi_{m-1,0}}} \right) \right), where\ \gamma_b . \xi_{m-1,0} \geq 1.8$$

There are, however, notable differences between equation 6.12 originally described by van der Meer (2002) and Pullen and others (2007) from that presented in equation D.4.5-19 in the FEMA West Coast methodology (NHC, 2005). For example, equation D.4.5-19 in the NHC report contains a higher coefficient value (1.77), along with one additional reduction factor (porosity) for calculating runup when the breaker parameter is less than 1.8. Similarly, for conditions where the breaker parameter exceeds 1.8 and the maximum runup equation is used, equation D.4.5-19 in the NHC report contains two extra reduction factors (berm and porosity reduction factors) that are not included in the original solution, which potentially could have a very significant effect on the calculated runup. Because of these differences, we have used the original solution presented as equation 6.12 of van der Meer (2002) and Pullen and others (2007).

6.2.2 Specific procedure for calculation of "barrier" runup

For those cases where the TAW method is used for determining runup on barriers (i.e., beaches backed by structures, cobble berms, and/or bluffs), we have followed the general approach laid out in section D.4.5.1.5.2 in NHC (2005), with the exception that we use Stockdon to define the $DWL_{2\%}$ (instead of DIM) at the structure toe, and TAW to calculate the incident swash on the barrier (i.e., equation 6-12). Because waves are depth limited at the barrier toe, H_{mo} may be estimated from $DWL_{2\%}$ using a breaker index of 0.78 (i.e., $H_{mo} = DWL_{2\%} * 0.78$). In performing these various derivations, $DWL_{2\%}$ was first determined using equation 6.13:

$$DWL_{2\%} = SWL + 1.1 * \left(\overline{\eta} + \frac{\widehat{\eta}}{2}\right) - D_{low} \qquad (6.13)$$

where:

SWL = measured tide,

$\overline{\eta} = 0.35 * \tan\ \beta\sqrt{H_s * L}$ *Eqn. 10 in Stockdon and others (2006)*

$\widehat{\eta} = 0.06 * \sqrt{H_s * L}$ *Eqn. 12 in Stockdon and others (2006)*

D_{LOW} = the toe of the structure or bluff, and

tan β = the beach slope defined for the region between 2 and 4 m.

Having calculated $DWL_{2\%}$ and H_{mo}, the TAW runup calculation can be implemented. equation 6.12 requires information on the slope of the barrier, used in the breaker parameter ($\xi_{m\text{-}1,0}$) calculation, which can be somewhat challenging to define. This is especially the case if the morphology of the barrier exhibits a composite morphology characterized by different slopes, such that errors in estimating the slope will translate to either significant underestimation or overestimation of the runup. According to van der Meer (2002) and Pullen and others (2007), because the runup process is influenced by the change in slope from the breaking point to the maximum wave runup, the characteristic slope should be specified for this same region. On the Oregon coast, the most common composite slope example is the case where a broad, dissipative sand beach fronts a structure or bluff that is perched relatively high on the back of the beach (structure toe > ~4-5 m). In this example, the wave runup is first influenced by the sandy beach slope and finally by the slope of the structure itself. To address this type of situation, we define a "local barrier slope," as the portion of the barrier that ranges from the calculated storm T_{WL} (calculated initially using equation 6.4) down to a lower limit defined by the wave setup plus the SWL (i.e., $(1.1 * \overline{\eta}) + SWL$). In a few cases, the T_{WL} was found to exceed the barrier crest in which case we used the structure crest as the upper limit for defining the local slope. This process is repeated for every storm condition. Having determined the barrier slope, the TAW runup is calculated using equation 6.12 and reduced based on the appropriate site specific reduction factors.

Under certain conditions, we identified events that generated extreme runup that made little physical sense. For these (rare) cases, we calculated the TAW runup using an iterative approach based on procedures outlined in the Eurotop (2007) manual. Because the maximum wave runup is the desired outcome and is unknown when initially defining the slope, the process is iterative requiring two steps. First, the breaking limit is defined as $1.5H_{mo}$ *below* the SWL, while $1.5H_{mo}$ *above* the SWL defines the upper limit of the first slope estimate (**Figure 6-5**). Having determined the first slope estimate, the TAW runup is calculated using equation 6.12 and reduced based on the appropriate reduction factors. A second slope estimate is then performed based on the initial runup calculation, while a third iteration is not necessary based on our tests because this method converges quickly. The breaking limit is again defined as $1.5H_{mo}$ *below* the SWL, while $R_{2\%}$ *above* the SWL defines the upper limit, and the final barrier runup estimate is again calculated using equation 6.12 and reduced based on the appropriate reduction factors.

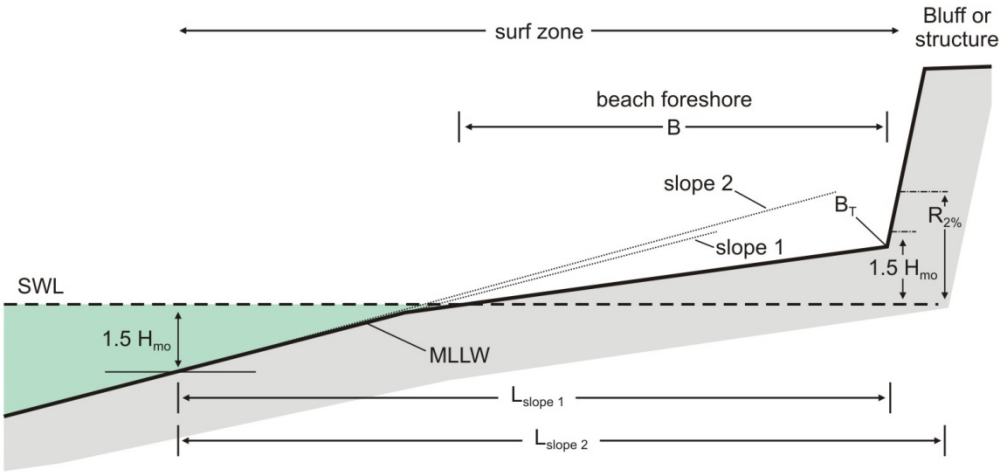

Figure 6-5. Determination of an average slope based on an iterative approach. The first estimate is initially based on 1.5 H_{mo} ±SWL, while the second estimate is based on 1.5H_{mo} below the SWL and the calculated $R_{2\%}$ above the SWL that is based on the first slope estimate.

Finally, it is important to note that the runup estimates based on the "barrier" runup calculations is sensitive to the slope. Similar to our study in Coos County, we identified several sites (primarily beaches backed by bluffs) along the Clatsop coast where the final T_{WLs} calculated using TAW was unreasonably low. These few cases are entirely due to there being a very wide dissipative surf zone at these transect locations that results in very low slopes being defined. For these sites where the calculated T_{WLs} seemed unreasonably low (relative to the morphology of the beach and observations of storm wave runup along this shore and elsewhere), we have defaulted to the T_{WLs} calculated using the Stockdon and others model.

6.2.3 "Barrier" runup reduction factors

Table 6-1 below presents information pertaining to the suite of parameters used to define wave runup (R) and ultimately the 1% T_{WLs} along the Clatsop County coast. In the case of bluff roughness along the Clatsop shore, we used a value of 0.6 for those situations here a bluff face was highly vegetated. These bluffs are typically located at or near their stable angle of repose and are covered with Salal plants (*Gaultheria shallon*), forming a deep, nearly impenetrable thicket. The decision to use 0.6 was based on discussions with Dr. WG McDougal (Coastal Engineer, OSU and Technical Coordinator of the North Pacific FEMA West Coast Guidelines, pers. comm., April 2010). At Cannon Beach Transects 3 and 13, and Seaside Transects 8 to 11, the reduction factor was set to 1 due to the presence of a seawall backing the beach. For those beaches backed by a significant riprap structure, fronted by a narrow gravel beach and broad dissipative sand beach, we used a reduction factor of 0.55. In other situations where a bluff is fronted by a narrow gravel beach and broad dissipative sand beach, we used a reduction factor of 0.8. Wave direction (γ_β) reduction factors were determined based on the shoreline orientation at every transect site and the actual wave directions measured during each storm condition. The reduction factor was calculated using equation D.4.5-22 (NHC, 2005, p. D.4.5-13). Finally, because none of the transects where structures are present contained a protective berm, no berm reduction factor was adopted for Clatsop County.

Table 6-1. Parameters used to define runup (*R*) and total water levels (TWLs) on beaches backed by dunes, structures, and bluffs.

Reach	Profile Number	D_{HIGH} (m)	D_{LOW} (m)	Beach Slope (tan β)	Wave Dir. (γ_β)	Rough-ness (Yr)	Approach	Description
Clatsop Plains	1	10.972	5.024	0.036	270	1.0	STK	dune-backed
	2	12.504	5.561	0.028	270	1.0	STK	dune-backed
	3	11.543	5.483	0.024	270	1.0	STK	dune-backed
	4	13.003	6.222	0.028	270	1.0	STK	dune-backed
	5	14.539	5.344	0.025	278	1.0	STK	dune-backed
	6	14.099	6.342	0.031	270	1.0	STK	dune-backed
	7	13.892	6.377	0.032	265	1.0	STK	dune-backed
	8	13.819	6.455	0.029	262	1.0	STK	dune-backed
	9	13.405	6.554	0.029	262	1.0	STK	dune-backed
	10	14.18	6.508	0.027	258	1.0	STK	dune-backed
	11	15.313	6.533	0.033	255	1.0	STK	dune-backed
	12	16.059	5.628	0.029	255	1.0	STK	dune-backed
	13	15.96	5.997	0.031	252	1.0	STK	dune-backed
	14	6.215	6.215	0.038	250	1.0	STK	dune-backed
Seaside	1	15.152	6.484	0.149	360	0.55	Snsh/TAW	cobble berm backed by high bluff
	2	5.639	5.639	0.165	360	0.55	Snsh/TAW	cobble berm backed by high bluff
	3	6.570	6.570	0.186	341	0.55	Snsh/TAW	sand backed by cobble berm
	4	6.810	6.810	0.028	298	1.0	STK	sand backed by cobble berm
	5	5.916	5.890	0.039	287	1.0	STK	sand backed by cobble berm
	6	8.328	5.778	0.045	284	1.0	STK	dune-backed
	7	7.288	5.576	0.026	281	1.0	STK	dune-backed
	8	8.040	6.500	0.018	281	1.0	STK	sand backed by seawall
	9	8.258	5.326	0.015	280	1.0	STK	sand backed by seawall
	10	7.894	6.379	0.021	280	1.0	STK	sand backed by seawall
	11	7.255	5.114	0.022	280	1.0	STK	sand backed by seawall
	12	9.679	4.362	0.014	293	1.0	STK	dune-backed
	13	8.019	4.680	0.009	281	1.0	STK	dune-backed
	14	7.410	4.280	0.007	264	0.60	Snsh/TAW	sand backed by low bluff
	15	6.864	3.149	0.005	272	0.60	Snsh/TAW	sand backed by low bluff
	16	5.800	2.400	0.005	269	0.55	Snsh/TAW	sand backed by riprap/low bluff
	17	5.418	2.330	0.005	275	1.0	Snsh/TAW	dune-backed

Reach	Profile Number	D_{HIGH} (m)	D_{LOW} (m)	Beach Slope (tan β)	Wave Dir. (γ_β)	Rough-ness (γr)	Approach	Description
Cannon Beach/ Tolovana	CB 1	16.651	4.869	0.026	282	0.80	STK	sand backed by high bluff
	CB 2	9.438	4.348	0.030	270	0.80	LocSlp/TAW	sand backed by riprap/mod high bluff
	TOL 1	8.29	4.696	0.031	273	0.70	LocSlp/TAW	sand backed by cobble, riprap/low bluff
	TOL 2	7.006	4.663	0.029	275	1.0	LocSlp/TAW	sand backed by cobble/low bluff
	TOL 3	7.832	4.938	0.030	275	0.70	STK	sand backed by cobble, riprap/low bluff
	TOL 4	8.222	4.942	0.028	275	0.80	LocSlp/TAW	sand backed by riprap/low bluff
	TOL 5	7.708	4.509	0.026	273	0.80	LocSlp/TAW	sand backed by cobble, riprap/low bluff
	CB 3	10.043	5.173	0.031	270	1.0	LocSlp/TAW	sand backed by seawall
	TOL 6	8.193	4.323	0.025	272	0.80	LocSlp/TAW	sand backed by riprap/low bluff
	TOL 7	7.697	4.812	0.025	272	0.80	LocSlp/TAW	sand backed by riprap/low bluff
	TOL 8	7.300	5.011	0.026	271	0.70	STK	sand backed by riprap/low bluff
	TOL 9	8.229	5.218	0.027	270	0.70	STK	sand backed by riprap
	TOL 10	7.644	4.130	0.029	270	0.80	LocSlp/TAW	sand backed by riprap/concrete foundation
	TOL 11	6.662	4.122	0.024	270	0.80	LocSlp/TAW	sand backed by riprap
	TOL 12	7.609	4.344	0.029	270	0.80	LocSlp/TAW	sand backed by riprap/low bluff
	CB 4	7.903	5.200	0.030	269	1.0	LocSlp/TAW	sand backed by low bluff
	TOL 13	7.955	4.565	0.028	269	1.0	LocSlp/TAW	wooden bulkhead/low bluff
	TOL 14	7.629	4.218	0.027	269	1.0	LocSlp/TAW	sand backed by riprap/low bluff
	TOL 15	7.537	4.068	0.025	270	1.0	LocSlp/TAW	sand backed by riprap/low bluff
	TOL 16	7.458	4.040	0.026	270	1.0	LocSlp/TAW	sand backed by riprap/low bluff
	TOL 17	7.980	4.528	0.026	270	1.0	LocSlp/TAW	sand backed by riprap/low bluff
	CB 5	7.035	4.713	0.028	270	1.0	LocSlp/TAW	sand backed by riprap/low bluff
	TOL 18	8.974	4.941	0.029	270	0.70	STK	sand backed by cobble, riprap/low bluff
	CB 6	12.826	4.285	0.027	270	1.0	LocSlp/TAW	sand backed by high bluff
	CB 7	16.011	4.607	0.032	270	0.70	LocSlp/TAW	sand backed by riprap/high bluff
	CB 8	15.746	6.869	0.031	275	0.70	STK	sand backed by high bluff
	CB 9	6.805	4.129	0.023	272	1.0	LocSlp/TAW	sand backed by seawall
	CB 10	9.752	6.966	0.028	270	0.70	STK	sand backed by mod high bluff
	CB 11	11.49	5.186	0.049	270	1.0	STK	dune-backed
	CB 12	10.964	4.231	0.051	279	0.55	LocSlp/TAW	sand backed by riprap/mod high bluff
	CB 13	6.709	4.127	0.012	283	1.0	LocSlp/TAW	sand backed by seawall
	CB 14	6.841	4.184	0.020	285	0.55	STK	sand backed by riprap
	CB 15	14.857	4.867	0.038	263	1.0	STK	dune-backed
	CB 16	16.764	4.723	0.043	256	1.0	STK	dune-backed
	CB 17	15.061	4.056	0.033	256	1.0	STK	dune-backed
Arcadia	1	15.322	6.201	0.060	270	1.0	LocSlp/TAW	sand, gravel backed by high bluff
	2	17.825	5.713	0.034	272	1.0	STK	sand, gravel backed by high bluff
	3	12.366	4.925	0.038	270	1.0	LocSlp/TAW	sand backed by mod high bluff

Reach	Profile Number	D_{HIGH} (m)	D_{LOW} (m)	Beach Slope (tan β)	Wave Dir. (γ_β)	Rough-ness (γr)	Approach	Description
Arch Cape	1	6.876	6.876	0.093	275	0.80	LocSlp/TAW	sand backed by gravel berm
	2	11.576	7.01	0.103	286	0.55	LocSlp/TAW	sand backed by gravel, riprap/low bluff
	3	8.001	5.22	0.087	286	0.55	LocSlp/TAW	sand backed by gravel, riprap/low bluff
	4	16.761	7.131	0.143	277	0.55	LocSlp/TAW	sand backed by gravel/mod high bluff
	5	12.149	5.291	0.168	277	0.80	Snsh/TAW	sand backed by gravel /seawall
	6	7.001	5.485	0.048	283	0.55	STK	sand backed by gravel /riprap
	7	15.219	6.849	0.079	278	0.55	STK	sand backed by gravel /high bluff
	8	18.065	4.031	0.071	289	0.55	LocSlp/TAW	sand backed by gravel/bulkhead/high bluff
	9	8.462	6.663	0.101	270	0.80	LocSlp/TAW	sand backed by gravel/low bluff
	10	7.897	5.366	0.085	270	0.55	LocSlp/TAW	sand backed by gravel, riprap/low bluff
Falcon Cove	1	15.935	7.027	0.101	278	0.80	LocSlp/TAW	sand, cobble berm backed by high bluff
	2	20.15	6.414	0.118	274	0.80	LocSlp/TAW	sand, cobble berm backed by high bluff
	3	15.612	6.091	0.101	280	0.80	LocSlp/TAW	sand, cobble berm backed by high bluff
	4	11.844	6.927	0.098	275	0.80	LocSlp/TAW	sand, cobble berm backed by high bluff
	5	6.453	1.25	0.119	272	0.80	Snsh/TAW	sand backed by cobble barrier
	6	11.585	5.388	0.065	274	0.80	LocSlp/TAW	sand, cobble berm backed by high bluff

Notes:

D_{HIGH} denotes the crest of the dune, bluff, or structure;

D_{LOW} denotes the toe of the dune (i.e., E_j), bluff, or structure;

Beach slope reflects the calculated slope spanning the region between 2- and 4-m elevation;

Wave direction denotes the shoreline orientation used to calculate the wave reduction (γ_β) factor used in TAW runup calculations;

Roughness (γ_r) defines the backshore roughness used in TAW runup calculations; and

Approach defines the final runup approach used to calculate the wave runup, where STK = Stockdon, Snsh/TAW = nearshore slope and TAW, and LocSlp/TAW = the local barrier slope and TAW.

6.3 Clatsop County Wave Runup and Total Water Level Calculations

The complete hourly combined time series is run through the lookup tables to derive alongshore varying transformed wave time series. Using the transformed wave conditions, and the measured alongshore varying beach and barrier slopes, initial TWL time series based on the Stockdon approach are developed at all transect locations. From these time series we identify the ~150 highest independent TWLs at each transect over the length of the record. Wave runup is then computed for each of these storm input conditions (about five events per year) at each of the beach profiles shown in **Figure 3-1** and **Figure 3-2** using a combination of the Stockdon and others (2006) runup equation for dune-backed beaches (equation 6.4; note that for the second round of runup computations undertaken using Stockdon, the calculated runup values are identical to the first) and TAW (equation 6-12) for wave runup on a barrier. The specific approaches used in our calculations are defined above in Table 6-1. For both models, the calculated runup is combined with the SWL (measured tides) to develop the T_{WL} conditions used to generate both the 100-year return level event and the 500-year return event. The input wave conditions from the SWAN modeling used in the various calculations were determined for each transect location by extending the shore-perpendicular transects from the backshore to where they intersected the 20-m contour, or the seaward most location of H_{mo}/depth = 0.4, whichever was farther offshore (but almost always shallower than 30 m). This ensured that only minor dissipation due to wave breaking influenced the model results. These intersections are where wave statistics from the SWAN output were extracted.

Having calculated the storm-induced TWLs, we used the generalized extreme value (GEV) family of distributions (specifically the peak over threshold (POT) approach) to estimate the 100-year and 500-year total water levels for each of the beach profile sites. Specific information about the extreme value techniques used to estimate these T_{WL}s is described in Section 4.6. **Figure 6-6** gives an example of the extreme value (GPD-Poisson) model for the Arch Cape 7 profile site in which the 100-year event is calculated to be 9.2 m (30.2 ft) and the 500-year event is estimated to be 9.8 m (32 ft). The results for all of the profiles can be found in **Table 6-2**.

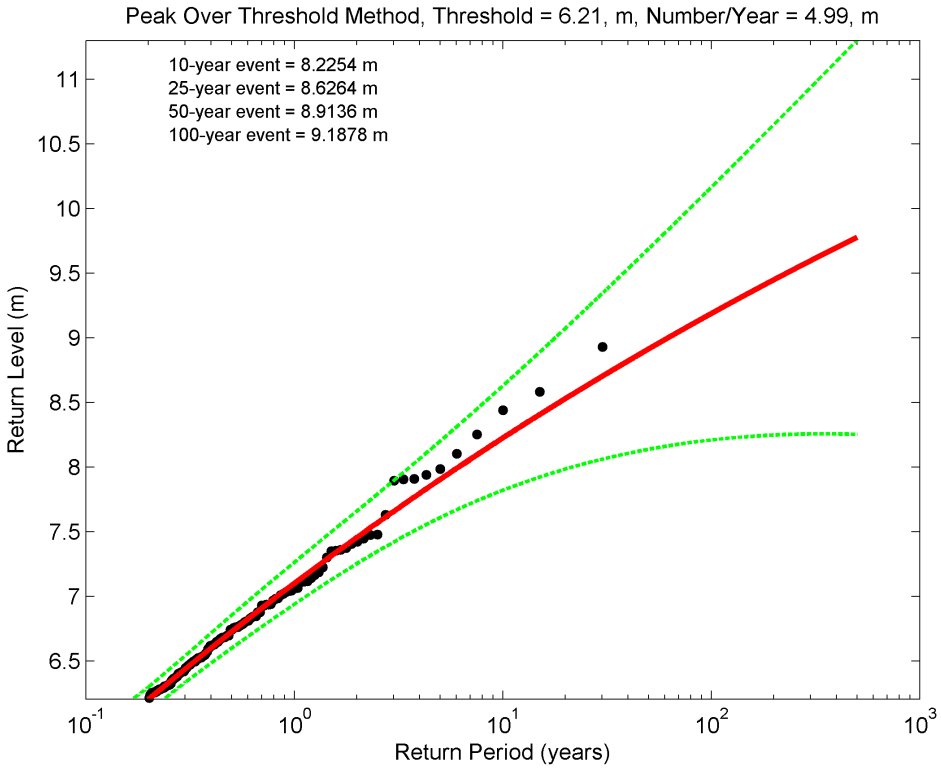

Figure 6-6. Example peak-over-threshold (POT) extreme value theory results for the Arch Cape 7 transect site (with 95% confidence levels). Note that y-axis vertical datum is relative to NAVD88. Black dots reflect the discrete peak total water level events and the red line is the extreme value distribution fit to those data. Green dashed line reflects the 95% confidence boundary.

Table 6-2. 100-year (1%) and 500-year (0.2%) total water levels calculated for the Clatsop County transect sites.

Reach	Profile Number	D_{HIGH} (m)	D_{LOW} (m)	100-Year (m)	500-Year (m)	Description
Clatsop Plains	1	10.972	5.024	6.91	7.27	dune-backed
	2	12.504	5.561	6.55	6.85	dune-backed
	3	11.543	5.483	6.49	6.88	dune-backed
	4	13.003	6.222	6.46	6.75	dune-backed
	5	14.539	5.344	6.28	6.56	dune-backed
	6	14.099	6.342	6.61	6.98	dune-backed
	7	13.892	6.377	6.68	7.05	dune-backed
	8	13.819	6.455	6.49	6.81	dune-backed
	9	13.405	6.554	6.58	6.94	dune-backed
	10	14.18	6.508	6.47	6.83	dune-backed
	11	15.313	6.533	6.74	7.13	dune-backed
	12	16.059	5.628	6.67	7.12	dune-backed
	13	15.96	5.997	6.69	7.09	dune-backed
	14	6.215	6.215	7.16	7.72	dune-backed
Seaside	1	15.152	6.484	8.06	8.12	cobble berm backed by high bluff
	2	5.639	5.639	8.82	8.87	cobble berm backed by high bluff
	3	6.57	6.57	9.94	10.10	sand backed by cobble berm
	4	6.81	6.81	6.54	6.83	sand backed by cobble berm
	5	5.916	5.89	7.01	7.38	sand backed by cobble berm
	6	8.328	5.778	7.27	7.61	dune-backed
	7	7.288	5.576	6.54	6.88	dune-backed
	8	8.040	6.500	6.18	6.48	sand backed by seawall
	9	8.258	5.326	6.02	6.27	sand backed by seawall
	10	7.894	6.379	6.21	6.47	sand backed by seawall
	11	7.255	5.114	6.28	6.58	sand backed by seawall
	12	9.679	4.362	6.02	6.30	dune-backed
	13	8.019	4.68	5.89	6.17	dune-backed
	14	7.410	4.28	5.33	5.49	sand backed by low bluff
	15	6.864	3.149	5.44	5.61	sand backed by low bluff
	16	5.800	2.400	8.10	8.20	sand backed by riprap/low bluff
	17	5.418	2.330	5.59	5.71	dune-backed

Reach	Profile Number	D_{HIGH} (m)	D_{LOW} (m)	100-Year (m)	500-Year (m)	Description
Cannon Beach/ Tolovana	CB 1	16.651	4.869	6.40	6.71	sand backed by high bluff
	CB 2	9.438	4.348	8.40	10.00	sand backed by riprap/mod high bluff
	TOL 1	8.29	4.696	6.59	6.92	sand backed by cobble, riprap/low bluff
	TOL 2	7.006	4.663	8.81	9.79	sand backed by cobble/low bluff
	TOL 3	7.832	4.938	6.61	6.92	sand backed by cobble, riprap/low bluff
	TOL 4	8.222	4.942	6.58	6.93	sand backed by riprap/low bluff
	TOL 5	7.708	4.509	7.16	7.92	sand backed by cobble, riprap/low bluff
	CB 3	10.043	5.173	7.19	7.85	sand backed by seawall
	TOL 6	8.193	4.323	7.80	9.11	sand backed by riprap/low bluff
	TOL 7	7.697	4.812	6.50	6.86	sand backed by riprap/low bluff
	TOL 8	7.3	5.011	6.47	6.80	sand backed by riprap/low bluff
	TOL 9	8.229	5.218	6.40	6.63	sand backed by riprap
	TOL 10	7.644	4.130	8.81	10.03	sand backed by riprap/concrete foundation
	TOL 11	6.662	4.122	7.91	8.33	sand backed by riprap
	TOL 12	7.609	4.344	7.87	9.04	sand backed by riprap/low bluff
	CB 4	7.903	5.2	7.67	9.47	sand backed by low bluff
	TOL 13	7.955	4.565	8.32	9.88	wooden bulkhead/low bluff
	TOL 14	7.629	4.218	8.81	9.35	sand backed by riprap/low bluff
	TOL 15	7.537	4.666	9.15	10.13	sand backed by riprap/low bluff
	TOL 16	7.458	4.04	9.81	10.74	sand backed by riprap/low bluff
	TOL 17	7.98	4.528	8.35	10.02	sand backed by riprap/low bluff
	CB 5	7.035	4.713	7.56	8.54	sand backed by riprap/low bluff
	TOL 18	8.974	4.941	6.59	6.90	sand backed by cobble, riprap/low bluff
	CB 6	12.826	4.285	10.31	13.97	sand backed by high bluff
	CB 7	16.011	4.607	7.07	7.62	sand backed by riprap/high bluff
	CB 8	15.746	6.869	6.70	7.02	sand backed by high bluff
	CB 9	6.805	4.129	11.76	13.00	sand backed by seawall
	CB 10	9.752	6.966	6.62	6.97	sand backed by mod high bluff
	CB 11	11.49	5.186	7.46	7.81	dune-backed
	CB 12	10.964	4.231	10.40	13.21	sand backed by riprap/mod high bluff
	CB 13	6.709	4.127	8.79	9.87	sand backed by seawall
	CB 14	6.841	4.184	6.20	6.46	sand backed by riprap
	CB 15	14.857	4.867	7.03	7.40	dune-backed
	CB 16	16.764	4.723	7.21	7.53	dune-backed
	CB 17	15.061	4.056	6.76	7.08	dune-backed
Arcadia	1	15.322	6.201	7.95	8.31	sand, gravel backed by high bluff
	2	17.825	5.713	6.80	7.13	sand, gravel backed by high bluff
	3	12.366	4.925	8.31	9.58	sand backed by mod high bluff
Arch Cape	1	6.876	6.876	9.60	10.05	sand backed by gravel berm
	2	11.576	7.01	10.56	11.32	sand backed by gravel, riprap/low bluff
	3	8.001	5.22	9.36	9.96	sand backed by gravel, riprap/low bluff
	4	16.761	7.131	11.41	11.69	sand backed by gravel/mod high bluff
	5	12.149	5.291	9.66	9.79	sand backed by gravel /seawall
	6	7.001	5.485	7.43	7.79	sand backed by gravel /riprap
	7	15.219	6.849	9.19	9.78	sand backed by gravel /high bluff
	8	18.065	4.031	11.15	12.2	sand backed by gravel/bulkhead/high bluff
	9	8.462	6.663	10.15	10.79	sand backed by gravel/low bluff
	10	7.897	5.366	9.70	10.58	sand backed by gravel, riprap/low bluff
Falcon Cove	1	15.935	7.027	9.93	10.33	sand, cobble berm backed by high bluff
	2	20.15	6.414	11.93	13.39	sand, cobble berm backed by high bluff
	3	15.612	6.091	10.33	11.17	sand, cobble berm backed by high bluff
	4	11.844	6.927	9.77	10.18	sand, cobble berm backed by high bluff
	5	6.453	1.25	9.07	9.38	sand backed by cobble barrier
	6	11.585	5.388	9.04	9.83	sand, cobble berm backed by high bluff

Notes: 100-year and 500-year total water level (T_{WL}) values relative to NAVD88 vertical datum.
D_{HIGH} is the crest of the dune, bluff or barrier determined for the eroded profile. *Red text denotes that the crest is overtopped*.

6.4 Overtopping Calculations

Overtopping of natural features such as foredunes, spits and coastal engineering structures and barriers occurs when the wave runup superimposed on the tide exceeds the crest of the foredune or structure (**Figure 6-7**). Hazards associated with wave overtopping can be linked to a number of simple direct flow parameters including (Pullen and others, 2007):

- mean overtopping discharge, *q*;
- overtopping velocities over the crest and farther landward, *V*;
- landward extent of green water and splash overtopping $y_{G,\,outer}$; and
- overtopping flow depth, *h* at a distance *y* landward of the foredune crest or "barrier."

NHC (2005) notes that there are three physical types of wave overtopping:

1. *Green water or bore overtopping* occurs when waves break onto or over the foredune or barrier and the overtopping volume is relatively continuous;
2. *Splash overtopping* occurs when the waves break seaward of the foredune or barrier, or where the foredune or barrier is high relative to the wave height and overtopping consists of a stream of droplets. Splash overtopping can be a function of its momentum due to the runup swashing up the barrier and/or may be enhanced due to onshore direct winds; and
3. *Spray overtopping* is generated by the effects of wind blowing droplets and spray that are derived from the wave crests.

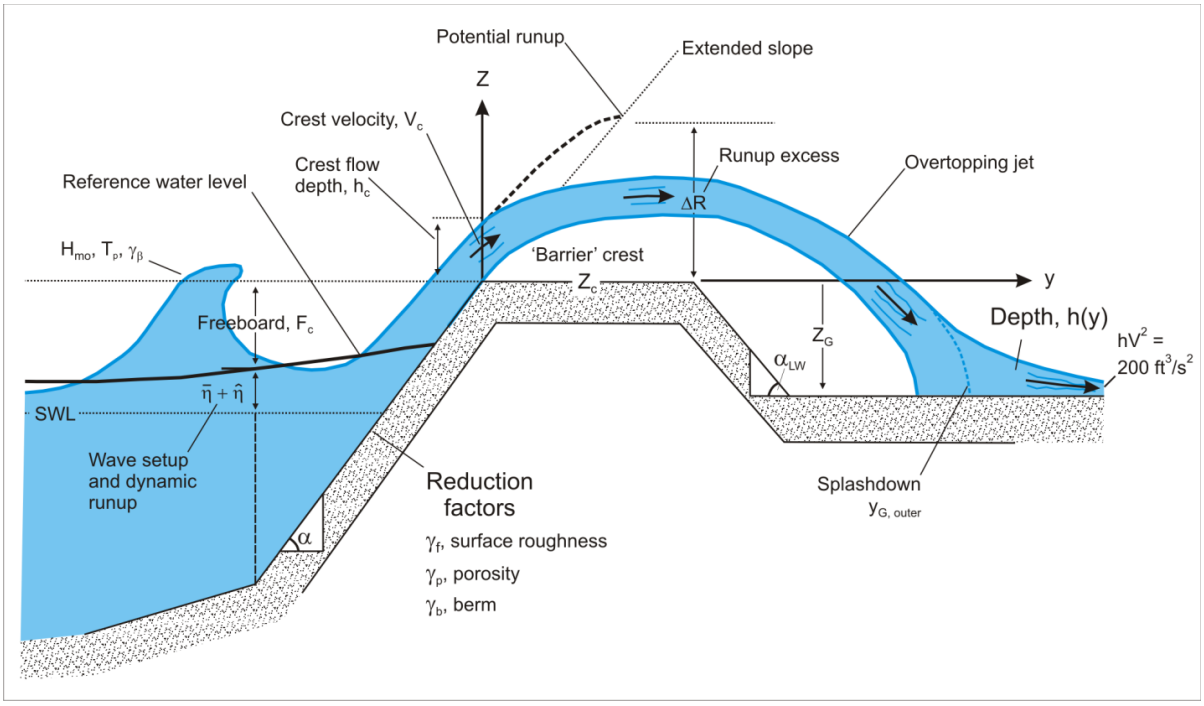

Figure 6-7. Nomenclature of overtopping parameters available for mapping base flood elevations (BFEs) and flood hazard zones (after NHC, 2005).

Mapping these respective flood inundation zones requires an estimate of the velocity, *V*, the overtopping discharge, *q*, of the water that is carried over the crest, the inland extent of green water and splash overtopping, and the envelope of the water surface that is defined by the water depth, *h*, landward of the barrier crest. According to NHC (2005) these hazard zones are ultimately defined based on the following two derivations:

- Base Flood Elevations (BFEs) are determined based on the water surface envelope landward of the barrier crest; and
- Hazard zones are determined based on the landward extent of green water and splash overtopping, and on the depth and flow velocity in any sheet flow areas beyond that, defined as $hV^2 = 5.7\ m^3/s^2$ *or* $200\ ft^3/s^2$.

A distinction can be made between whether green water (or bore) or splash overtopping predominates at a particular location that is dependent on the ratio of the calculated wave runup height relative to the barrier crest elevation, R/Z_c. When $1 < R/Z_c < 2$, splash overtopping dominates and for $R/Z_c > 2$, bore propagation occurs. In both cases, R and Z_c are relative to the 2% Dynamic Water Level ($DWL_{2\%}$) at the barrier (Figure D.4.5-12 in NHC [2005, p. D.4.5-22]).

6.4.1 Mean overtopping rate at the "barrier" crest

Wave overtopping of dunes and barrier is a function of both hydraulic and barrier structure parameters whereby:

$$q = f(H_{mo}, T_p, \beta, F_c, DWL_{2\%}, geometry) \qquad (6.14)$$

where q is the overtopping discharge (expressed as cubic meters per second per meter, $m^3/s/m$ [$ft^3/s/ft$]), H_{mo} is the significant wave height at the toe of the structure, T_p is the peak period, β is the angle of wave attack, F_c is the freeboard, and $DWL_{2\%}$ is 2% depth of water at the toe of the structure (**Figure 6-7**).

Prior to calculating the mean overtopping rate at the barrier crest it is necessary to first distinguish between four contrasting types of wave breaking situations that may impact a particular barrier or dune overtopping situation. There four conditions include *non-breaking* or *breaking* on a normally sloped barrier (where $0.067 < \tan\alpha < 0.67$), and *reflecting* or *impacting* on steeply sloping or vertical barriers (where $\tan\alpha \geq 0.67$). Of these, the breaking wave situation is the dominant condition in Clatsop County, where the waves have already broken across the surf zone and are reforming as bores prior to swashing up the beach face or barrier.

For beaches and normally sloping barriers (where $0.067 < \tan\alpha < 0.67$), a distinction can be made between situations where waves break directly on the barrier versus those conditions where the waves have not yet broken. These conditions can be determined using the surf similarity parameter (Iribarren number) defined here in terms of the beach or structure slope ($\tan\alpha$), and the wave steepness ($S_{op} = H_{mo}/L_o$):

$$\xi_{op} = \frac{\tan\alpha}{\sqrt{\frac{H_{mo}}{L_o}}} = \frac{\tan\alpha}{\sqrt{S_{op}}} \qquad (6.15)$$

Breaking on normally sloping surfaces generally occurs where the surf similarity number, $\xi_{op} \leq 1.8$, while non-breaking conditions occur when $\xi_{op} > 1.8$. As noted above, for the Clatsop County coastline the identified Iribarren numbers always fell below the 1.8 criteria indicating that the incident waves are always broken prior to reaching the beach or the barrier face.

At the beach or barrier crest, the relative freeboard (F_c/H_{mo}), **Figure 6-7**, is a particularly important parameter because changing these two parameters controls the volume of water that flows over the barrier crest. For example, increasing the wave height or period increases the overtopping discharge, as does reducing the beach or barrier crest height or raising the water level.

A variety of prediction methods are available for calculating the overtopping discharge and are almost entirely based on laboratory experiments based on a range of structure slopes (slopes between 1:1 and 1:8, with occasional tests at slopes around 1:15 or lower). Factors that will serve to reduce the potential over-

topping discharge include the barrier *surface roughness* (γ_f), the presence of a *berm* (γ_b), *wave approach directions* (γ_β), and the *porosity* of the barrier (γ_p) (Figure 6-7). In terms of porosity, increasing this variable effectively reduces the wave runup and overtopping discharge because more of the water is able to be taken up by the voids between the clasts and particles. As noted by NHC (2005), the effect of the *porosity* factor makes it convenient to distinguish between impermeable and permeable structures. Methods for determining the various reduction factors are described in Table D.4.5-3 in NHC (2005, p. D.4.5-13), with one difference whereby the approach recommended for determining the wave approach (γ_β) reduction factor for wave overtopping calculations is based on the following equation:

$$\gamma_\beta = \begin{Bmatrix} 1 - 0.0033|\beta|, (0 \le |\beta| \le 80°) \\ 1 - 0.0033|80|, (|\beta| \ge 80°) \end{Bmatrix} \quad (6.16)$$

Table D.4.5-3 in NHC (2005, p. D.4.5-13) identifies four general categories of overtopping applications: overtopping on a normally sloping barrier (e.g., riprap structure), steep sloping or vertical barrier (e.g., seawall or bluff where some waves broken); steep sloping or vertical barrier (all waves broken), and shallow foreshore slopes subject to large Iribarren numbers.

For a normally sloping barrier, where 0.05 < tan α < 0.67 and the Iribarren number (ξ_{op}) ≤ 1.8 (breaking wave condition), the following formulation can be used to determine the mean overtopping discharge (both dimensional (q) and non-dimensional (Q) forms) at the barrier crest:

$$q = Q\sqrt{\frac{gH_{mo}\tan\alpha}{S_{op}}} \text{ where:} \quad (6.17)$$

$$Q = 0.06e^{-4.7F'}, \text{ and}$$

$$F' = \frac{F_c}{H_{mo}}\frac{\sqrt{S_{op}}}{\tan\alpha}\frac{1}{\gamma_f\gamma_b\gamma_\beta\gamma_p}$$

For non-breaking conditions (Iribarren number [ξ_{op}] > 1.8):

$$q = Q\sqrt{gH_{mo}^3} \text{ where:} \quad (6.18)$$

$$Q = 0.2e^{-2.3F'}, \text{ and}$$

$$F' = \frac{F_c}{H_{mo}}\frac{1}{\gamma_f\gamma_\beta}$$

For steep sloping or vertical barrier, where tan α > 0.67 and $h_* \ge 0.3$ (reflecting condition, where

$$h_* = \frac{h}{H_{mo}}\left(\frac{2\pi h}{gT_m^2}\right)$$

and h is the water depth at the structure toe), the following formulation can be used:

$$q = Q\sqrt{gH_{mo}^3} \text{ where:} \quad (6.19)$$

$$Q = 0.05e^{-2.78F_c/H_{mo}}$$

For impacting conditions (h_* < 0.3):

$$q = Q\sqrt{gh^3}\ h_*^2 \text{ where:} \quad (6.20)$$

$$Q = 1.37 * 10^{-4}(F')^{-3.24}, \text{ and}$$

$$F' = \frac{F_c}{H_{mo}}\ h_*$$

For steep sloping or vertical barrier (all waves are broken) where the structure toe <$DWL_{2\%}$ water level and where (F_c/H_{mo})*h_*≤0.03:

$$q = Q\sqrt{gh^3}\ h_*^2 \text{ where:} \quad (6.21)$$

$$Q = 0.27 * 10^{-4}e^{-3.24\,(F_c/H_{mo})h_*}$$

For steep sloping or vertical barrier (all waves are broken) where the structure toe >$DWL_{2\%}$ water level:

$$q = Q\sqrt{gh^3}\ h_*^2 \text{ where:} \quad (6.22)$$

$$Q = 0.06e^{-4.7\,F_c S_{op}^{-0.17}}$$

We have implemented two additional overtopping calculations following discussions with Dr. W.G. McDougal, which may be applied to beaches subject to gently sloping ($\tan\beta < 0.4$), dissipative foreshores:

$$q = Q\sqrt{gh^3}h_*^2 \text{ where:} \quad (6.23)$$

$$Q = 0.21\sqrt{gH_{mo}^3}e^{-F'}, \text{ and}$$

$$F' = \frac{F_c}{\gamma_f\gamma_\beta H_{mo}(0.33 + 0.022\xi_{op})}$$

and cases where there is negative freeboard. The latter occurs when the still water level ($DWL_{2\%}$) is higher than the barrier crest, which produces a negative freeboard (i.e., $-F_c$). In this situation we apply the well-known weir type formula to define the volume of water that is overflowing the crest (Eurotop, 2007). The formulation used is:

$$q = Q_s + q_w \text{ where:} \quad (6.24)$$

$$Q_s = 0.4583(-F_C)\sqrt{-F_C g} \text{ and}$$

$$Q_w = 0.21\sqrt{gH_{mo}^3} \text{ and}$$

$$q_w = Q_w\sqrt{gh^3}h_*^2$$

6.4.2 Overtopping limits and flood hazard zones landward of the "barrier" crest

Estimates of the landward limit of the splashdown distance associated with wave overtopping and the landward limit of the hazard zone require several calculation steps. These steps include:

1. The excess potential runup, $\Delta R = R - Z_c$, crest flow rate, $V_c\cos\alpha$ (where $V_c = 1.1\sqrt{g\Delta R}$), and initial flow depth, h_c (where $h_c = 0.38\Delta R$) are first calculated.
2. The associated onshore wind component, *Wy* is determined from available wind data. For the purposes of this study, we used *Wy = 19.6 m/s (64.3 ft/s)*, which was determined from an analysis of winds (mean from a select number of storms) measured at the Cape Arago C-MAN station operated by the NDBC. In the absence of wind data, NHC (2005) recommends a wind speed of *13.4 m/s (44 ft/s)*.

3. The enhanced onshore water velocity component $(V_c\cos\alpha)'$ is then calculated using equation 6.25:

$$(V_c cos\ \alpha)' = V_c\cos\alpha + 0.3(W_y - V_c\cos\alpha) \quad (6.25)$$

4. The effective angle, α_{eff}, is calculated from:

$$\tan\alpha_{eff} = \frac{V_c\sin\alpha}{(V_c\cos\alpha)'}.$$

5. Having determined the above parameters, the outer limit of the splash region, $y_{G\,outer}$ is calculated using equation 6.26. Here we have used an algorithm developed by Dr. Bill McDougal (Coastal Engineer, OSU and Technical Coordinator of the North Pacific FEMA West Coast Guidelines) of the form:

$$y_{G\ outer} = \frac{(V_c cos\alpha)'}{g} * V_c sin\alpha - mBackshore * (V_c cos\alpha)' * \left(1 + \sqrt{1 - \frac{2g * bBackshore}{(V_c sin\alpha - mBackshore * (V_c cos\alpha)'^2}}\right) \quad (6.26)$$

and

$$Z_G = bBackshore + (mBackshore * y_{G\ outer}) \quad (6.27)$$

where *bBackshore* is the intercept for the backshore slope adjacent to the barrier crest and *mBackshore* is the slope of the backshore. equation 6.26 is ultimately based on Figure D.4.5-15 in NHC (2005, p. D.4.5-30).

6. The total energy, E, of the splashdown is calculated from $E = \Delta R - Z_G$.
7. Finally, the initial splashdown velocity, V_o (where $V_o = 1.1\sqrt{gE}$), and depth, h_o (where $h_o = 0.19E$) are calculated. In the case of green water or bore overtopping, the splashdown velocity, V_o, can be calculated from $V_o = 1.1\sqrt{g\Delta R}$, while the flow depth is determined as $h_o = 0.38E$

Having determined the initial splashdown velocity, V_o, and flow depth, h_o, the landward extent of the overland flow is calculated using an approach modified from that originally proposed by Cox and Machemehl (1986). The version presented in NHC (2005) effectively calculates the flow depth, h, with distance, y, from the barrier crest, such that the flow depth decays asymptotically as y-distance increases away from the barrier crest, eventually approaching zero. The NHC (2005) equation is shown as equation 6.28:

$$h(y) = \left[\sqrt{h_o} - \frac{5(y - y_o)}{A\sqrt{gT^2}}\right]^2 \quad (6.28)$$

where h_o is determined from step 7 above and for an initial approximation the non-dimensional A parameter may be taken as unity. For sloping backshores, the A parameter in equation 6.28 can be modified such that $A_m = A(1 - 2 * \tan\alpha_{LW})$, and the value in parentheses is limited to the range 0.5 to 2. According to NHC (2005) if the maximum distance of splash or bore propagation calculated using equation 6.28 does not appear reasonable or match field observations, the A parameter can be adjusted in order to increase or decrease the landward wave propagation distance. In addition, for green water or bore propagation the A parameter value is taken initially to be 1.8.

For the purposes of this study we have adopted a modified version of equation 6.28 developed by Dr. WG McDougal of the form:

$$h(y) = \left[h_o^{1/2} - \frac{y - y_o}{2\alpha(\alpha + 1)^{\frac{3}{2}}(1 - 2m)\, g^{0.5} T}\right]^2 \quad (6.29)$$

where m is the slope of the backshore and α is a constant that can be varied in order to increase or decrease the landward wave propagation distance.

Finally, the landward limit of the hazard zone defined as $hV^2 = 5.7\ m^3/s^2$ *(or 200* ft^3/s^2*)* is determined, whereby h is the water depth given by the modified Cox and Machemehl (1986) method (equation 6.29) and $V = V_o$ calculated from step 7 above.

6.4.3 Initial testing of the landward limit of wave overtopping

Our initial computations of the landward extent of wave overtopping using the steps outlined above yielded narrow hazard zones for our original coastal FIRM study in Coos County. To calibrate equation 6.29, we performed wave overtopping calculations and inundation for a site on the northern Oregon coast where there are field observations of wave overtopping. The site is Cape Lookout State Park, Tillamook County (Allan and others, 2006; Allan and Komar, 2002a; Komar and others, 2003). The southern portion of Cape Lookout State Park is characterized by a wide, gently sloping, dissipative sand beach backed by a moderately steep gravel berm and, ultimately, by a low foredune that has undergone significant erosion since the early 1980s (Komar and others, 2000).

On March 2-3, 1999, the crest of the cobble berm/dune at Cape Lookout State Park was overtopped during a major storm; significant wave heights reached 14.1 m (46.3 ft), while the peak periods were 14.3 s measured by a deepwater NDBC wave buoy (Allan and Komar, 2002b). Wave overtopping of the dune and flooding extended 70 m (230 ft) into the park (Dr. P. Komar, Emeritus Professor, College of Oceanic and Atmospheric Sciences, pers. comm., 2010), proof for which included photos and field evidence including pockmarks at the base of the tree trunks located in the park. These pockmarks were caused by cobbles carried into the park from the beach by the overtopping waves, where the cobbles eventually slammed into the bases of trees as ballistics. Because the average beach slopes at Cape Lookout State park are analogous to those observed along the beaches of Coos County (and those in Clatsop County) and because large wave events associated with extratropical storms affect significant stretches (100s to 1000 kilometers) of the coast at any single point in time, we believe these data provide a reasonable means in which to investigate a range of alpha (α) values that may be used to determine the landward extent of wave inundation in the park.

Using beach morphology data (slope [tan β] = 0.089, barrier crest = 5.5 m [18 ft]) from Cape Lookout State Park and deepwater wave statistics from a nearby NDBC wave buoy (#46050), we experimented with a range of alpha values (**Figure 6-8**) in order to replicate the landward extent of the inundation. As can be seen in **Figure 6-8**, in order to emulate the landward extent of flooding observed at Cape Lookout our analyses yielded an α of 0.58. Using alpha = 0.58, we in turn calculated the extent of the hazard zone where $h(y)$ = 200 ft^3/s^2, which was found to be ~34 m from the crest of the cobble berm/dune, consistent with damage to facilities in the park.

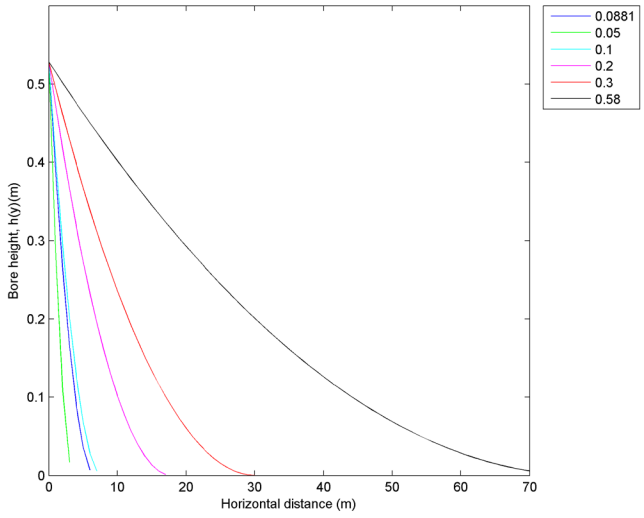

Figure 6-8. Calculations of bore height decay from wave overtopping at Cape Lookout State Park at the peak of the March 2-3, 1999, storm based on a range of alpha (α) values.

6.4.4 Wave overtopping and hazard zone limits calculated for Clatsop County

Table 6-3 presents the results of the calculated splashdown distances ($y_{G\,outer}$) and the landward extent of the flow (hV^2) where the flows approach *5.7 m^3/s^2 (or 200 ft^3/s^2)*. **Table 6-3** includes a more conservative splashdown distance, based on an enhanced wind velocity of 19.6 m/s (64.3 ft/s); this contrasts with the default wind speed of 13.4 m/s (44 ft/s) suggested by NHC (2005). This enhanced wind velocity was determined from an analysis of wind speeds measured by the Cape Arago C-MAN station (http://www.ndbc.noaa.gov/station_page.php?station=CARO3) located adjacent to the mouth of Coos Bay (Allan and others, 2012b). Essentially, Allan and others examined the wind speeds identified at Cape Arago for a range of storm events and identified a wide range of values, with a maximum mean wind speed of 19.6 m/s (64.3 ft/s). Because the measured wind speeds reflect a 2-min average such that higher wind speeds have been measured throughout the entire record (e.g., the maximum 2-min average wind speed is 29.3 m/s [96 ft/s], while the maximum 5-s wind gust reached 38.1 m/s [125.0 ft/s]), we believe it is justified to use the more conservative enhanced wind velocity of 19.6 m/s (64.3 ft/s). Furthermore, comparisons by Allan and others (2012b) indicated that the relative difference between the value suggested by NHC (2005) and the enhanced wind used here differs by about 30%. As can be seen from the **Table 6-3**, the calculated splashdown distances ($y_{G\,outer}$) indicate splash distances that range from as little as 0.9 m (3 ft) to a maximum of 5.9 m (19.4 ft); the mean splash distance is 2.9 m (9.6 ft), while the standard deviation is 1.6 m (5.2 ft). Thus, adopting the reduced wind velocity would cause the zones to narrow by ~1.8 m for the highest splash distance and 0.3 m for the smallest. Overall, these differences are negligible given the tremendous uncertainties in calculating splash and overtopping (NHC, 2005).

Hazard zone calculations shown in **Table 6-3** indicate a similarly broad range of values that vary from negligible (i.e., effectively where the 1% T_{WL} intersects with the backshore, plus the width of the splash zone where applicable) to as much as 73 m (240 ft) wide, with the widest zones having occurred where overtopping significantly exceeds the eroded beach crest elevations such as at Falcon Cove and at the south end of Seaside. Qualitative field observations of past storm wave overtopping events at all sites subject to overtopping calculated in this study confirm that this is indeed the case. Hence, field-based observations appear to be consistent with the calibrated results identified in **Table 6-3**. The depth of flooding at each mapped overtopping zone is indicated in **Table 6-4**.

Table 6-3. Splashdown and hazard zone limits calculated for Clatsop County detailed coastal sites. Values reflect the maximum values derived from all the storm runup and overtopping calculations. Dist_3, Dist_2, and Dist_1 reflect the landward extent at which the calculated bore height decreases from 0.9 m (3 ft), to 0.6 m (2 ft), and, finally, to 0.3 m (1 ft). In all cases, the hazard zones are ultimately defined relative to the location of the dune/structure crest. Note: *sup* denotes a supplemental line established adjacent to the Clatsop Plains 14 transect site.

Reach	Profile	Splashdown $y_{G\ outer}$ (m)	Bore Ht (m)	Dist_3 (≥0.91 m)	Dist_2 (>0.61 < 0.91 m)	Dist_1 (≤0.31 m)	hV^2 > 5.7 m^3/s^2 (m)
Falcon Cove	5	5.87	0.71		9.53	43.9	73.26
Arch Cape	1	2.13	0.48			19.68	39.76
	3	4.15	0.40			12.93	25.05
	6	2.42	0.16				
	9	3.82	0.32			2.05	4.94
	10	5.65	0.44			18.70	35.09
Tolovana/	T2	4.83	0.46			17.21	31.96
Cannon Beach	T10	0.60	0.21				
	T11	3.37	0.34			4.34	9.50
	T12	0.00	0.00				
	T13	3.57	0.25				
	T14	4.22	0.40			12.16	23.57
	T15	4.48	0.48			20.90	38.29
	T16	4.90	0.58			29.15	50.89
	T17	3.26	0.22				
	CB5	1.90	0.18				
	CB9	6.46	0.92	0.70	24.36	55.18	87.39
	CB13	4.40	0.41			14.56	27.98
Seaside	2	2.10	0.47			16.57	35.77
	3	4.45	0.70		7.33	36.67	63.48
	5	1.23	0.23				
	16	3.32	0.40			8.65	16.85
	17	0.11	0.04				
Clatsop Plains	14	1.31	0.14				
	sup	1.49	0.08				

Table 6-4. Depth of flooding at the overtopping zones landward of the structure crest.

Reach	Profile	Dist_3 Depth (m)	Dist_2 Depth (m)	Dist_1 Depth (m)	hV^2 > 5.7 m^3/s^2 Depth (m)	Comment
Arch Cape	1			0.3	0.3	
	3			0.3	0.3	
	9			0.3	0.3	hV2 zone too narrow to map
	10			0.3	0.3	
Tolovana/	T2			0.3	0.3	
Cannon Beach	T11			0.3	0.3	hV2 zone too narrow to map
	T14			0.3	0.3	
	T15			0.3	0.3	
	T16			0.3	0.3	
	CB9	0.91	0.61	0.3	0.3	Dist_3 zone too narrow to map
	CB13			0.3	0.3	hV2 zone too narrow to map
Seaside	2			0.3	0.3	
	3		0.61	0.3	0.3	
	16			0.3	0.3	

7.0 COASTAL EROSION CAUSED BY INDIVIDUAL STORM EVENTS

In order to estimate beach (or bluff) erosion and the resulting profile changes that occur during a particular storm, it is important to first establish the initial profile conditions that existed prior to that storm. As outlined in Section 3.2, this initial profile morphology is represented by the most likely winter profile (MLWP), which forms the basis for determining profile changes that could eventuate as a result of a particularly severe storm(s). Having established the MLWP for a site, the profile is then modified according to the amount of erosion estimated to occur during a specified storm as a result of the increased water levels (tide + surge + ENSO) as well as from wave processes, specifically the wave runup. This section explores two approaches described in the revised FEMA guidelines, which may be used to establish the eroded profiles along the Clatsop County coastline. The second half of the section describes the specific approach adopted for Clatsop County and the results from our erosion analyses.

7.1 Models of Foredune Erosion

7.1.1 The Komar and others (1999) model

The erosion potential of sandy beaches and foredunes along the Pacific Northwest coast of Oregon and Washington is a function of the total water level produced by the combined effect of the wave runup plus the tidal elevation (E_T), exceeding some critical elevation of the fronting beach, typically the elevation of the beach-dune junction (E_J). This basic concept is depicted conceptually in **Figure 7-1A** based on the model developed by Ruggiero and others (1996), and in the case of the erosion of a foredune backing the beach the application of a geometric model (**Figure 7-1B**) formulated by Komar and others (1999). Clearly, the more extreme the total water level elevation, the greater the resulting erosion that occurs along both dunes and bluffs.

As can be seen from **Figure 7-1B**, estimating the maximum potential dune erosion (DE_{max}) is dependent on first determining the total water level elevation, T_{WL}, diagrammed in **Figure 7-1A**, which includes the combined effects of extreme high tides plus storm surge plus wave runup, relative to the elevation of the beach-dune junction (E_J). Therefore, when the $T_{WL} > E_J$ the foredune retreats landward by some distance, until a new beach-dune junction is established, whose elevation approximately equals the extreme water level. Because beaches along the high-energy Oregon coast are typically wide and have a nearly uniform slope (tan β), the model assumes that this slope is maintained, and the dunes are eroded landward until the dune face reaches point B in **Figure 7-1B**. As a result, the model is geometric in that it assumes an upward and landward shift of a triangle, one side of which corresponds to the elevated water levels, and then the upward and landward translation of that triangle and beach profile to account for the total possible retreat of the dune (Komar and others, 1999). An additional feature of the geometric model is its ability to accommodate further lowering of the beach face due to the presence of a rip current, which has been shown to be important to occurrences on the Oregon coast of localized "hot spot" erosion and property impacts (Komar, 1997). This feature of the model is represented by the beach-level change ΔBL shown in **Figure 7-1B**, which causes the dune to retreat some additional distance landward until it reaches point C. As can be seen from **Figure 7-1B**, the distance from point A to point C depicts the total retreat, DE_{max}, expected during a particularly severe storm event (or series of storms) that includes the localized effect enhancement by a rip current. Critical then in applying the model to evaluate the susceptibility of coastal properties to erosion, is an evaluation of the occurrence of extreme tides (E_T), the runup of waves, and the joint probabilities of these processes along the coast (Ruggiero and others, 2001), this having been the focus of Section 6 described previously.

The geometric model gives the maximum potential equilibrium cross-shore change in the shoreline position landward of the MLWP resulting from a storm. However, in reality it is unlikely that this extreme degree of response is ever fully realized,

because of the assumptions that had been made in deriving the geometric model with the intent of evaluating the maximum potential dune erosion. As noted by Komar and others (1999), in the first instance the geometric model projects a mean linear beach slope. As a result, if the beach is more concave, it is probable that the amount of erosion would be less, though not by much. Perhaps of greater significance is that the geometric model assumes an instantaneous erosional response, with the dunes retreating landward as a result of direct wave attack. However, the reality of coastal change is that it is far more complex, there in fact being a lag in the erosional response behind the forcing processes. As noted by Komar and others (1999), the extreme high runup elevations typically occur for only a relatively short period of time (e.g., the period of time in which the high wave runup elevations coincide with high tides). Because the elevation of the tide varies with time (e.g., hourly), the amount of erosion can be expected to be much less when the water levels are lower. Thus, it is probable that several storms during a winter may be required to fully realize the degree of erosion estimated by the geometric model; this did, for example, occur during the winter of 1998-99, with the last in the series of 5 storms having been the most extreme and erosive (Allan and Komar, 2002). In addition, as beaches erode, the sediment is removed offshore (or farther along the shore) into the surf zone where it accumulates in near shore sand bars. This process helps to mitigate the incoming wave energy by causing the waves to break farther offshore, dissipating some of the wave energy, and forming the wide surf zones that are characteristic of the Oregon coast. In turn, this process helps to reduce the rate of beach erosion that occurs. In summary, the actual amount of beach erosion and dune recession is dependent on many factors, the most important of which include the incident wave conditions, the T_{WL}, and the duration of the storm event(s).

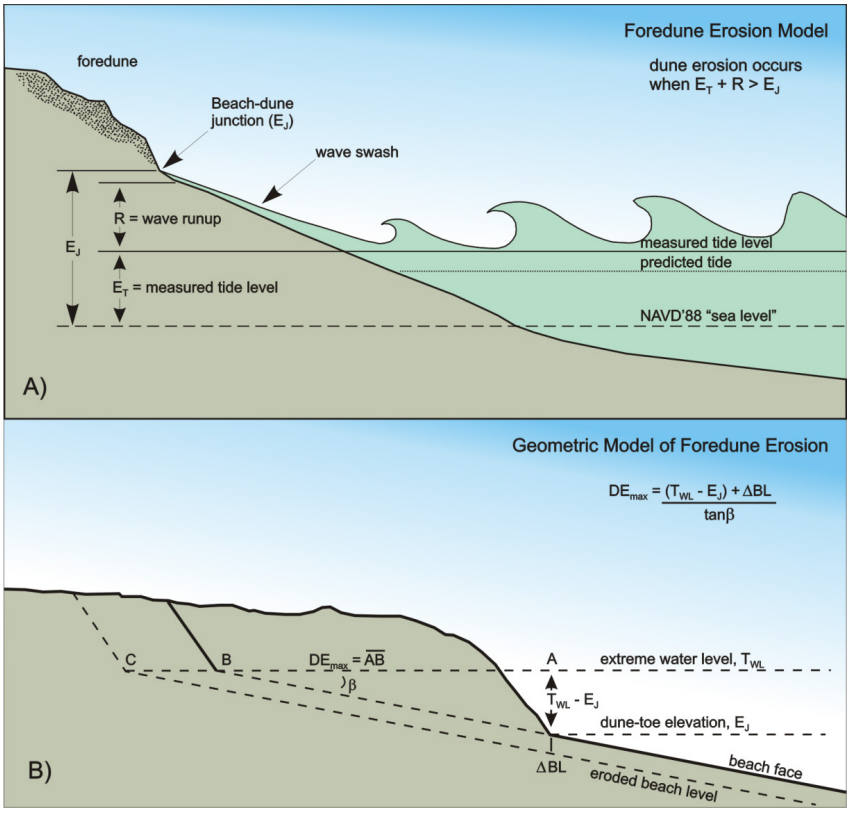

Figure 7-1. A) The foredune erosion model. B) The geometric model used to assess the maximum potential beach erosion in response to an extreme storm (Komar and others, 1999).

7.1.2 The Kriebel and Dean (1993) model

Kriebel and Dean (1993), hereafter known as K&D, developed a dune erosion model that is broadly similar to the Komar and others (1999) geometric model. At its core is the assumption that the beach is in statistical equilibrium with respect to the prevailing wave climate and mean water levels (Bruun, 1962). As water levels increase, the beach profile is shifted upward by an amount equal to the change in water level (S) and landward by an amount R_∞, until the volume of sand eroded from the subaerial beach matches the volume deposited offshore in deeper water (**Figure 7-2**); note that DE_{MAX} and R_∞ are essentially synonymous with each other. One important distinguishing feature in the K&D model relative to Bruun (1962) is that it relies on the equilibrium beach profile theory proposed by Dean (1977) to account for the erosion following an increase in the water level. The Dean model is a simplified yet realistic equilibrium form for open-coast beach profiles expressed as a power-law curve of the form:

$$h = Ay^{2/3} \text{ or equivalently as } x = \left(\frac{h}{A}\right)^{3/2} \qquad (7.1)$$

where h is the water depth at a distance x offshore from the still-water level and A is a parameter that governs the overall steepness (and slope) of the profile and is a function of the beach grain size. Thus, incorporating the assumed components of Bruun (1962) and Dean (1977), the maximum erosion potential, R_∞, was determined by K&D to be a function of the increase in mean water level (S) caused by a storm, the breaking wave water depth (h_b), surf zone width (W_b), berm or dune height (B or D), and the slope (β_f) of the upper foreshore beach face. The breaking wave depth (h_b) may be calculated from the wave breaker height (equation 6.8) multiplied by 0.78 (the breaker index).

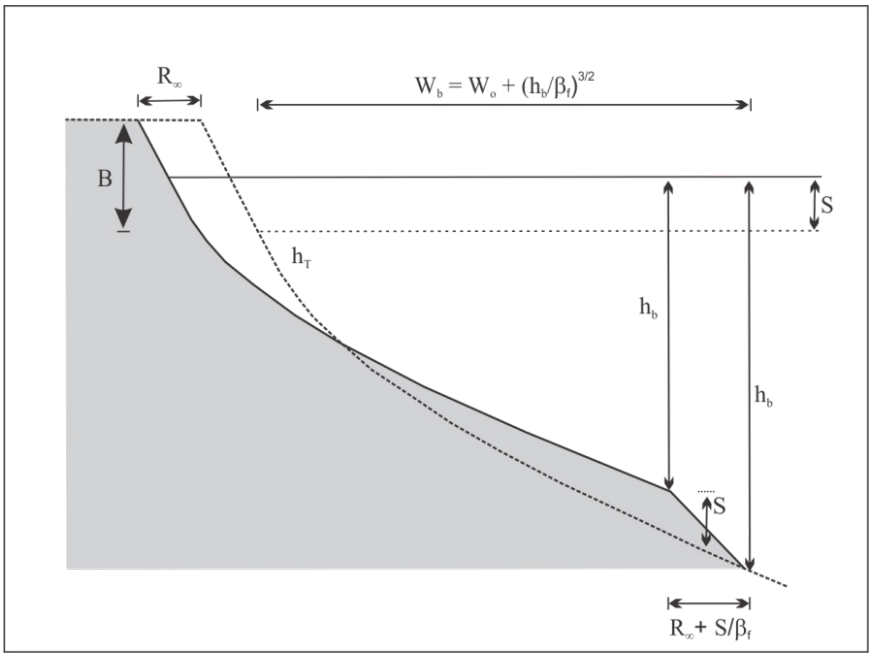

Figure 7-2. Maximum potential erosion ($R\infty$) due to a change in water levels (after Kriebel and Dean, 1993).

As a result of the above concepts, K&D developed two approaches for determining the maximum erosion potential. These include:

- A beach backed by a low sand berm

$$R_\infty = \frac{S\left(W_b - h_b/\beta_f\right)}{B + h_b - S/2} \tag{7.2}$$

- A beach backed by high sand dune

$$R_\infty = \frac{S\left(W_b - h_b/\beta_f\right)}{D + h_b - S/2} \tag{7.3}$$

Like the Komar and others (1999) model, the Kriebel and Dean (1993) dune erosion models estimates of the maximum potential erosion (DE_{MAX}) associated with a major storm, and assume that a particular storm will last sufficiently long enough to fully erode the dune. In reality, DE_{MAX} is almost never fully realized because storms rarely last long enough to fully erode the dune to the extent of the model predictions. Because the duration of a storm is a major factor controlling beach and dune erosion, K&D developed an approach to account for the duration effects of storms with respect to the response time scale required to fully erode a beach profile. The time scale for the erosion of a dune to the extent R given by equation (7.2) can be estimated using equation 7.4:

$$T_S = C_1 \frac{H_b^{3/2}}{g^{1/2} A^3} \left(1 + \frac{h_b}{B} + \frac{\beta_f W_b}{h_b}\right)^{-1} \tag{7.4}$$

where T_S is the time scale of response, C_1 is an empirical constant (320), H_b is the breaker height, h_b is the breaker depth, g is acceleration due to gravity, B is the berm elevation, β_f is the slope of the foreshore, W_b is the surf zone width and A is the beach profile parameter that defines an equilibrium profile. Using equation 7.4 yields typical response times for complete profile erosion that are on the order of 10 to 100 hours (NHC, 2005). In general, as the surf zone width increases due to larger wave heights, smaller grain sizes or gentler slopes, the response time increases. In addition, the response time will also increase as the height of the berm increases.

The beach profile response is determined by a convolution integral. According to NHC (2005), the time dependency of the storm hydrograph may be approximated by:

$$f(t) = \sin^2\left(\pi \frac{t}{T_D}\right) \text{ for } 0 < t < T_D \tag{7.5}$$

where t is time from the start of the storm and T_D is the storm duration. The convolution integral is:

$$DE(t) = \frac{DE_{MAX}}{T_S} \int_0^t f(\tau) e^{-(t-\tau)/T_S}\, d\tau \tag{7.6}$$

which integrates to:

$$\frac{DE(t)}{DE_{MAX}} = 0.5 \left\{ 1 - \frac{\beta^2}{1+\beta^2} \exp\left(-\frac{t}{T_S}\right) - \frac{1}{1+\beta^2} \left[\cos\left(\frac{2\pi t}{T_D}\right) + \beta \sin\left(\frac{2\pi t}{T_D}\right) \right] \right\} \tag{7.7}$$

where $\beta = 2\pi T_S/T_D$ and DE_{MAX} is the maximum potential recession that would occur if the storm duration was infinite. Thus, if the storm duration, T_D, is long relative to the time scale of profile response, T_S, then a significant portion of the estimated erosion determined by the K&D or geometric model will occur. As the ratio of these two values decreases, the amount of erosion will also decrease. The time required for maximum beach and dune recession is determined by setting the derivative of equation 7.7 to zero and solving for time. This yields:

$$exp\left(-\frac{t_m}{T_D}\right) = \cos\left(\frac{2\pi t_m}{T_S}\right) - \frac{T_D}{2\pi T_S} \sin\left(\frac{2\pi t_m}{T_S}\right) \tag{7.8}$$

in which t_m is the time that the maximum erosion occurs with respect to the beginning of the storm. Unfortunately, this equation can only be solved by approximation or numerically. Thus the maximum recession associated with a duration limited storm can be calculated by:

$$\alpha = \frac{DE_m}{DE_{MAX}} = 0.5\left[1 - \cos\left(2\pi\frac{t_m}{T_D}\right)\right] \qquad (7.9)$$

where α is the duration reduction factor and DE_m is the maximum recession that occurs for a given storm duration that occurs at time t_m. As a result, the duration limited recession is:

$$DE_m = \alpha DE_{MAX} \qquad (7.10)$$

7.2 Erosion modeling on Clatsop County beaches

In order to determine the duration reduction factor, α, the duration of each storm event has to be first identified. The approach used here involved an analysis of the number of hours a specific total water level (T_{WL}) event was found to exceed a particular beach profile's beach-dune junction elevation, applying the Ruggiero and others (2001) analysis approach. **Figure 7-3** is an example of the approach we used, which is based on a script developed in MATLAB. In essence, the blue line is the TWL time series for a particular profile, ±3 days from the event. The script moves backwards and forwards in time from the identified event until the TWL falls below the critical threshold shown as the black line in **Figure 7-3**, which reflects the beach-dune junction elevation. The duration of the storm was then determined as the period where the TWL exceeds the threshold and includes the shoulders of the event (i.e., when the TWL first falls below the critical threshold). This process was undertaken for every storm and for each of the profile sites. One limitation of this approach that was encountered is that it is possible for the duration to be underestimated if the TWL dips below the threshold for an hour or more and then rises again above the threshold, as seen in the example in **Figure 7-3**.

As described previously, the breaker height, H_b, was calculated using equation 6.8 and the breaker depth, h_b, was claculated using a breaker index of 0.78. The berm elevation was established at 3 m (typical for PNW beaches), while the surf zone width, W_b, was determined for each breaker depth value by interpolating along a profile line of interest (**Figure 7-4**). Although we have grain size information available that could have been used to define the *A*-parameter for Clatsop County, the approach we took was to iteritively determine an equilibrium *A* value based on the actual beach profile data. Here we used the profile data seaward to the 8 m (26.3 ft) water depth; a range of *A*-values were fit to the data until a value was found that best matched the profile morphology. This approach was adopted for all the profile sites. **Figure 7-5** presents the alongshore varying dune erosion parameters (beach slope, A, surfzone width and breaker depth) calculated for each transect site and averaged over every storm. These data are also summarized in **Table 7-1**.

Figure 7-6 presents the alongshore varying time scale for the erosion of a dune (T_S), storm duration (T_D), and duration reduction factor (α) values determined for those transect sites characterized as "dune-backed" in Clatsop County. In all cases, we used the surf zone width, breaking depth, and water levels determined at the respective transect site (along with information pertaining to the sites beach/dune morphology) to calculate T_S, and T_D for each storm, while the final parameter, *Tm*, was solved numerically using equation 7.8 in order to define the duration reduction factor (α). These data have subsequently been averaged for each of the transect locations and are ultimately included in **Table 7-1** and presented in **Figure 7-5** and **Figure 7-6**.

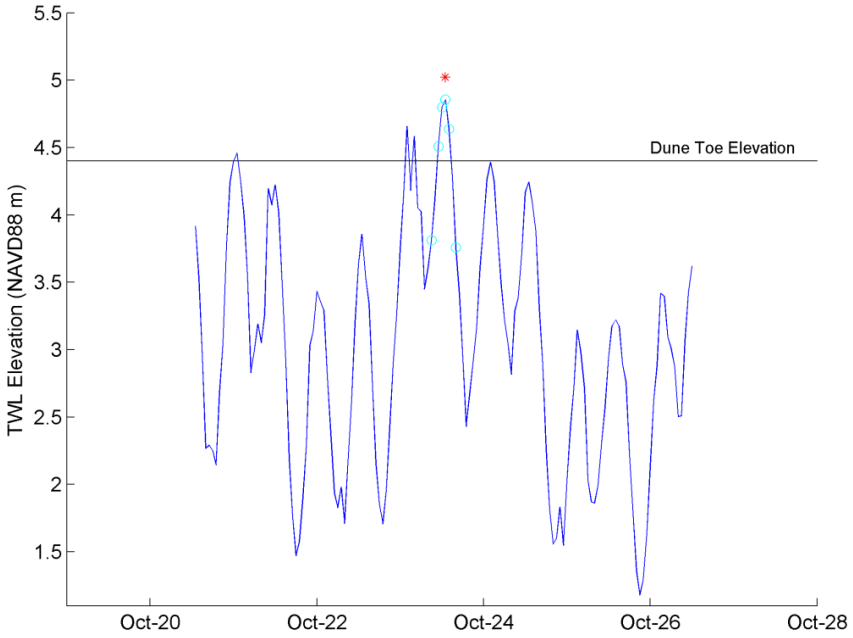

Figure 7-3. Example plot of the approach used to define storm duration along the Coos County shoreline. Note: The red asterisk denotes the location of the storm peak. The blue circles denote the hours when the event exceeded the critical beach-dune junction toe elevation (including the shoulders) that are used to define the "duration" of the event.

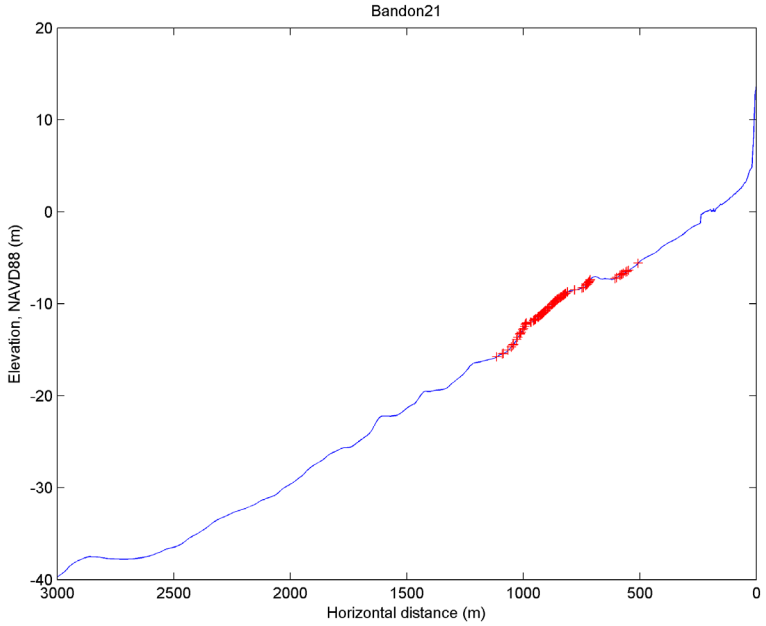

Figure 7-4. Example transcect from Coos County showing the locations of h_b (red crosses), used to define the cross-shore width (W_b) of the surf zone.

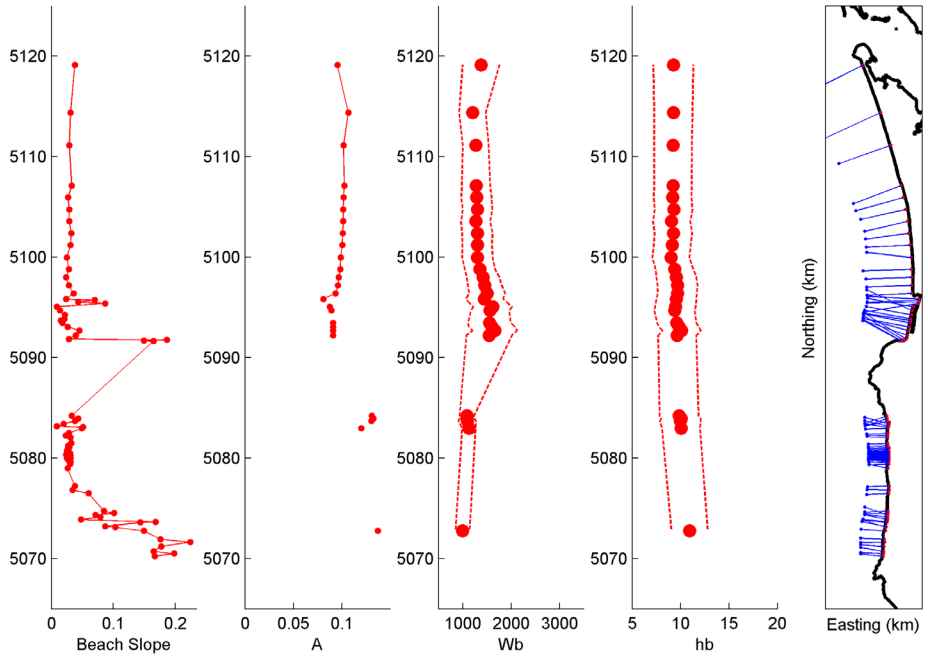

Figure 7-5. Plot showing the dune erosion parameters (tan β, *A*, W_b, and h_b) used to calculate the profile responses (T_S), storm durations (T_D), alpha, and the storm-induced dune erosion. For W_b and h_b we show the mean value and ±1 standard deviation computed using all of the storms.

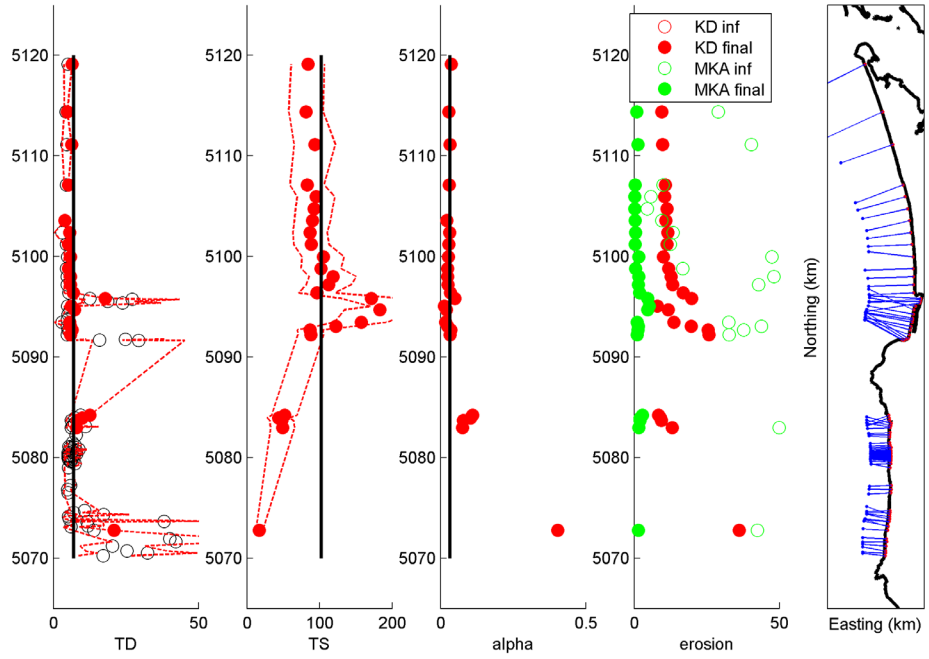

Figure 7-6. Plot showing the storm duration hours (TD), the calculated time scale of profile response hours (T_S), alpha, and the storm induced K&D and geometric model erosion adjusted using equation 7.10 for the dune-backed profiles along the Clatsop County shore.

Having defined the duration reduction factor (α) for each transect location, the storm-induced erosion was calculated using equation 7.10. As can be seen in **Table 7-1**, calculations of the maximum potential dune erosion (DE_{MAX}) using the Komar and others (1999) Geometric model yielded results that are considerably smaller than those derived using the Kriebel and Dean (1993) approach. These differences are largely due to the effect of the surf zone width parameter and the low nearshore slopes used in the K&D calculations. Our initial calculations of storm-induced erosion based on the K&D approach indicated several sites with anomalously large estimates of dune erosion (>20 m), when compared with actual field observations observed by DOGAMI staff over the past two decades. In contrast, storm-induced erosion estimates based on the maximum potential dune erosion (DE_{MAX}) calculated using the geometric model produced very negligible erosion responses that made little physical sense. As a result, our final calculation of the storm-induced erosion (DE_m) is based on the K&D approach. To reduce the large erosion responses observed at several of the transect sites, we ultimately defined an alongshore averaged duration reduction factor (α) of 0.03 (**Table 7-1**), which was used to calculate the storm-induced erosion (DE_m) at each of the dune-backed transect sites present along Clatsop County. As can be seen from **Table 7-1**, this resulted in erosion responses that range from a minimum of 7.9 m to as much as 25.5 m, while the mean storm-induced erosion response is calculated to be 12.8 m. These results are entirely consistent with actual field observations derived from both GPS beach surveys and from previous analyses of topographic change data measured using lidar (Allan and Harris, 2012; Allan and Stimely, 2013).

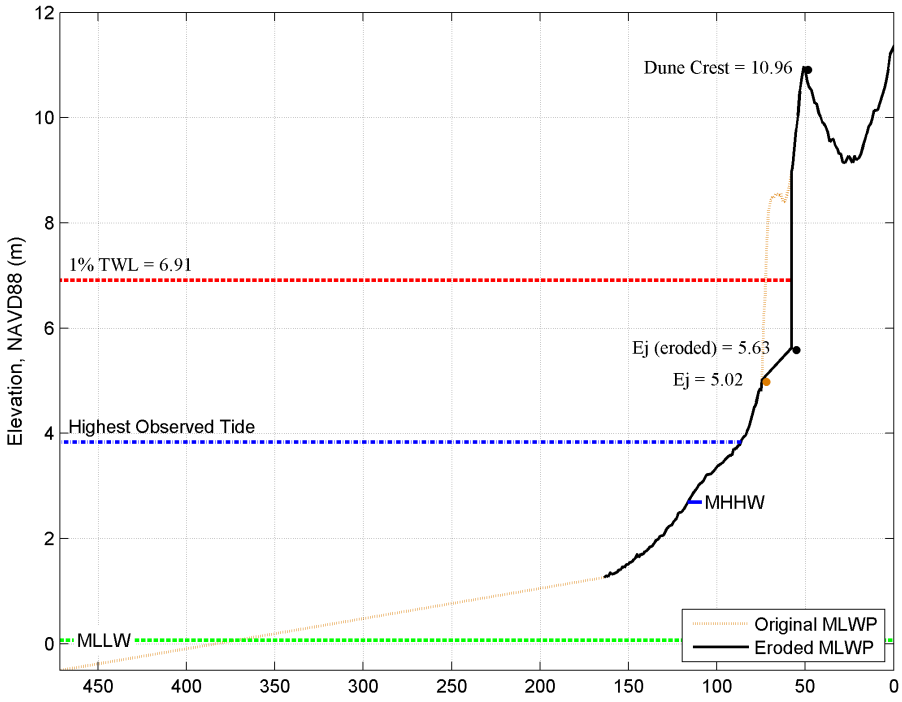

Figure 7-7. Application of the duration reduced erosion estimate to the most likely winter profile at Clatsop Plains 1.

Table 7-1. Calculated storm-induced erosion parameters for dune-backed beaches in Clatsop County. Note: MKA denotes the Geometric model and K&D is the Kriebel and Dean model.

Profiles		*A*	W_B	T_D	T_S	α	MKA (DE_{MAX})	MKA (DE_m)	K&D (DE_{MAX})	K&D (DE_m)
Cannon Beach	11	0.120	1128	8.0	49.2	0.076	49.9	1.7	396.9	13.2
	15	0.131	1095	8.1	47.9	0.078	61.4	2.0	282.0	9.4
	16	0.133	1091	10.0	43.4	0.030	62.3	2.1	274.4	9.1
	17	0.131	1086	12.6	51.7	0.030	86.1	2.9	252.9	8.4
Seaside	6	0.091	1665	6.4	87.0	0.036	37.7	1.3	767.9	25.5
	7	0.091	1608	5.9	122.5	0.024	43.8	1.5	591.4	19.6
	8	0.091	1551	5.6	157.2	0.018	32.6	1.1	412.0	13.7
	12	0.090	1566	7.3	183.1	0.019	138.1	4.6	353.8	11.7
	13	0.088	1621	6.2	227.4	0.013	155.9	5.2	239.0	7.9
	17	0.081	1448	17.8	171.4	0.050	138.3	4.6	595.8	19.8
Clatsop Plains	1	0.094	1505	6.8	96.6	0.034	56.2	1.9	508.9	16.9
	2	0.096	1455	5.9	112.7	0.026	42.8	1.4	398.4	13.2
	3	0.097	1423	5.9	118.5	0.024	48.1	1.6	381.7	12.7
	4	0.099	1356	5.2	102.2	0.025	16.7	0.6	358.4	11.9
	5	0.099	1305	6.0	105.0	0.028	47.4	1.6	304.2	10.1
	6	0.100	1302	5.2	88.9	0.029	12.5	0.4	340.6	11.3
	7	0.101	1303	5.6	87.1	0.031	13.3	0.4	349.0	11.6
	8	0.102	1268	4.0	90.2	0.022	9.6	0.3	329.0	10.9
	9	0.102	1306		92.6	0.030	4.5	0.1	340.2	11.3
	10	0.102	1284		95.3	0.030	5.8	0.2	314.1	10.4
	11	0.103	1276	5.2	82.9	0.031	10.0	0.3	324.4	10.8
	12	0.102	1270	6.3	93.6	0.033	40.3	1.3	295.8	9.8
	13	0.107	1202	4.8	81.4	0.029	28.9	1.0	285.9	9.5
	14	0.096	1381	6.5	83.9	0.037	51.9	1.7	539.1	17.9
Mean		**0.102**	**1354**	**7.1**	**102.4**	**0.03**	**49.8**	**1.7**	**384.8**	**12.8**

Note: *A* is the beach profile parameter that defines an equilibrium profile; W_b is the surf zone width; T_D is the storm duration; T_S is the time scale of response; α is the duration reduction factor.

Figure 7-7 and **Figure 7-8** provide two examples where the most eroded winter profile is eroded to reflect the storm-induced erosion values identified in **Table 7-1**. The first example is the Clatsop Plains 1 profile site where the beach is backed by a prominent foredune. In this example, the calculated duration reduced recession is ~16.9 m (55 ft). The location of the beach-dune junction is depicted in **Figure 7-7** by the brown circle, while the most eroded winter profile is shown as the black line. Because the underlying principle of the K&D and Geometric models is for the slope to remain constant, the dune is eroded landward by shifting the location of the beach-dune junction landward by 16.9 m (55 ft) and upward to its new location where it forms an erosion scarp (**Figure 7-7**). Due to the high dune crest, overtopping does not occur at this location.

Figure 7-8 provides an example where dune breaching and overtopping occurs in response to the calculated 1% TWL for the Clatsop Plains 14 profile site. The calculated dune erosion for Clatsop Plains 14 is ~17.9 m (59 ft). The location of the beach-dune junction is depicted in **Figure 7-8** by the shaded black circle, while the most eroded winter profile is shown as the black line. As noted by NHC (2005), when dunes are subject to major overtopping events, breaching of the dune typically results in significant lowering of the dune morphology and the development of an overwash fan on the lee side of the dune. Because the present methodologies are unable to account for such

responses, NHC recommends that the dune profile is adjusted by extending the *most likely winter profile* slope to the backside of the dune. This type of adjustment is demonstrated in **Figure 7-8** where the entire foredune is assumed to be eroded and removed as a result of a major storm.

Unfortunately, there are no measured examples of the type of response depicted in **Figure 7-8** for the Clatsop County area that can be used to make comparisons against. However, monitoring of beaches by DOGAMI on the Oregon coast provides some suggestion that this approach is probably reasonable. **Figure 7-9** is an example of beach profile changes measured along a barrier beach adjacent to Garrison Lake, Port Orford, located to the south of Bandon. In this example, the barrier beach, which has a crest elevation of 8-9 m NAVD88 (26–29 ft), is known to have been overtopped during several major storms in February/March 1999 (**Figure 7-10**) (Allan and others, 2003). Analyses of the mean shoreline position at this site indicate that changes in the morphology of the beach is controlled primarily by the occurrence of these major storms as well as by El Niño climate events that result in hotspot erosion. Examination of the beach profile changes along the Garrison Lake shore indicate that during major events characterized by overtopping, the crest of the barrier beach is lowered, with some of the eroded sand having been carried landward where they form washover fans, while the bulk is removed seaward to form sand bars. Ultimately, though, any dune located at the back of the profile is removed entirely, as the barrier rolls landward, consistent with the response depicted in **Figure 7-7**.

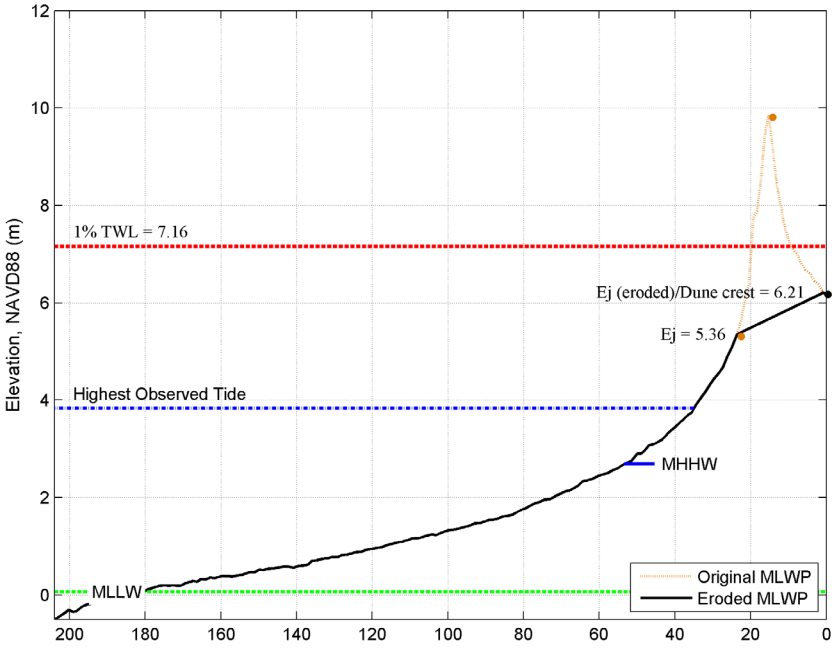

Figure 7-8. Application of the duration reduced erosion estimate to the most likely winter profile at Clatsop Plains 14 where overtopping and breaching occurs.

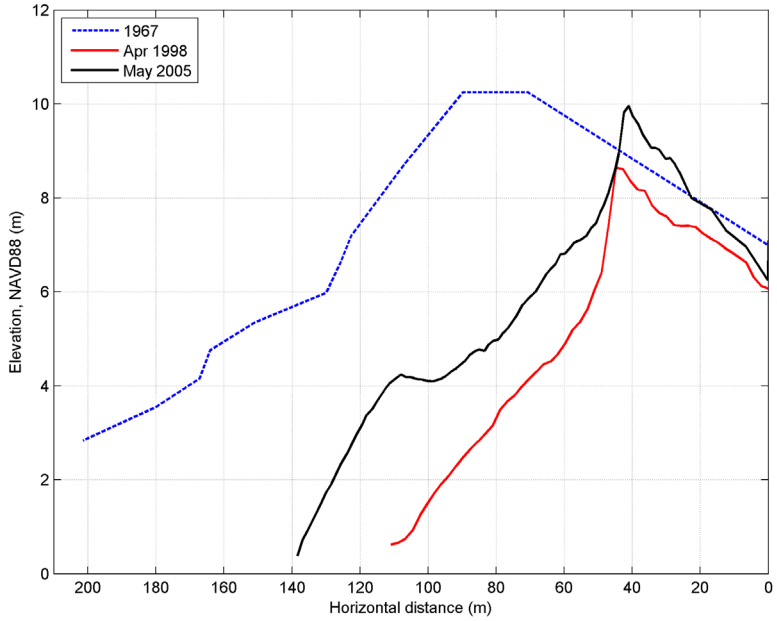

Figure 7-9. Example profile where a barrier beach is overtopped and eroded. This example is based on measured beach profile changes at Garrison Lake, Port Orford on the southern Oregon coast. The 1967 morphology was derived from Oregon Department of Transportation surveys of the beach on September 25, 1967, used to define the Oregon statutory vegetation line.

Figure 7-10. Overtopping of the barrier beach adjacent to Garrison Lake during a major storm on February 16, 1999 (photo: courtesy of a resident at Port Orford).

8.0 FLOOD MAPPING

8.1 Detailed Coastal Zone VE Flood Zone Mapping

Detailed mapping of the 1% chance flood event within selected areas of Clatsop County was performed using two contrasting approaches, controlled ultimately by the geomorphology of the beach and backshore. In all cases we followed the methods described in section D.4.9 in the final draft guidelines of the Coastal Flood Hazard Analysis and Mapping for the Pacific Coast of the United States (NHC, 2005). Due to the complexities of each mapping approach for the 0.1% chance flood event, it was not possible to reasonably map the 0.2% chance event. The reasons for this are described in more detail in the following sections.

8.1.1 Bluff-backed beaches

For bluff-backed beaches the total water level (T_{WL}) values calculated in Section 6.3 were extended into the bluff. The first step involved identifying specific contours of interest, which were extracted from the 1-meter resolution bare earth lidar grid DEM (surveyed in 2009). In all cases, the calculated total water level (T_{WL}) values were rounded to the nearest whole foot. For the bluff-backed beaches the landward extent of the coastal Zone VE is defined by the contour representing the total water level (T_{WL}) elevation calculated for each of the represented detailed surveyed transects (e.g., **Figure 8-1** and **Table 6-2**). FEMA Operating Guidance 9-13 (2013) dictates that areas near the landward extent of Zone VE, where the difference between the total water level (TWL) and ground elevation are less than 3 feet, be designated as Zone AE. However, due to the steepness of the shoreline along bluff-backed beaches such areas are too thin to be visible at the prescribed map scale, and therefore Zone AE was not designated in these environments. Similarly, 0.2% annual chance zones were not mapped due to the steepness of the shoreline.

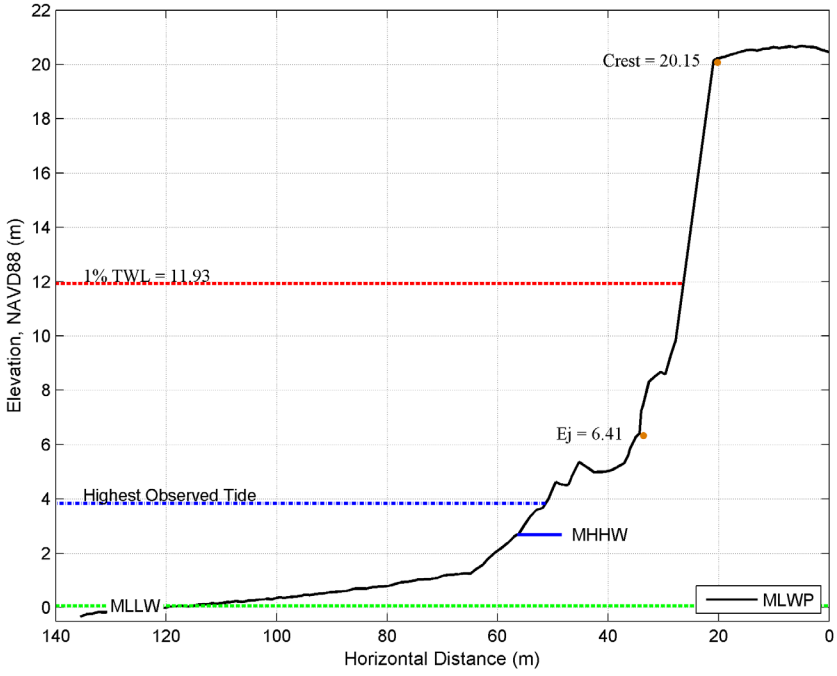

Figure 8-1. Example of a bluff-backed beach (Falcon Cove 2) where the calculated total water level and defined velocity (VE) zone extends into the bluff.

To define the velocity zones between transects, we used professional judgment to establish appropriate zone breaks between the various transects. For example, along-shore geomorphic barriers were identified within which the transect total water level (T_{WL}) value is valid (**Figure 8-2**). Slope and hillshade derivatives of the lidar DEM, as well as 1-meter orthophotos (acquired in 2009), provided the base reference. An effort was made to orient zone breaks perpendicular to the beach at the location of the geomorphic barrier. The seaward extent for the majority of bluff-backed Zone VE were inherited from the effective DFIRM (2010). In some cases adopting the effective extent produced inconsistent zone widths (too thin) and the boundaries were subsequently extended seaward.

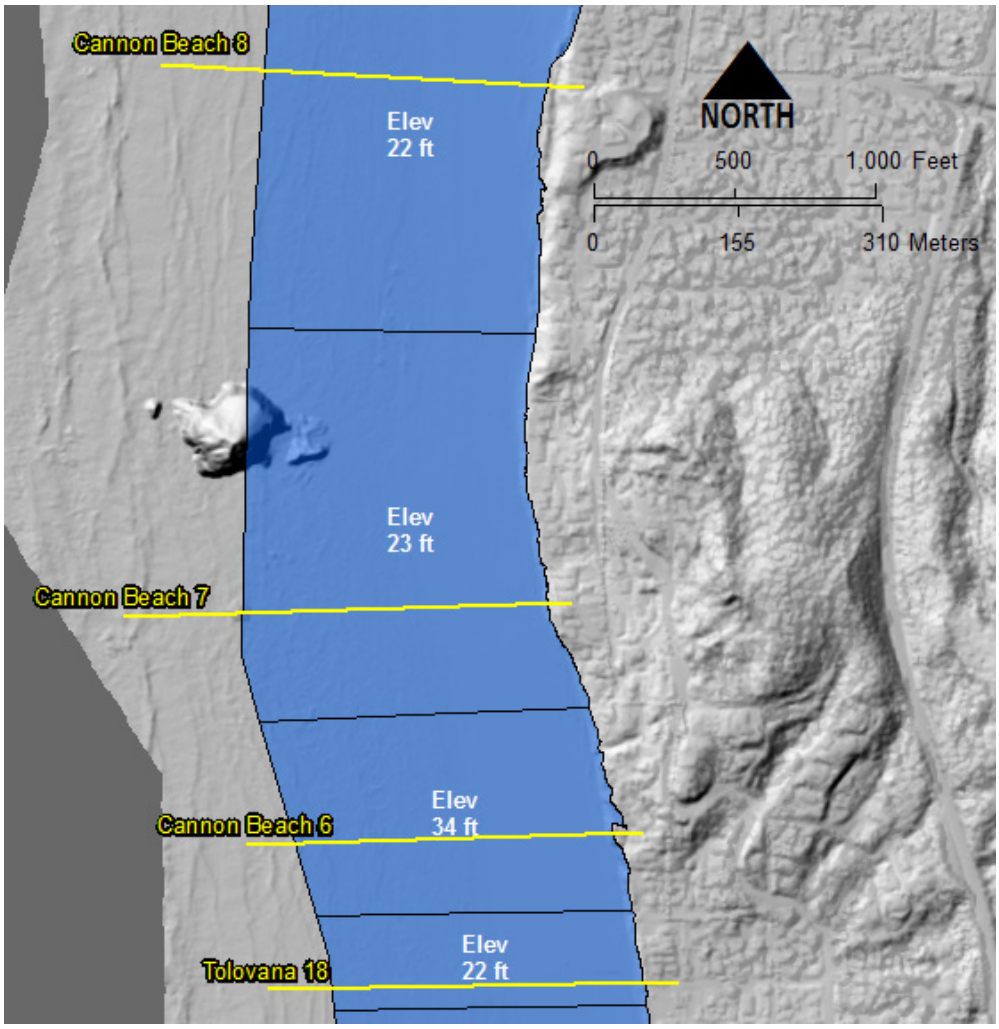

Figure 8-2. Example of along-shore zone breaks and their relationship to geomorphic barriers and surveyed transects. Surveyed transects are symbolized as yellow lines; zone breaks are solid black lines.

8.1.2 Dune-backed beaches

For dune-backed beaches, the VE flood zone was determined according to one or more criteria specified in the NHC (2005) guidelines. These include:

1. The ***wave runup zone***, which occurs where the total water level (T_{WL}) exceeds the (eroded) ground profile by ≥ 0.91 m (3 ft);
2. The ***wave overtopping splash zone*** is the area landward of the dune/bluff/structure crest where splashover occurs. The landward limit of the splash zone is only mapped in cases where the wave runup exceeds the crest elevation by ≥ 0.91 m (3 ft);
3. The ***high-velocity flow zone*** occurs landward of the overtopping splash zone, where the product of flow times the flow velocity squared (hV^2) is ≥ 5.7 m^3/s^2 (or 200 ft^3/s^2);
4. The ***breaking wave height zone*** occurs where wave heights ≥ 0.91 m (3 ft) could occur and is mapped when the wave crest profile is 0.64 m (2.1 ft) or more above the static water elevation; and
5. The ***primary frontal dune (PFD) zone*** as defined in Part 44 of the U.S. Code of Federal Regulations, Section 59.1; FEMA Coastal Hazard Bulletin, No. 15.

Table 6-3 lists the overtopping calculations for those transects where overtopping occurs, including the calculated splashdown distances ($Y_{G\,outer}$), bore height associated with wave overtopping (h_o) and the landward extent of the high-velocity flow (hV^2) where the flows approach 5.7 m^3/s^2 (or 200 ft^3/s^2). As noted above, hV^2 reflects the furthest point landward of the dune/bluff/structure crest that experiences coastal flooding due to overtopping and is ultimately controlled by the extent of the landward flow where it approaches 5.7 m^3/s^2 (or 200 ft^3/s^2); values greater than 5.7 m^3/s^2 (or 200 ft^3/s^2) are located within the high-velocity flow (VE) zone while lower values are located within the passive overland flooding (AE) zone. "Dist_3" (where the bore height is ≥ 3 ft) identifies the landward extent of flood zones where the bore height (h_o) was determined to be ≥ 0.91 m and were ultimately rounded up to the nearest whole foot (i.e., having an elevation of 0.91 m [3 ft] above the land surface). "Dist_2" (where the bore height is > 2 < 3 ft) identifies the landward extent of flood zones where the bore height (h_o) was determined to be between 0.61 and 0.91 m (2 and 3 ft high) and were ultimately rounded up to the nearest whole foot (i.e., having an elevation of 0.91 m [3 ft] above the land surface). "Dist_1" marks the seaward extent of flood zones where the bore height falls below 0.3 m (1 ft [i.e., having an elevation of 0.3 m (1 ft)] above the land surface (all values less than 0.3 m [1 ft] were rounded up to the nearest whole foot). Areas where flood zones exhibited bore height elevations of 0.61 m (2 ft) above the land surface were inferred as existing in the area between the two previously described regions (i.e., between "Distance from "x" Where Bore >2 <3 ft" and "Distance from "x" Where Bore <1").

Similar to the bluff-backed beaches, professional judgment was once again used to establish appropriate zone breaks between the detailed transects. This was achieved through a combination of having detailed topographic information of the backshore and from knowledge of the local geomorphology. Some interpretation was required to produce flood zones appropriate for the printed map scale. Elevations were identified from the 1-meter resolution bare earth lidar DEM to aid in establishing zone breaks due to changes in flood depth landward of the dune crest (**Figure 8-3**). Slope and hillshade derivatives of the lidar DEM, as well as 1-m orthophotos, provided base reference.

In overtopping splash transect situations, the flood zone was determined by adding the splashdown distances (YG outer) to the Dhigh distance. For all overtopping splash situations on the Clatsop coast, the splash distance was very short and not visible at a mapping scale. Therefore, it was added to the VE zone extent (**Figure 8-4**).

For flood zones seaward of the dune crest, the calculated T_{WL} values were used. As with the bluff-backed beaches, along-shore geomorphic barriers were identified within which the transect T_{WL} value is valid. In all cases, an effort was made to orient zone breaks perpendicular to the beach at the location of the geomorphic barrier. The seaward extent of the flood zones were inherited from the effective DFIRM (2010).

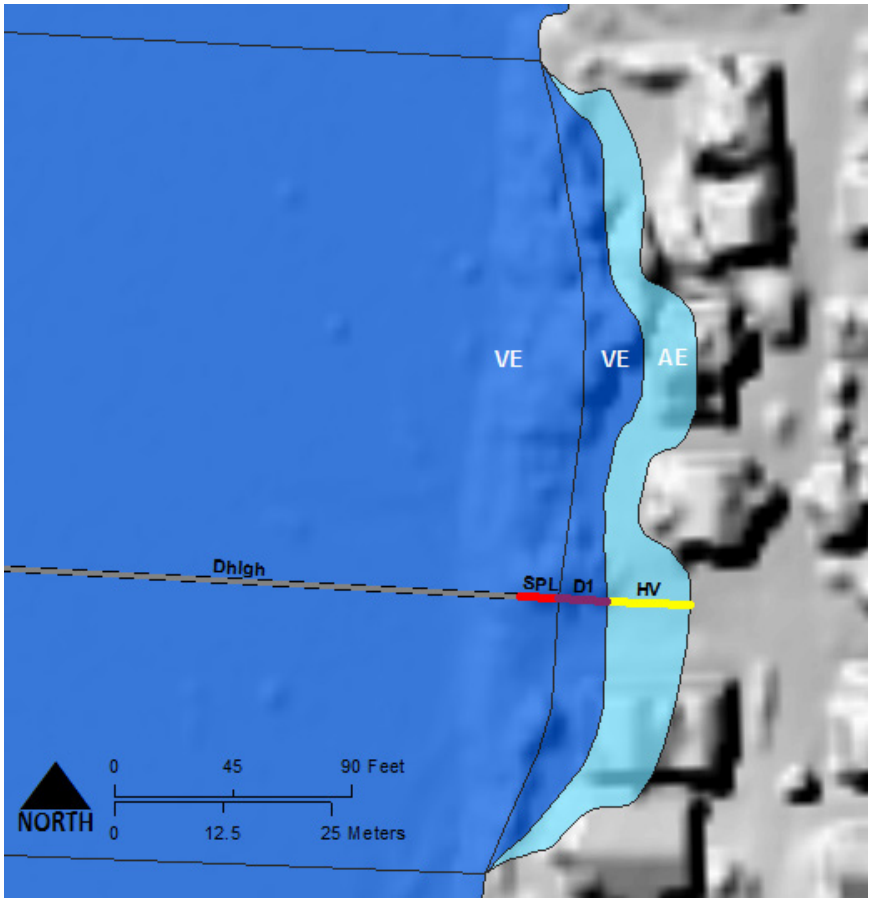

Figure 8-3. Breaking wave height overtopping along Tolovana Park 2 transect, where Dhigh is the area seaward of Dhigh distance, SPL is the splashdown distance, D1 is depth ≤0.31 m, HV is flow < 5.7 m^3/s^2 (or 200 ft^3/s^2. Zone breaks are solid gray lines. Dark blue flood zones are VE zones; light blue are AE zones.

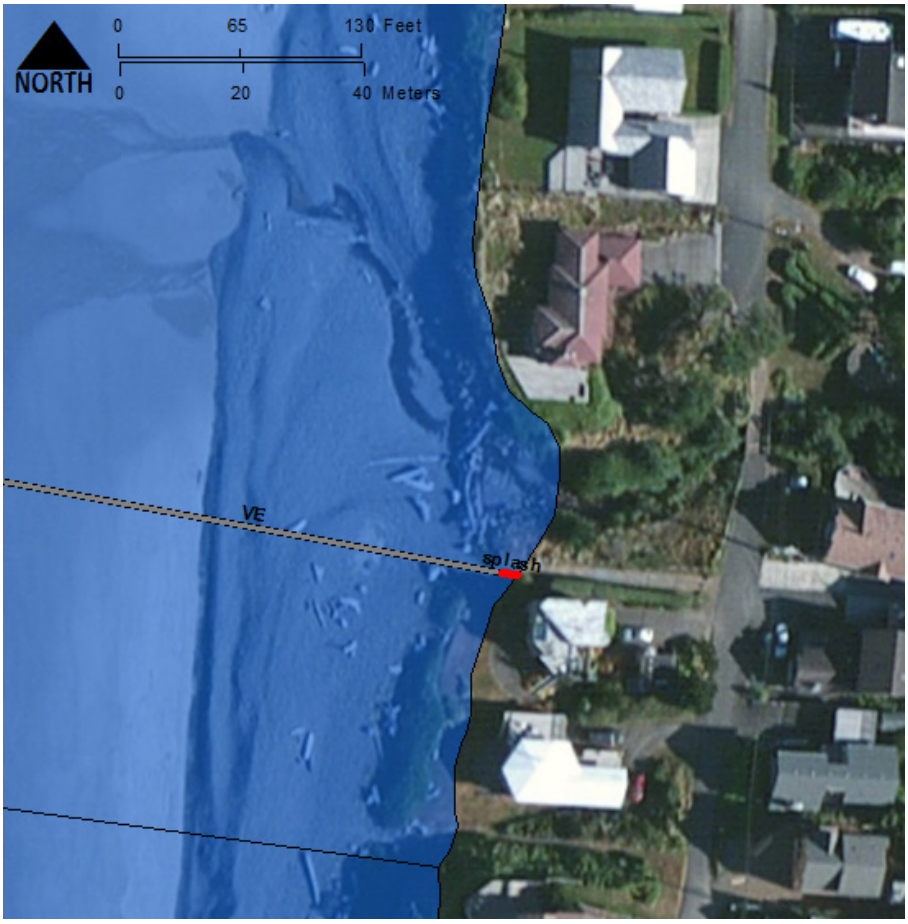

Figure 8-4. Transect (gray) at Arch Cape with overtopping Splash zone. The short splash zone distance (red) was added to the extent of Zone VE.

The PFD is defined as "a continuous or nearly continuous mound or ridge of sand with relatively steep seaward and landward slopes immediately landward and adjacent to the beach and subject to erosion and overtopping from high tides and waves during major coastal storms. The landward limit of the primary frontal dune, also known as the toe or heel of the dune, occurs at a point where there is a distinct change from a relatively steep slope to a relatively mild slope. The primary frontal dune toe represents the landward extension of the Zone VE coastal high hazard velocity zone" (Part 44 of the U.S. Code of Federal Regulations, Section 59.1, as modified in FEMA Coastal Hazard Bulletin, No. 15, https://www.¬floodmaps.fema.gov/listserv/ch_jul02.shtml).

The approach developed by DOGAMI to define the morphology of the beach and dune system, including the location of the PFD, follows procedures developed in our Coos Bay study (Allan and others, 2012) and was based on detailed analyses of light detection and ranging (lidar) data measured by the USGS/NASA/NOAA in 1997, 1998, and 2002 and by DOGAMI in 2009. However, because the lidar data flown by the USGS/NASA/NOAA are of relatively poor resolution (~1 point/m^2) and reflect a single return (i.e., include vegetation where present), while the lidar data flown by DOGAMI have a higher resolution (8 points/m^2) and are characterized by multiple returns enabling the development of a bare-earth DEM, determination of the PFD was based entirely on analysis of the 2009 lidar data.

Lidar data flown in 1997, 1998 and 2002 were downloaded from NOAA's Coastal Service Center (http://coast.noaa.gov/dataregistry/search/collection/info/coastallidar) and gridded in ArcGIS using a triangulated irregular network (TIN) algorithm (Allan

and Harris, 2012). Transects spaced 25 m apart were cast for the full length of the county coastline using the Digital Shoreline Analysis System (DSAS) developed by the USGS (Thieler and others, 2009); this process yielded 1951 individual transects throughout Clatsop County. For each transect, x,y,z values for the 1997, 1998, 2002, and 2009 lidar data were extracted at 1=m intervals along each transect line and saved as a text file using a customized ArcGIS script.

Processing of the lidar data was undertaken in MATLAB using a custom beach profile analysis script developed by DOGAMI. This script requires the user to interactively define various morphological features including the dune/bluff/structure crest/top, bluff/structure slope, landward edge of the PFD(s), beach-dune juncture elevations for various years, and the slopes of the beach foreshore (Allan and Harris, 2012). Although we evaluated all 1,951 transects, not all morphological features were applicable and therefore the PFD could be defined for only a subset of transects. **Figure 8-5** provides an example from Clatsop #12 derived from the northern tip of the Clatsop Plains. In this example, the dune crest in 2009 is presently located at 7.3 m (24 ft); prior to 2009, the dune crest was as high as 9.5 m (31 ft). As can be seen from the figure, the seaward face of the dune eroded landward by ~16.5 m (54 ft) between 1998 and 2009; shoreline change (erosion/accretion) was determined based on the change in position of the 6 m (19.7 ft) contour elevation, which is an excellent proxy for determining the effects of storm erosion (Allan and others, 2003). **Figure 3-13** (Clatsop Plains to Seaside) and **Figure 3-14** (Cannon Beach to Falcon Cove) depict changes in the position of the 6 m (19.6 ft) contour along the length of the Clatsop County shoreline. As can be seen from the figures, erosion is occurring at the extreme north end of the Clatsop Plains adjacent to the south Columbia River jetty (**Figure 3-13**), and along much of the Cannon Beach/Falcon Cove shore (**Figure 3-14**), albeit at relatively low rates. In contrast, accretion dominates much of the Clatsop Plains (**Figure 3-13**).

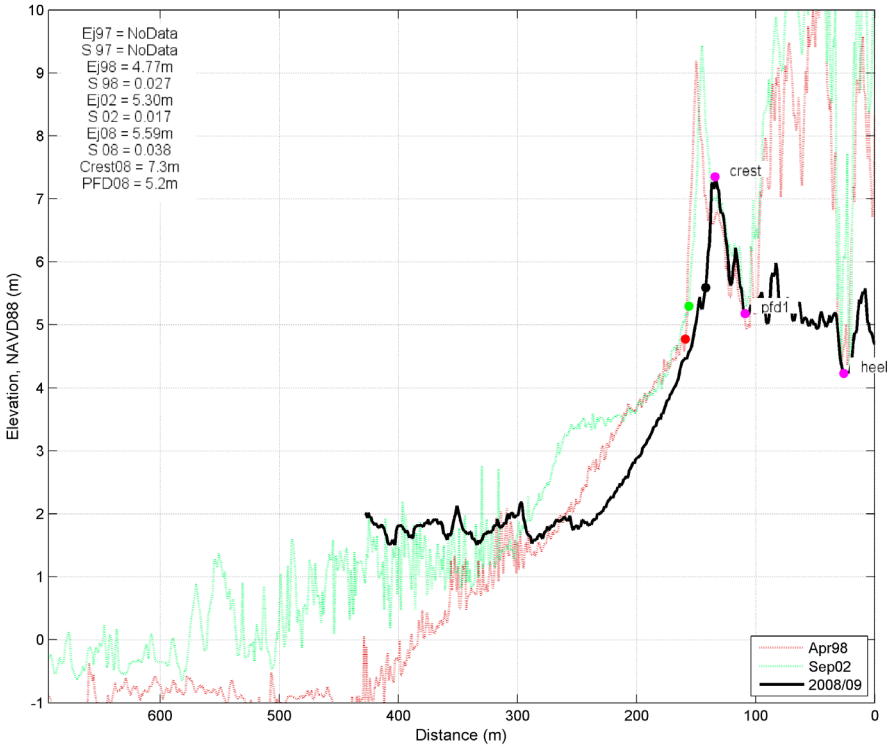

Figure 8-5. Example beach profile (#12) for the northern Clatsop Plains derived from 1997, 1998, 2002 and 2009 lidar data (Allan and Harris, 2012).

Having interpolated the lidar transect data in order to define the various morphological parameters, the actual locations of the PFDs were subsequently plotted in ArcGIS and overlaid on both current and historical aerial photos of the county, and shaded relief derived from the 2009 lidar. (In many cases, multiple PFD locations were defined along a single transect.) In a number of locations the PFD was found to be located either farther landward or seaward relative to adjacent PFD locations. This response is entirely a function of the degree to which the morphology of foredunes vary along a coast, and further the ambiguity of defining the PFD as defined above in the FEMA definition. Our observations of the PFD approach highlighted a number of uncertainties, including:

1. There were numerous examples of smaller dune features that have begun to develop in front of a main dune (or are the product of erosion of the dune), but have not yet attained dimensions and volumes where they would be considered an established dune or may continue to erode and could disappear entirely. However, the PFD approach does not adequately account for such features. In this example, the smaller dunes are almost certainly subject to erosion and periodic over-topping, and have morphologies that resemble the FEMA PFD definition. However, because they are subject to short-term erosion responses they are more ephemeral in nature and thus it is debatable whether they should be defined as PFDs. Furthermore, over the life of a typical map (~10 years) these dunes could be eroded and removed entirely leaving a "gap" between the original polygon boundary and the eroding dune. For example, from repeated observations of beach profile transects on the northern Oregon coast, single storm events have been documented to remove as much as 9–25 m (30–82 ft) of the dune (Allan and Hart, 2007, 2008);
2. The PFD does not adequately account for a large established foredune, where the dune may have attained heights of 10–15 m (33–49 ft), with cross-shore dimensions on the order of 100–200 m (328–656 ft) wide due to prolonged aggradation and progradation of the beach. In this example, although there may be a clear landward heel located well inland away from the beach (e.g., profile #840 in **Figure 8-6**), the PFD is clearly not subject to "frequent" wave over-topping due to its height and erosion (because of its large volume of sand). Defining the PFD at the location of the heel is consistent within the definition provided by FEMA, but would almost certainly generate a very conservative V zone.
3. Although numerous transects exhibited clear examples of single PFD locations, many others were characterized by more than one PFD. Profile #840 (**Figure 8-6**) is an example where multiple potential PFDs were defined.

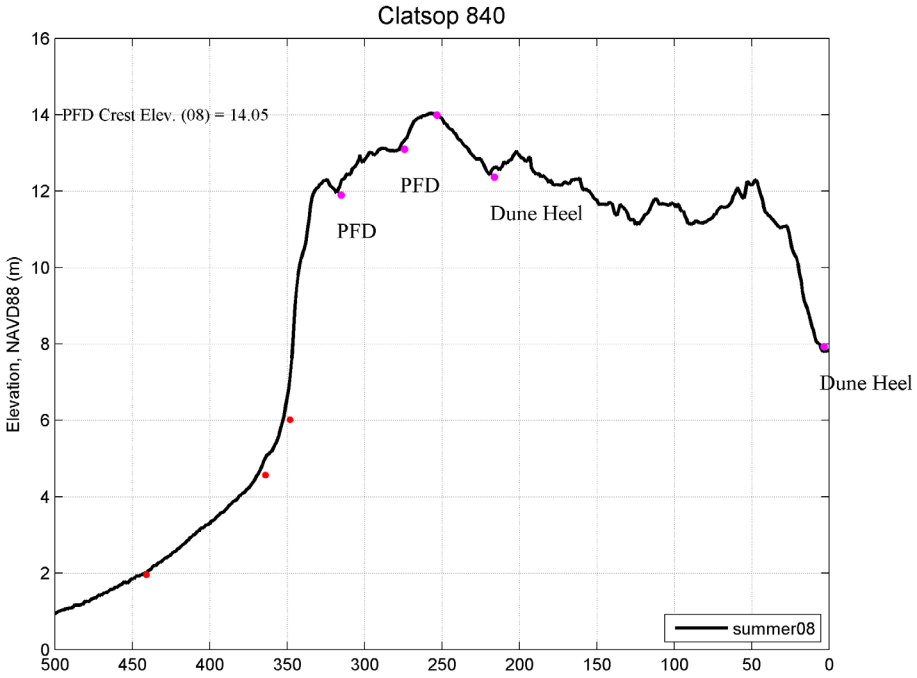

Figure 8-6. Example profile from the Clatsop Plains where considerable aggradation and progradation of the dune has occurred. In this example, the PFD could conceivably be drawn at a variety of locations and meet the FEMA definition.

To account for these variations and uncertainties, the PFD shown on the profile plots (e.g., **Figure 8-5** and **Figure 8-6**) were re-examined and adjustments were made where necessary in order to define a single PFD line. For example, in a few locations along the Clatsop Plains, the PFD extent for a particular transect was physically moved in ArcGIS so that it was more in keeping with the adjacent PFD locations to its immediate north and south. As can be seen in **Figure 8-7**, the final PFD designation was invariably some distance inland, often representing the clearest signal determined from all available data and adhering best to the FEMA definition.

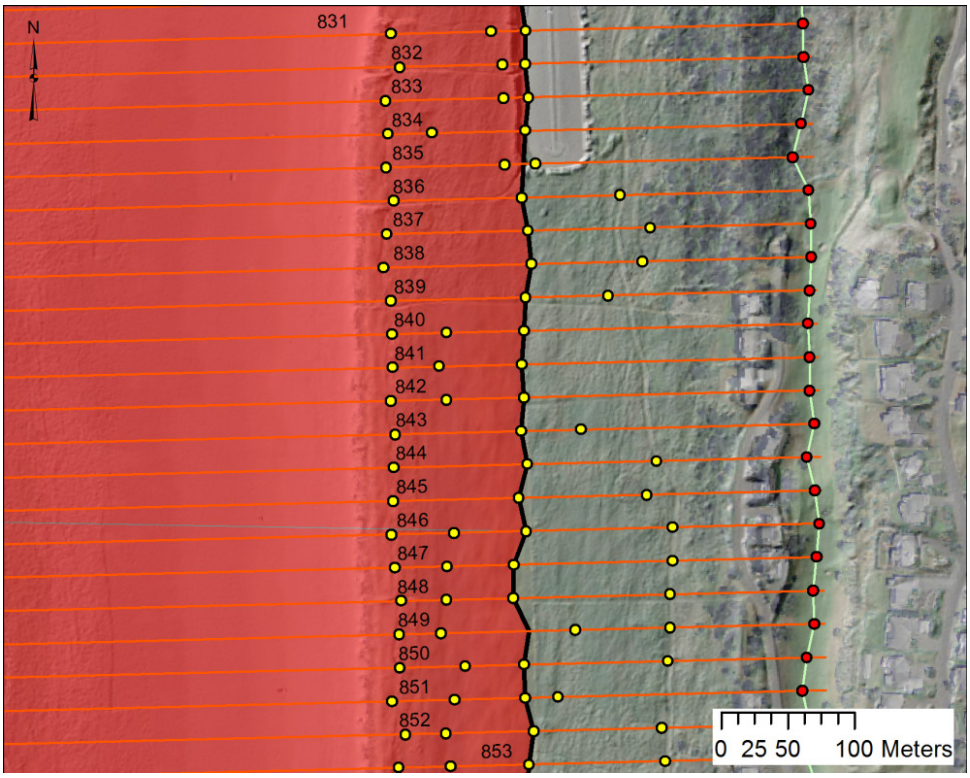

Figure 8-7. Plot showing identified PFD locations (yellow dots) along each transect, landward most dune heel (red dots), and derived PFD line (black line). Red zone depicts the VE zone having accounted for all possible criteria. Red lines depict the locations of the lidar transects, which were spaced 25 m (82 ft) apart.

In one example (Seaside 5 transect) the VE zone was physically moved slightly farther inland due to the presence of field evidence of historical overtopping. The Seaside 5 example (**Figure 8-8**) is located at the south end of Seaside (**Figure 3-1**). The red and blue solid lines indicate our transect locations (red=overtopped (inundation is shown at the bottom of the image as orange and yellow shading), blue=no overtopping). This section of shore reflects an extensive gravel/cobble berm fronted by a low sloping dissipative sand beach. The figure shows the calculated BFEs (i.e., T_{WL}) for the various transects, which increases to the south due to there being less fronting beach and the increasing effect of the steep cobble face. The cobble berm broadens significantly in the reach covered by our cp59 transect. The predominant sediment source is from landsliding off of Tillamook Head to its immediate south (**Figure 3-10**), and the subsequent northward transport of those sediment (in fact much of seaside is built on a sequence of barrier berms composed of gravels that have formed over the past 5,000 years). The red zone in **Figure 8-8** indicates the calculated VE zone. At the Seaside 5 transect site, the waves barely overtop the crest of the berm due to the dissipative effect from the fronting sand beach. Landward of the calculated VE zone is a red line which marks the back edge of one of the barrier berms. These berms are characterized with abundant logs on the top of the berm landward of our VE zone, which is the product of runup and overtopping from historical events, followed by progradation of the berm. In this example, although technically a cobble berm fronted by a sand beach, we map the VE to the line depicted by the back-edge of the berm.

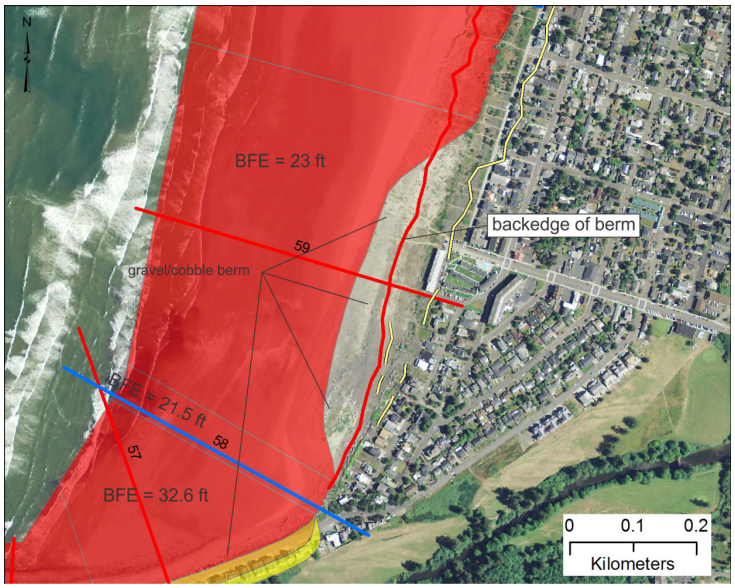

Figure 8-8. Profile Seaside 5 showing the calculated VE zone and various geomorphic indicators used to finalize the VE zone.

Finally, there was one exception where the flood zone landward of the hV2 transition was designated as Zone AH instead of Zone AE. The exception was at Falcon Cove 5 where waves overtop the barrier and fill the lagoon like a bathtub (**Figure 8-9**). This zone can only hold water levels equal or less than their height of the barrier (D_{high}); all additional floodwater pours back out into the ocean. Therefore, it is a ponding zone and the static BFE for Falcon Cove 5 is the same as the elevation of D_{high}.

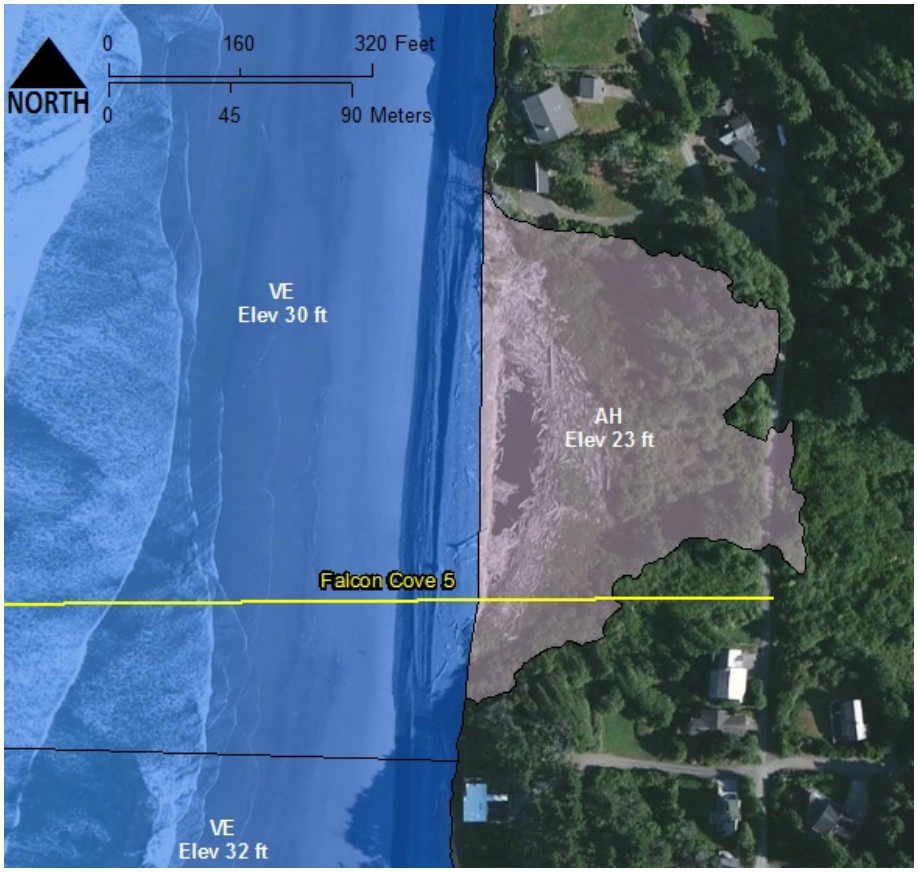

Figure 8-9. Falcon Cove 5 transect where a Zone AH was designated landward of *Dhigh* due to the presence of a lagoon.

8.1.3 Mapping of estuarine flooding

The confluences of Ecola Creek and Necanicum River with the Pacific Ocean form the two primary estuarine features along the Clatsop County open coast south of the Columbia River jetty. The total water level (TWL) parameter calculated at each surveyed transect includes wave setup and runup components that are not applicable in the sheltered waters of the estuaries. Due to the lack of wave energy the still water level (SWL) was used to map the coastal backwater effect of the 1% and 0.2% flood events into the estuaries. Procedures for developing the SWL are described in Section 4.6. The 1% SWL value for the Clatsop County coast is 3.60 m (11.8 ft, NAVD88) and 0.2% SWL is estimated to be 3.68 m (12.1 ft, NAVD88).

Coastal backwater flooding into the Necanicum River estuary was reduced by approximately 2 feet. Flood profiles published in the effective Flood Insurance Study report (2010) for the Necanicum River and Neawanna Rivers were edited to show the change in coastal backwater flooding. Because Ecola Creek is not a studied riverine flooding source the only mapped flood zones are the result of coastal backwater flooding (**Figure 8-10**).

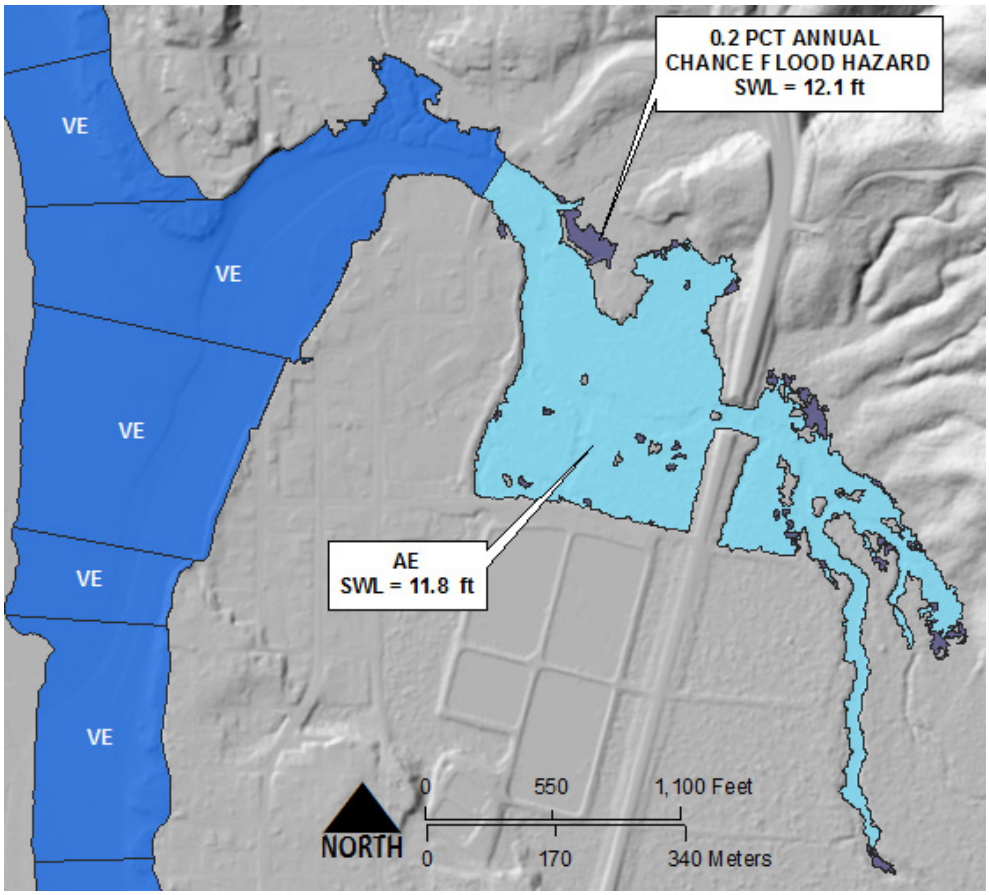

Figure 8-10. Coastal backwater flooding mapped from SWLs for the Ecola Creek estuary.

8.2 Coastal V-Zone Mapping along the Clatsop County Shoreline

8.2.1 Dune-backed beaches

The FEMA guidelines provide little direct guidance for mapping approximate coastal velocity zones (Zone V) in areas where no detailed studies have occurred, other than by defining the location of the PFD, using the methodology described above. In the case of the Clatsop Plains, we have endeavored to undertake detailed mapping in all areas backed by dunes.

8.2.2 V-zone mapping on coastal bluffs and headlands

Significant sections of the Clatsop County coastline are characterized by coastal bluffs and cliffs of varying heights. For these areas, the approach adopted by DOGAMI was to map the top of the active bluff (**Figure 8-11**) that is most likely subject to wave erosion, which is a readily identifiable feature that can be used to constrain the landward extent of the Zone V. **Figure 8-11** provides an example of a lidar transect from just north of Ecola State Park, where the top of the active bluff face is located at 20.2 m. **Figure 8-12** depicts the derived bluff top line based on a synthesis of all available information, including the lidar transect data, analyses of lidar contours, and hillshades.

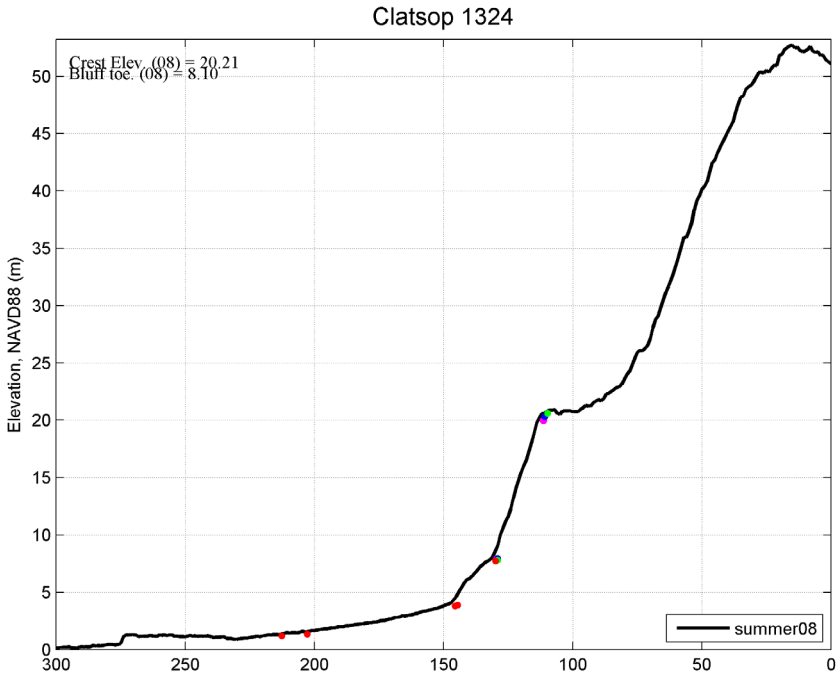

Figure 8-11. Zone V mapping morphology designation along coastal bluffs and cliffs. Example is from just north of Ecola State Park (Clatsop #1324). Blue dot denotes the location of the bluff/cliff top, while the red dots reflect locations where slopes were calculated, as well as the bluff toe.

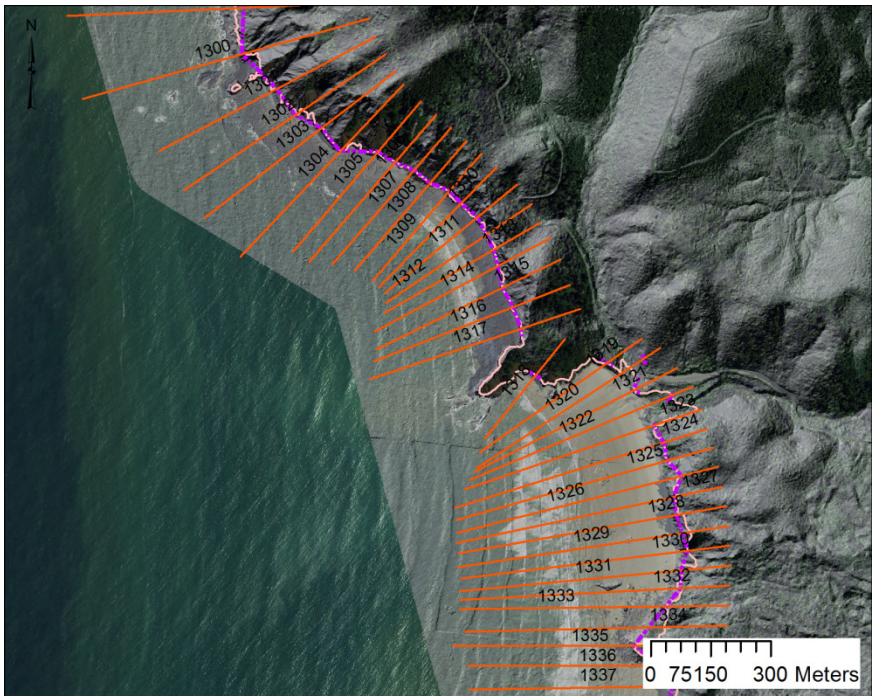

Figure 8-12. Zone V mapping example showing the locations of the individual transects (red lines), bluff top (magenta line) derived from analyses of the lidar transects, and the final derived bluff line (pink line), which incorporates all available data (transects, contours, hillshade, and orthophotos).

9.0 ACKNOWLEDGMENTS

Funding for this study was provided by the Federal Emergency Management Agency as part of the Flood Map Modernization program under Cooperating Technical Partner award EMS-2010-GR-0014. We are grateful to Dr. Bill McDougal for his technical advice throughout this project. We would especially like to acknowledge Nicole Walker from Atkins Global and Dr. Paul Komar for their insightful reviews of the report.

10.0 REFERENCES

Aguilar-Tunon, N.A., and Komar, P.D., 1978, The annual cycle of profile changes of two Oregon beaches: Ore Bin, v. 40, no. 2, p. 25-39.

Allan, J.C., and Priest, G.R., 2001, Evaluation of coastal erosion hazard zones along dune and bluff backed shorelines in Tillamook County, Oregon: Cascade Head to Cape Falcon: Oregon Department of Geology and Mineral Industries Open-File Report O-01-03, 126 p.

Allan, J.C., and Komar, P.D., 2002, Extreme storms on the Pacific Northwest Coast during the 1997-98 El Niño and 1998-99 La Niña: Journal of Coastal Research, v. 18, no. 1, p. 175-193.

Allan, J.C., Komar, P.D., and Priest, G.R., 2003, Shoreline variability on the high-energy Oregon coast and its usefulness in erosion-hazard assessments, *in* Byrnes, M.R., Crowell, M., and Fowler, C., eds., Shoreline mapping and change analysis: Technical considerations and management implications: Journal of Coastal Research, Special Issue No. 38, p. 83-105.

Allan, J.C., Hart, R., and Geitgey, R., 2005, Dynamic revetments for coastal erosion stabilization: A feasibility analysis for application on the Oregon Coast: Oregon Department of Geology and Mineral Industries Special Paper 37, 71 p.

Allan, J.C., and Komar, P.D., 2006, Climate controls on U.S. West Coast erosion processes: Journal of Coastal Research, v. 22, no. 3, p. 511-529.

Allan, J.C., and Hart, R., 2007, Assessing the temporal and spatial variability of coastal change in the Neskowin littoral cell: Developing a comprehensive monitoring program for Oregon beaches: Oregon Department of Geology and Mineral Industries Open-File Report O-07-01, 27 p.

Allan, J.C., and Hart, R., 2008, Oregon beach and shoreline mapping and analysis program: 2007-2008 beach monitoring report: Oregon Department of Geology and Mineral Industries Open-File Report O-08-15, 60 p.

Allan, J.C., Komar, P.D., and Ruggiero, P., 2011, Storm surge magnitudes and frequenciy on the central Oregon coast, *in* Solutions to Coastal Disasters 2011, Anchorage, Alaska, American Society of Civil Engineers, p. 53-64.

Allan, J.C., and Harris, E.L., 2012, An "expanded" geospatial database of beach and bluff morphology determined from LIDAR data collected on the northern Oregon coast; Tillamook to Clatsop County: Oregon Department of Geology and Mineral Industries Open-File Report O-12-08, 23 p.

Allan, J.C., Komar, P.D., Ruggiero, P., and Witter, R.C., 2012a, The March 2011 Tōhoku tsunami and its impacts along the U.S. West Coast: Journal of Coastal Research, v. 28, no. 5, p. 1142-1153.

Allan, J.C., Ruggiero, P., and Roberts, J.T., 2012b, Coastal flood insurance study, Coos County, Oregon: Oregon Department of Geology and Mineral Industries Special Paper 44, 132 p.

Anders, F.J., and Byrnes, M.R., 1991, Accuracy of shoreline change rates as determined from maps and aerial photographs: Shore and Beach, v. 59, no. 1, p. 17-26.

Atwater, B.F., Satoko, M.-R., Satake, K., Yoshinobu, T., Kazue, U., and Yamaguchi, D.K., 2005, The orphan tsunami of 1700—Japanese clues to a parent earthquake in North America: U.S. Geological Survey Professional Paper 1707, 144 p.

Baird & Associates, 2005, Pacific Ocean wave information study: Validation of wave model results against satellite altimeter data. Prepared for U.S. Army Corp of Engineers, Engineering Research and Development Center, Vicksburg, Miss.: Madison, Wisconsin, 13 p.

Bernstein, D.J., Freeman, C., Forte, M.F., Park, J.-Y., Gayes, P.T., and Mitasova, H., 2003, Survey design analysis for three-dimensional mapping of beach and nearshore morphology, *in* Fifth International Symposium on Coastal Engineering and Science of Coastal Sediment Processes (Coastal Sediments '03), Clearwater Beach, Fla., American Society of Civil Engineers, p. 12.

Booij, N., Ris, R.C., and Holthuijsen, L.H., 1999, A third-generation wave model for coastal regions, Part I: Model description and validation: Journal of Geophysical Research, v. 104, no. C4, p. 7649-7666.

Boon, J.D., 2004, Secrets of the tide: Tide and tidal current analysis and predictions, storm surges and sea level trends: Cambridge, U.K., Woodhead Publishing, 224 p.

Bruun, P., 1962, Sea level rise as a cause of shore erosion: Journal of Waterways, Harbors Division, Amer. Soc. Civil Engrs., v. 88, p. 117-130.

Burgette, R.J., Weldon, R.E., III, and Schmidt, D.A., 2009, Interseismic uplift rates for western Oregon and along-strike variation in locking on the Cascadia subduction zone: Journal of Geophysical Research, v. 114, no. B01408, p. 24.

Carignan, K.S., Taylor, L.A., Eakins, B.W., Warnken, R.R., Sazonova, T., and Schoolcraft, D.C., 2009a, Digital elevation model of Garibaldi, Oregon: Procedures, data sources and analysis: National Geophysical Data Center NOAA Technical Memorandum NESDIS NGDC-16, 28 p.

Carignan, K.S., Taylor, L.A., Eakins, B.W., Warnken, R.R., Sazonova, T., and Schoolcraft, D.C., 2009b, Digital elevation model of Astoria, Oregon: Procedures, data sources and analysis: National Geophysical Data Center, Marine Geology and Geophysics Division NOAA Technical Memorandum NESDIS NGDC-22, 43 p.

Clemens, K.E., and Komar, P.D., 1988, Oregon beach-sands compositions produced by the mixing of sediments under a transgressing sea: Journal of Sedimentary Petrology, v. 58, no. 3, p. 519-529.

Coles, S., 2001, An introduction to statistical modeling of extreme values: London, Springer-Verlag, 208 p.

Cooper, W.S., 1958, Coastal sand dunes of Oregon and Washington: Geological Society of America Memoir 72, 169 p.

Davis, R.E., and Dolan, R., 1993, Nor'easters: American Scientist, v. 81, p. 428-439.

Dean, R.G., 1977, Equilibrium beach profiles: U.S. Atlantic and Gulf Coasts; Ocean Engineering Technical Report No. 12: Newark, Del., University of Delaware, Department of Civil Engineering and College of Marine Studies, 45 p.

FEMA, 2010, Flood insurance study: Clatsop County, Oregon: FEMA, 122 p.

Gelfenbaum, G., Buijsman, M.C., Sherwood, C.R., Moritz, H.R., and Gibbs, A.E., 2001, Coastal evolution and sediment budget at the mouth of the Columbia River, USA, *in* 4th International Conference on Coastal Dynamics, Lund, Sweden.

Gelfenbaum, G., and Kaminsky, G.M., eds., 2002, Southwest Washington coastal erosion workshop report 2000, Washington Department of Ecology, Olympia, WA, and U.S. Geological Survey, Menlo Park, CA, OFR 02-229, 308 p.

Goldfinger, C., Nelson, C.H., and Johnson, J.G., 2003, Holocene earthquake records from the Cascadia Subduction Zone and Northern San Andreas fault based on precise dating of offshore turbidites: Annual Review of Earth and Planetary Sciences, v. 31, p. 555-577.

Goldfinger, C., 2009, Paleoseismically derived probabilities for Cascadia great earthquakes [abs.]: Geological Society of America Abstracts with Programs, v. 41, no. 7, p. 520.

Goldfinger, C., and others, 2009, Turbidite event history: methods and implications for Holocene paleoseismicity of the Cascadia subduction zone Professional Paper 1661-F.

Gorman, L., Morang, A., and Larson, R., 1998, Monitoring the coastal environment; Part IV: Mapping, shoreline changes and bathymetric analysis: Journal of Coastal research, v. 14, no. 1, p. 61-92.

Hedges, T.S., and Mase, H., 2004, Modified Hunt's equation incorporating wave setup: Journal of Waterway, Port, Coastal, and Ocean Engineering, v. 130, no. 3, p. 109-113.

Jennings, R., and Shulmeister, J., 2002, A field based classification scheme for gravel beaches: Marine Geology, v. 186, p. 211-228.

Kelsey, H.M., Nelson, A.R., Hemphill-Haley, E., and Witter, R.C., 2005, Tsunami history of an Oregon coastal lake reveals a 4600 yr record of great earthquakes on the Cascadia subduction zone: Geological Society of America Bulletin, v. 117, no. 7/8, p. 1009-1032.

Komar, P.D., Torstenson, R.W., and Shih, S.-M., 1991, Bandon, Oregon: Coastal development and the potential for extreme ocean hazards: Shore & Beach, v. 59, no. 4, p. 14-22.

Komar, P.D., 1997, The Pacific Northwest Coast: Living with the shores of Oregon and Washington: Durham and London, Duke University Press, 195 p.

Komar, P.D., 1998, Beach processes and sedimentation (2nd ed.): Englewood Cliffs, New Jersey, Prentice Hall, Inc., 544 p.

Komar, P.D., McDougal, W.G., Marra, J.J., and Ruggiero, P., 1999, The rational analysis of setback distances: Applications to the Oregon coast: Shore & Beach, v. 67, p. 41-49.

Komar, P.D., McManus, J., and Styllas, M., 2004, Sediment Accumulation in Tillamook Bay, Oregon: Natural Processes versus Human Impacts: Journal of Geology, v. 112, p. 455-469.

Komar, P.D., Allan, J.C., and Ruggiero, P., 2011, Sea level variations along the U.S. Pacific Northwest Coast: Tectonic and climate controls: Journal of Coastal Research, v. 27, no. 5, p. 808-823.

Leach, D.S., 1989, Seaside beach management plan (revised 1990 by Husing, O., and Ternik, W.): Newport, Oreg., report, 45 p.

Legaard, K.R., and Thomas, A.C., 2006, Spatial patterns in seasonal and interannual variability of chlorophyll and sea surface temperature in the California Current: Journal of Geophysical Research, v. 111, no. C06032.

Lockett, J.B., 1963, Phenomena affecting improvement of the lower Columbia estuary and entrance, *in* Federal Interagency Sedimentation Conference, Jackson, Mississippi, U.S. Department of Agriculture, p. 626-668.

Moore, L.J., 2000, Shoreline mapping techniques: Journal of coastal research, v. 16, no. 1, p. 111-124.

Mori, N., Takahashi, T., Yasuda, T., and Yanagisawa, H., 2011, Survey of 2011 Tohoku Earthquake Tsunami Inundation and Run-up: Geophysical Research Letters, v. 38, no. L00G14, p. 6.

Morton, R.A., Leach, M.P., Paine, J.G., and Cardoza, M.A., 1993, Monitoring beach changes using GPS surveying techniques: Journal of Coastal Research, v. 9, no. 3, p. 702-720.

Northwest Hydraulic Consultants, Inc. (NHC), 2005, Final draft guidelines for coastal flood hazard analysis and mapping for the Pacific Coast of the United States, report prepared for FEMA: West Sacramento, Calif., Northwest Hydraulic Consultants, Inc., 344 p.

Oceanweather Inc., 2010, Global Reanalysis of Ocean Waves Fine Northeast Pacific Hindcast (GROW-FINE NEPAC): Oceanweather Inc., 39 p.

Ozkan-Haller, H.T., Allan, J.C., Barth, J.A., Haller, M.C., Holman, R.A., and Ruggiero, P., 2009, Baseline observations and modeling for the Reedsport wave energy site: Oregon State University and the Oregon Department of Geology and Mineral Industries on behalf of Oregon Wave Energy Trust, 35 p.

Peterson, C., Scheidegger, K., Komar, P.D., and Niem, W., 1984, Sediment composition and hydrography in six high-gradient estuaries of the northwestern United States: Journal of Sedimentary Petrology, v. 54, no. 1, p. 86-97.

Peterson, C.D., Darienzo, M.E., Hamilton, D., Pettit, D.J., Yeager, R.K., Jackson, P.L., Rosenfeld, C.L., and Terich, T.A., 1994, Beach-shoreline database, Pacific Northwest Region, USA: Oregon Department of Geology and Mineral Industries Open-File Report O-94-2, 29 p.

Pullen, T.A., Allsop, N.W.H., Bruce, T., Kortenhaus, A., Schuttrümpf, H., and van der Meer, J.W., 2007, EurOtop - wave overtopping of sea defences and related structures: Assessment manual, 193 p.

Ris, R.C., Booij, N., and Holthuijsen, L.H., 1999, A third-generation wave model for coastal regions, Part II: Verification: Journal of Geophysical Research, v. 104, no. C4, p. 7667-7681.

Ruggiero, P., Komar, P.D., McDougal, W.G., and Beach, R.A., 1996, Extreme water levels, wave runup and coastal erosion, *in* Proceedings of the 25th International Conference on Coastal Engineering, Sept. 2-6, 1996, Orlando, Fla., American Society of Civil Engineers, p. 2793-2805.

Ruggiero, P., and Voigt, B., 2000, Beach monitoring in the Columbia River littoral cell, 1997-2000: Coastal Monitoring & Analysis Program, Washington Department of Ecology Publication No. 00-06-026, 113 p.

Ruggiero, P., Komar, P.D., McDougal, W.G., Marra, J.J., and Beach, R.A., 2001, Wave runup, extreme water levels and the erosion of properties backing beaches: Journal of Coastal Research, v. 17, no. 2, p. 407-419.

Ruggiero, P., Holman, R.A., and Beach, R.A., 2004, Wave run-up on a high-energy dissipative beach: Journal of Geophysical Research, v. 109, p. C06025.

Ruggiero, P., Kaminsky, G.M., Gelfenbaum, G., and Voight, B., 2005, Seasonal to interannual morphodynamics along a high-energy dissipative littoral cell: Journal of Coastal Research, v. 21, no. 3, p. 553-578.

Ruggiero, P., Buijsman, M.C., Kaminsky, G.M., and Gelfenbaum, G., 2010a, Modeling the effects of wave climate and sediment supply variability on large-scale shoreline change: Marine Geology, v. 273, p. 127-140.

Ruggiero, P., Komar, P.D., and Allan, J.C., 2010b, Increasing wave heights and extreme value projections: The wave climate of the U.S. Pacific Northwest: Coastal Engineering, v. 57, no. 5, p. 539-552.

Satake, K., Shemazaki, K., Yoshinobu, T., and Ueda, K., 1996, Time and size of a giant earthquake in Cascadia inferred from Japanese tsunami records of January 1700: Nature, v. 379, no. 6562, p. 246-249.

Schlicker, H.G., Deacon, R.J., Beaulieu, J.D., and Olcott, G.W., 1972, Environmental geology of the coastal region of Tillamook and Clatsop Counties, Oregon: Oregon Department of Geology and Mineral Industries Bulletin 74, 164 p.

Sherwood, C.R., Jay, D.A., Harvey, R.B., Hamilton, P., and Simenstad, C.A., 1990, Historical changes in the Columbia River Estuary: Progress in Oceanography, v. 25, p. 299-352.

Smith, J.M., Sherlock, A.R., and Resio, D.T., 2001, STWAVE: Steady-state spectral wave model user's manual for STWAVE, Version 3.0: U.S. Army Engineer Research and Development Center, Coastal and Hydraulics Laboratory Technical Report ERDC/CHL SR-01-1, 81 p.

Soler, T., Weston, N.D., and Foote, R.H., 2011, The "Online Positioning User Service" suite (OPUS-S, OPUS-RS, OPUS-DB), *in* Soler, T., ed., CORS and OPUS for Engineers: Tools for Surveying and Mapping Applications Reston, Va., American Society of Civil Engineers, p. 17-26.

Stockdon, H.F., Holman, R.A., Howd, P.A., and Sallenger, A.H., 2006, Empirical parameterization of setup, swash, and runup: Coastal Engineering, v. 53, no. 7, p. 573-588.

Thieler, E.R., Himmelstoss, E.A., Zichichi, J.L., and Ayhan, E., 2009, Digital Shoreline Analysis System (DSAS) version 4.0—An ArcGIS extension for calculating shoreline change: U.S. Geological Survey Open-File Report 2008-1278.

Tillotson, K., and Komar, P.D., 1997, The wave climate of the Pacific Northwest (Oregon and Washington): A comparison of data sources: Journal of Coastal Research, v. 13, no. 2, p. 440-452.

Trimble, 2005, Trimble 5700 GPS system datasheet: Dayton, Ohio, Trimble Navigation Limited, Engineering & Construction Group, p. 2.

van der Meer, J.W., 2002, Technical report wave run-up and wave overtopping at dikes: Deflt, Netherlands, Technical Advisory Committee on Flood Defence, Road and Hydraulic Engineering Institute, 50 p.

Witter, R.C., Kelsey, H.M., and Hemphill-Haley, E., 2003, Great Cascadia earthquakes and tsunamis of the past 6700 years, Coquille River estuary, southern coastal Oregon: Geological Society of America Bulletin, v. 115, p. 1289-1306.

Witter, R.C., Horning, T., and Allan, J.C., 2009, Coastal erosion hazard zones in southern Clatsop County, Oregon: Seaside to Cape Falcon: Oregon Department of Geology and Mineral Industries Open-File Rport O-09-06, 39 p. [Open-File Report].

Witter, R.C., Zhang, Y.J., Goldfinger, C., Priest, G.R., and Wang, K., 2010, Validating numerical tsunami simulations in southern Oregon using late Holocene records of great Cascadia earthquakes and tsunamis [abs.]: Seismological Research Letters, v. 81, no. 2, p. 290.

Woxell, L.K., 1998, Prehistoric beach accretion rates and long-term response to sediment depletion in the Columbia River littoral system, USA: Portland, OR, Portland State University, M.S., 206 p.

Yamamoto, M., 2011, Tōhoku Tsunami March 11, 2011 as of 30 March 2011: United Nations Educational, Scientific and Cultural Organization, Intergovernmental Oceanographic Comission IOC/UNESCO Bulletin No. 13.

Zhang, K., Douglas, B.C., and Leatherman, S., 2001, Beach erosion potential for severe nor'easters: Journal of Coastal Research, v. 17, no. 2, p. 309-321.

11.0 APPENDICES

Appendix A: Ground Survey Accuracy Assessment Protocols

Appendix B: Clatsop County Beach and Bluff Profiles

11.1 Appendix A: Ground Survey Accuracy Assessment Protocols

See report by Watershed Sciences, Inc., dated December 21, 2009.

11.2 Appendix B: Clatsop County Beach and Bluff Profiles

11.2.1 Clatsop Plains

Clatsop 1

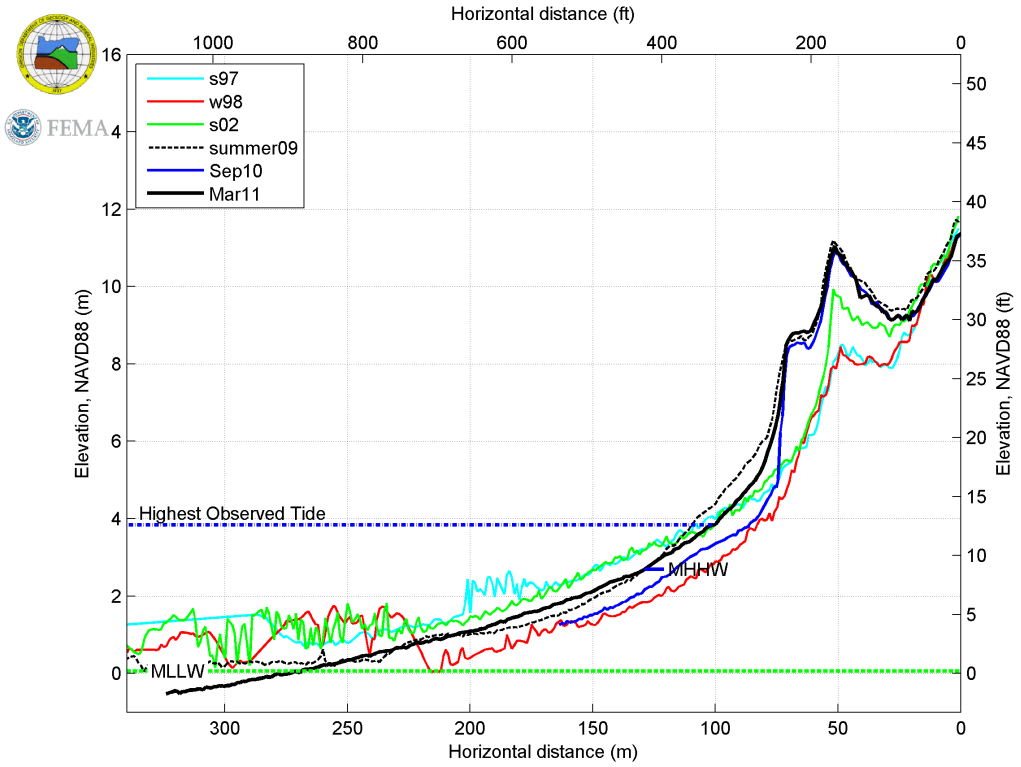

Clatsop 2

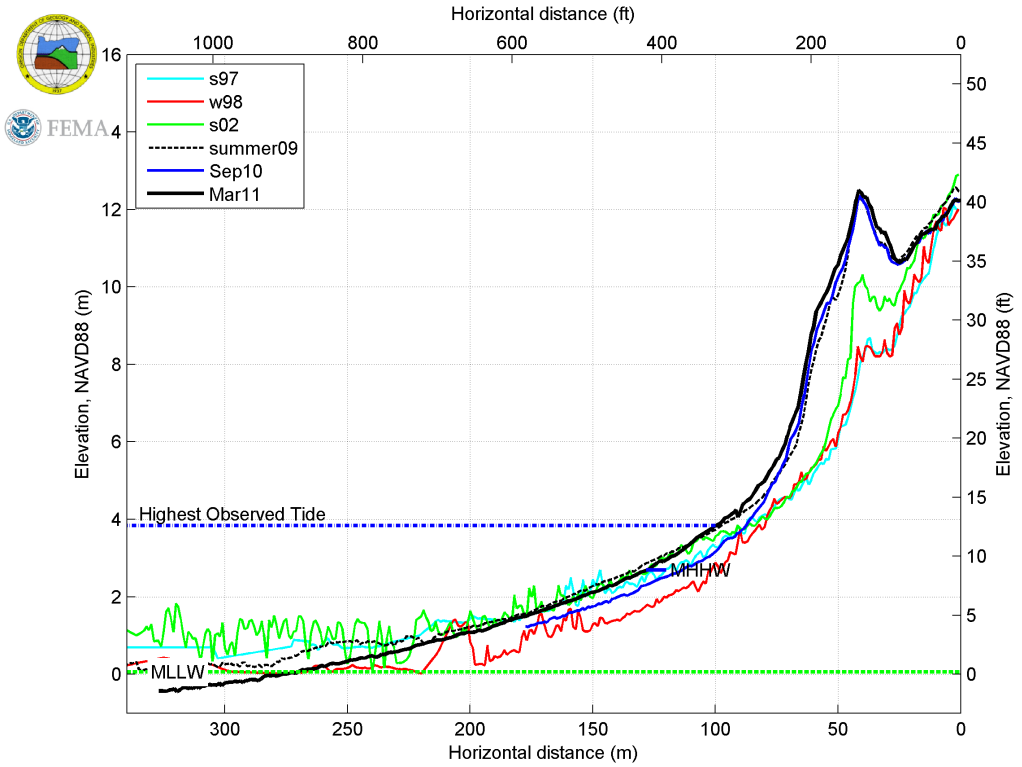

Clatsop 3

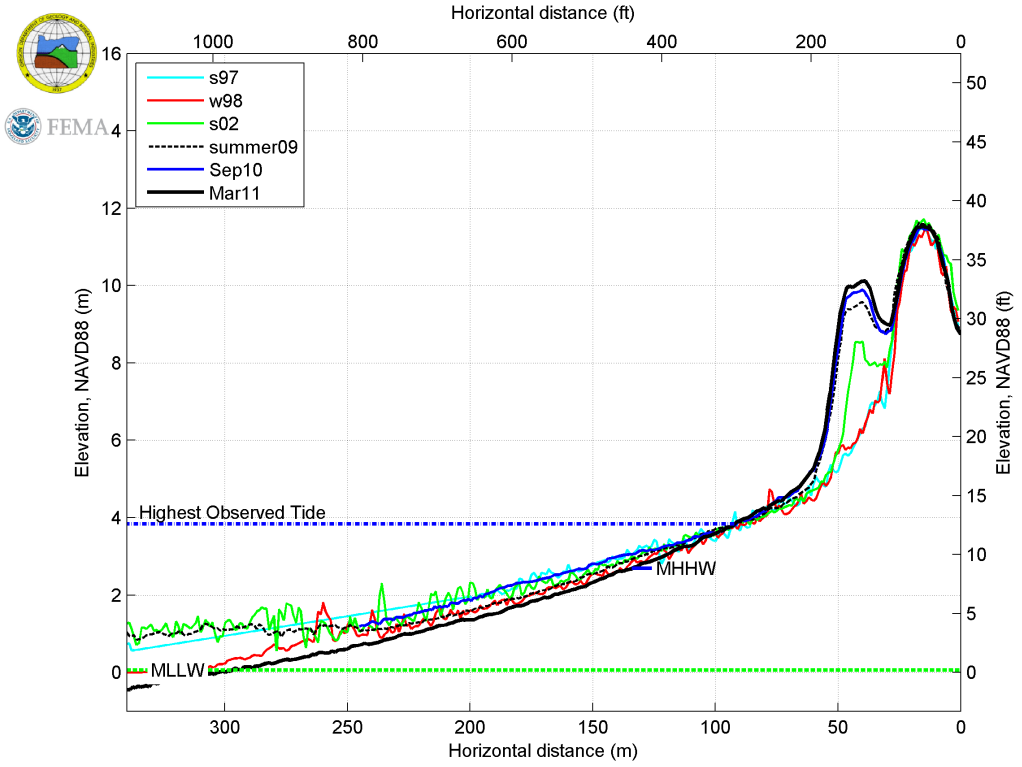

Clatsop 4

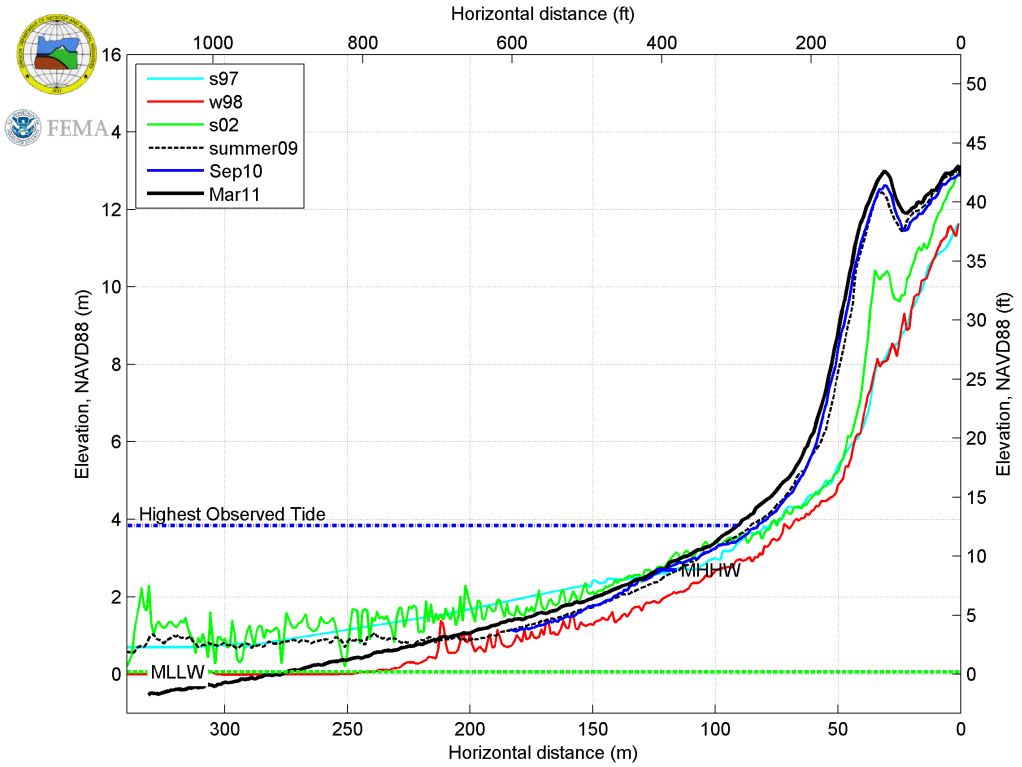

Clatsop 5

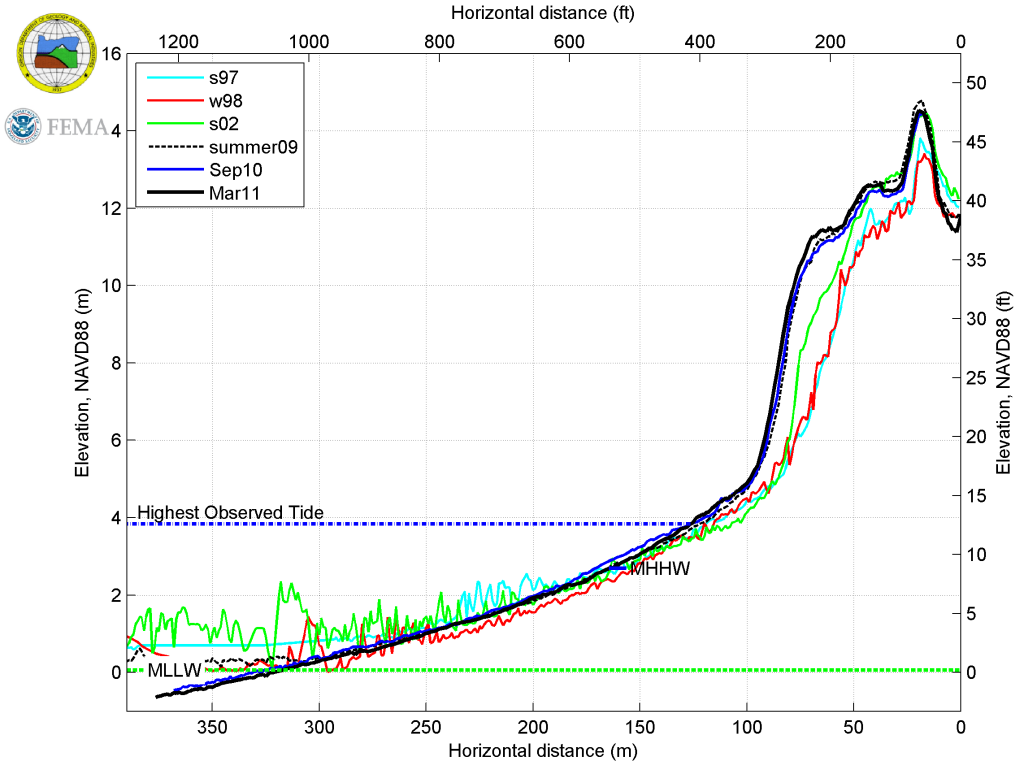

Clatsop 6

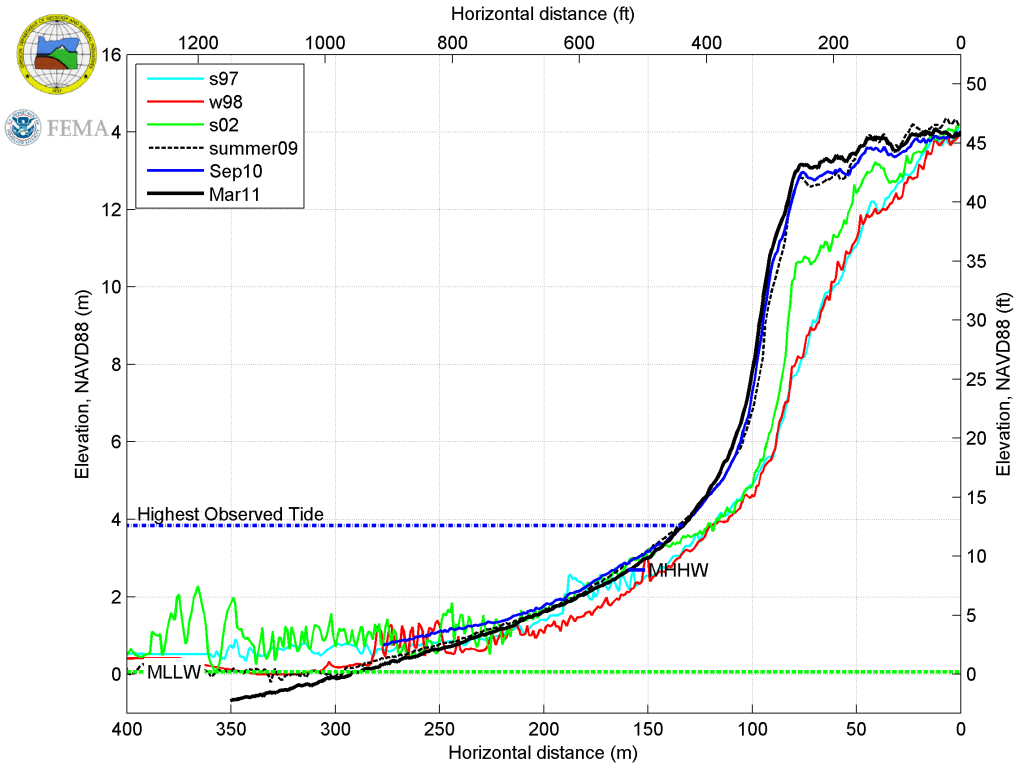

Clatsop 7

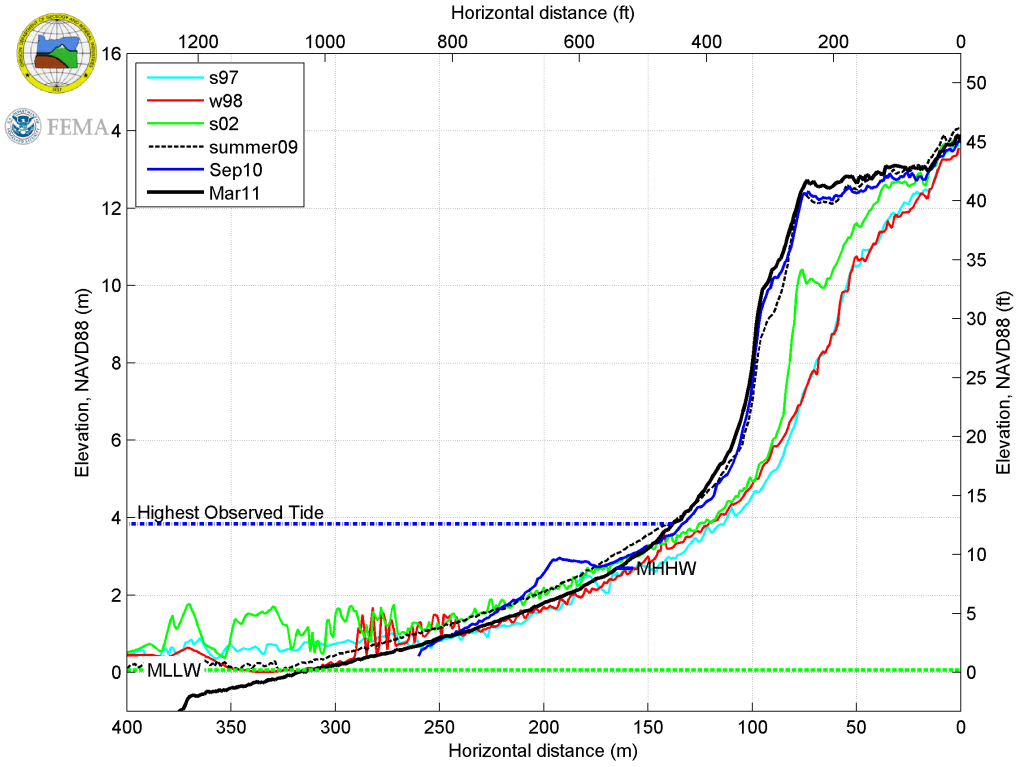

Clatsop 8

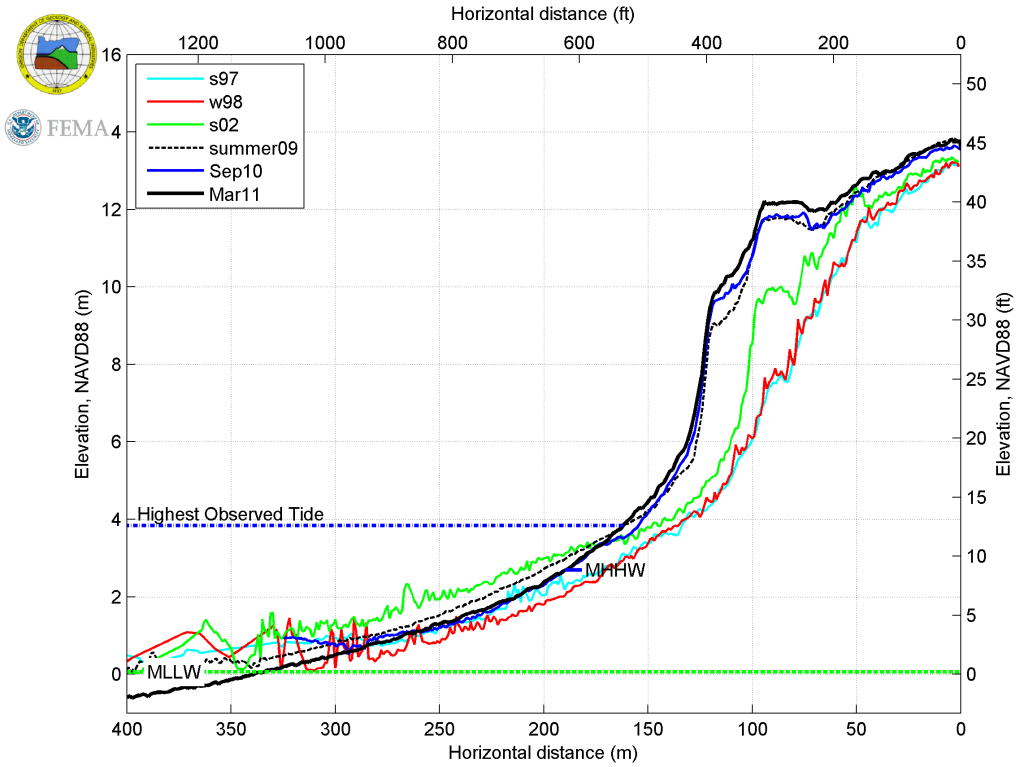

Clatsop 9

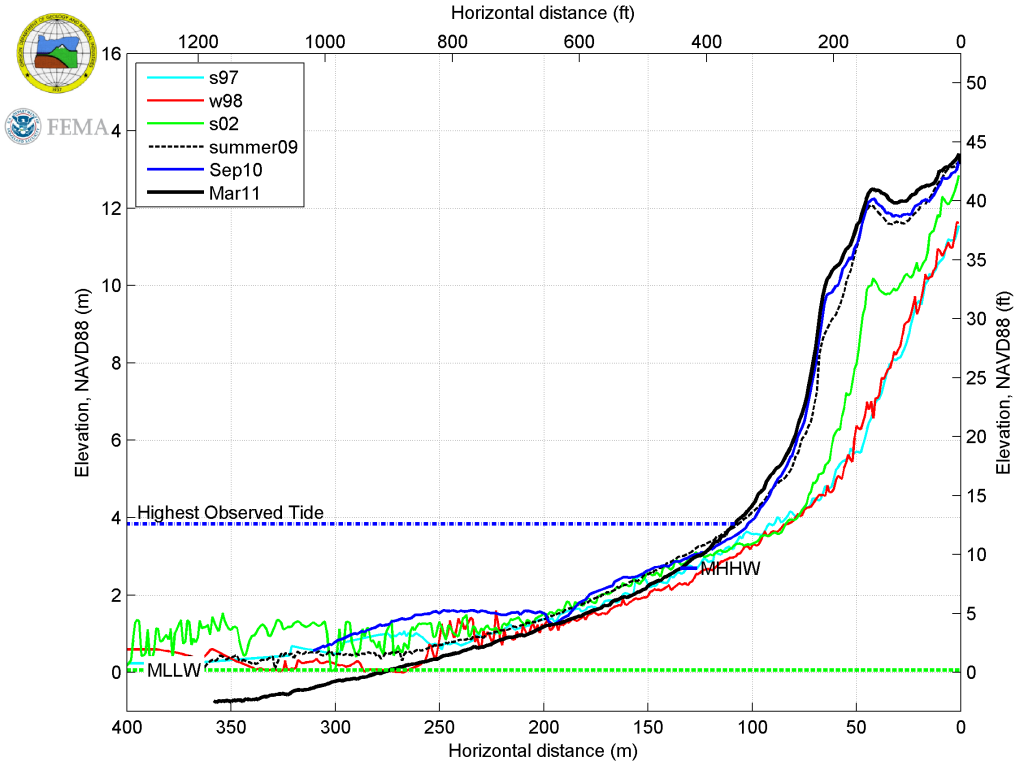

Clatsop 10

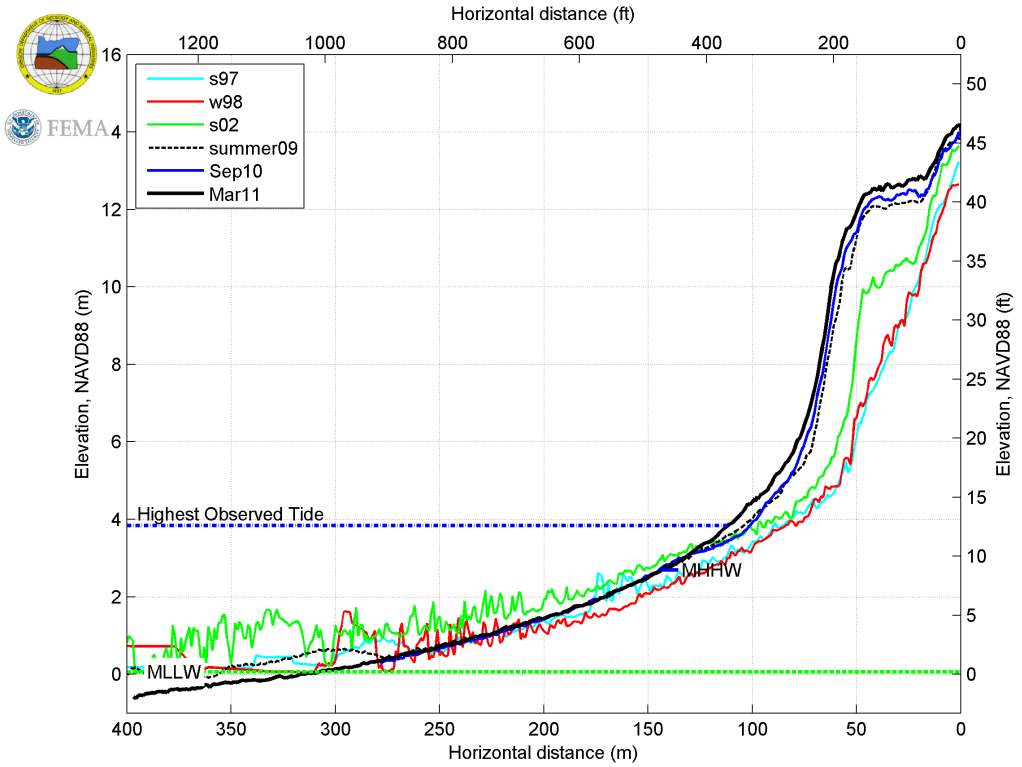

Clatsop 11

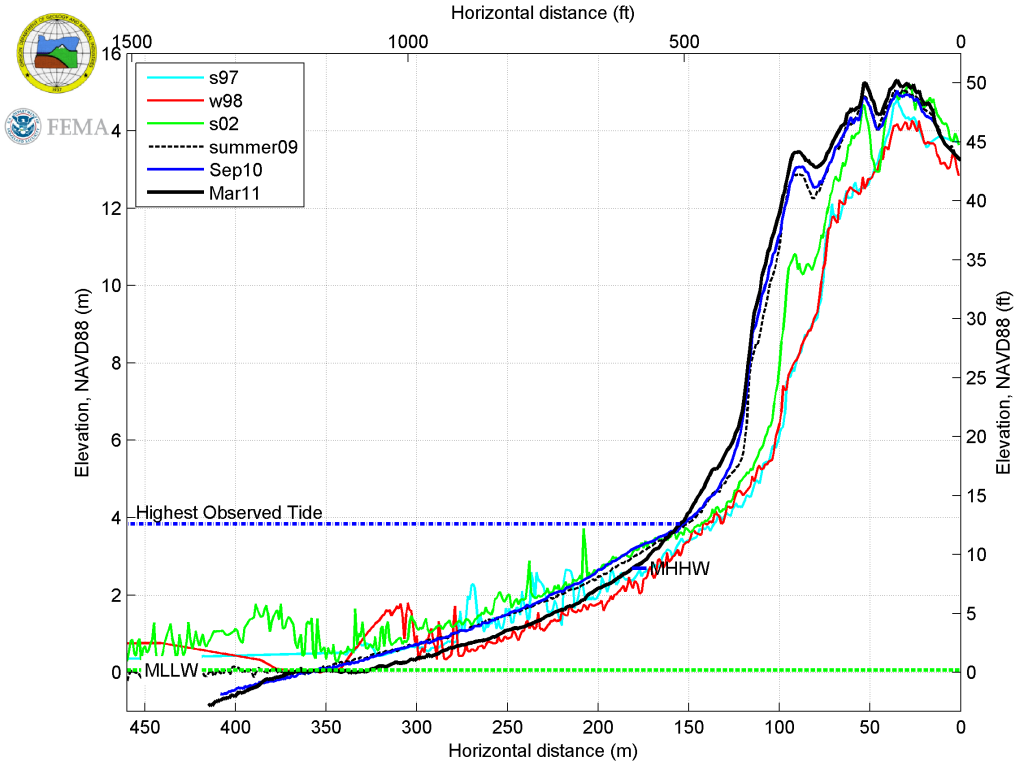

Clatsop 12

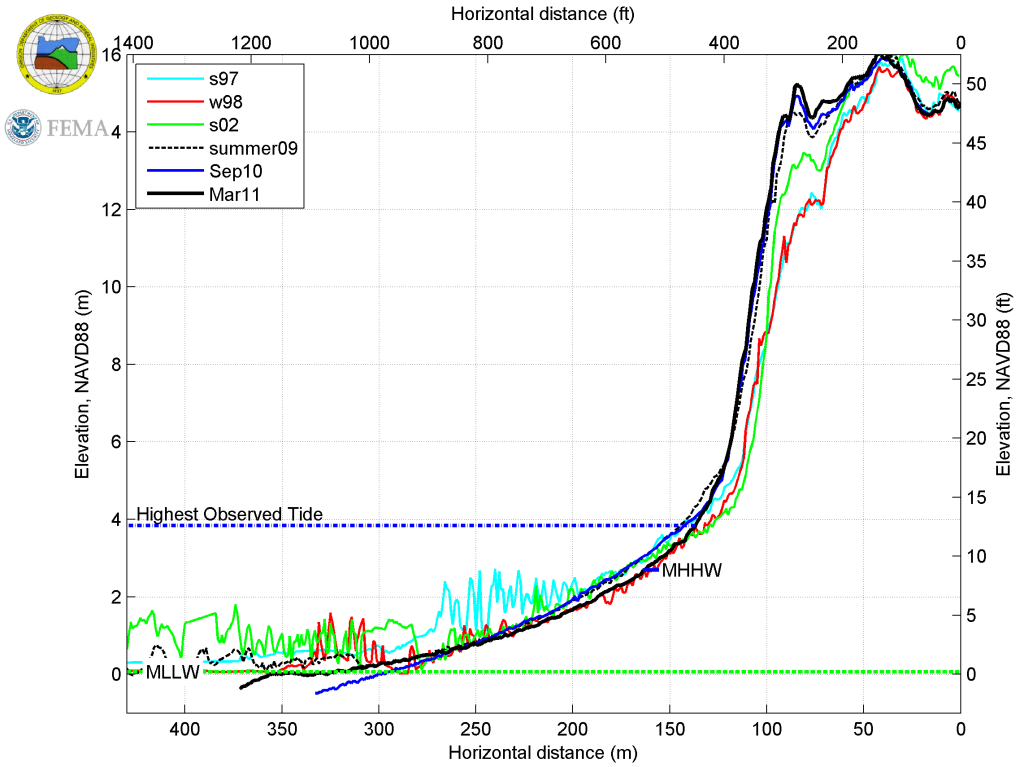

Clatsop 13

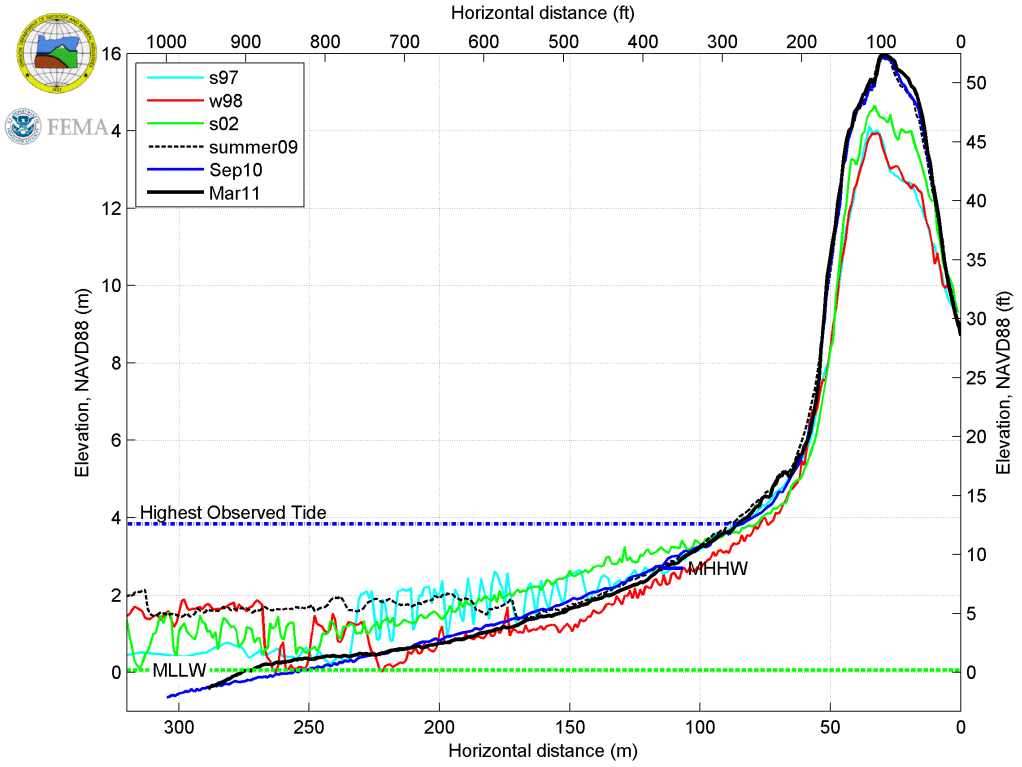

Clatsop 14

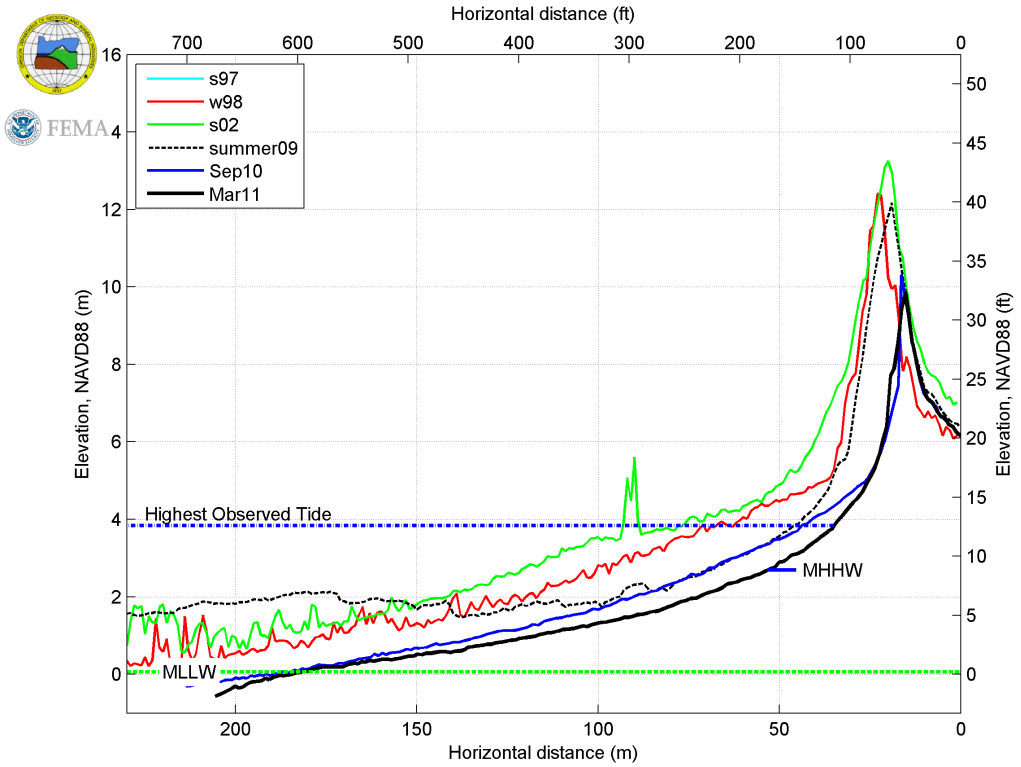
Horizontal distance (ft)
700
600
500
400
300
200
100
0
s97
w98
s02
summer09
Sep10
Mar11
Elevation, NAVD88 (m)
Elevation, NAVD88 (ft)
Highest Observed Tide
MHHW
MLLW
200
150
100
50
0
Horizontal distance (m)

11.2.2 Seaside

Seaside 1

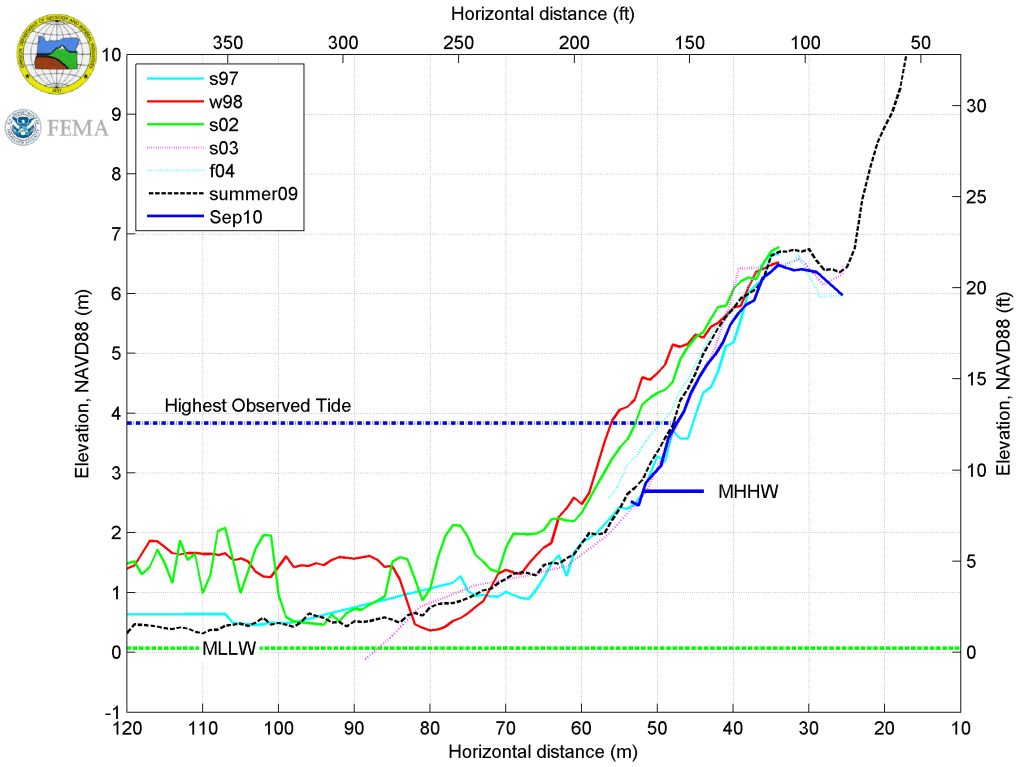

Seaside 2

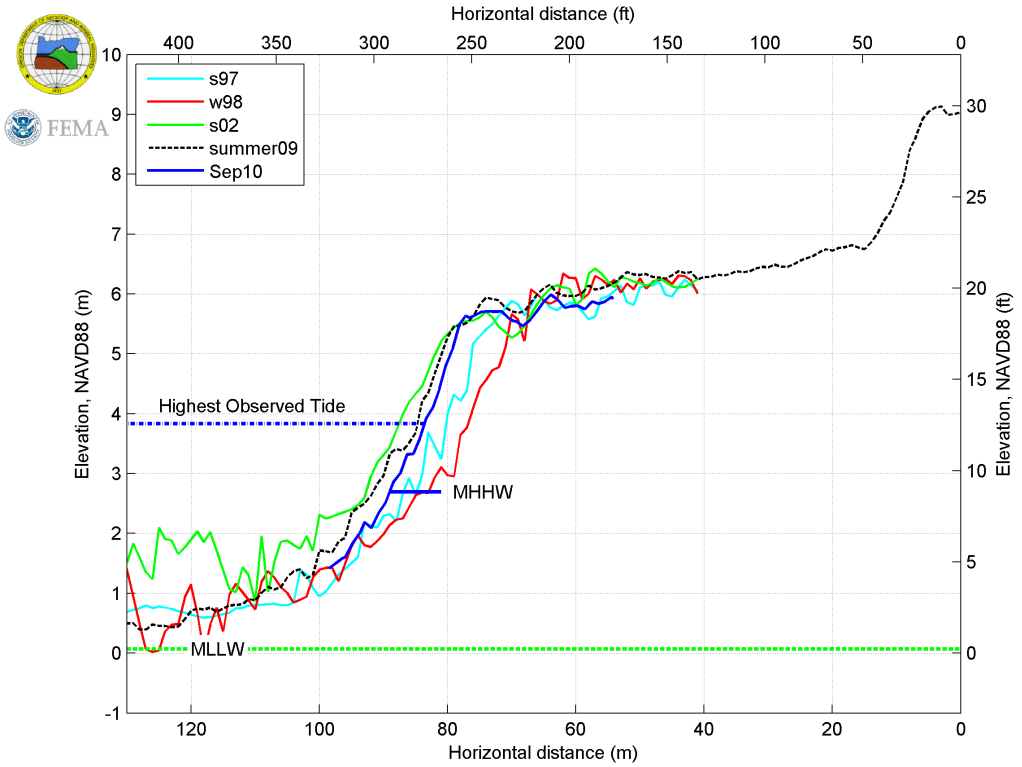

Seaside 3

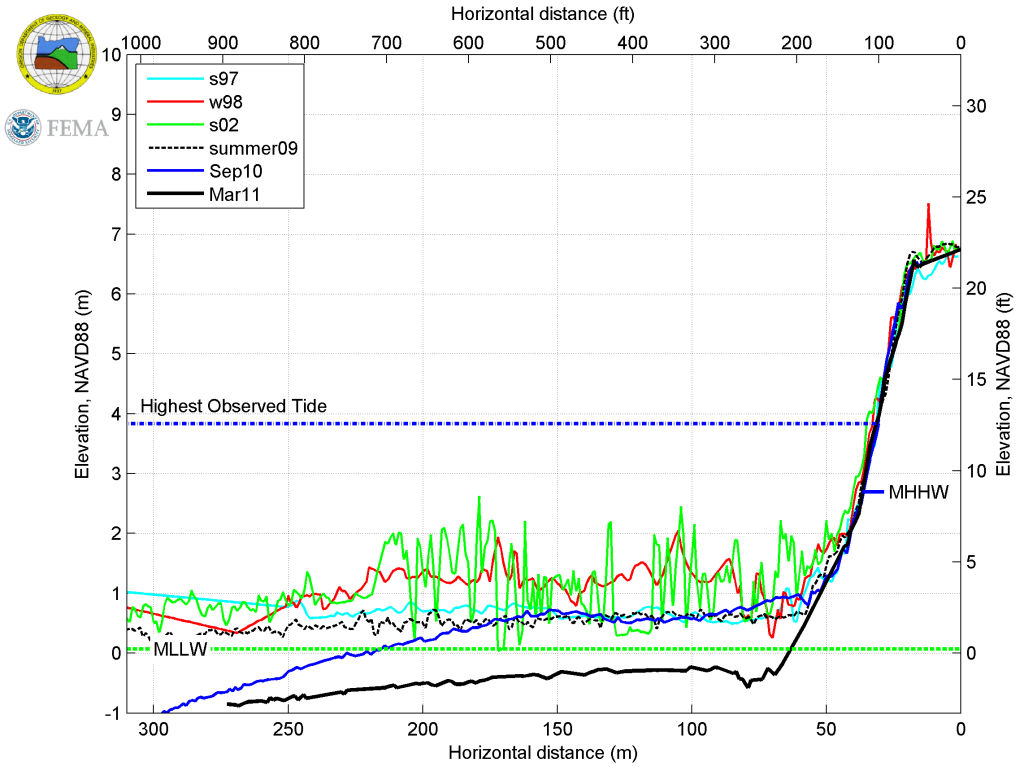

Seaside 4

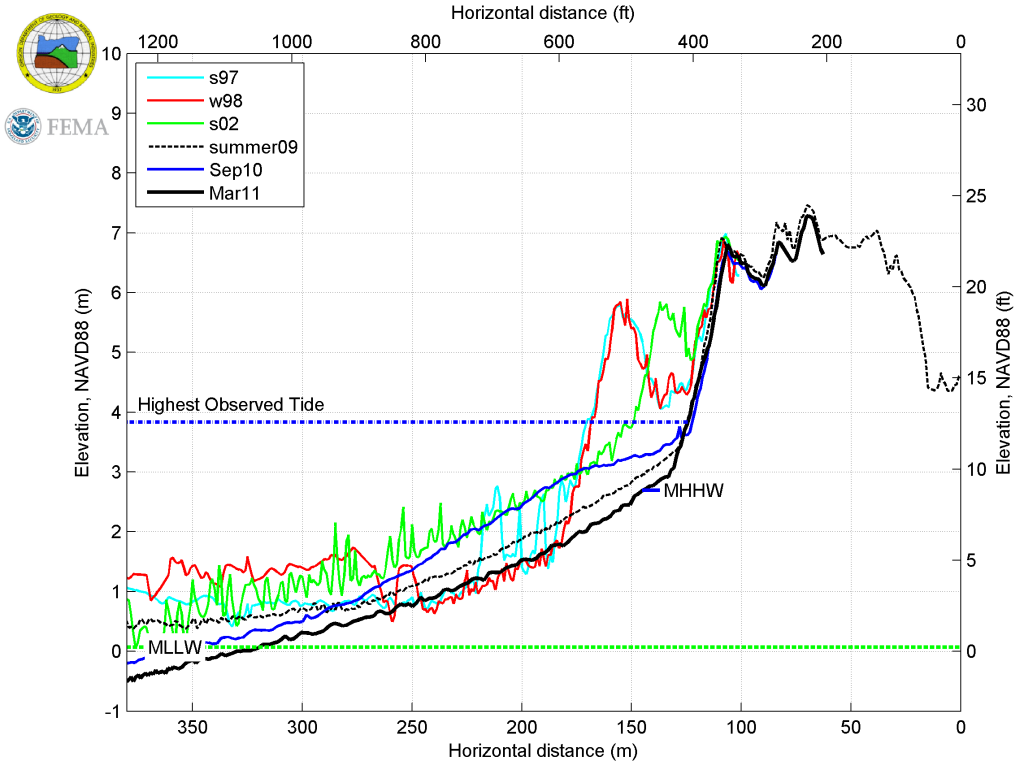

Seaside 5

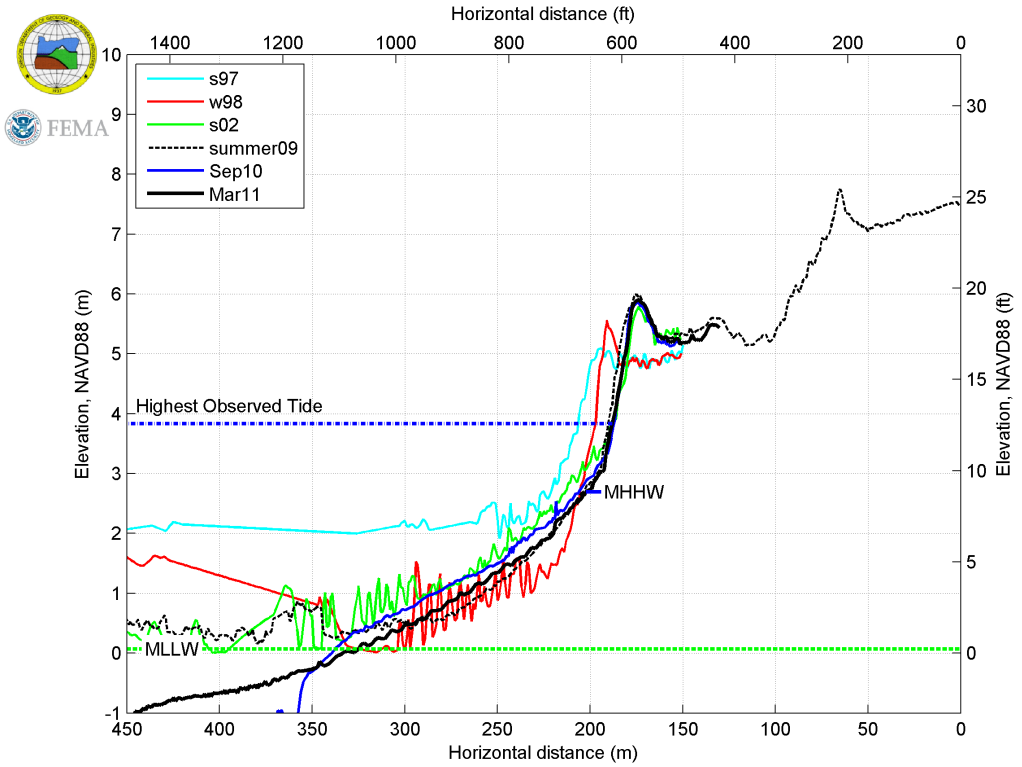

Seaside 6

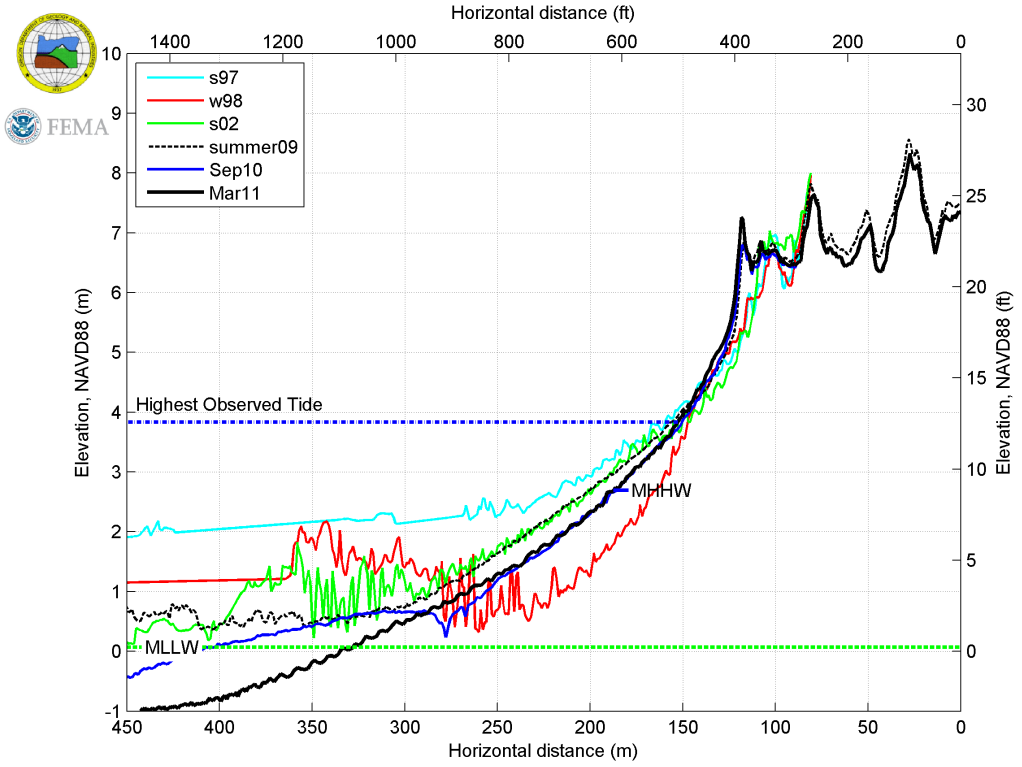

Seaside 7

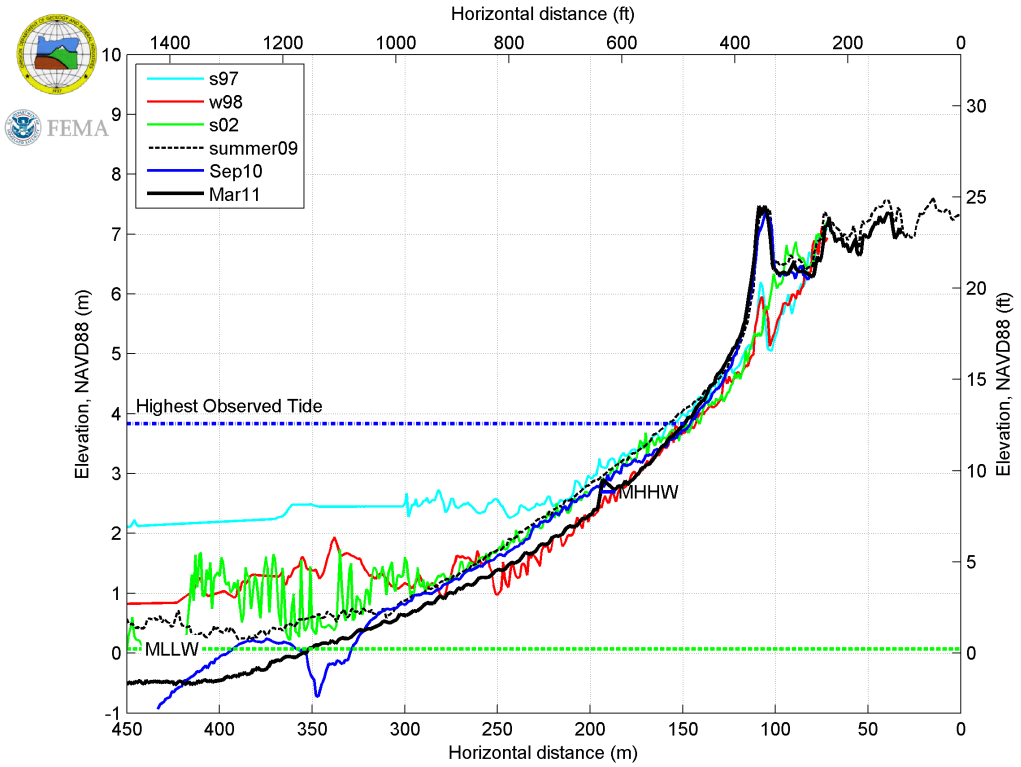

Seaside 8

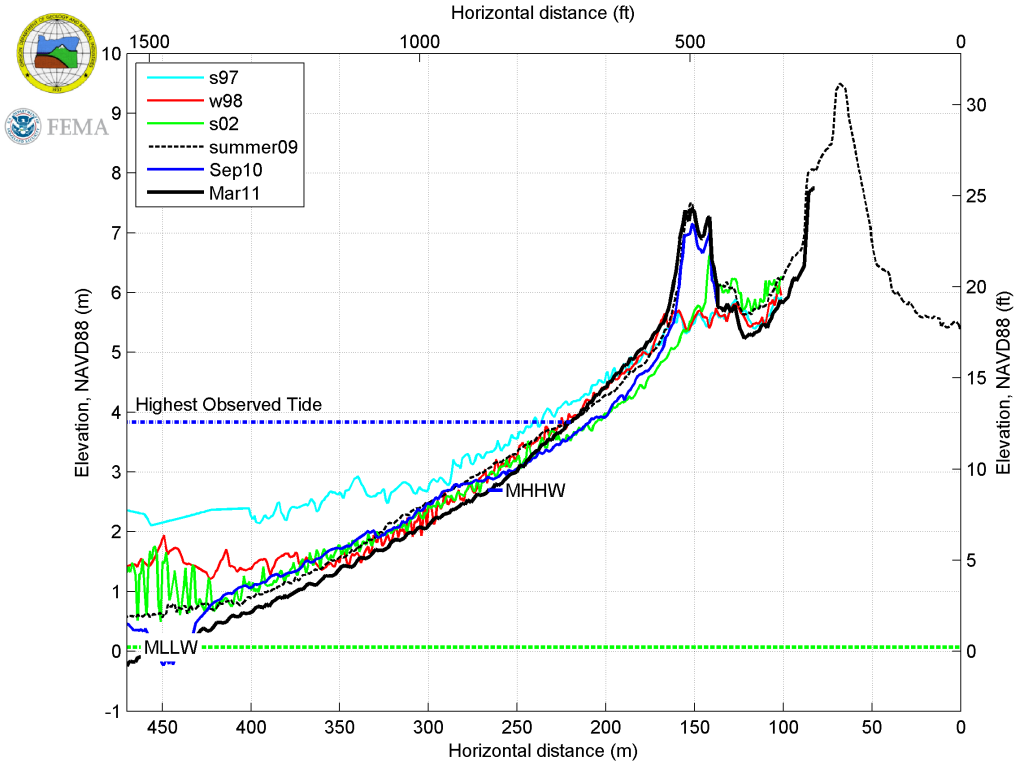

Seaside 9

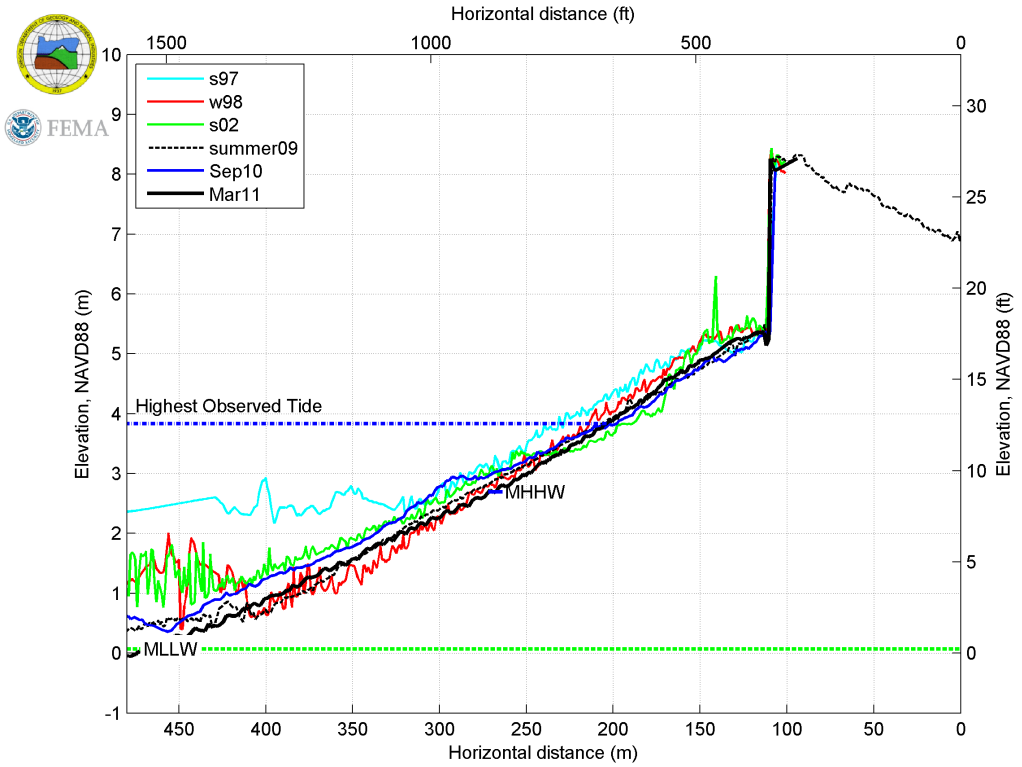

Seaside 10

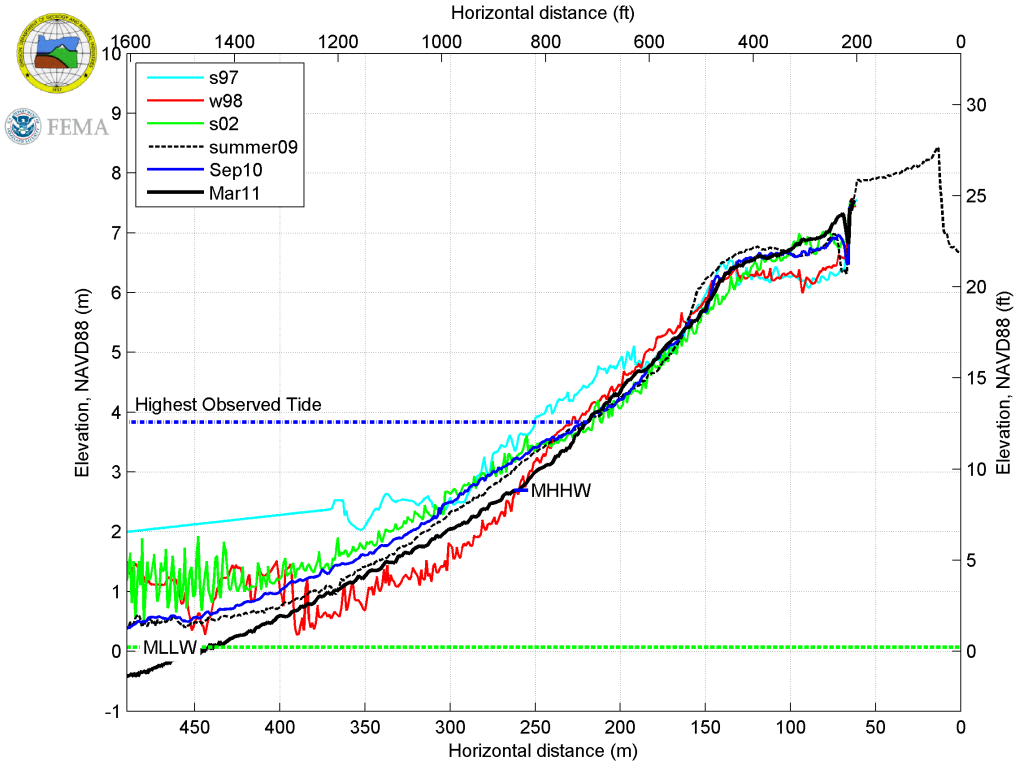

Seaside 11

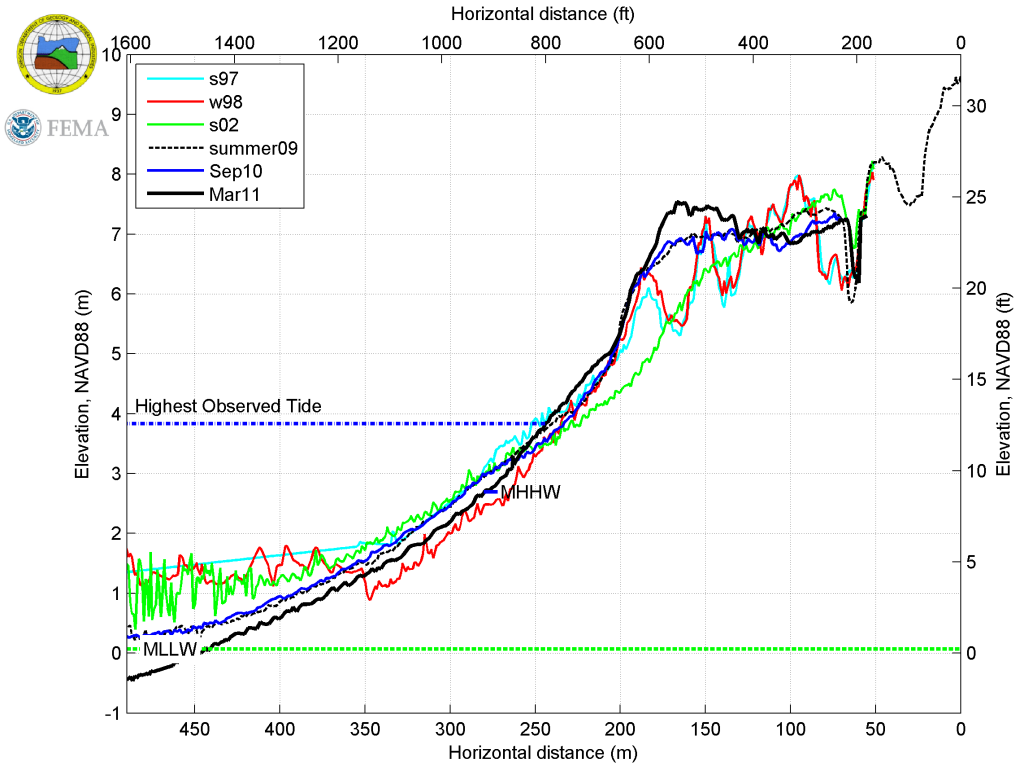

Seaside 12

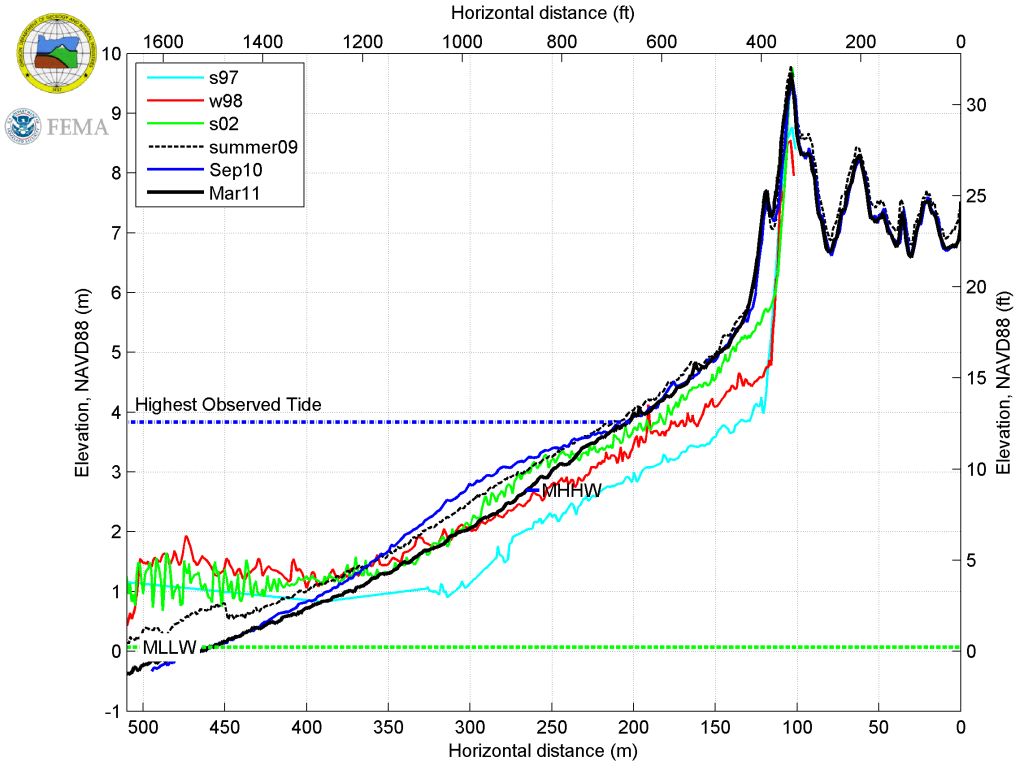

Seaside 13

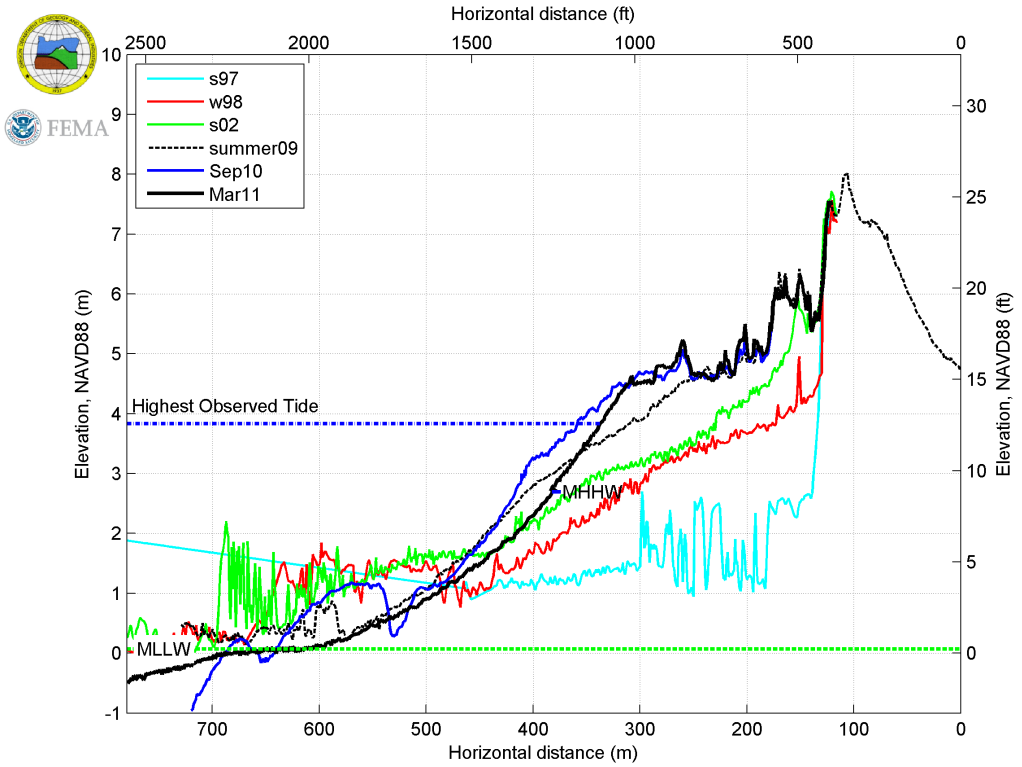

Seaside 14

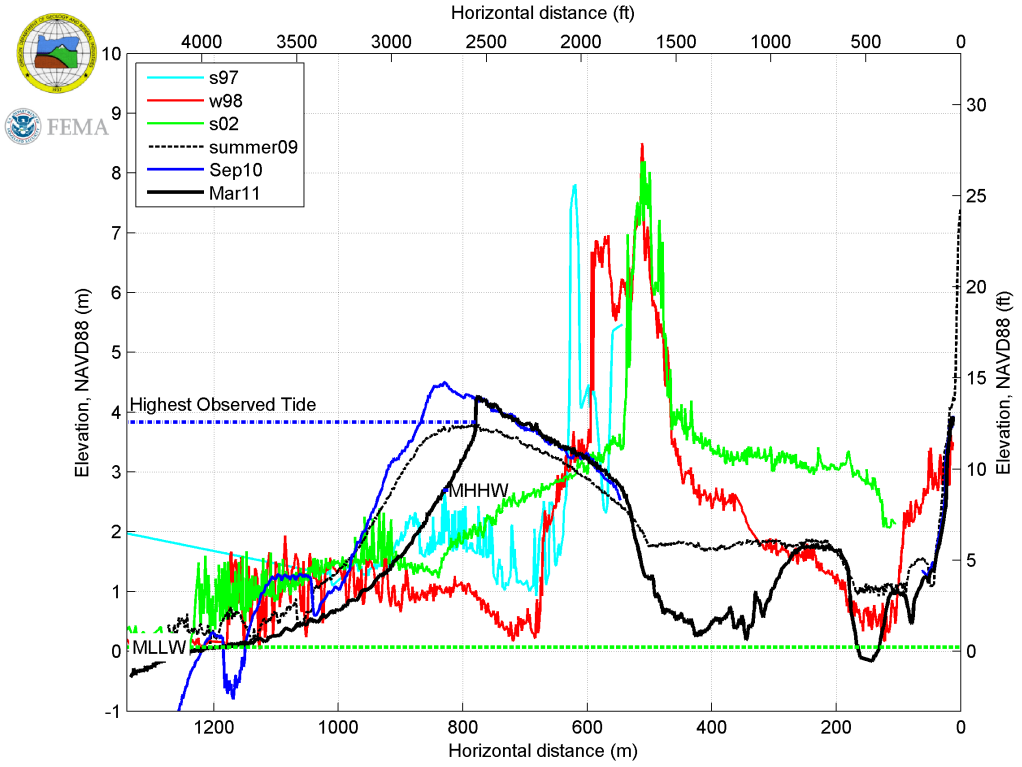

Seaside 15

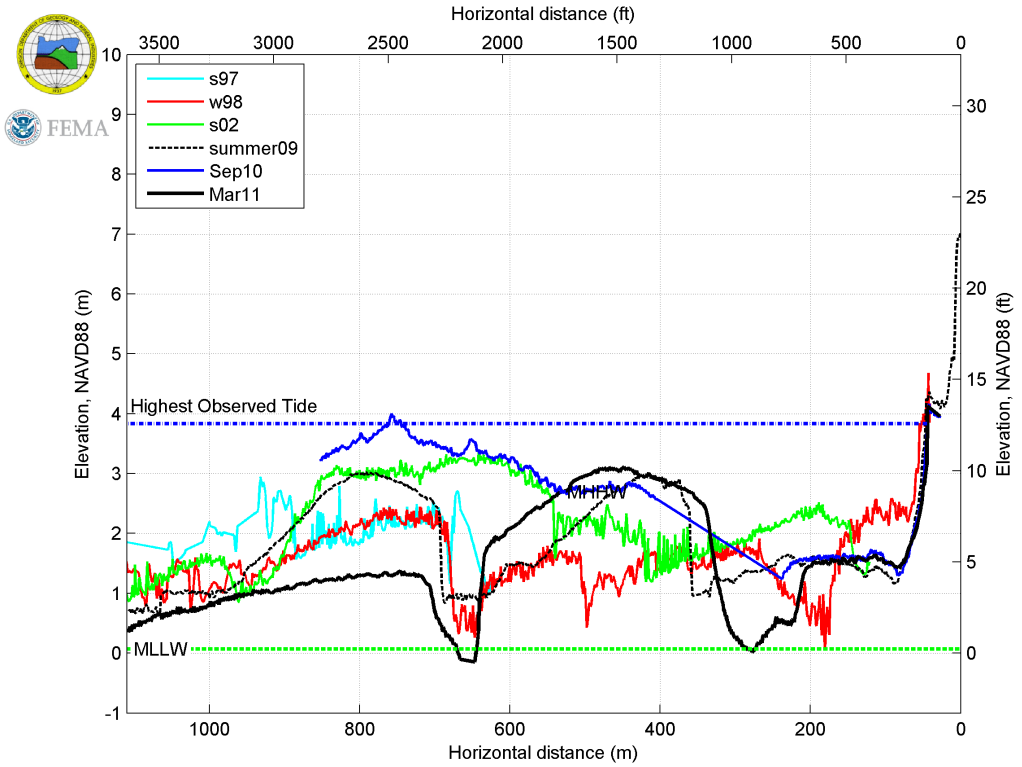

Seaside 16

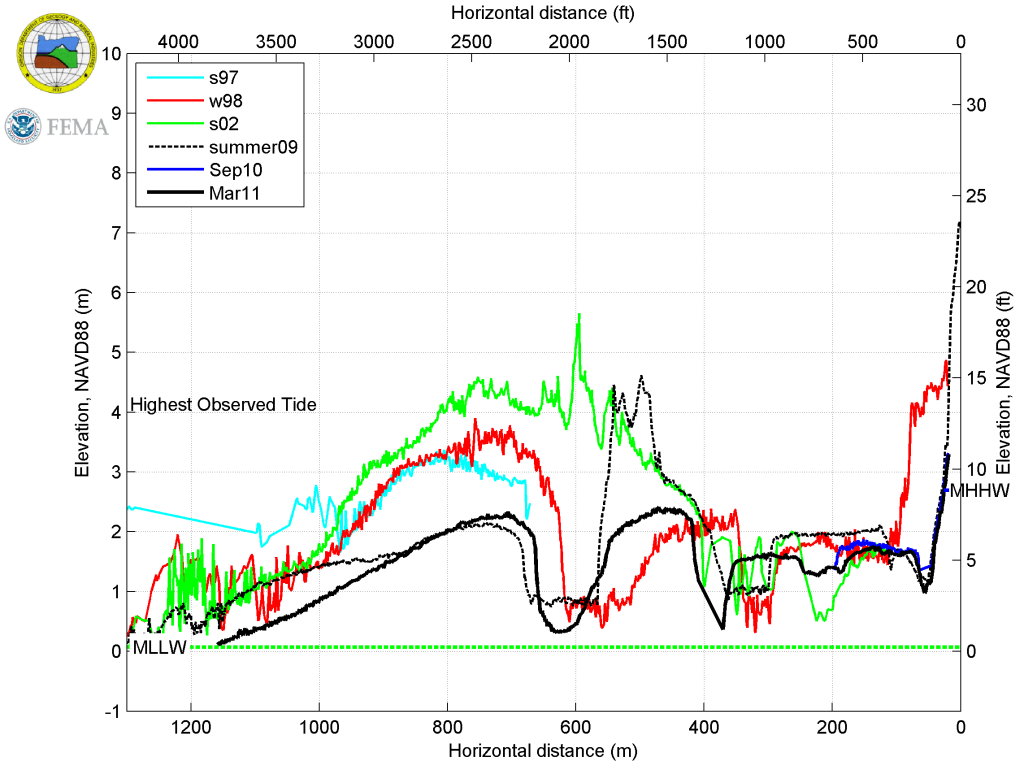

Seaside 17

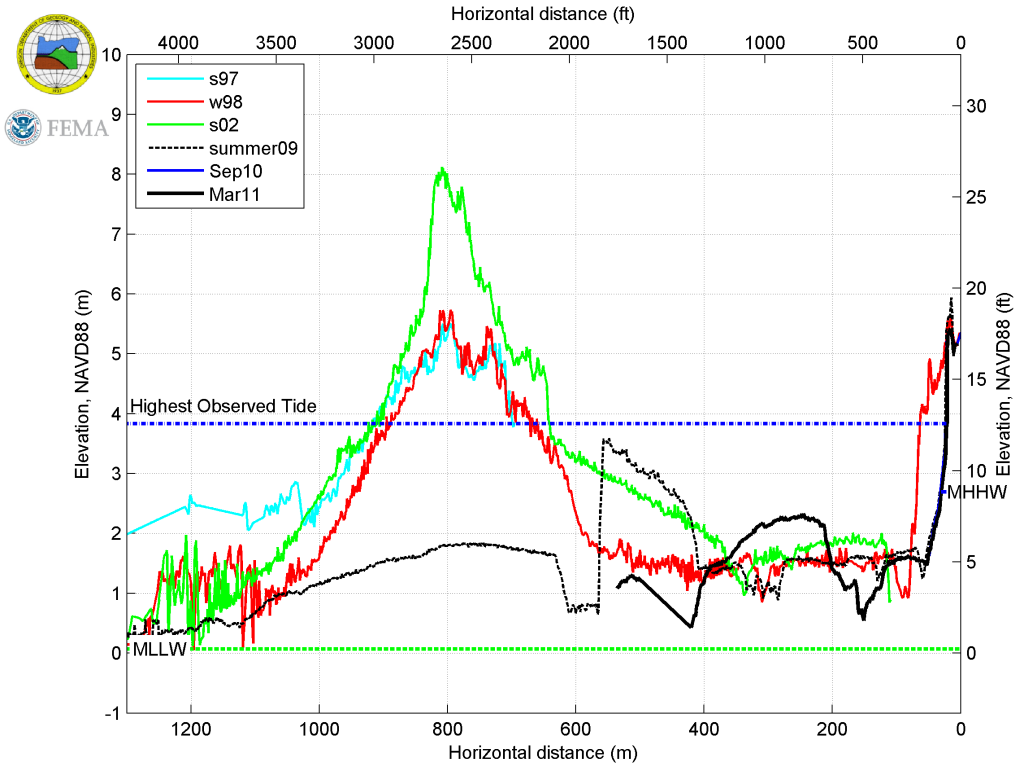
Horizontal distance (ft)
4000
3500
3000
2500
2000
1500
1000
500
0
s97
w98
s02
summer09
Sep10
Mar11
Highest Observed Tide
MLLW
MHHW
Elevation, NAVD88 (m)
Elevation, NAVD88 (ft)
10
9
8
7
6
5
4
3
2
1
0
-1
30
25
20
15
10
5
0
1200
1000
800
600
400
200
0
Horizontal distance (m)

11.2.3 Cannon Beach

CB 1

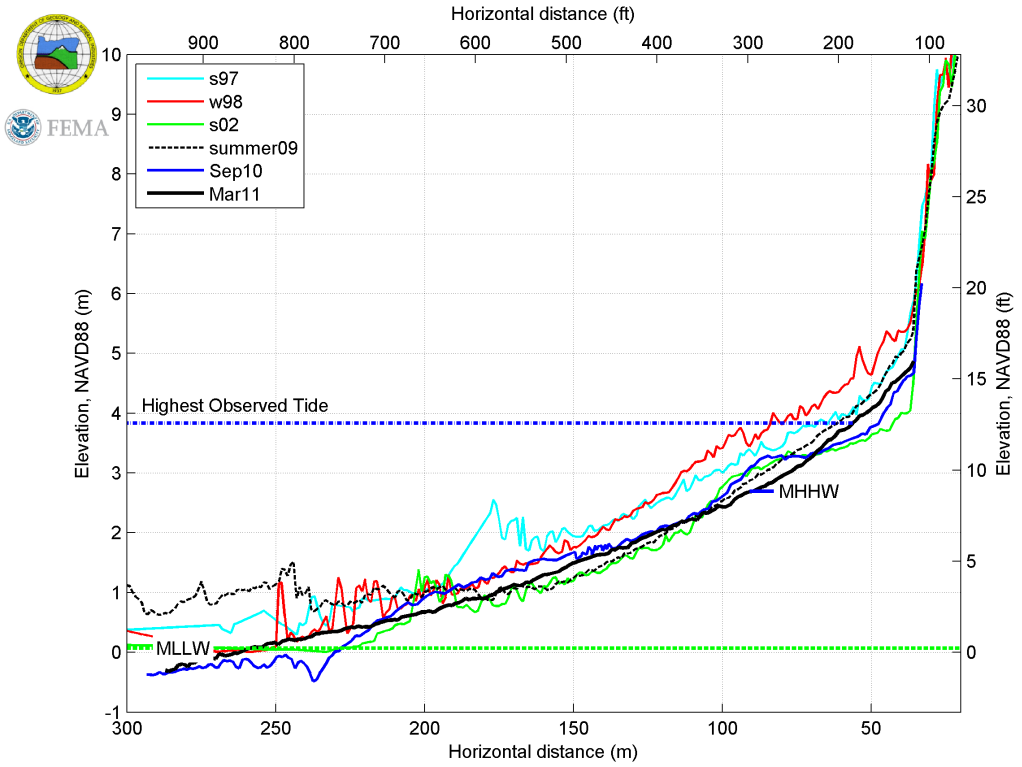

CB 2

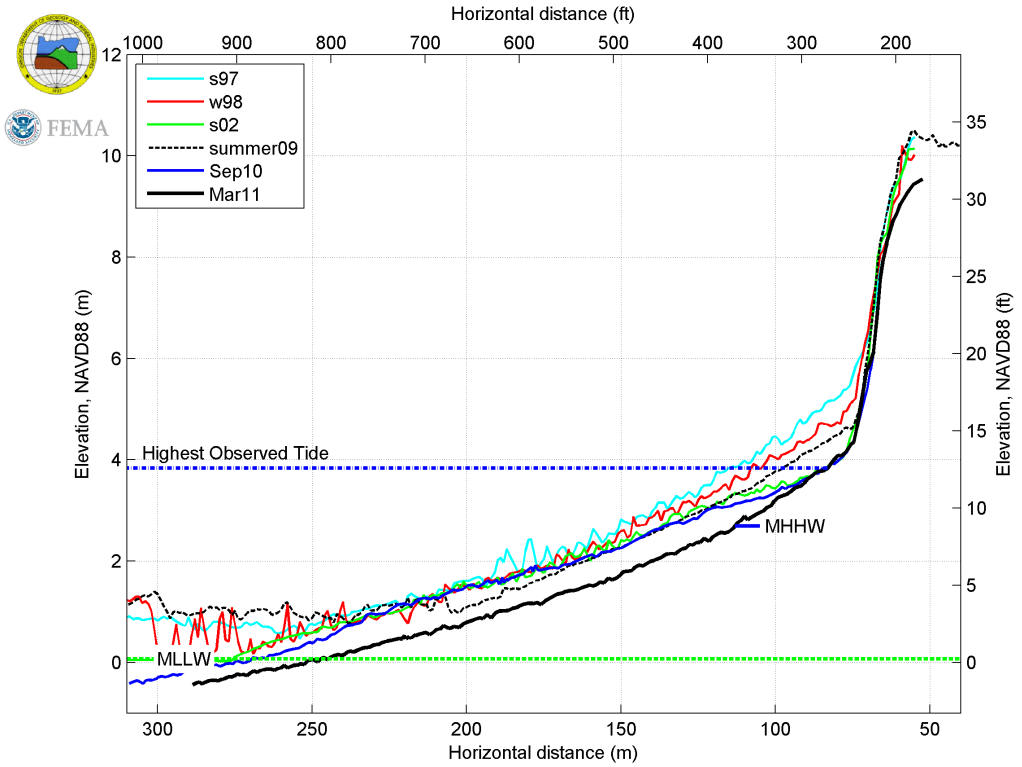

CB 3

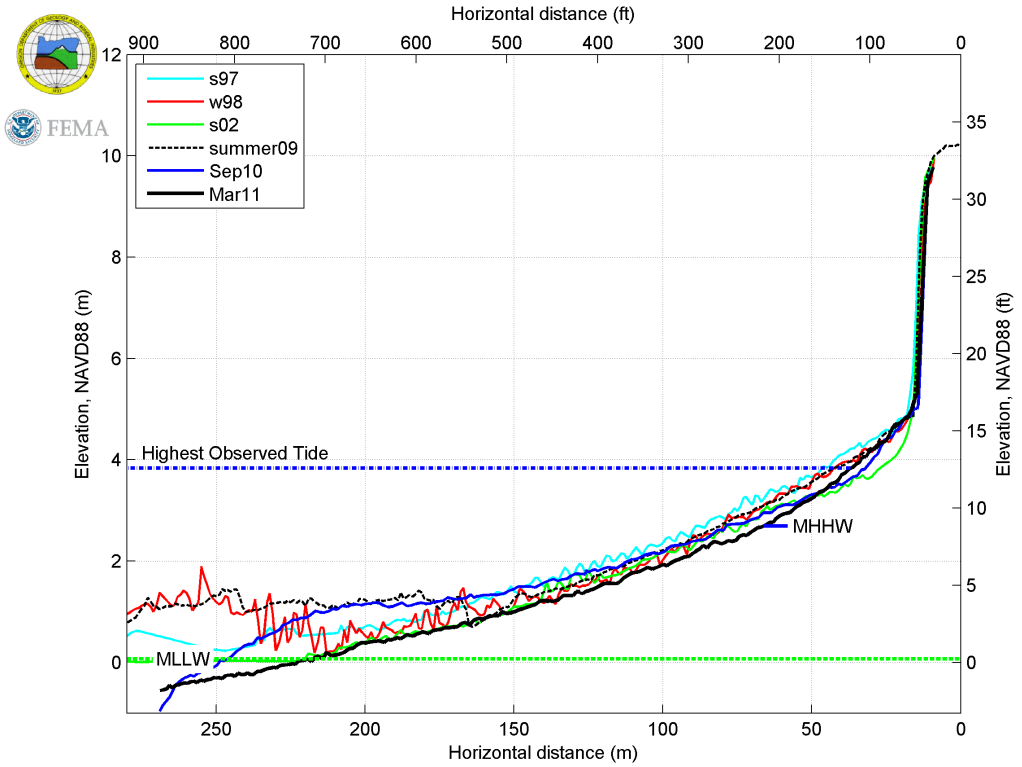
Horizontal distance (ft)
900
800
700
600
500
400
300
200
100
0
s97
w98
s02
summer09
Sep10
Mar11
Highest Observed Tide
MHHW
MLLW
Elevation, NAVD88 (m)
Elevation, NAVD88 (ft)
250
200
150
100
50
0
Horizontal distance (m)

CB 4

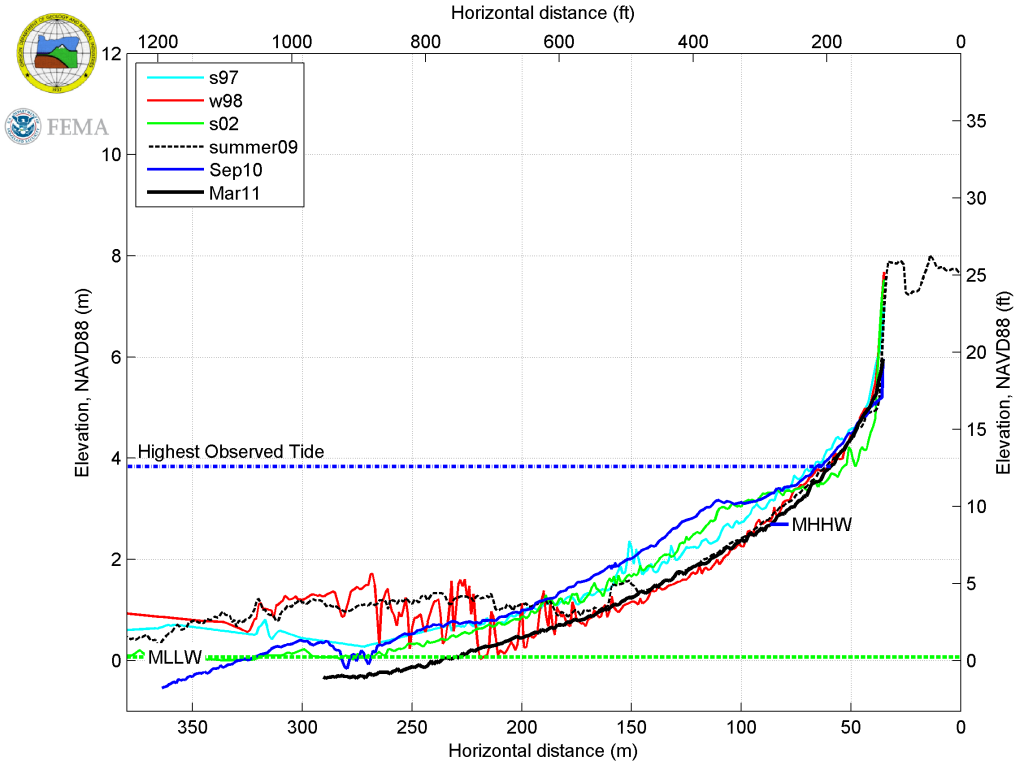
Horizontal distance (ft)
1200
1000
800
600
400
200
0
s97
w98
s02
summer09
Sep10
Mar11
Highest Observed Tide
MHHW
MLLW
Elevation, NAVD88 (m)
Elevation, NAVD88 (ft)
350
300
250
200
150
100
50
0
Horizontal distance (m)

CB 5

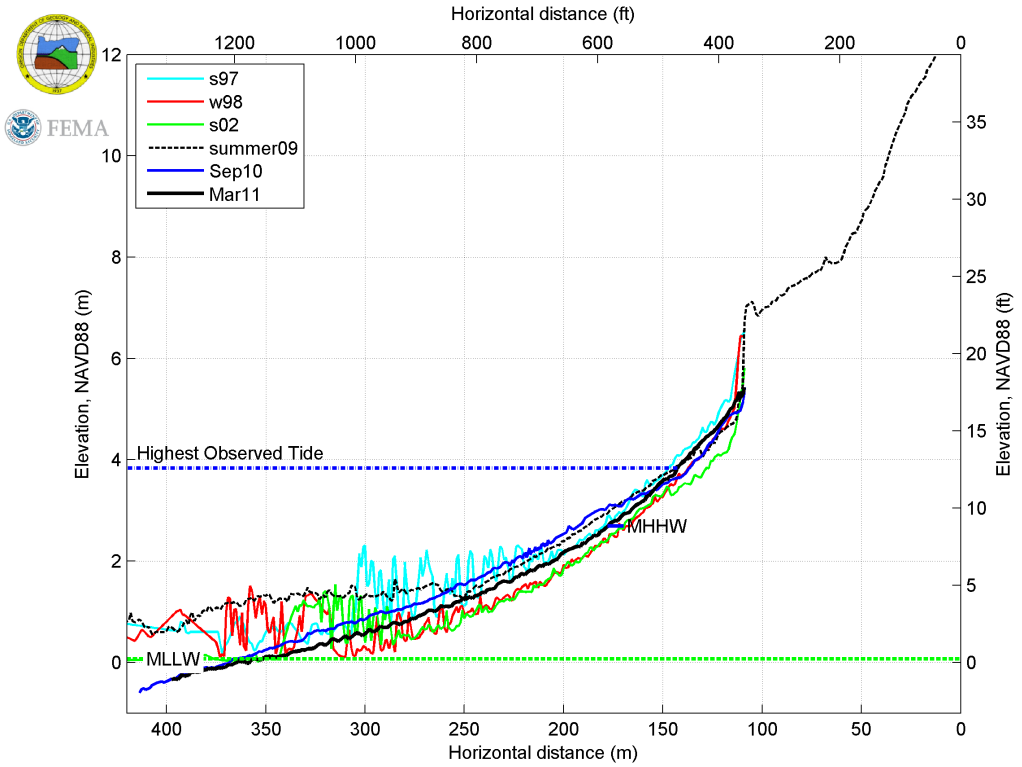
Horizontal distance (ft)
1200
1000
800
600
400
200
0
s97
w98
s02
summer09
Sep10
Mar11
Elevation, NAVD88 (m)
Elevation, NAVD88 (ft)
Highest Observed Tide
MHHW
MLLW
400
350
300
250
200
150
100
50
0
Horizontal distance (m)

CB 6

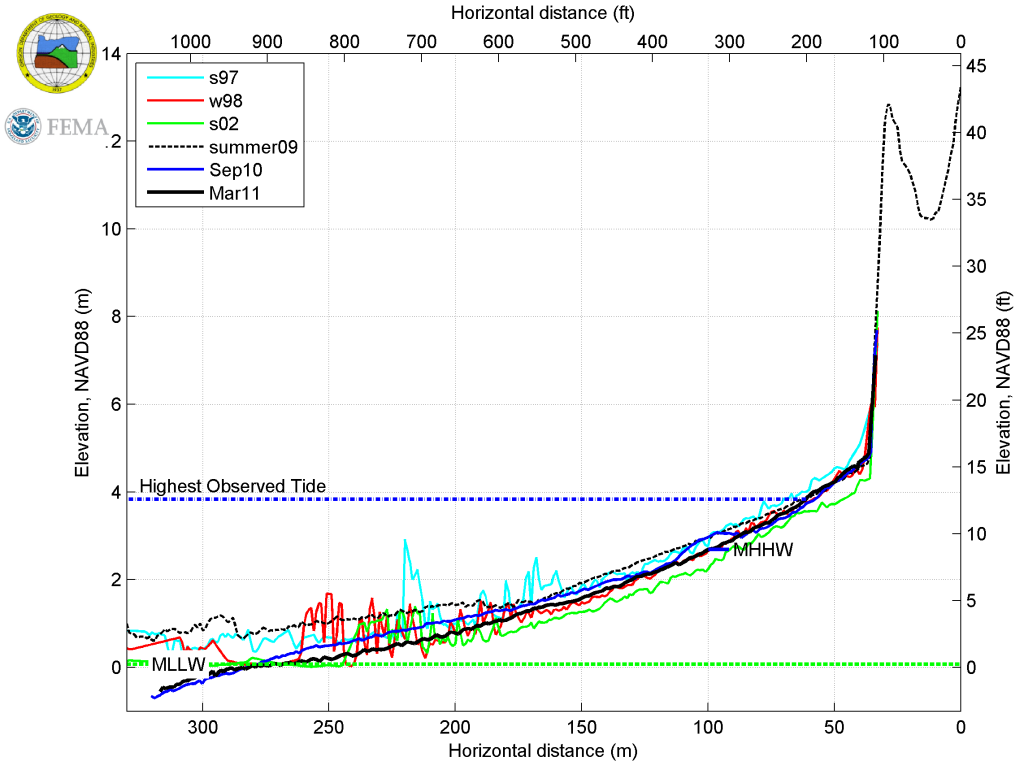
Horizontal distance (ft)
1000
900
800
700
600
500
400
300
200
100
0
s97
w98
s02
summer09
Sep10
Mar11
Elevation, NAVD88 (m)
Elevation, NAVD88 (ft)
Highest Observed Tide
MHHW
MLLW
300
250
200
150
100
50
0
Horizontal distance (m)

CB 7

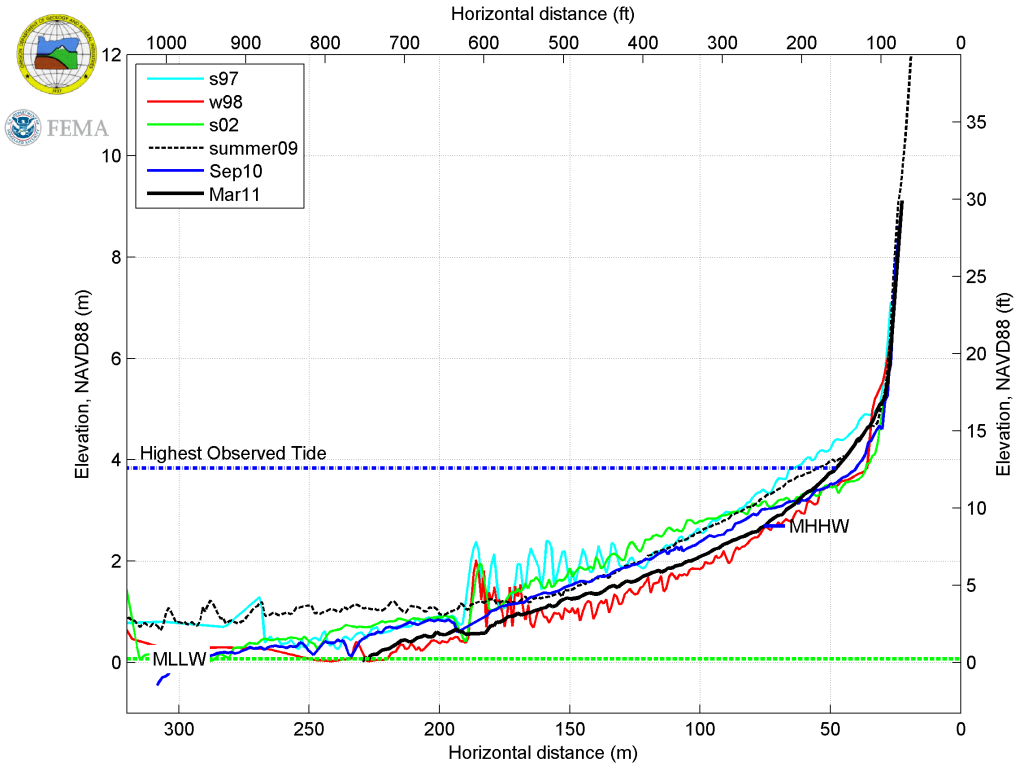
Horizontal distance (ft)
1000 900 800 700 600 500 400 300 200 100 0
s97
w98
s02
summer09
Sep10
Mar11
Highest Observed Tide
MHHW
MLLW
Elevation, NAVD88 (m)
Elevation, NAVD88 (ft)
300 250 200 150 100 50 0
Horizontal distance (m)

CB 8

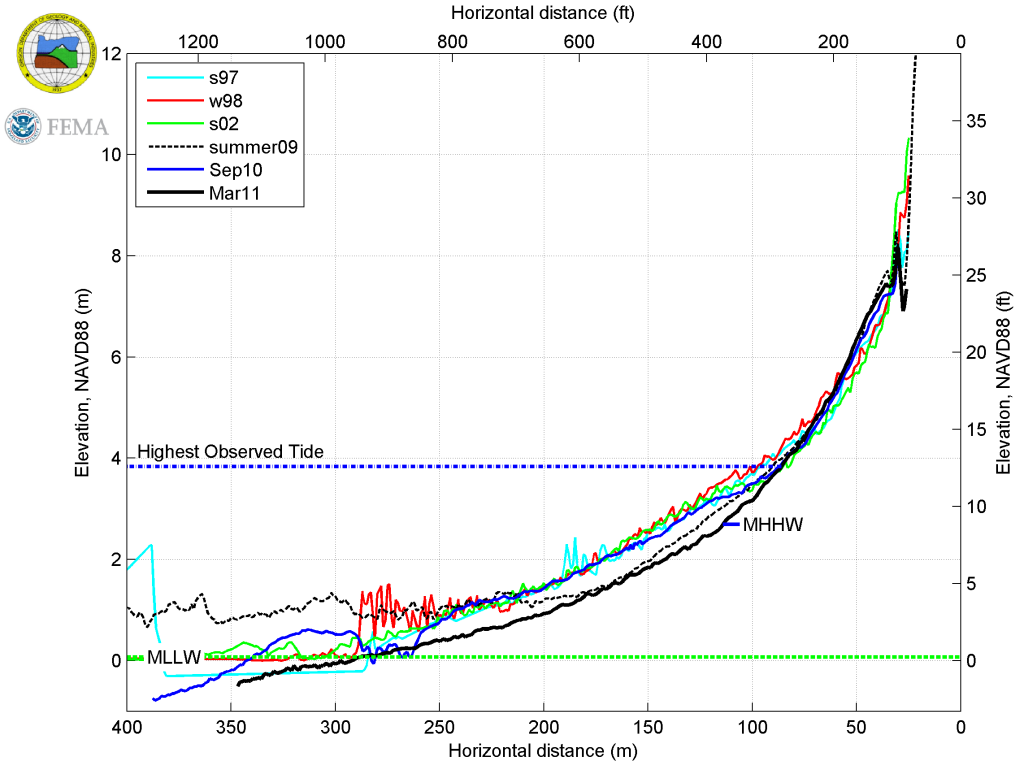
Horizontal distance (ft)
1200 1000 800 600 400 200 0
s97
w98
s02
summer09
Sep10
Mar11
Highest Observed Tide
MHHW
MLLW
Elevation, NAVD88 (m)
Elevation, NAVD88 (ft)
400 350 300 250 200 150 100 50 0
Horizontal distance (m)

CB 9

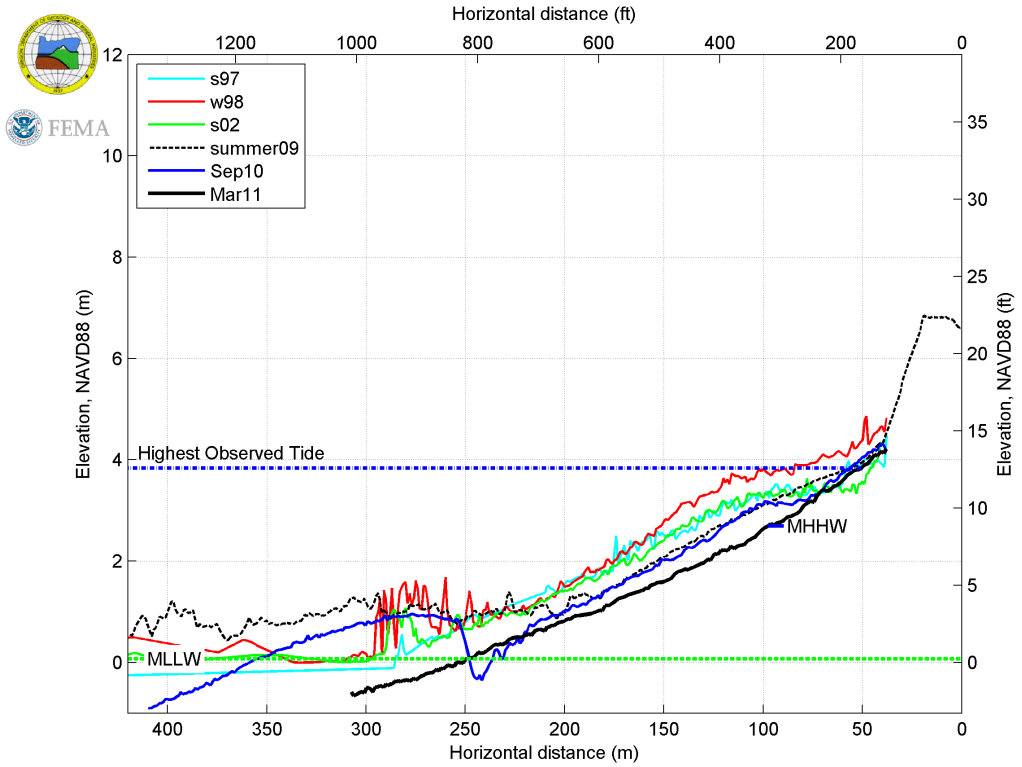
Horizontal distance (ft)
1200
1000
800
600
400
200
0
s97
w98
s02
summer09
Sep10
Mar11
Elevation, NAVD88 (m)
Elevation, NAVD88 (ft)
Highest Observed Tide
MHHW
MLLW
Horizontal distance (m)
400
350
300
250
200
150
100
50
0

CB 10

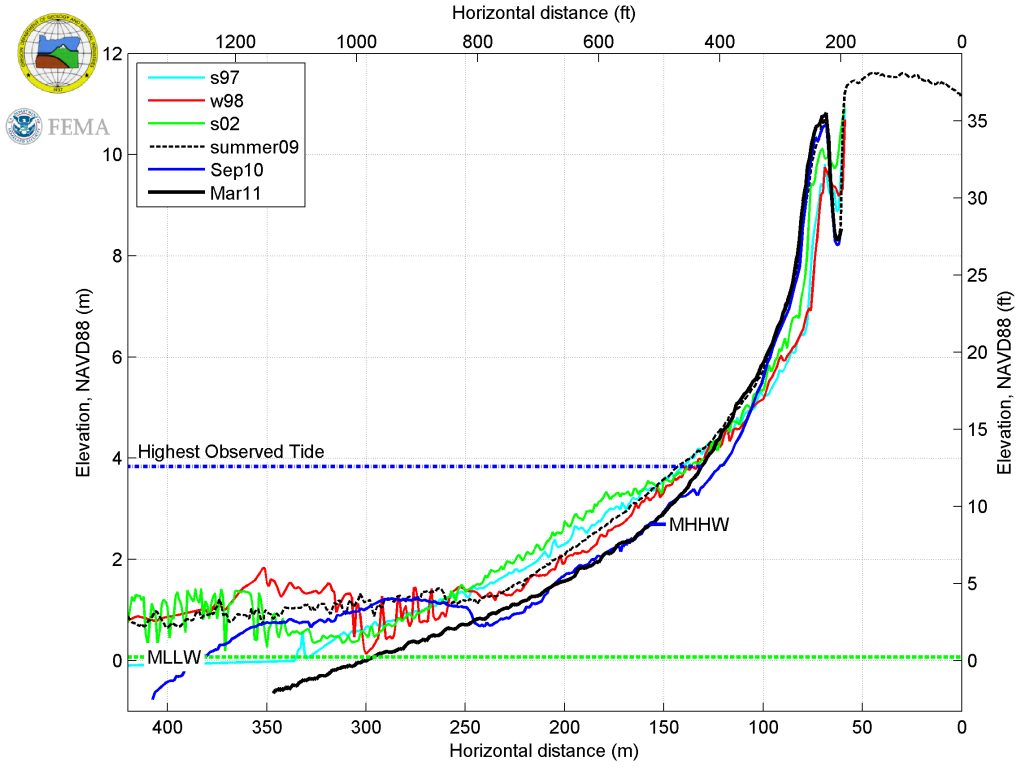
Horizontal distance (ft)
1200
1000
800
600
400
200
0
s97
w98
s02
summer09
Sep10
Mar11
Elevation, NAVD88 (m)
Elevation, NAVD88 (ft)
Highest Observed Tide
MHHW
MLLW
Horizontal distance (m)
400
350
300
250
200
150
100
50
0

CB 11

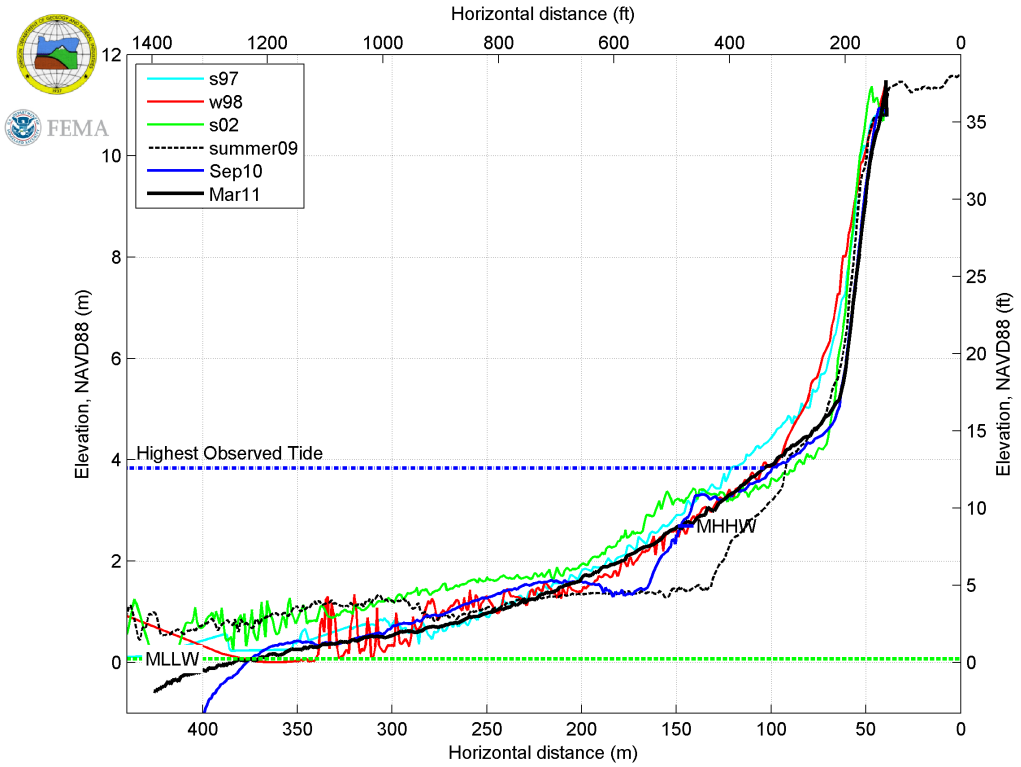
Horizontal distance (ft)
1400
1200
1000
800
600
400
200
0
s97
w98
s02
summer09
Sep10
Mar11
Highest Observed Tide
MHHW
MLLW
Elevation, NAVD88 (m)
Elevation, NAVD88 (ft)
Horizontal distance (m)
400
350
300
250
200
150
100
50
0

CB 12

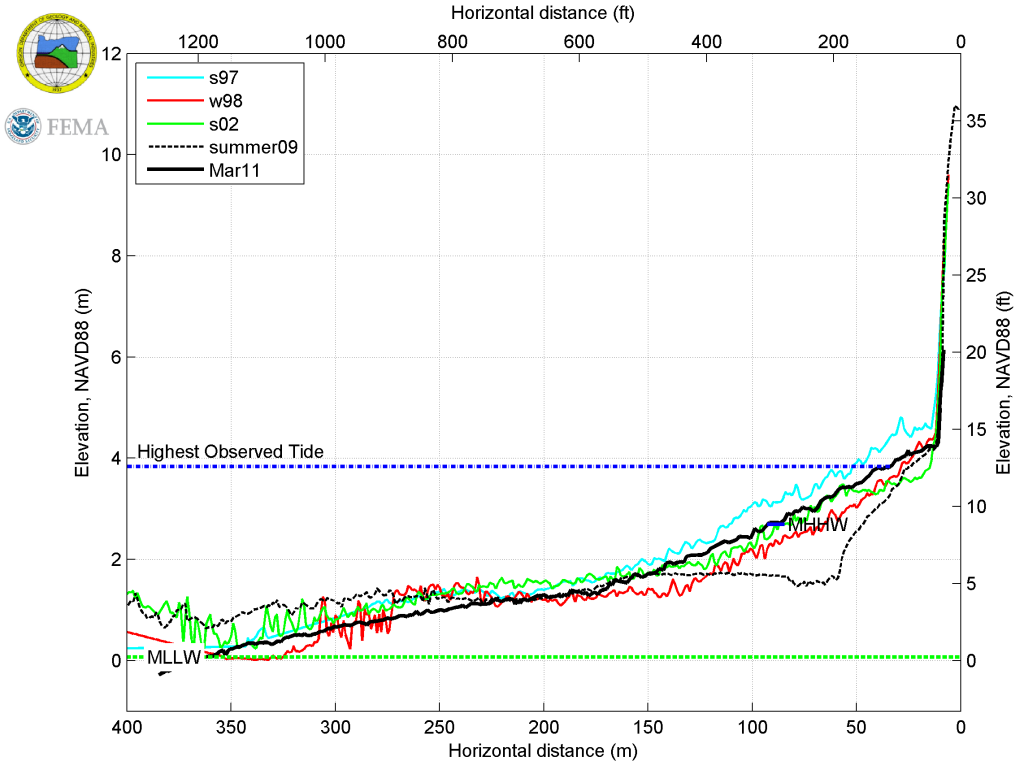
Horizontal distance (ft)
1200
1000
800
600
400
200
0
s97
w98
s02
summer09
Mar11
Highest Observed Tide
MHHW
MLLW
Elevation, NAVD88 (m)
Elevation, NAVD88 (ft)
Horizontal distance (m)
400
350
300
250
200
150
100
50
0

CB 13

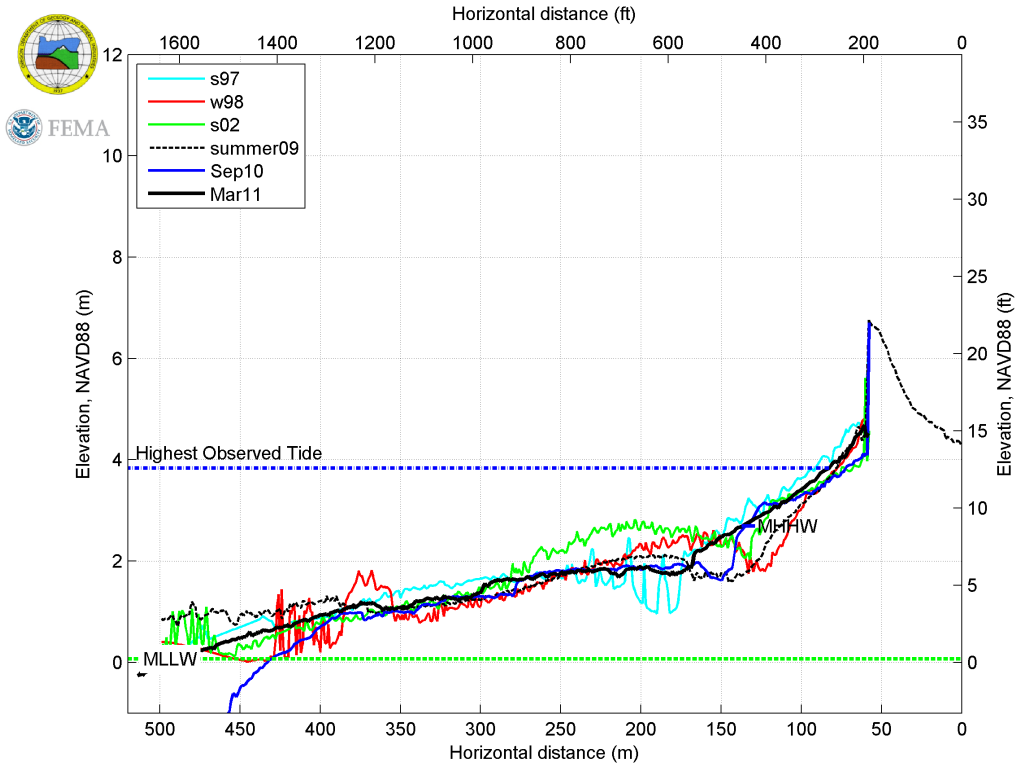
Horizontal distance (ft)
1600
1400
1200
1000
800
600
400
200
0
s97
w98
s02
summer09
Sep10
Mar11
Elevation, NAVD88 (m)
Elevation, NAVD88 (ft)
Highest Observed Tide
MHHW
MLLW
500
450
400
350
300
250
200
150
100
50
0
Horizontal distance (m)

CB 14

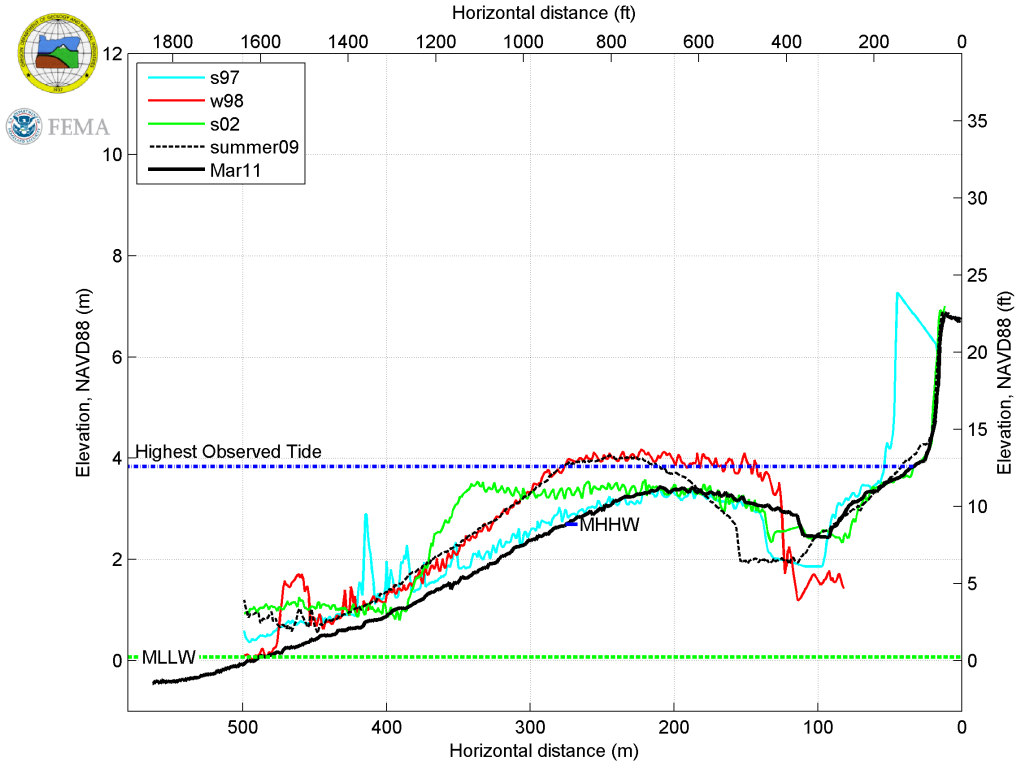
Horizontal distance (ft)
1800
1600
1400
1200
1000
800
600
400
200
0
s97
w98
s02
summer09
Mar11
Elevation, NAVD88 (m)
Elevation, NAVD88 (ft)
Highest Observed Tide
MHHW
MLLW
500
400
300
200
100
0
Horizontal distance (m)

CB 15

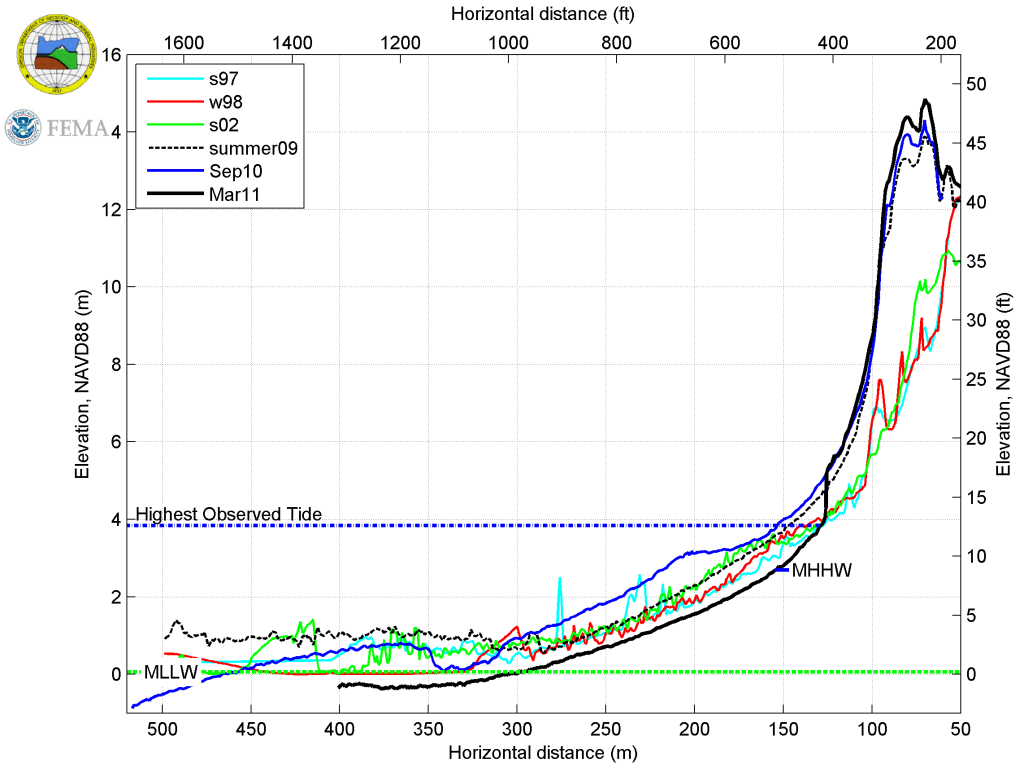
Horizontal distance (ft)
1600
1400
1200
1000
800
600
400
200
s97
w98
s02
summer09
Sep10
Mar11
Elevation, NAVD88 (m)
Elevation, NAVD88 (ft)
Highest Observed Tide
MHHW
MLLW
500
450
400
350
300
250
200
150
100
50
Horizontal distance (m)

CB 16

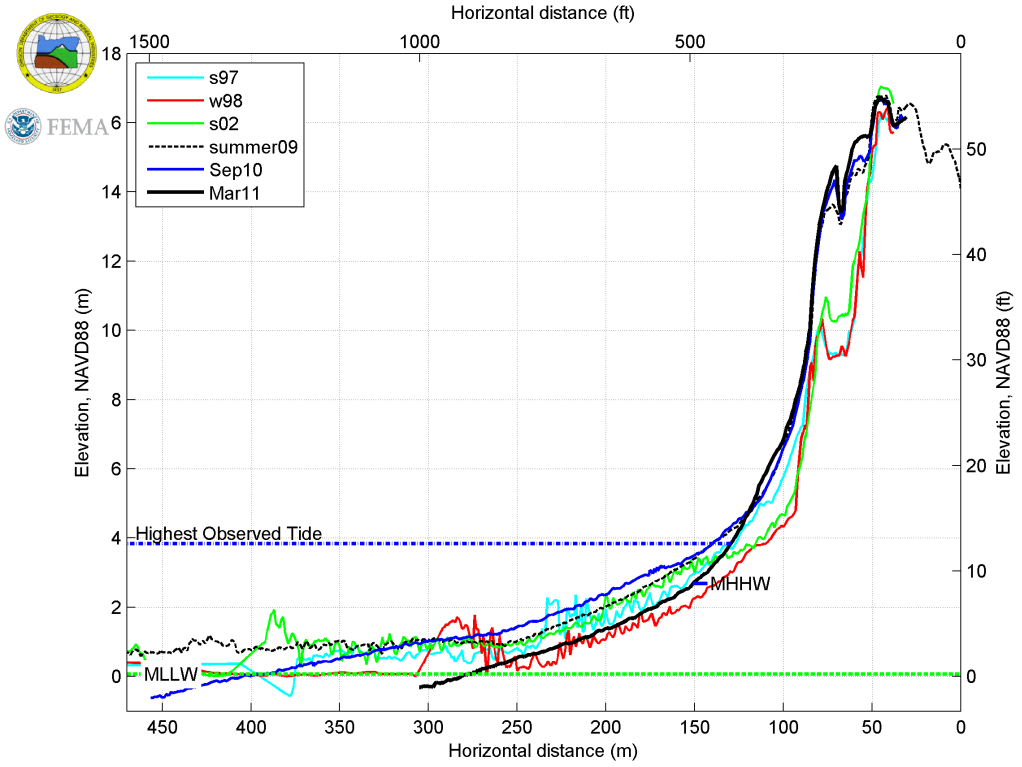
Horizontal distance (ft)
1500
1000
500
0
s97
w98
s02
summer09
Sep10
Mar11
Elevation, NAVD88 (m)
Elevation, NAVD88 (ft)
Highest Observed Tide
MHHW
MLLW
450
400
350
300
250
200
150
100
50
0
Horizontal distance (m)

CB 17

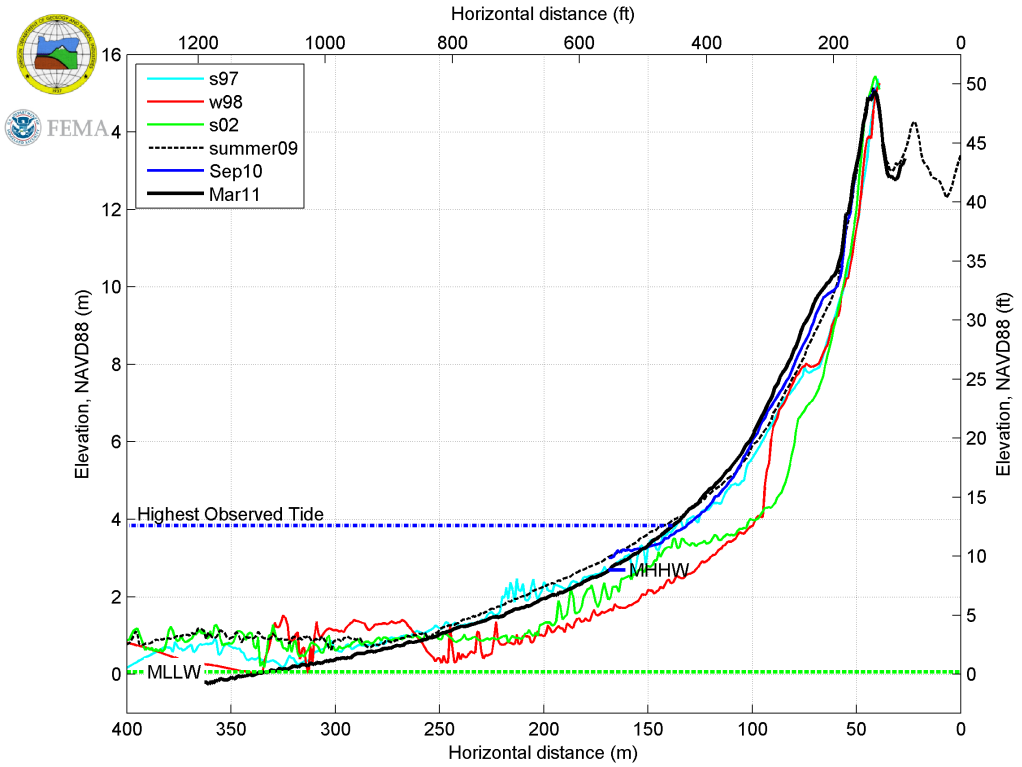
Horizontal distance (ft)
1200
1000
800
600
400
200
0
s97
w98
s02
summer09
Sep10
Mar11
Elevation, NAVD88 (m)
Elevation, NAVD88 (ft)
Highest Observed Tide
MHHW
MLLW
400
350
300
250
200
150
100
50
0
Horizontal distance (m)

11.2.4 Tolovana Beach

TOL 1

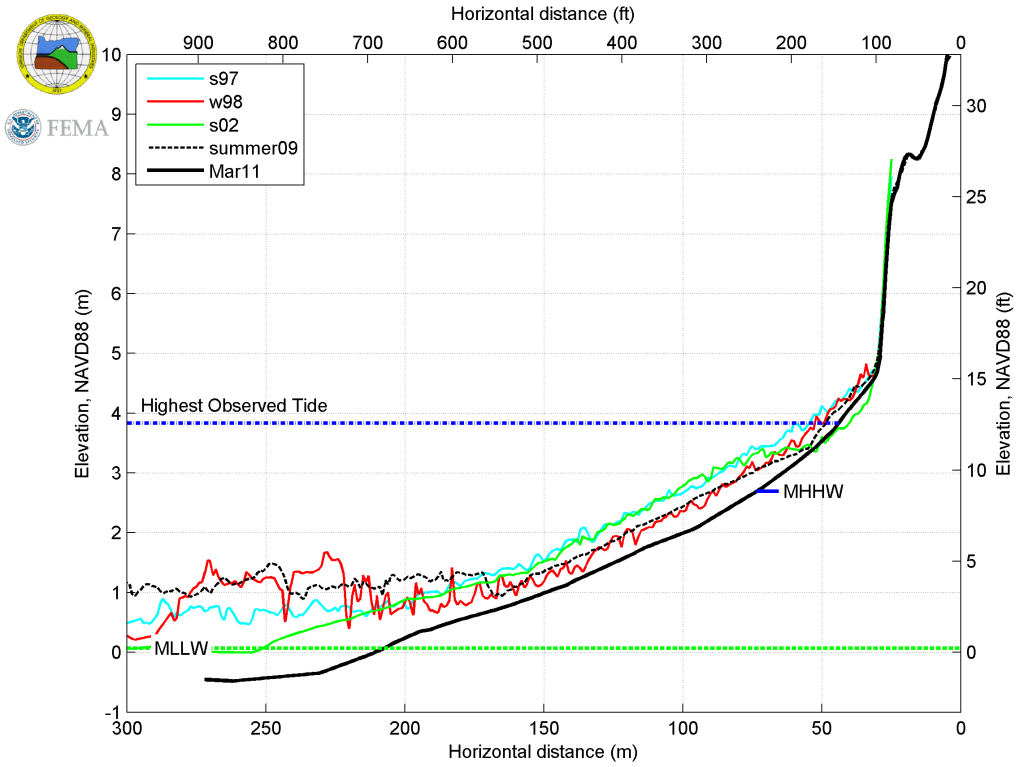

TOL 2

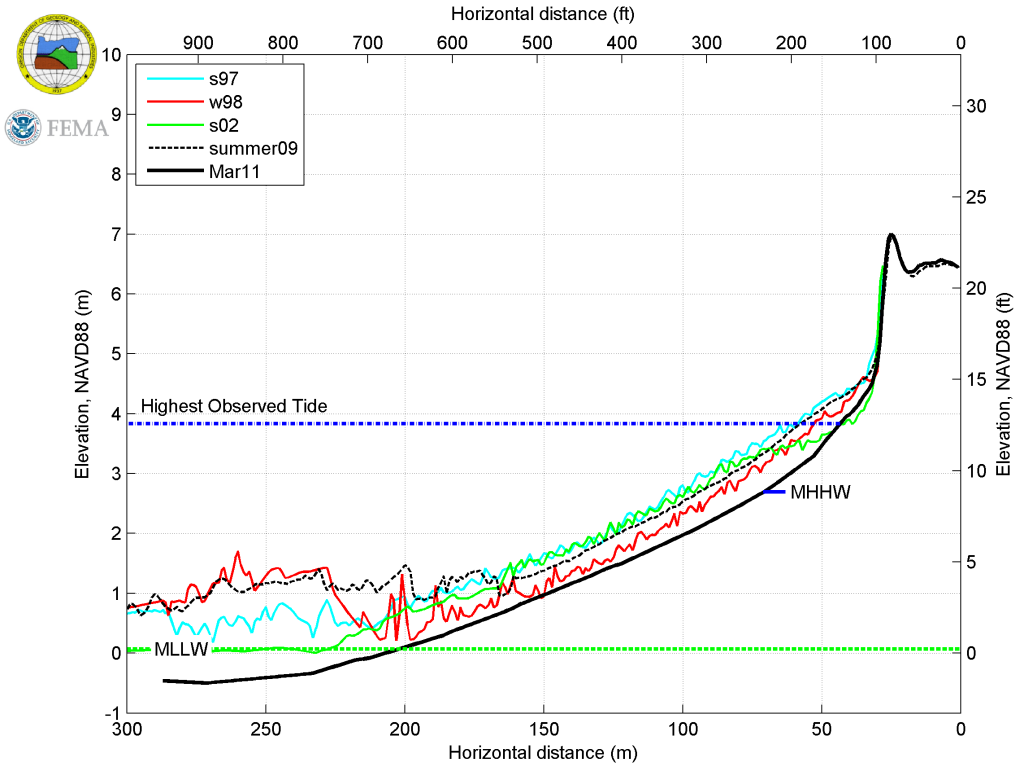

TOL 3

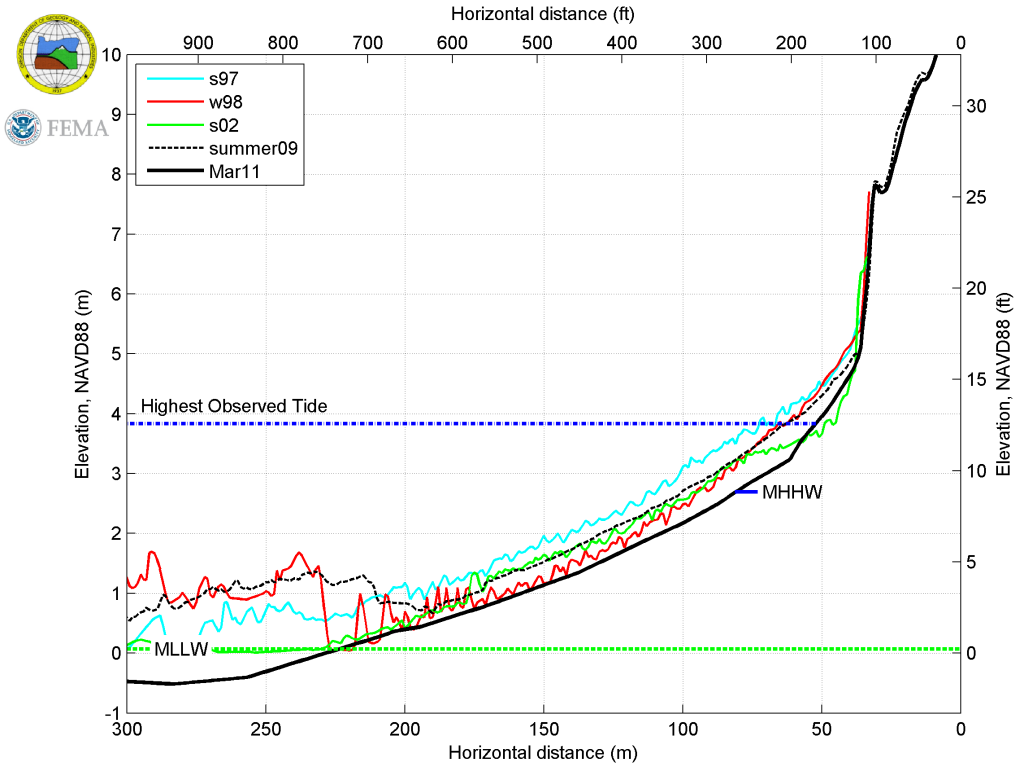
Horizontal distance (ft)
900 800 700 600 500 400 300 200 100 0
s97
w98
s02
summer09
Mar11
Highest Observed Tide
MHHW
MLLW
Elevation, NAVD88 (m)
Elevation, NAVD88 (ft)
300 250 200 150 100 50 0
Horizontal distance (m)

TOL 4

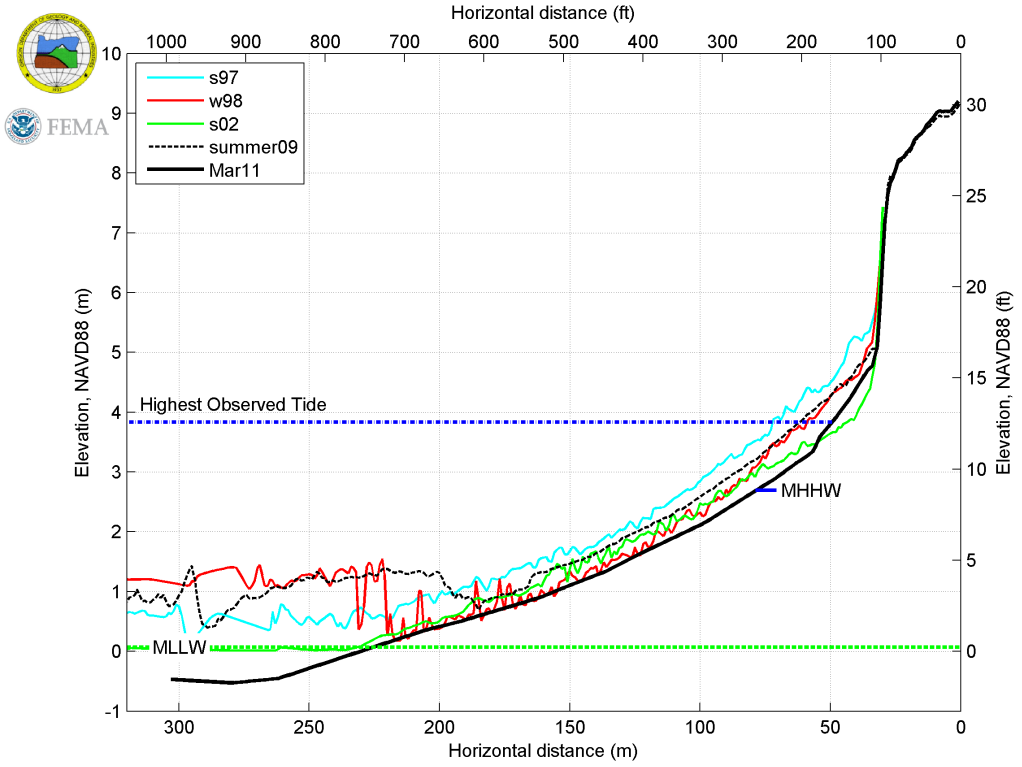
Horizontal distance (ft)
1000 900 800 700 600 500 400 300 200 100 0
s97
w98
s02
summer09
Mar11
Highest Observed Tide
MHHW
MLLW
Elevation, NAVD88 (m)
Elevation, NAVD88 (ft)
300 250 200 150 100 50 0
Horizontal distance (m)

TOL 5

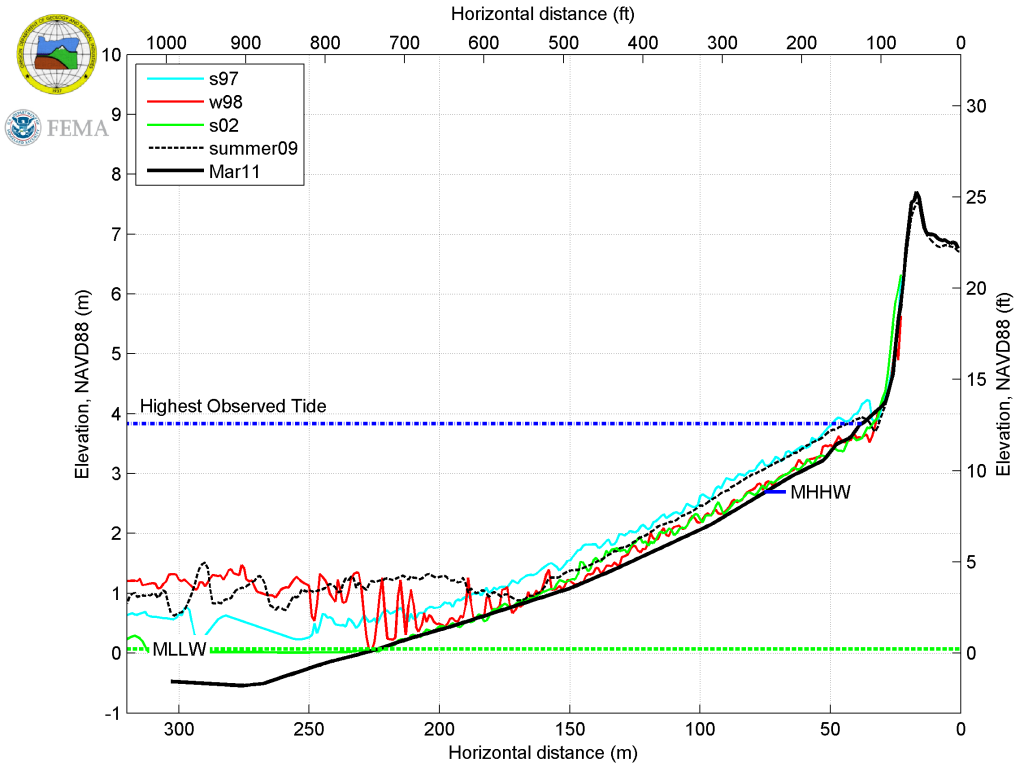
Horizontal distance (ft)
1000 900 800 700 600 500 400 300 200 100 0
s97
w98
s02
summer09
Mar11
Highest Observed Tide
MHHW
MLLW
Elevation, NAVD88 (m)
Elevation, NAVD88 (ft)
300 250 200 150 100 50 0
Horizontal distance (m)

TOL 6

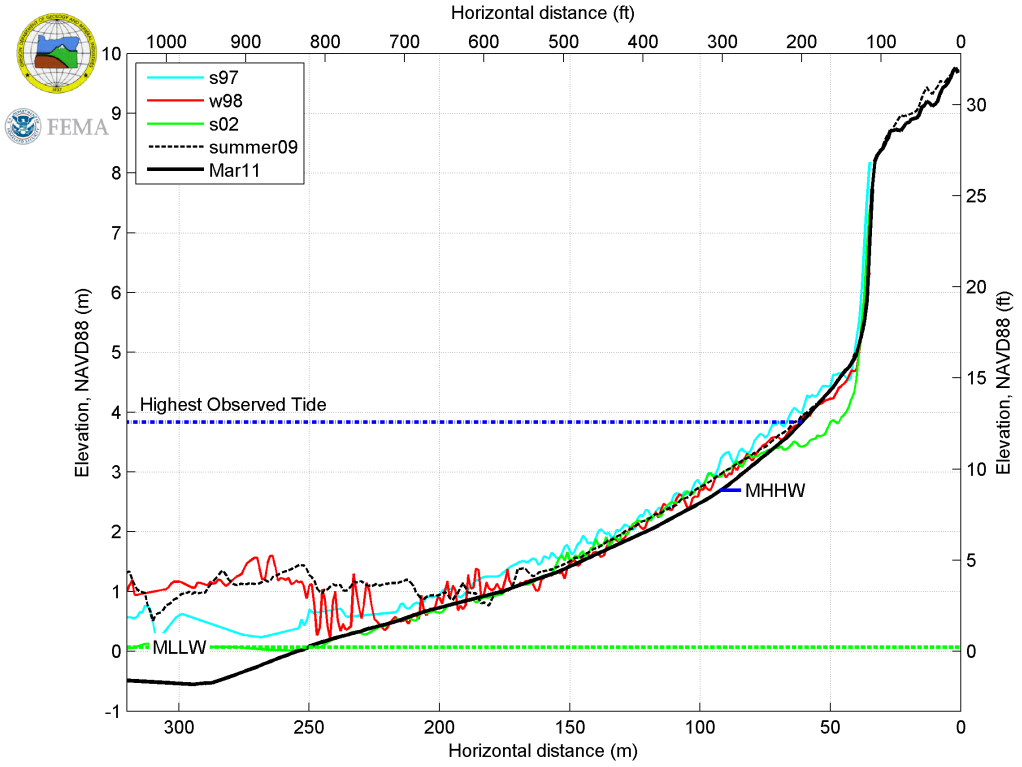
Horizontal distance (ft)
1000 900 800 700 600 500 400 300 200 100 0
s97
w98
s02
summer09
Mar11
Highest Observed Tide
MHHW
MLLW
Elevation, NAVD88 (m)
Elevation, NAVD88 (ft)
300 250 200 150 100 50 0
Horizontal distance (m)

TOL 7

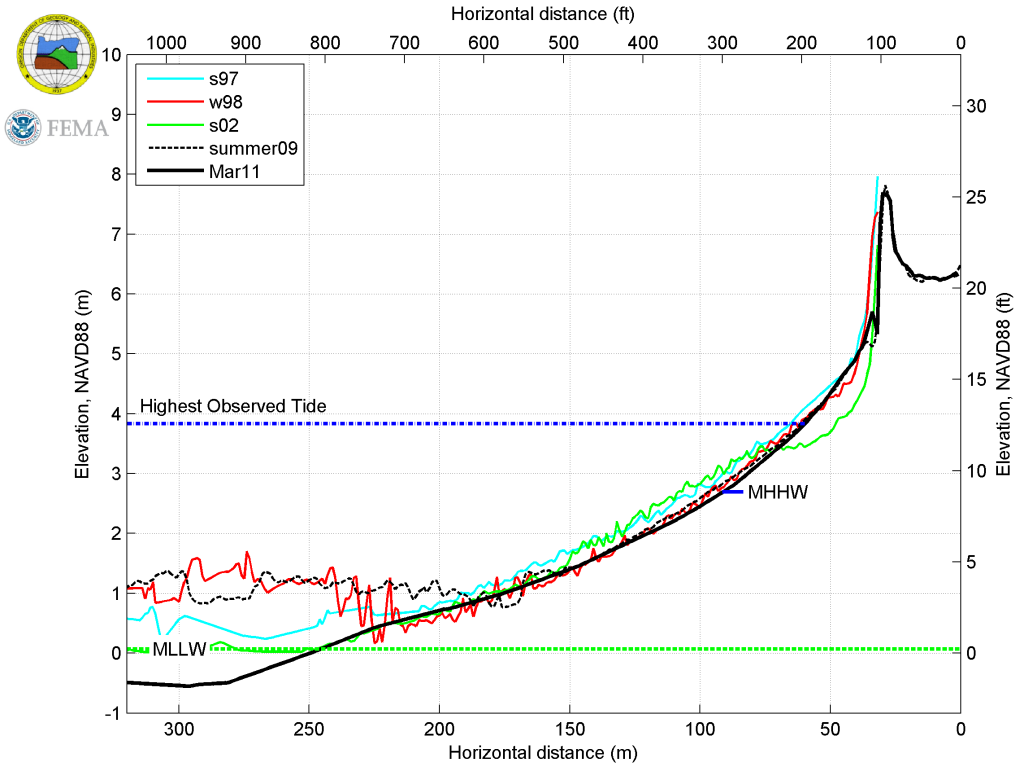
Horizontal distance (ft)
1000 900 800 700 600 500 400 300 200 100 0
s97
w98
s02
summer09
Mar11
Highest Observed Tide
MHHW
MLLW
Elevation, NAVD88 (m)
Elevation, NAVD88 (ft)
300 250 200 150 100 50 0
Horizontal distance (m)

TOL 8

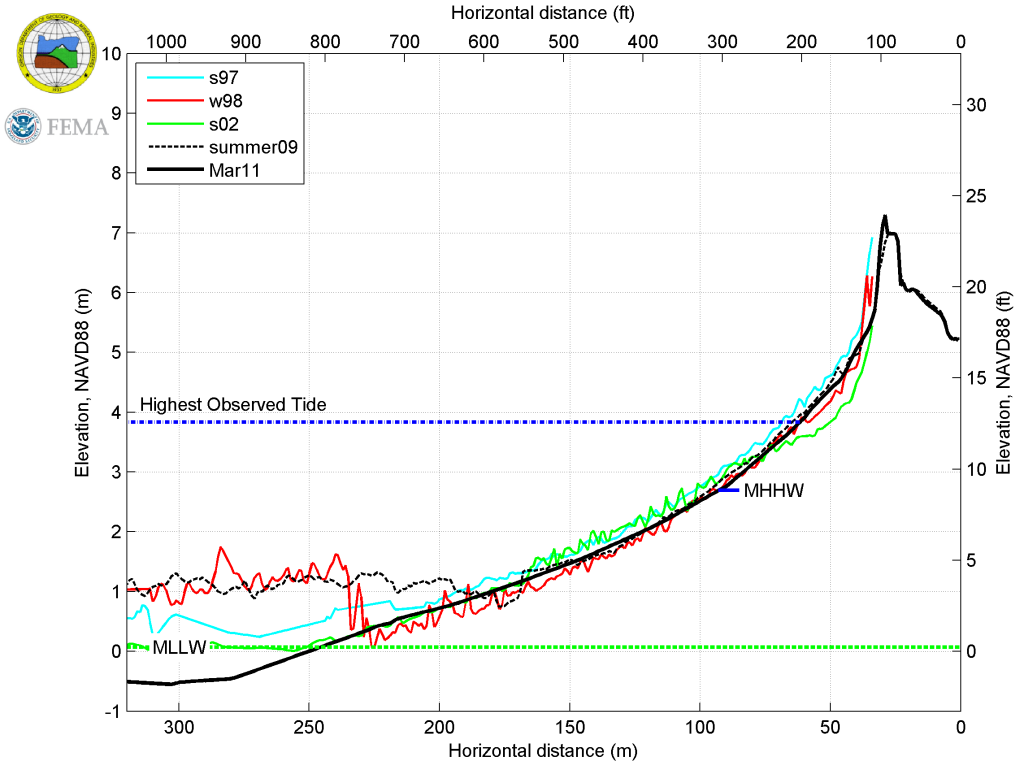
Horizontal distance (ft)
1000 900 800 700 600 500 400 300 200 100 0
s97
w98
s02
summer09
Mar11
Highest Observed Tide
MHHW
MLLW
Elevation, NAVD88 (m)
Elevation, NAVD88 (ft)
300 250 200 150 100 50 0
Horizontal distance (m)

TOL 9

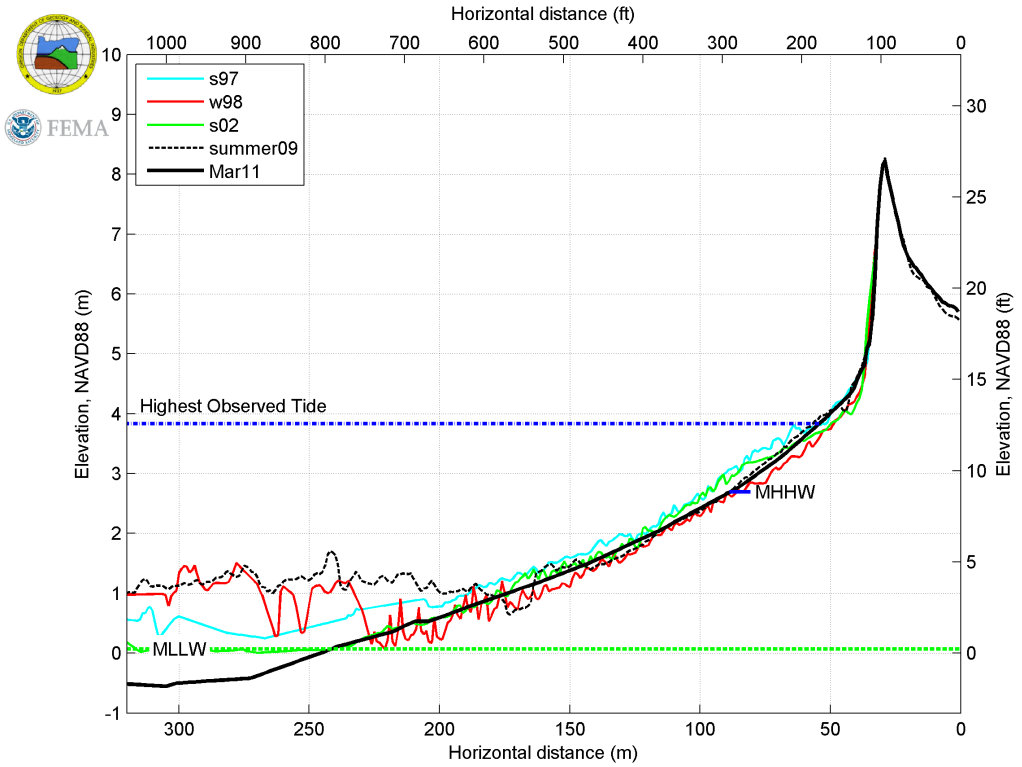
Horizontal distance (ft)
1000 900 800 700 600 500 400 300 200 100 0
s97
w98
s02
summer09
Mar11
Highest Observed Tide
MHHW
MLLW
Elevation, NAVD88 (m)
Elevation, NAVD88 (ft)
300 250 200 150 100 50 0
Horizontal distance (m)

TOL 10

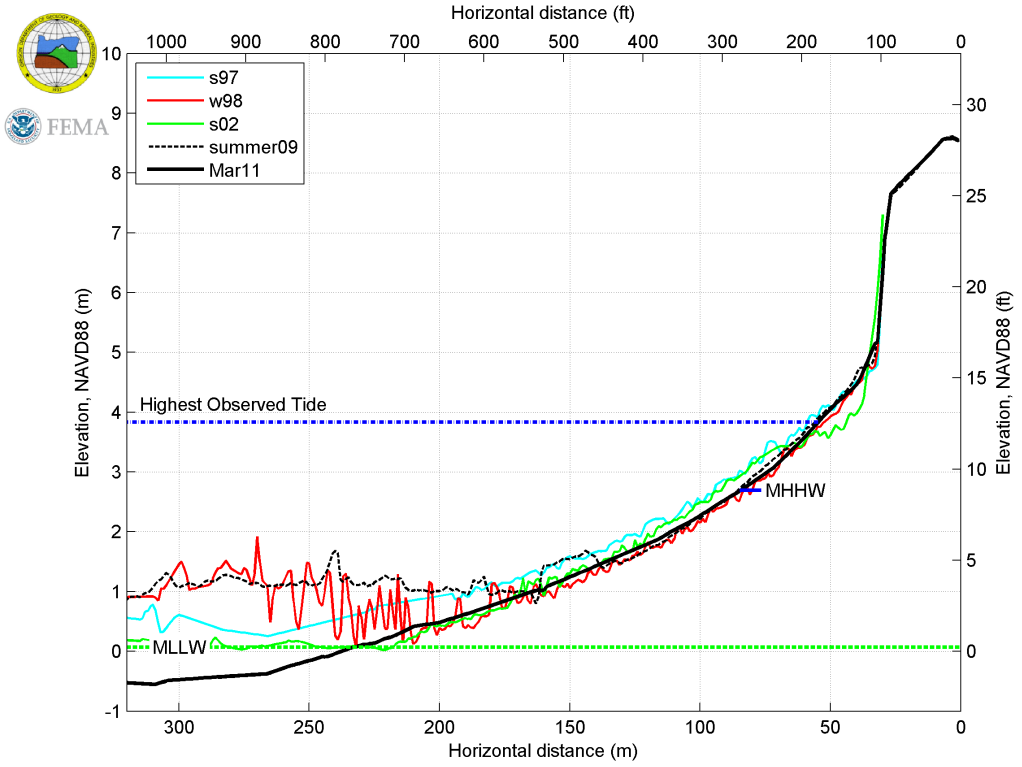
Horizontal distance (ft)
1000 900 800 700 600 500 400 300 200 100 0
s97
w98
s02
summer09
Mar11
Highest Observed Tide
MHHW
MLLW
Elevation, NAVD88 (m)
Elevation, NAVD88 (ft)
300 250 200 150 100 50 0
Horizontal distance (m)

TOL 11

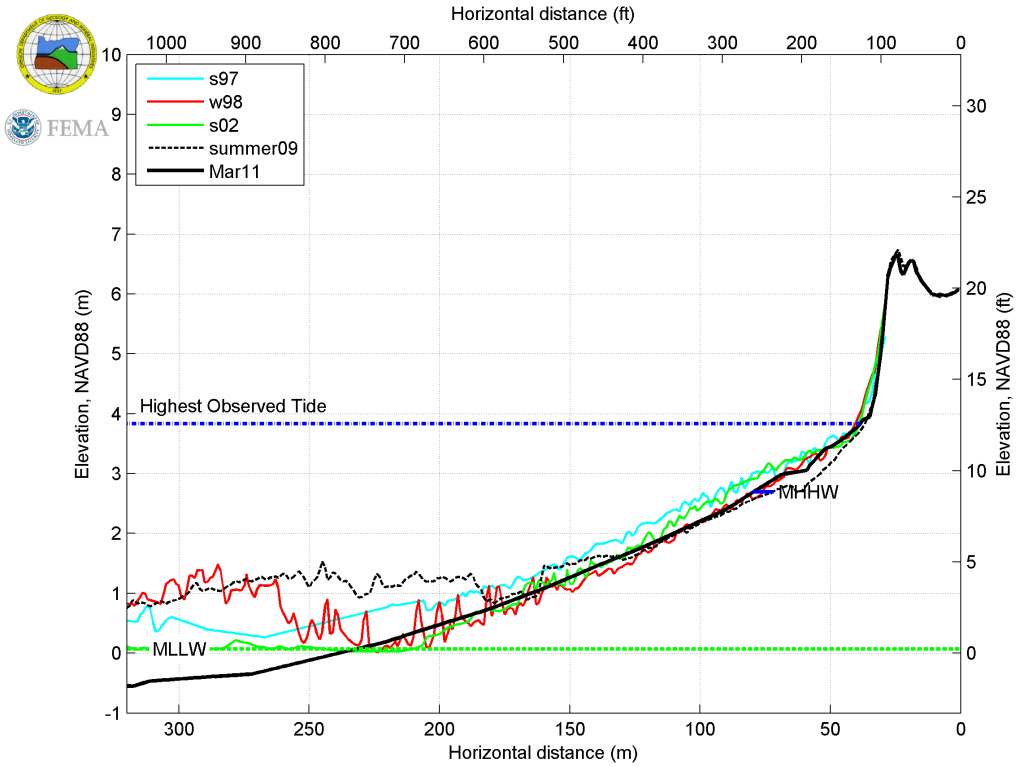
Horizontal distance (ft)
1000 900 800 700 600 500 400 300 200 100 0
s97
w98
s02
summer09
Mar11
Highest Observed Tide
MHHW
MLLW
Elevation, NAVD88 (m)
Elevation, NAVD88 (ft)
300 250 200 150 100 50 0
Horizontal distance (m)

TOL 12

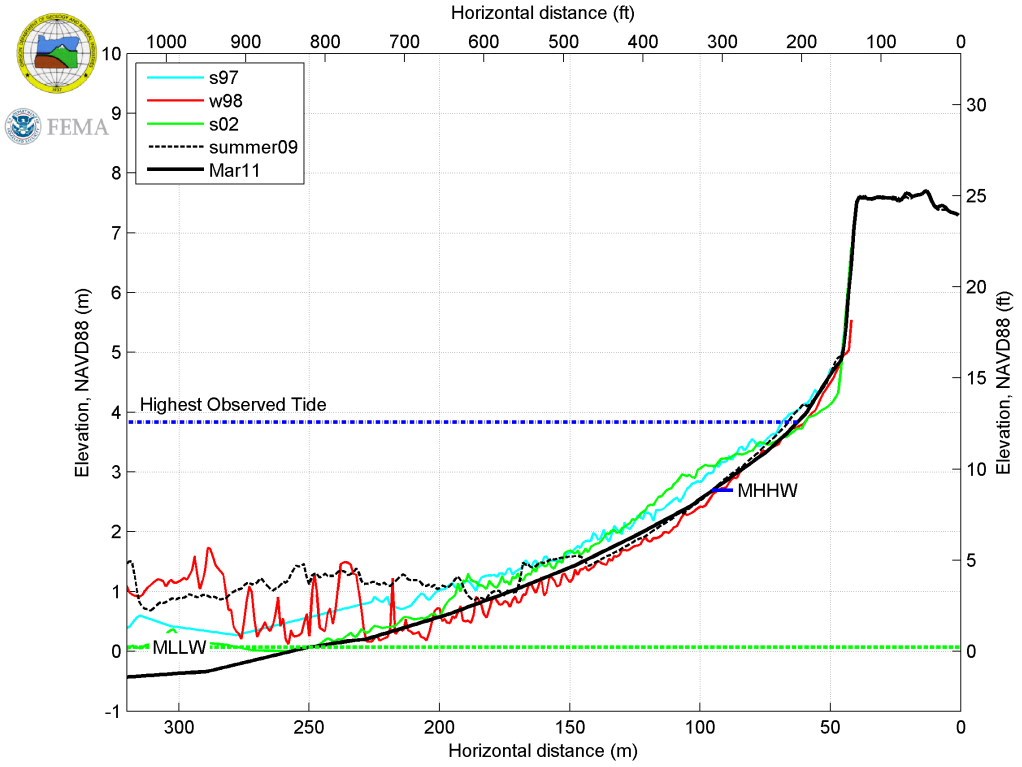
Horizontal distance (ft)
1000 900 800 700 600 500 400 300 200 100 0
s97
w98
s02
summer09
Mar11
Highest Observed Tide
MHHW
MLLW
Elevation, NAVD88 (m)
Elevation, NAVD88 (ft)
300 250 200 150 100 50 0
Horizontal distance (m)

TOL 13

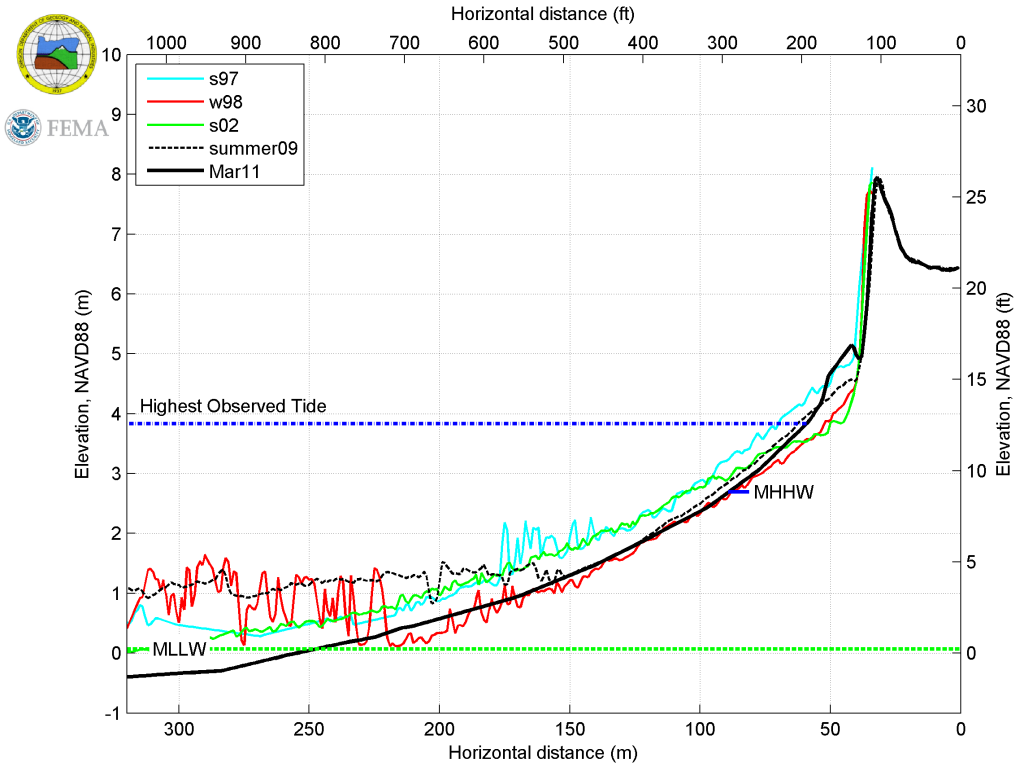
Horizontal distance (ft)
1000 900 800 700 600 500 400 300 200 100 0
s97
w98
s02
summer09
Mar11
Highest Observed Tide
MHHW
MLLW
Elevation, NAVD88 (m)
Elevation, NAVD88 (ft)
300 250 200 150 100 50 0
Horizontal distance (m)

TOL 14

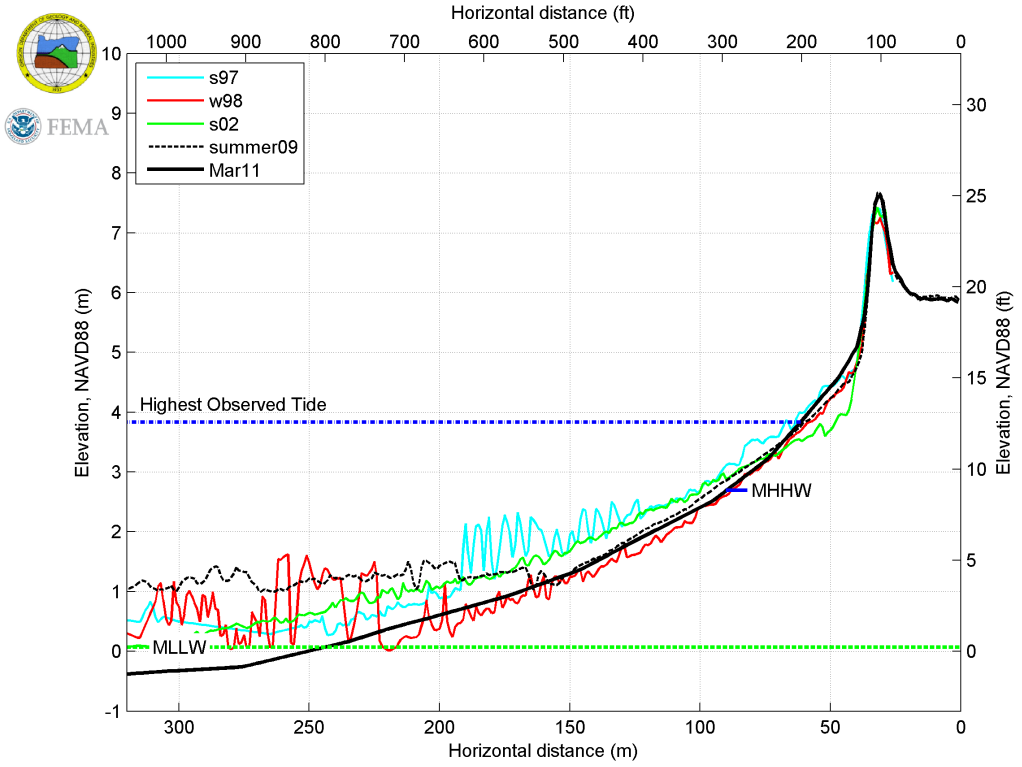
Horizontal distance (ft)
1000 900 800 700 600 500 400 300 200 100 0
s97
w98
s02
summer09
Mar11
Highest Observed Tide
MHHW
MLLW
Elevation, NAVD88 (m)
Elevation, NAVD88 (ft)
300 250 200 150 100 50 0
Horizontal distance (m)

TOL 15

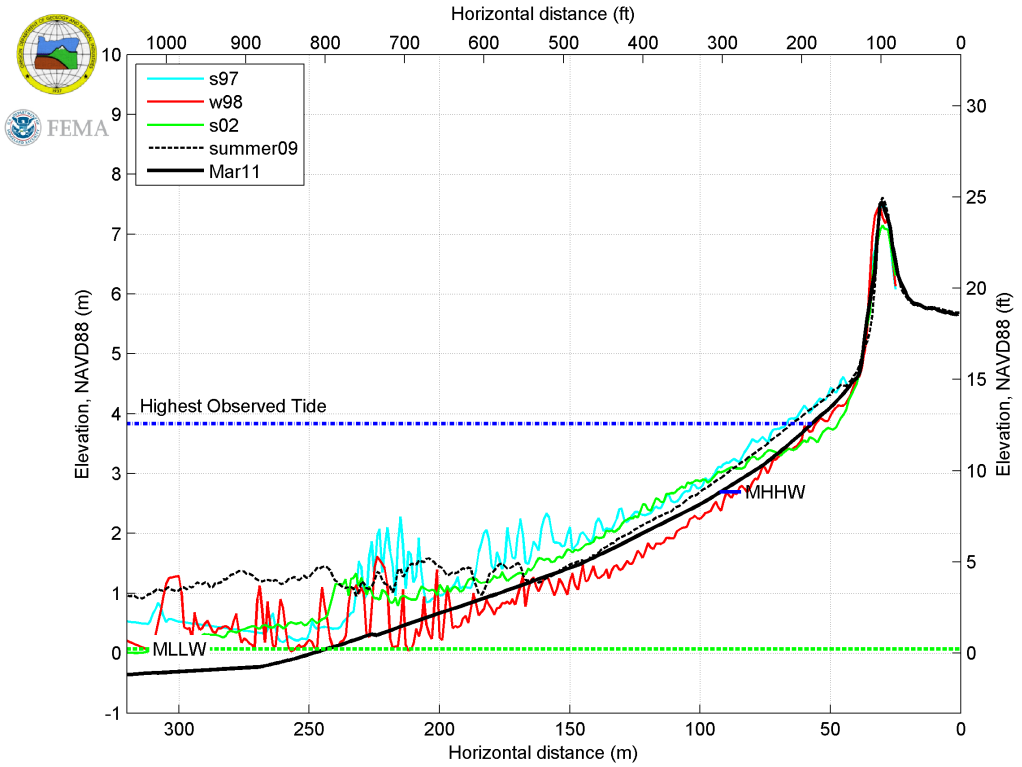
Horizontal distance (ft)
1000 900 800 700 600 500 400 300 200 100 0
s97
w98
s02
summer09
Mar11
Highest Observed Tide
MHHW
MLLW
Elevation, NAVD88 (m)
Elevation, NAVD88 (ft)
300 250 200 150 100 50 0
Horizontal distance (m)

TOL 16

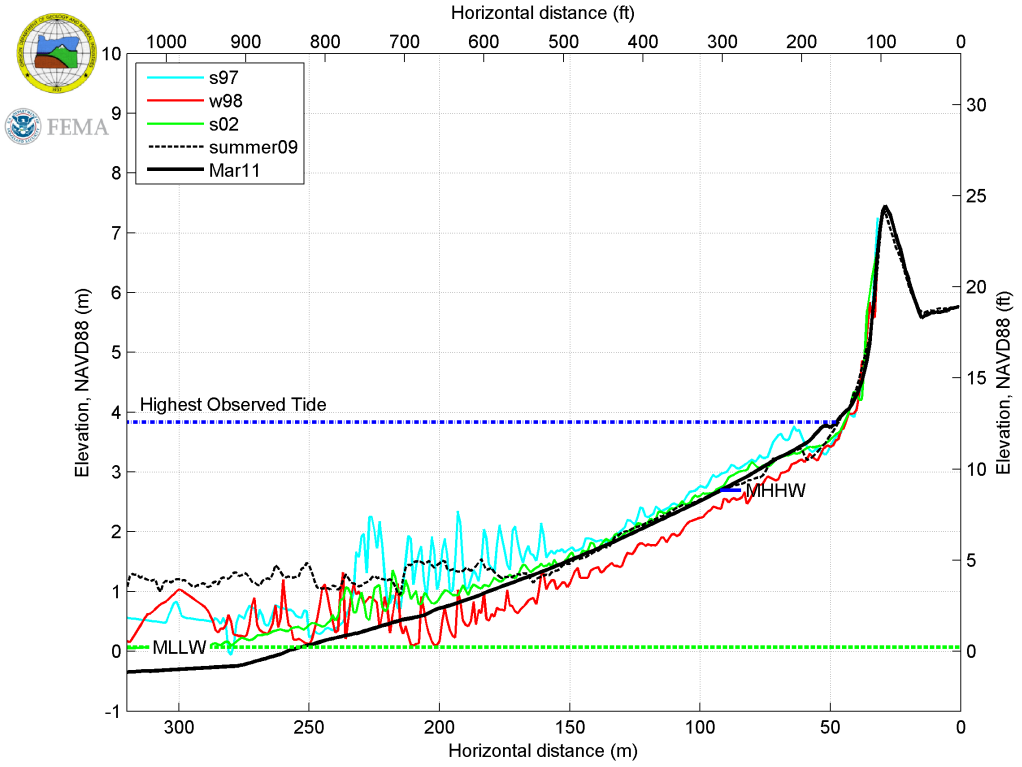
Horizontal distance (ft)
1000 900 800 700 600 500 400 300 200 100 0
s97
w98
s02
summer09
Mar11
Highest Observed Tide
MHHW
MLLW
Elevation, NAVD88 (m)
Elevation, NAVD88 (ft)
300 250 200 150 100 50 0
Horizontal distance (m)

TOL 17

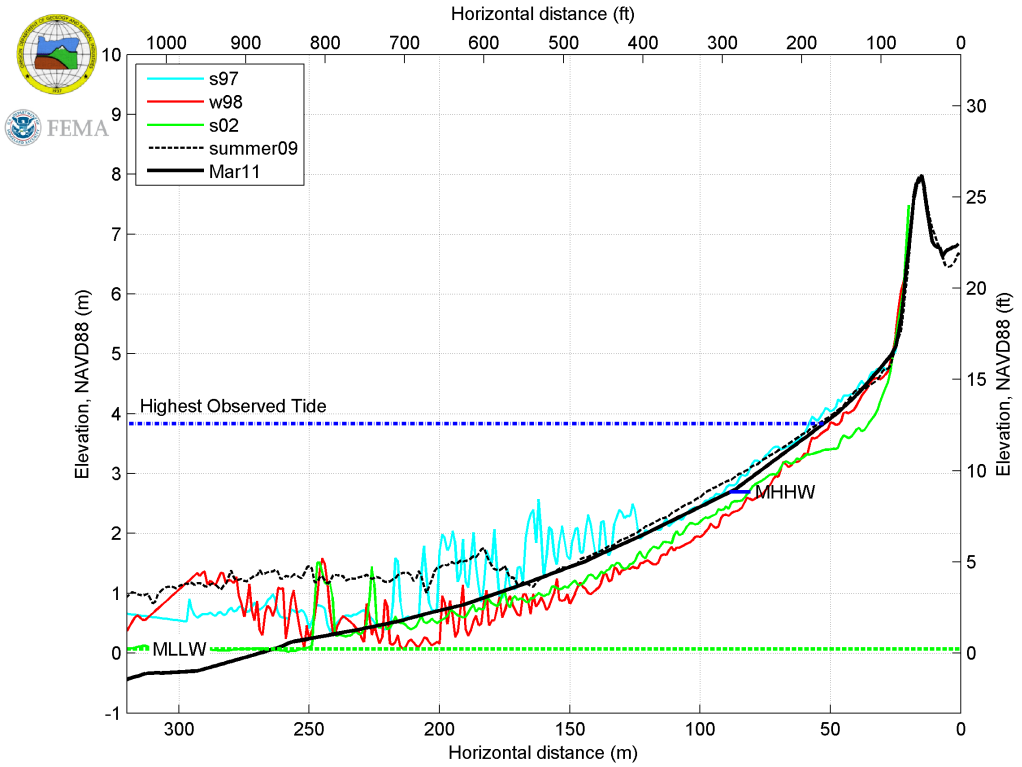
Horizontal distance (ft)
1000 900 800 700 600 500 400 300 200 100 0
s97
w98
s02
summer09
Mar11
Highest Observed Tide
MHHW
MLLW
Elevation, NAVD88 (m)
Elevation, NAVD88 (ft)
300 250 200 150 100 50 0
Horizontal distance (m)

TOL 18

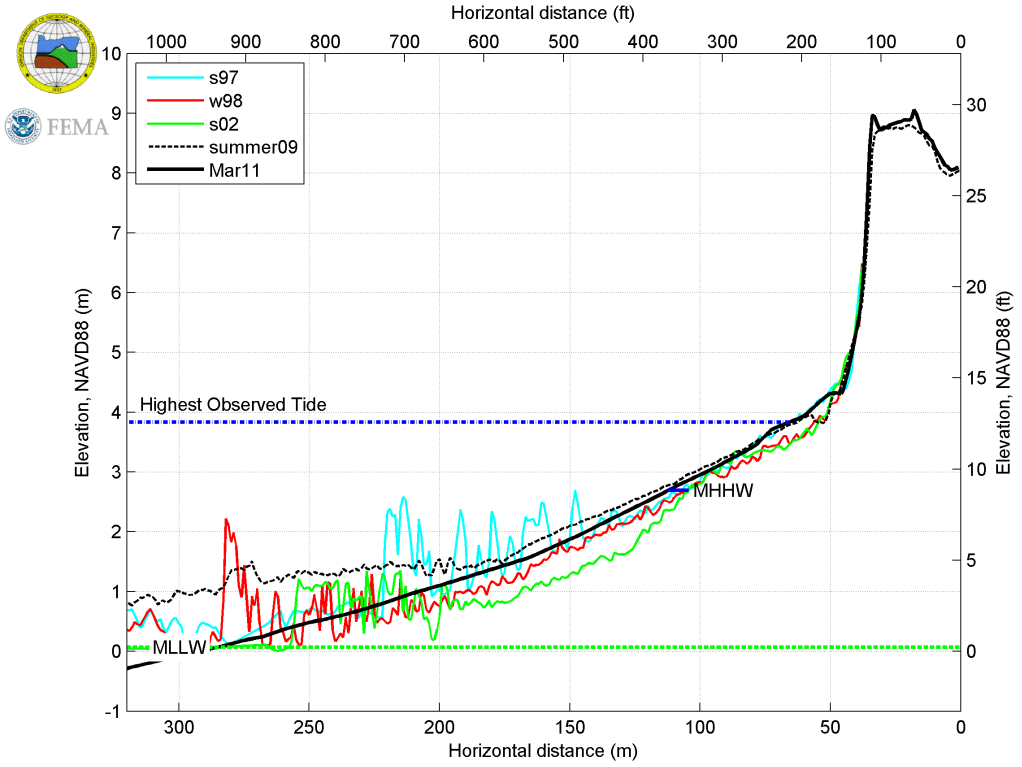
Horizontal distance (ft)
1000 900 800 700 600 500 400 300 200 100 0
s97
w98
s02
summer09
Mar11
Highest Observed Tide
MHHW
MLLW
Elevation, NAVD88 (m)
Elevation, NAVD88 (ft)
300 250 200 150 100 50 0
Horizontal distance (m)

11.2.5 Arcadia Beach

ARC 1

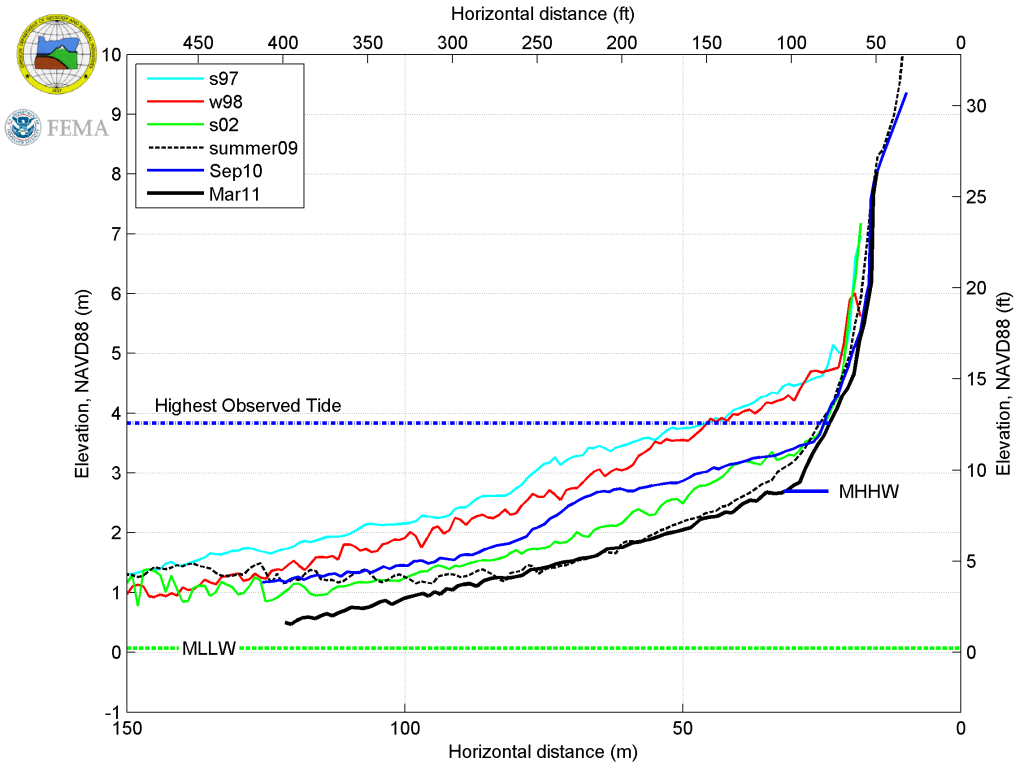

ARC 2

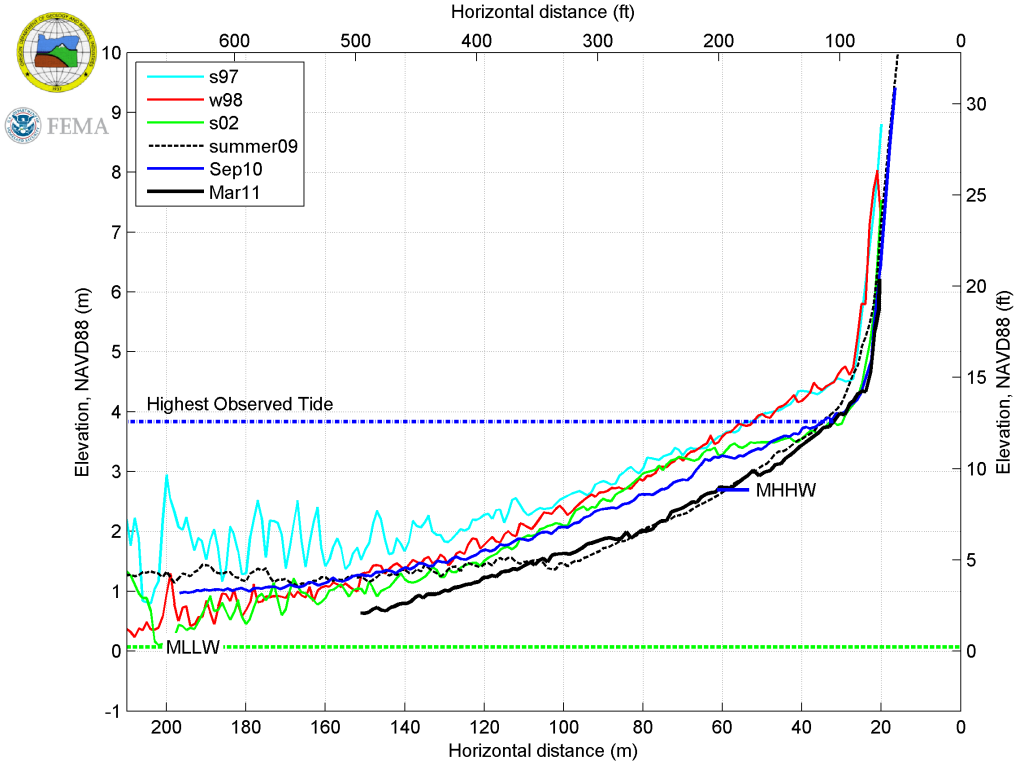

ARC 3

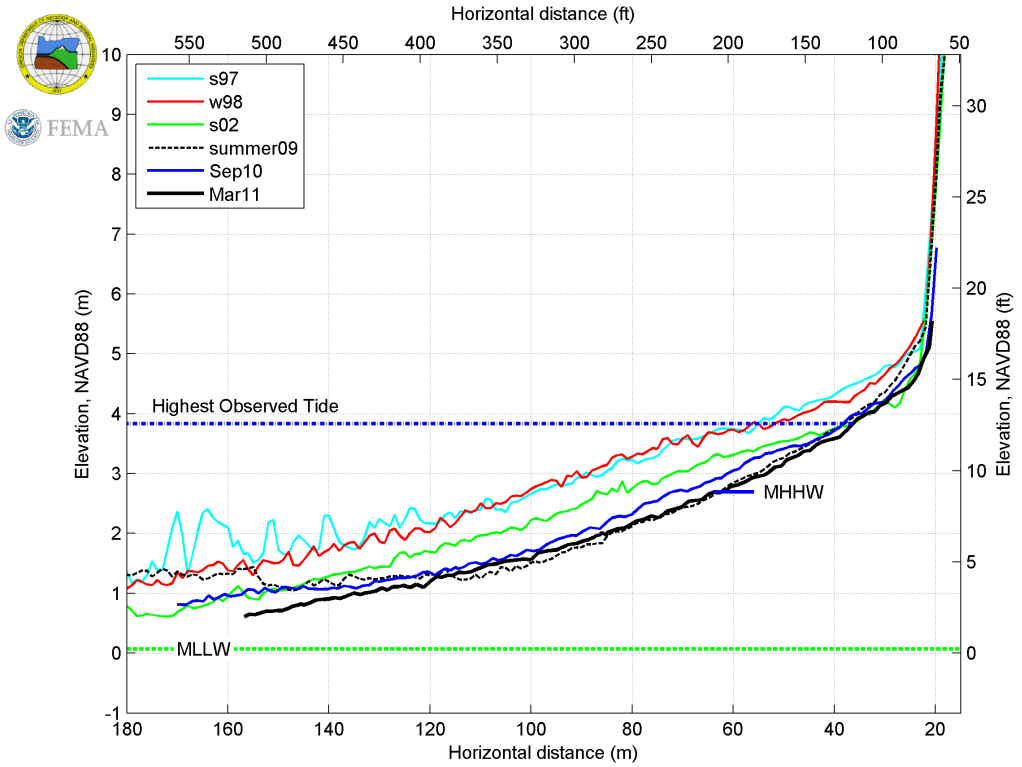
Horizontal distance (ft)
550
500
450
400
350
300
250
200
150
100
50
s97
w98
s02
summer09
Sep10
Mar11
Highest Observed Tide
MHHW
MLLW
Elevation, NAVD88 (m)
Elevation, NAVD88 (ft)
Horizontal distance (m)
180
160
140
120
100
80
60
40
20

11.2.6 Arch Cape

AC 1

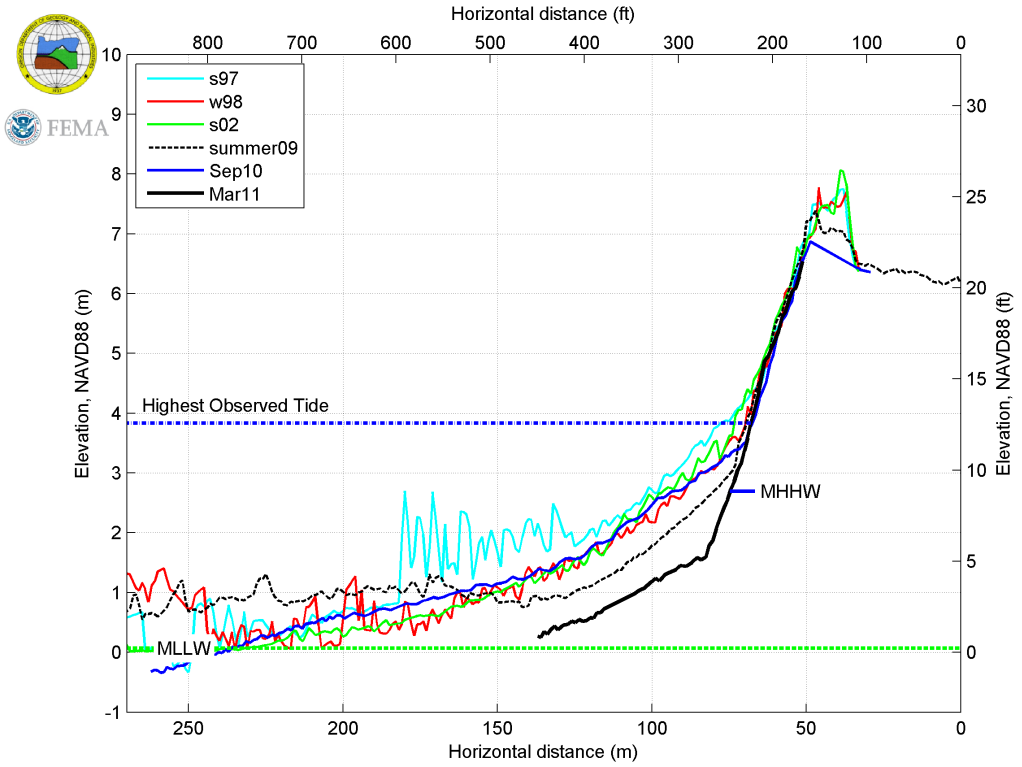

AC 2

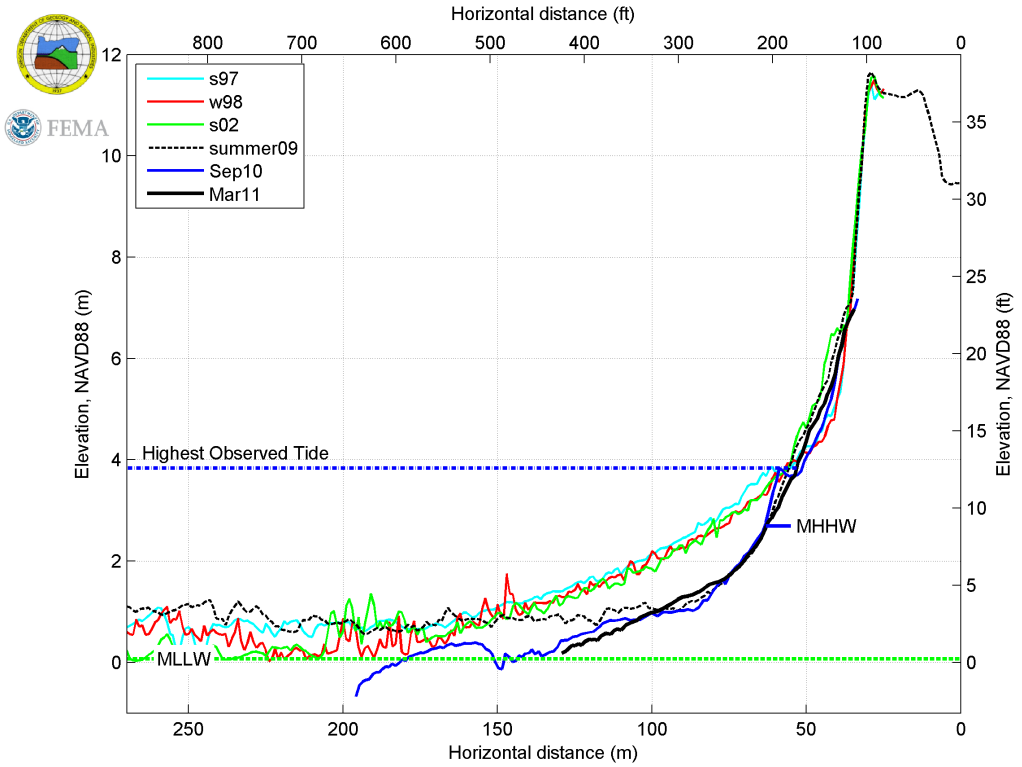

AC 3

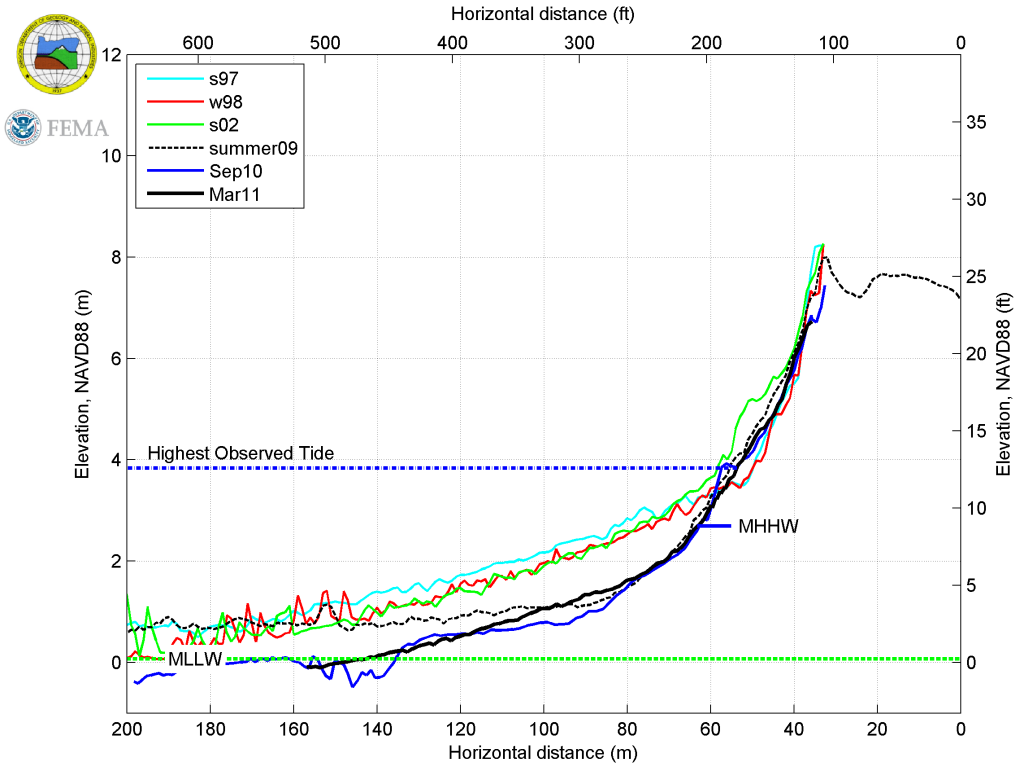
Horizontal distance (ft)
600
500
400
300
200
100
0
s97
w98
s02
summer09
Sep10
Mar11
Highest Observed Tide
MHHW
MLLW
Elevation, NAVD88 (m)
Elevation, NAVD88 (ft)
200
180
160
140
120
100
80
60
40
20
0
Horizontal distance (m)

AC 4

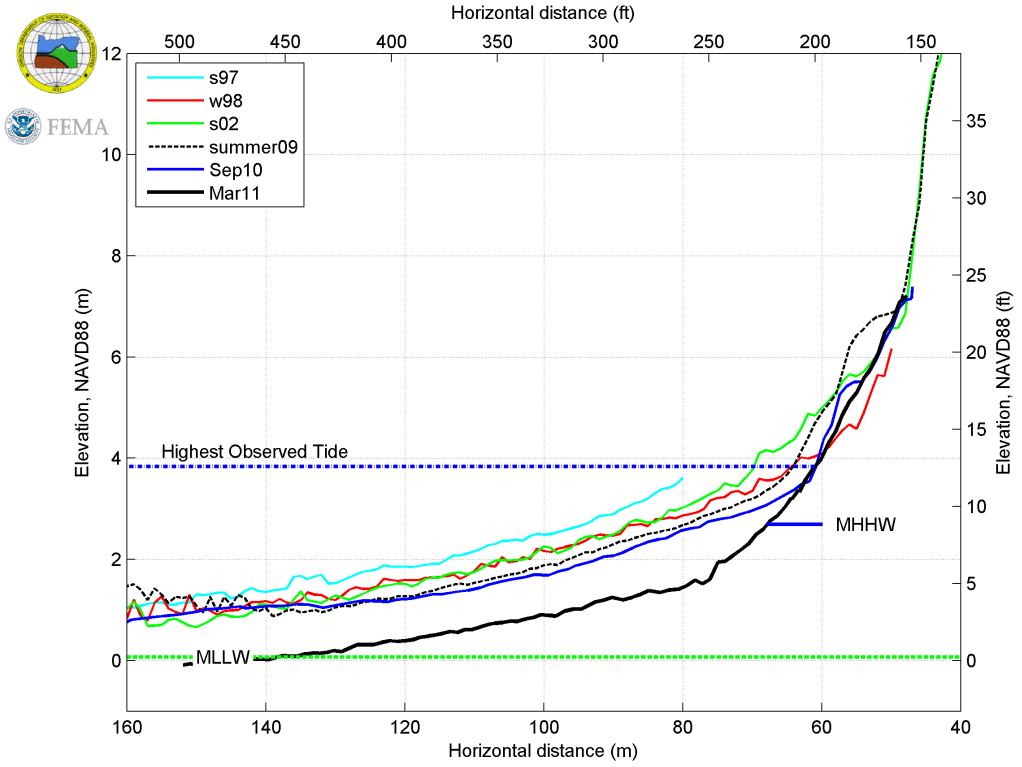
Horizontal distance (ft)
500
450
400
350
300
250
200
150
s97
w98
s02
summer09
Sep10
Mar11
Highest Observed Tide
MHHW
MLLW
Elevation, NAVD88 (m)
Elevation, NAVD88 (ft)
160
140
120
100
80
60
40
Horizontal distance (m)

AC 5

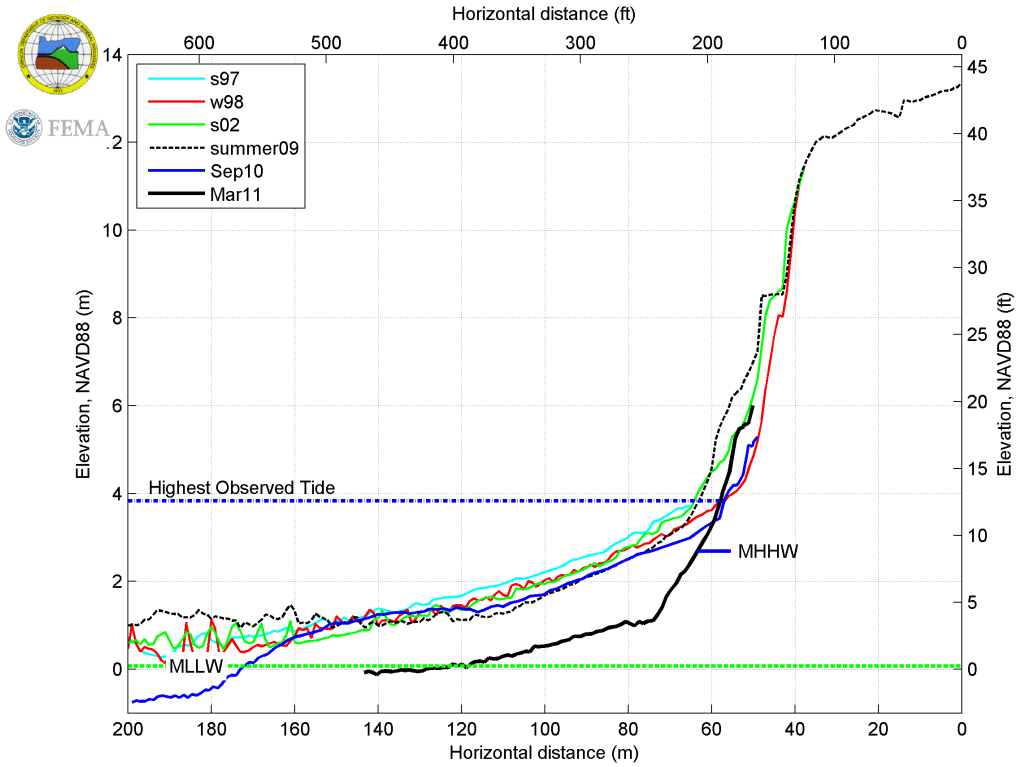
Horizontal distance (ft)
600
500
400
300
200
100
0
s97
w98
s02
summer09
Sep10
Mar11
Highest Observed Tide
MHHW
MLLW
Elevation, NAVD88 (m)
Elevation, NAVD88 (ft)
Horizontal distance (m)
200
180
160
140
120
100
80
60
40
20
0

AC 6

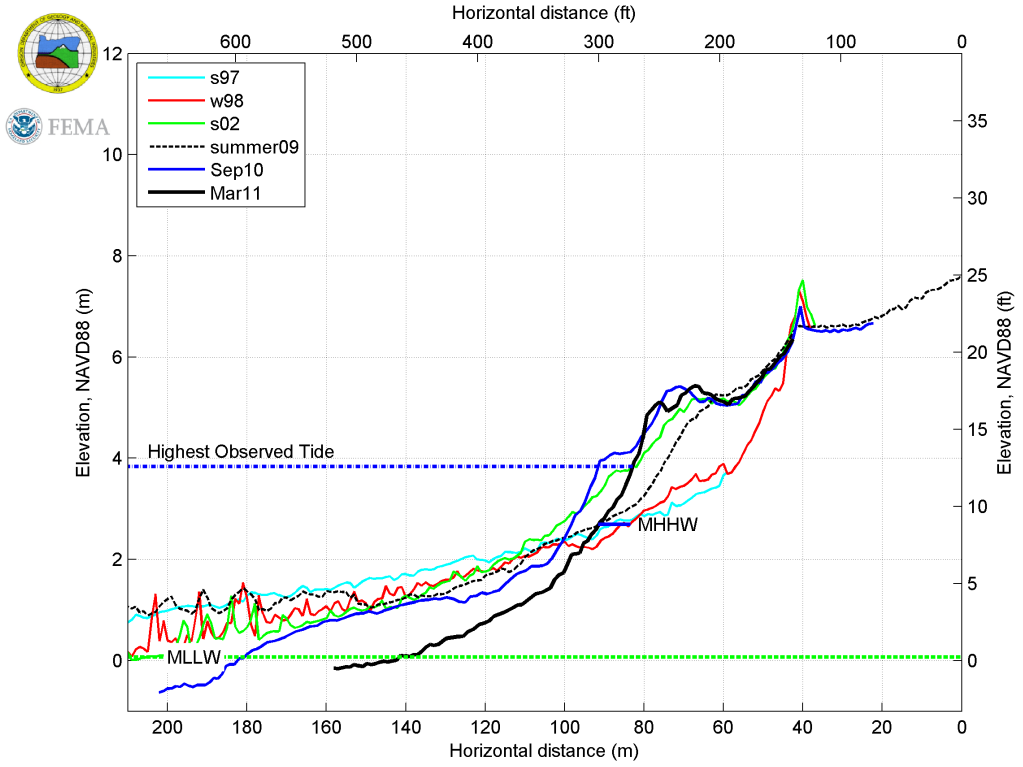
Horizontal distance (ft)
600
500
400
300
200
100
0
s97
w98
s02
summer09
Sep10
Mar11
Highest Observed Tide
MHHW
MLLW
Elevation, NAVD88 (m)
Elevation, NAVD88 (ft)
Horizontal distance (m)
200
180
160
140
120
100
80
60
40
20
0

AC 7

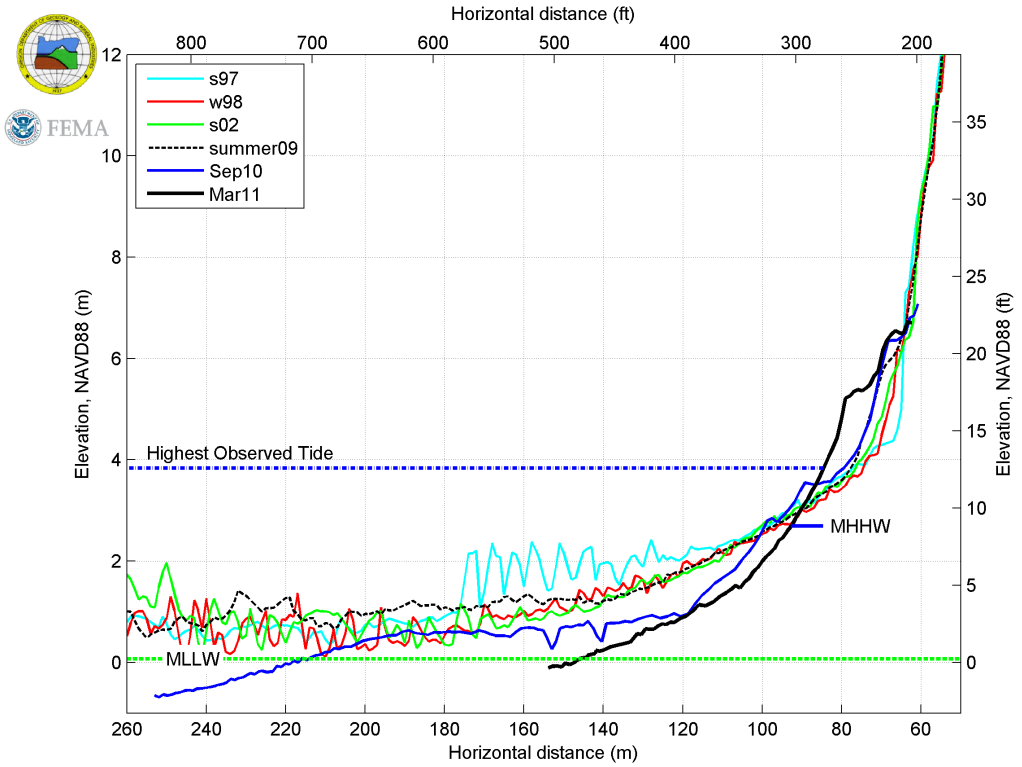
FEMA
Horizontal distance (ft)
800
700
600
500
400
300
200
s97
w98
s02
summer09
Sep10
Mar11
Highest Observed Tide
MHHW
MLLW
Elevation, NAVD88 (m)
Elevation, NAVD88 (ft)
Horizontal distance (m)
260
240
220
200
180
160
140
120
100
80
60

AC 8

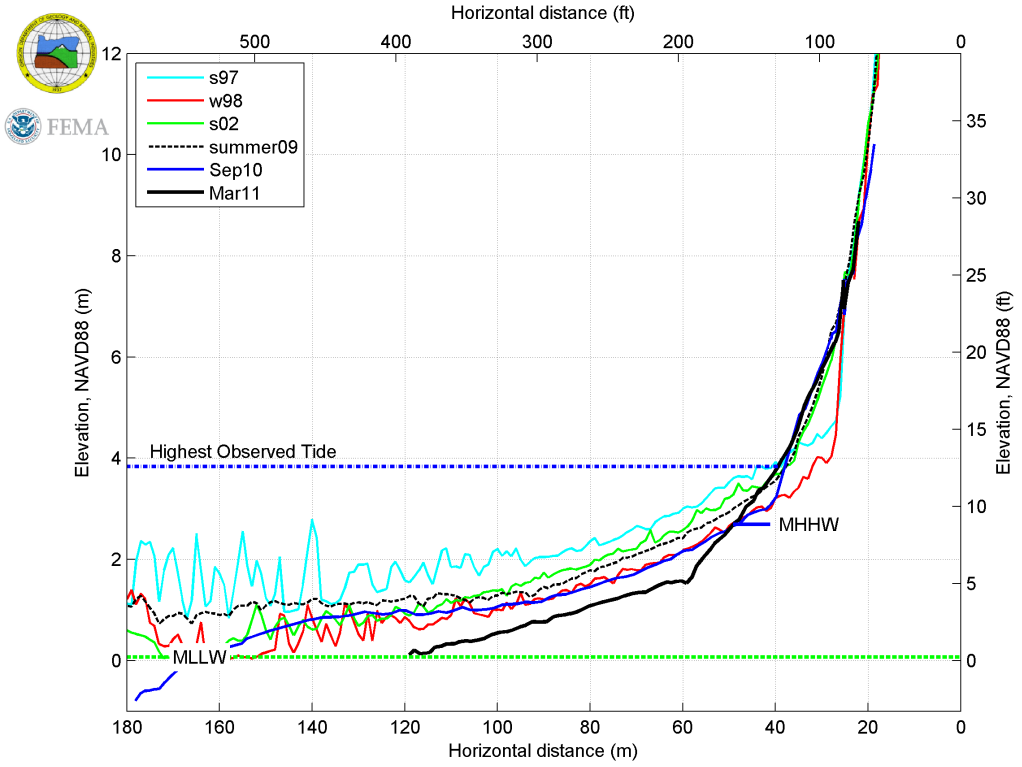
FEMA
Horizontal distance (ft)
500
400
300
200
100
0
s97
w98
s02
summer09
Sep10
Mar11
Highest Observed Tide
MHHW
MLLW
Elevation, NAVD88 (m)
Elevation, NAVD88 (ft)
Horizontal distance (m)
180
160
140
120
100
80
60
40
20
0

AC 9

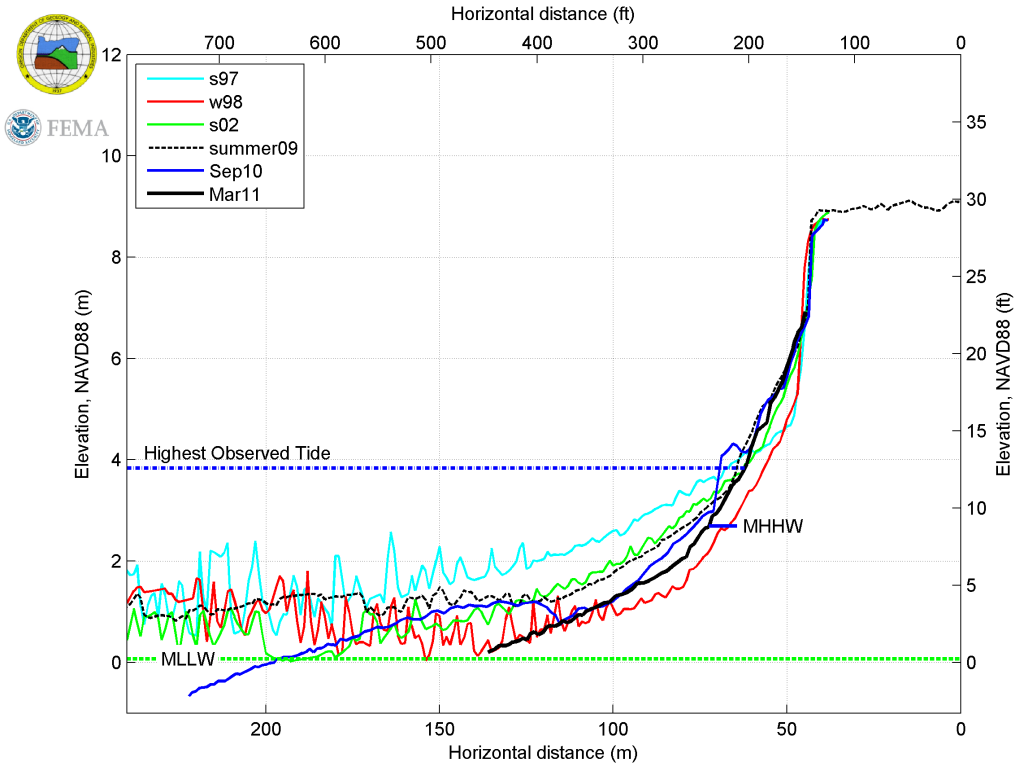
Horizontal distance (ft)
700
600
500
400
300
200
100
0
s97
w98
s02
summer09
Sep10
Mar11
Highest Observed Tide
MHHW
MLLW
Elevation, NAVD88 (m)
Elevation, NAVD88 (ft)
Horizontal distance (m)
200
150
100
50
0

AC 10

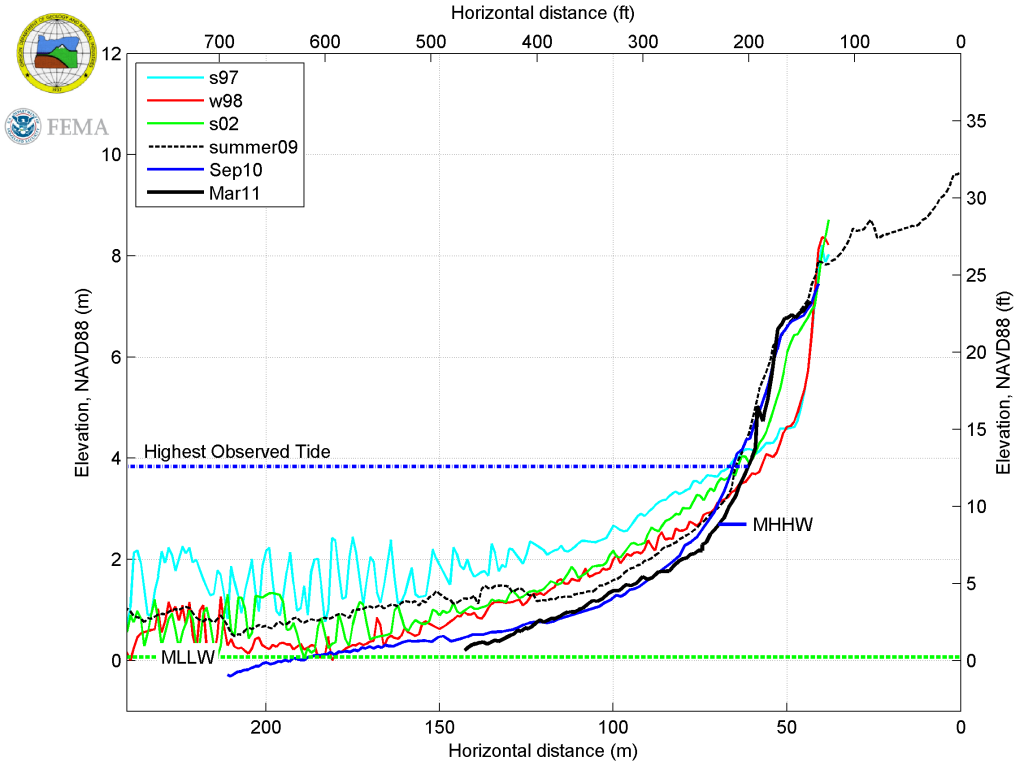
Horizontal distance (ft)
700
600
500
400
300
200
100
0
s97
w98
s02
summer09
Sep10
Mar11
Highest Observed Tide
MHHW
MLLW
Elevation, NAVD88 (m)
Elevation, NAVD88 (ft)
Horizontal distance (m)
200
150
100
50
0

11.2.7 Falcon Cove

FC 1

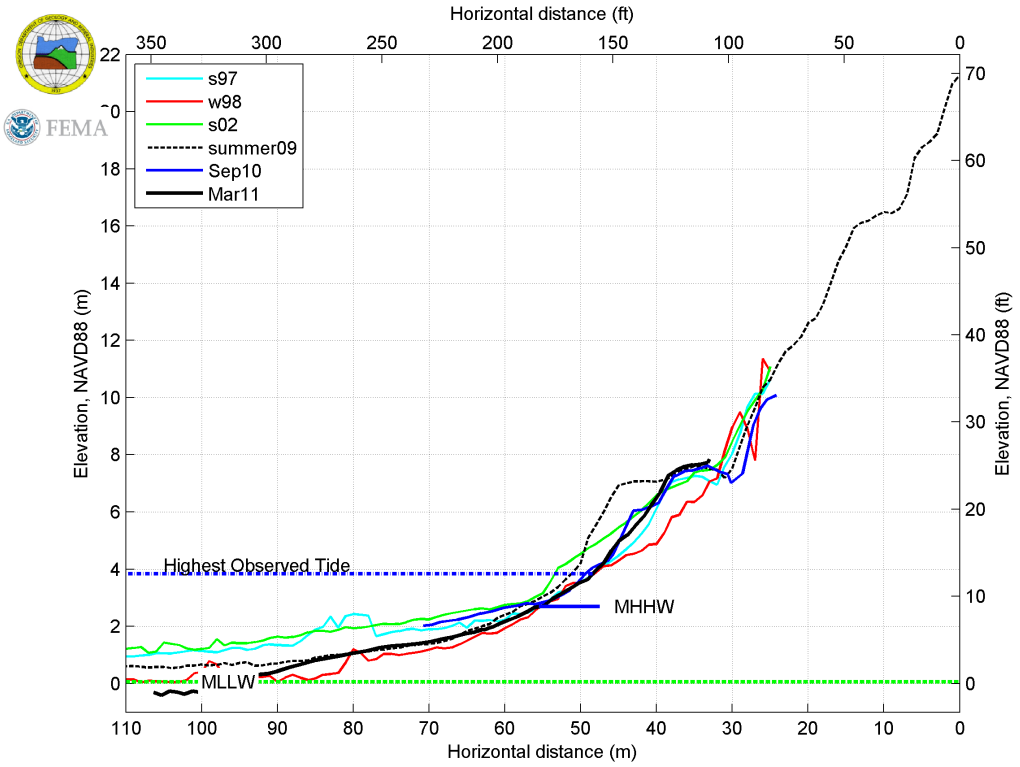

FC 2

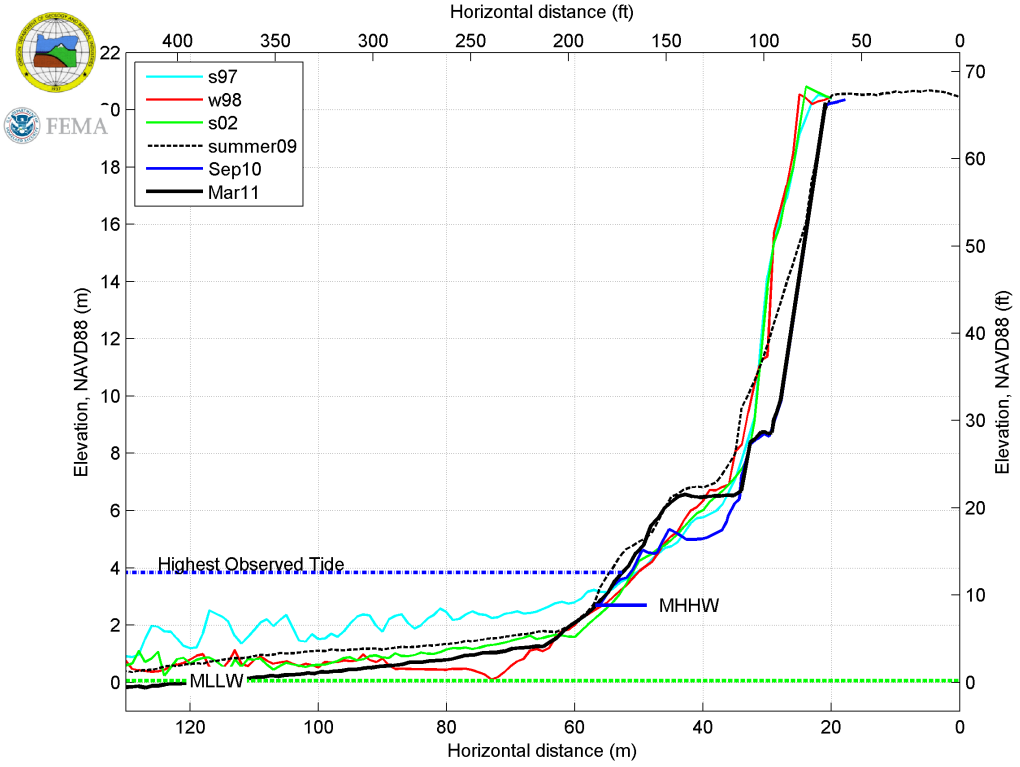

FC 3

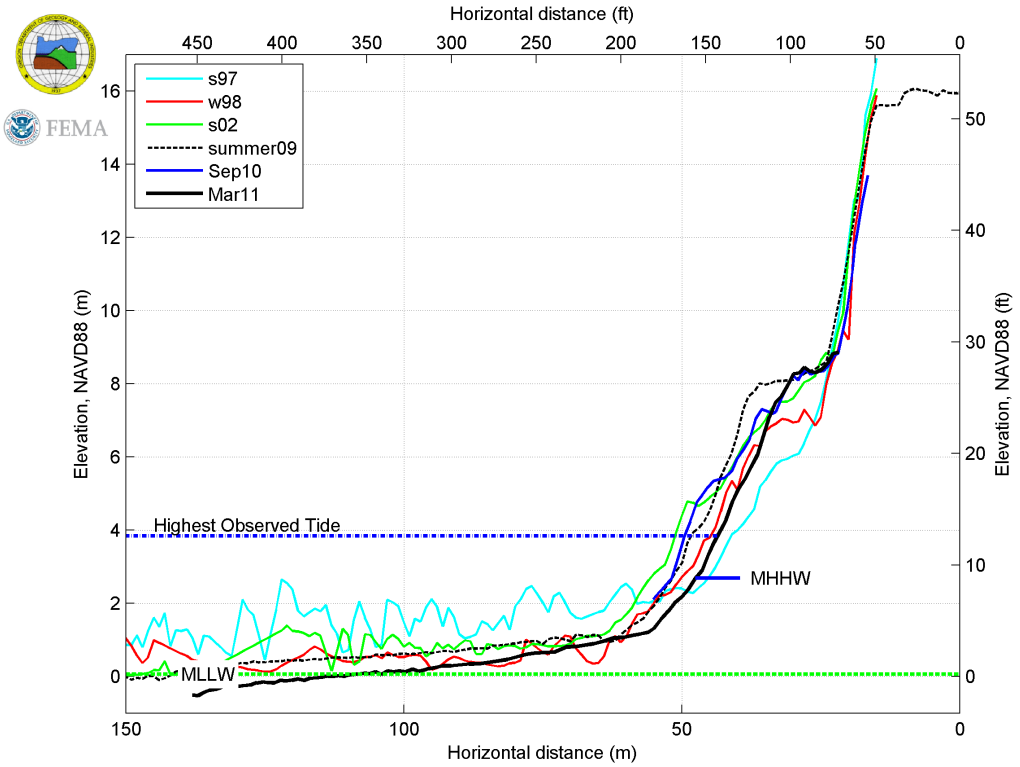
Horizontal distance (ft)
450 400 350 300 250 200 150 100 50 0
s97
w98
s02
summer09
Sep10
Mar11
Highest Observed Tide
MHHW
MLLW
Elevation, NAVD88 (m)
Elevation, NAVD88 (ft)
150 100 50 0
Horizontal distance (m)

FC 4

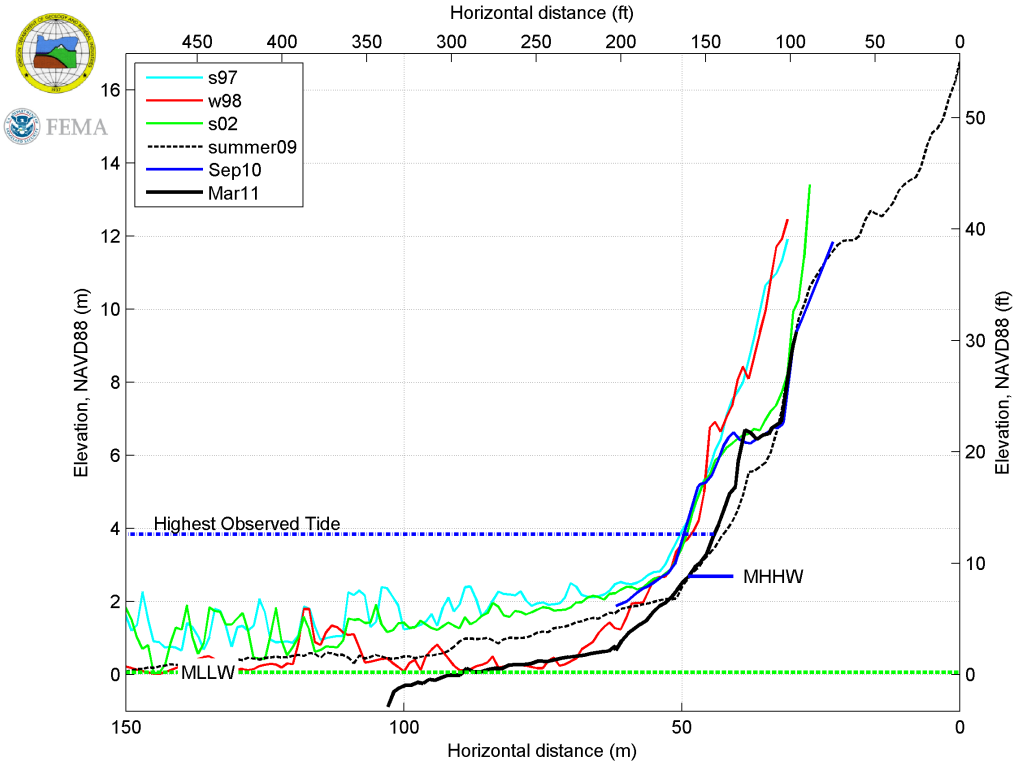
Horizontal distance (ft)
450 400 350 300 250 200 150 100 50 0
s97
w98
s02
summer09
Sep10
Mar11
Highest Observed Tide
MHHW
MLLW
Elevation, NAVD88 (m)
Elevation, NAVD88 (ft)
150 100 50 0
Horizontal distance (m)

FC 5

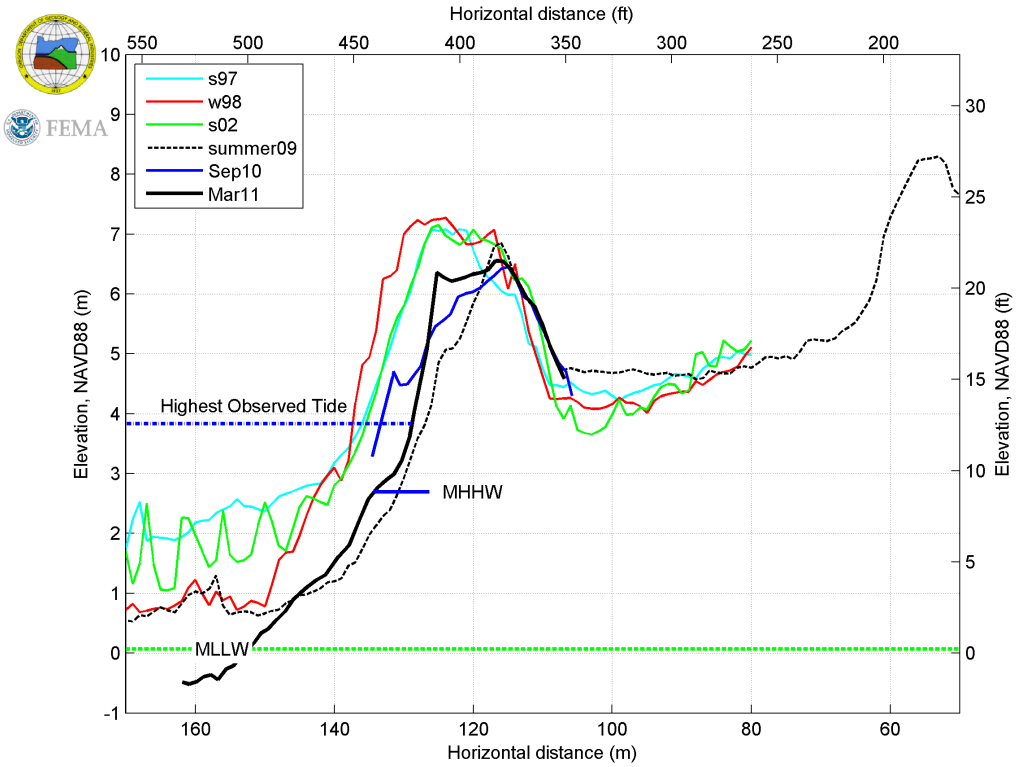
Horizontal distance (ft)
550
500
450
400
350
300
250
200
s97
w98
s02
summer09
Sep10
Mar11
Highest Observed Tide
MHHW
MLLW
Elevation, NAVD88 (m)
Elevation, NAVD88 (ft)
Horizontal distance (m)
160
140
120
100
80
60

FC 6

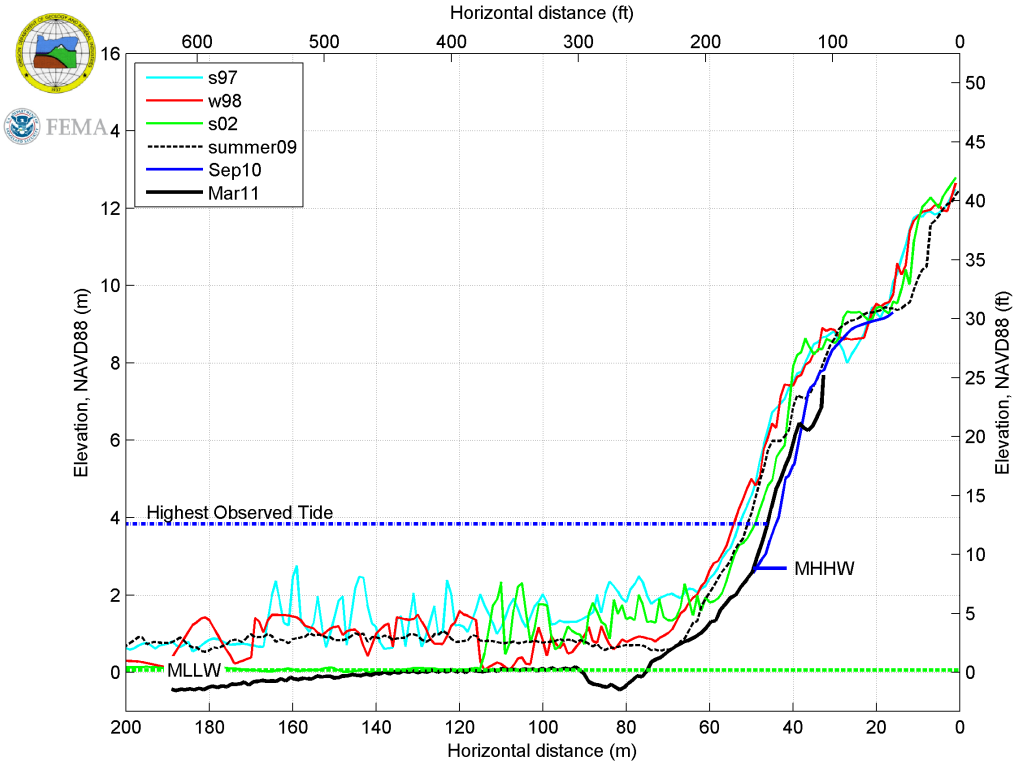
Horizontal distance (ft)
600
500
400
300
200
100
0
s97
w98
s02
summer09
Sep10
Mar11
Highest Observed Tide
MHHW
MLLW
Elevation, NAVD88 (m)
Elevation, NAVD88 (ft)
Horizontal distance (m)
200
180
160
140
120
100
80
60
40
20
0